Establishing an *in vitro* system for the ABC transporter Pleiotropic Drug Resistance 8 from *Arabidopsis thaliana*

Inaugural-Dissertation

zur Erlangung des Doktorgrades
der Mathematisch-Naturwissenschaftlichen Fakultät
der Heinrich-Heine-Universität Düsseldorf

vorgelegt von

Katharina Gräfe

aus Krefeld

Düsseldorf, August 2018

aus dem Institut für Biochemie
der Heinrich-Heine-Universität Düsseldorf

Gedruckt mit der Genehmigung der
Mathematisch-Naturwissenschaftlichen Fakultät der
Heinrich-Heine-Universität Düsseldorf

Berichterstatter:

1. Prof. Dr. rer. nat. Lutz Schmitt

2. Prof. Dr. rer. nat. Karl-Erich Jaeger

Tag der mündlichen Prüfung: 17.10.2018

Table of contents

Summary

As sessile organisms plants are exposed to many environmental stressors. Although they cannot move they react to their environment by activating stress response and signaling pathways. This response includes detoxification mechanisms as well as herbivore and pathogen response. ATP-binding cassette (ABC) transporters were shown to be involved in all these processes. Interestingly, plants contain high numbers of ABC transporters compared to organisms from other kingdoms and also compared to microalgae, the ancestor of plants. Therefore it was hypothesized that ABC transporter genes multiplied and obtained new functions during the adaption of plants to the sessile lifestyle on dry land. The plasma membrane ABC transporter PDR8 from *Arabidopsis thaliana* belongs to the Pleiotropic Drug Resistance (PDR) family, which only exists in plants and fungi. Applying mutant studies and reverse genetics the protein was shown to be involved in diverse physiological processes including heavy metal detoxification, hormone transport, drought and salt resistance and pathogen response. *At*PDR8 was furthermore assigned a key role in nonhost resistance in *A. thaliana*. The physiological studies imply that *At*PDR8 transports a variety of structurally unrelated compounds. However, this hypothesis lacks direct evidence and the possibility that *At*PDR8 transports only one stress-inducible compound cannot be excluded at the moment. Additionally, contradictory results exist complicating the understanding of *At*PDR8 function in plant immunity. Knowledge about the transported substrate(s) will help to clarify the physiological role of the transporter. This requires biochemical studies and the establishment of an *in vitro* system to ensure that interfering processes do not mask the role of the transporter. This project aimed the establishment of an *in vitro* system for the ABC transporter *At*PDR8. To realize this, five steps were required: 1) Cloning, 2) Heterologous expression, 3) Purification, 4) Reconstitution into liposomes and 5) Establishment of a suitable transport assay. The *AtPDR8* gene was cloned into expression vectors for prokaryotic and eukaryotic systems and different affinity tags were fused to the N- or the C-terminus of the protein sequence. During the cloning and expression tests potential toxicity of *At*PDR8 to the (pro- and eukaryotic) hosts was encountered resulting in the need to explore multiple cloning strategies and strains. Expression of a construct with N-terminal affinity tags was successful in the yeast *Pichia pastoris*. In this study, for the first time a plant ABC transporter was expressed in *P. pastoris*. However, the position of the tag was crucial for successful overexpression. Density gradient centrifugation and confocal fluorescence microscopy could show that *At*PDR8 was targeted to the plasma membrane in *P. pastoris*, which implies correct

folding and processing of the protein. *At*PDR8 was subsequently purified, for which the purification protocol was established. That included the screening of different detergents as well as a screening of different affinity chromatography approaches and the evaluation of a size exclusion chromatography. The reconstitution protocol for *At*PDR8 was also established, which comprised the liposomes preparation using different lipid compositions, the optimization of the destabilization process and the integration of *At*PDR8 into the liposomes. Floating density gradient centrifugation could proof the success of the reconstitution. This study represents the first purification and reconstitution of a PDR transporter from *A. thaliana*. In order to clarify which substrates are transported and to identify unknown substrates of the transporter a transport assay was established, which allows the usage of a mixture of unknown compounds, e.g. cytosolic extracts. The establishment required the evaluation of optimal conditions for the transport reaction and the evaluation of different methods for the disruption of membrane vesicles. Tandem mass spectrometry even allows the identification of transported compounds of low abundance. The knowledge gained in this project will facilitate the establishment of *in vitro* systems for other plant full-size ABC transporters. Since several eukaryotic ABC transporters display broad substrate spectra these systems will be needed to biochemically characterize the transporters regarding substrate specificity and transport characteristics.

Zusammenfassung

Als sessile Organismen sind Pflanzen einer Vielzahl von Stressfaktoren ausgesetzt. Obwohl sie darauf nicht durch Relokalisierung reagieren können schützen sie sich durch die Aktivierung von Verteidigungs- und Signalstoffwechselwegen. Diese beinhalten Mechanismen zur Entgiftung sowie zur Verteidigung gegen pathogene und herbivore Organismen. Es wurde gezeigt, dass „ATP-binding cassette“ (ABC)-Transporter an diesen Prozessen beteiligt sind. Interessanterweise beinhalten Pflanzen eine Vielzahl an ABC-Proteinen im Vergleich zu Organismen der anderen Reiche und auch im Vergleich zu Mikroalgen, den Vorfahren von Pflanzen. Daher wird vermutet, dass während der Anpassung der Landpflanzen an die sessile Umgebung ABC-Transporter-Gene multipliziert wurden und neue Funktionen entwickelt haben. Der Transporter PDR8 aus *Arabidopsis thaliana* gehört zu der Familie der ABC-Transporter mit pleiotropischer Wirkstoffresistenz (englisch: Pleiotropic drug resistance, PDR), welche bisher nur in Pflanzen und Pilzen entdeckt wurden. *At*PDR8 ist in der Plasmamembran lokalisiert und durch Mutationsstudien und reverse Genetik an *A. thaliana* wurde herausgefunden, dass *At*PDR8 an diversen physiologische Prozessen beteiligt ist. Dazu gehören Entgiftung, Hormontransport, Resistenz gegen Salz und Trockenheit sowie Pathogenabwehr. Des Weiteren wurde gezeigt, dass *At*PDR8 eine Schlüsselfunktion in der Resistenz von Nicht-Wirtspflanzen einnimmt. Die Physiologischen Studien weisen darauf hin, dass *At*PDR8 eine Vielzahl verschiedener Substanzen transportiert. Allerdings fehlt der direkte Nachweis für diese Hypothese und es kann daher nicht ausgeschlossen werden, dass *At*PDR8 nur eine einzige, Stress-induzierbare Substanz transportiert. Darüber hinaus existieren widersprüchliche Studien bezüglich der Rolle von *At*PDR8 in der Pflanzenimmunität. Das Wissen über die transportierten Substrate würde Aufschluss über die tatsächliche physiologische Rolle von *At*PDR8 geben. Dazu werden biochemische Analysen und die Etablierung eines *In vitro*-Systems benötigt um zu verhindern, dass andere Proteine die Charakterisierung stören. Diese Arbeit zielte auf die Etablierung eines *In vitro*-Systems des ABC-Transporters PDR8 ab. Für die Umsetzung mussten folgende Schritte realisiert werden: 1) Klonierung, 2) Heterologe Expression, 3) Proteinreinigung, 4) Rekonstitution sowie 5) die Etablierung einer Transportanalyse. Das *PDR8*-Gen wurde in Expressionsvektoren für pro- und eukaryotische Systeme kloniert. Dabei wurden verschiedene Affinitätsmarkierungen an den C- oder N-terminus der Proteinsequenz angefügt. Während der Klonierungs- und Expressionsstudien wurde deutlich, dass *At*PDR8 möglicherweise toxisch für die getesteten pro- und eukaryotischen Systeme ist. Aus diesem

Grund wurden verschiedene Klonierungsstrategien und Stämme analysiert. Die Expression mit N-terminaler Markierung war erfolgreich in der Hefe *Pichia pastoris*. In dieser Arbeit wurde zum ersten Mal ein pflanzlicher ABC-Transporter in *P. pastoris* exprimiert, wobei die Position der Affinitätsmarkierung entscheidend für die erfolgreiche Expression war. Durch Dichtegradientenzentrifugation und konfokaler Fluoreszenzmikroskopie konnte gezeigt werden, dass *At*PDR8 auch in *P. pastoris* in der Plasmamembrane lokalisiert ist. Daher kann angenommen werden, dass das Protein korrekt gefaltet und prozessiert wurde. Anschließend wurde *At*PDR8 aufgereinigt, wofür das Protokoll in dieser Arbeit erstellt wurde. Dazu wurden verschiedene Detergenzien analysiert sowie verschiedene Ansätze der Affinitätschromatographie in Kombination mit Größenausschlusschromatographie. Das Protokoll für die Rekonstitution von *At*PDR8 in Liposomen wurde ebenfalls etabliert. Dazu wurde die Herstellung von Liposomen aus verschiedenen Lipidansätzen, die Optimierung der Liposomendestabilisierung und die Integration von *At*PDR8 in die Liposomen untersucht. Der Erfolg der Rekonstitution konnte durch Dichtegradientenzentrifugation bestätigt werden. In dieser Arbeit wurde zum ersten Mal ein PDR-Transporter aus *A. thaliana* gereinigt und rekonstituiert. Um zu klären welche Substrate transportiert werden und um unbekannte Substrate zu identifizieren, wurde eine Transportanalyse etabliert, welche die Verwendung eines Komponentengemischs, wie zum Beispiel ein zytosolischer Extrakt, ermöglicht. Dazu wurde der Transporter Pdr5 aus *Saccharomyces cerevisiae* verwendet, da dessen Substrate schon studiert wurden. Die Etablierung umfasste die Evaluation der optimalen Transportbedingungen sowie die Analyse verschiedener Methoden zum Membranvesikelaufschluss. Der Einsatz von Tandem-Massenspektroskopie ermöglicht die Identifikation unbekannter Substanzen, selbst wenn diese in geringen Konzentrationen vorliegen. Das durch dieses Projekt gewonnene Wissen erleichtert die Etablierung weiterer *in vitro*-Systeme für Volllängen-ABC-Transporter. Mehrere eukaryotische ABC-Transporter weisen breite Substratspektren auf. Daher werden *in vitro*-Systeme benötigt um die Transporter biochemisch zu charakterisieren in Bezug auf die Substratspezifität und die Transportcharakteristika.

Abbreviations

2,4-D	2,4-Dichlorophenoxyacetic acid
4MI3G	4-methoxyindol-3-ylmethylglucosinulate
4OGGlcI3F	4-*O*-β-D-glucosyl-1-H-indole-3-yl formamide
4-OH-I3G	4-hydroxy-indol-3-ylmethylglucosinulate
aa	amino acids
ADP	Adenosine 5'-diphosphate
ABC	ATP-binding cassette
AOH	ABC one homolog
Appr.	approximately
At	*Arabidopsis thaliana*
ATH	ABC two homolog
ATP	Adenosine 5'-triphosphate
BSEP	Bile salt export pump
CaM	calmoduline or calcium modulated protein
CBP	Calmoduline-binding peptide
CBP-AC	CBP affinity chromatography
cDNA	copy DNA
CDPK	Calcium-dependent protein kinase
cmc	critical micellar concentration
CML	Calmodulin-like
Cr	*Catharanthus roseus*
CYP81F2	Cytochrome P450, family 81, subfamily F, polypeptide 2
DDAO	n-dodecyl-N,N-dimethylamine-N-oxide
DDM	n-Dodecyl-β-D-maltopyranoside
DNA	Deoxyribonucleic acid
EDTA	Ethylenediamine tetraacetic acid
ER	Endoplasmic reticulum
EQ	E1036Q mutation in *Sc*Pdr5
FLS2	Flagellin sensitive 2
g	Grams
HeLa	Henrietta Lacks
HEPES	2-(4-(2-Hydroxyethyl)-1-piperazinyl)-ethansulfonsäure

Hs	*Homo sapiens*
Hv	*Hordeum vulgare*
I3G	Indole-3-ylmethyl glucosinulate
IAA	Indole-3-acetic acid
IBA	Indole-3-butyric acid
IGMT	*O*-methyltransferase
IMAC	Immobilized metal ion affinity chromatography
IPTG	Isopropyl β-D-1-thiogalactopyranoside
K_D	Dissociation constant
kDa	kilo Dalton
L	Liters
LC	Liquid chromotography
Lr	Leaf rust resistance
M	mol per liter
MAPK	Mitogen-activated protein kinase
MDR	Multidrug resistance
m	milli, factor 10^{-3}
mRNA	messenger RNA
MRP	Multi-drug resistance-associated protein
MS	Mass spectrometry
MS/MS	Tandem mass spectrometry
Mt	*Medicago truncatula*
MWCO	Molecular weight cut off
n	nano, factor 10^{-9}
NAA	1-Naphthaleneacetic acid
NBD	Nucleotide binding domain
Np	*Nicotiana plumbaginifolia*
NPA	N-1-naphthylphthalamic acid
Nt	*Nicotiana tabacum*
OD	Optical density
Os	*Oryza sativa*
PAMP	Pathogen associated molecular pattern
PCC-α-M	*trans*-4-(*trans*-4′-propylcyclohexyl)-cyclohexyl-α-D-maltoside
PCR	Polymerase chain reaction

PDR	Pleiotropic drug resistance
Pgp	P-glycoprotein
Ph	*Petunia hybrida*
Pp	*Pichia pastoris*
RNA	Ribonucleic acid
RNAi	RNA interference
RT	Room temperature
Sc	*Saccharomyces cerevisiae*
SDS	Sodium dodecylsulfate
SDS-PAGE	SDS-polyacrylamide gel electrophoresis
SEC	Size exclusion chromatography
SP	*Spirodela polyrrhiza*
Spa	*Spathaspora passalidarum*
Ta	*Triticum aestivum*
TMD	Transmembrane domain
TNP	Trinitro phenyl
TAP	Transporter associated with antigen processing
Tris	Tris-(hydroxymethyl)-aminomethan
TUR2	Turion 2
UGT	UDP-glycosoltransferase
Vm	*Vinca minor*
WT	Wild-type
µ	micro, factor 10^{-6}

Amino acid	**3-letter code**	**1-letter code**	**Amino acid**	**3-letter code**	**1-letter code**
Alanine	Ala	A	Leucine	Leu	L
Arginine	Arg	R	Lysine	Lys	K
Asparagine	Asn	N	Methionine	Met	M
Aspartic acid	Asp	D	Phenylalanine	Phe	F
Cysteine	Cys	C	Proline	Pro	P
Glutamic acid	Glu	E	Serine	Ser	S
Glutamine	Gln	Q	Threonine	Thr	T
Glycine	Gly	G	Tryptophan	Trp	W
Histidine	His	H	Tyrosine	Tyr	Y
Isoleucine	Ile	I	Valine	Val	V

1 Introduction

1.1 Plants in their environment – how to hold your ground when you are sessile

Plants are highly specialized organisms that have presumed the sessile lifestyle (Hwang et al., 2016). They are exceptional compared to other organisms. They have a unique body structure with a big relative surface area for light collection as energy input for photosynthesis. To avoid damage of UV light plants are coated with cutin and wax layers. In contrast, the wide surface area prevents rapid movement, which could have been a reason why plants have adopted the sessile lifestyle (Hwang et al., 2016). Due to the sessile lifestyle plants are subjected to many environmental stressors, which they cannot avoid by simply moving away. These stressors, which may occur simultaneously, can be UV radiation, drought, salinity, extreme temperatures, lack of nutrients and the exposure to toxic compounds (Dicke and Hilker, 2003). Furthermore, plants have no excretory organs like animals; therefore detoxification must take place on a cellular level (Sanchez-Fernandez et al., 2001a). Although plants cannot move they actively interact with the surrounding environment and respond to the conditions they are exposed to with physiological and morphological mechanisms (phenotypic plasticity). Upon stress the plant metabolism is radically changed by activating stress response and signaling pathways and only maintaining the indispensible basic metabolism (Gechev and Hille, 2012, Dicke et al., 2003, Kretzschmar et al., 2011).

1.1.1 Detoxification

Due to the sessile lifestyle plants are exposed to a variety of detrimental compounds. These compounds can be xenobiotics like pollutants or biocides, toxic microbial metabolites, soil-born minerals that are taken up together with nutrients, but also products of internal metabolic pathways that become toxic if not modified or removed. Since plants cannot avoid these compounds they have developed detoxification mechanisms (Rea, 2007). The detoxification process comprises two successive processes: the modification and the compartmentation. The first step of the modification is the hydrolysis or oxidation of the toxic compound. The hydrolysis is performed by esterases and the oxidation by cytochrome P450s. Thereby reactive sites are added to the toxic compound, which enables conjugation. The compound then gets conjugated to a hydrophilic molecule in order to prevent diffusion across membranes. The hydrophilic molecules can be glucose, malonate or glutathione. The

conjugations are catalyzed by glucosyl, malonyl or glutathione transferases. Through the modification toxicity of the compound is reduced and the distribution in cells and tissues is avoided. In the compartmentation process the compound is exported from the cytosol either into the vacuole or into the apoplast. The export is generally mediated by ATP-dependent membrane transporters. Heavy metals are mainly bound by phytochelatins, which are synthesized from glutathione by the phytochelatin synthase. The phytochelatin synthase is in turn activated by heavy metals. *At*ABCC1 and *At*ABCC2 were shown to transport phytochelated arsenic, cadmium and mercury into the vacuole (Kang et al., 2011, Coleman et al., 1997). The plasma membrane located ABC transporter *At*PDR8 mediates cadmium transport into the apoplast and *At*PDR12 is involved in lead tolerance (Lee et al., 2005, Kim et al., 2007). *At*ABCI16/*At*ALS3 and *At*ABCI17/*At*STAR1 were shown to be involved in aluminum resistance (Larsen et al., 2005, Huang et al., 2010). However, it is unclear in what form the heavy metals are translocated by these transporters (Kang et al., 2011).

1.1.2 Plant resistance to pathogens

During the adaption to dry land, plants have evolved different mechanisms to defend pathogen attack. Most plants are resistant to a broad range of pathogens and are only colonized by a small number of adapted pathogens. The term “nonhost resistance” describes the nonspecific resistance of a plant species to all genotypes of non-adapted pathogen species. Nonhost resistance includes physical barriers avoiding pathogen entry into the cell, penetration resistance and postpenetration resistance. It is a multi-layered process and includes constitutive and inducible mechanisms (Mysore and Ryu, 2004). The first step is the pathogen associated molecular pattern (PAMP)-triggered immunity. PAMPs are general elicitor molecules that are recognized by the plants through plasma membrane-localized receptors (Mysore and Ryu, 2004, Niks and Marcel, 2009). One general elicitor is flagellin, a protein that forms the filament in flagellated bacteria. The conserved 22 amino acids long sequence flg22 of the N-terminus is recognized by the receptor-like kinase flagellin sensitive 2 (FLS2) (Chinchilla et al., 2006). Fungal elicitors are for example xylanase and chitin (Benschop et al., 2007, Underwood and Somerville, 2013).

The elicitor recognition activates defense mechanisms, which include the expression of defense genes, the enhancement of resistance to diseases, the activation of the mitogen-activated protein kinase (MAPK) cascade, ethylene biosynthesis, induction of phospholipases

and the production of reactive oxygen species by the plasma membrane localized NADPH oxidase and apoplastic peroxidases (Johansson et al., 2014, Benschop et al., 2007). The signal transduction pathways that are activated after elicitor recognition involve *inter alia* ion fluxes across the plasma membrane, extracellular alkalinization, temporary elevation of the cytosolic calcium ion concentration, protein phosphorylation/dephosphorylation by MAPK and the calcium ion-dependent protein kinases (CDPKs) as well as the production of jasmonate. The proteins involved in these signal transduction pathways are activated by post-translational modifications, conformational changes or by changes in complex formation. The activated defense responses include closure of stomata, reinforcement of the cell wall, formation of papillae, synthesis of phytoalexins and secretion of secondary metabolites (Johansson et al., 2014, Benschop et al., 2007, Underwood and Somerville, 2013). Some pathogens have evolved ways to circumvent the PAMP-triggered immunity. They produce effector proteins that repress the plant defense signaling. This process is called effector-triggered susceptibility. In turn, some plants recognize the effector molecules and activate defense mechanisms in response (effector-triggered immunity), which includes the hypersensitive response, the programmed cell death of the infected tissue (Johansson et al., 2014, Mysore and Ryu, 2004).

In *A. thaliana* the *PENETRATION* (*PEN*) mutants show enhanced susceptibility to nonhost pathogens. PEN1 is a membrane-located syntaxin, which is involved in vesicle-dependent secretory defense (Nielsen and Thordal-Christensen, 2013). PEN2 and PEN3 were shown to act together in the same pathway for extracellular defense, which is distinct from the PEN1 pathway. The PEN2/PEN3 pathway is especially important in nonhost resistance because it restricts the growth of a broad range of pathogens (Lipka et al., 2005, Bednarek et al., 2009, Stein et al., 2006). PEN2 is a myrosinase, which is peroxisome-localized and hydrolyzes indole glucosinulates to form antimicrobially active compounds. PEN3 is the plasma membrane-localized ABC transporter *At*PDR8, which likely exports the PEN2-activated compounds. The proposed pathway is shown in Figure 1. The tryptophan-derived indole-3-ylmethyl glucosinulate (I3G) is converted to 4-hydroxy-indol-3-ylmethylglucosinulate (4-OH-I3G) by the P450 monooyxgenase CYP81F2, which can be further converted to 4-methoxyindol-3-ylmethylglucosinulate (4MI3G) by *O*-methyltransferases (IGMTs). 4MI3G was shown to accumulate in *pen2* mutants, however, the necessity of functional IGMTs for pathogen resistance is not clarified. Both 4-OH-I3G and 4MI3G could be activated by PEN2 through hydrolysis. It was speculated that the produced bioactive compound is exported by *At*PDR8/PEN3 (Bednarek et al., 2009, Lu et al., 2015).

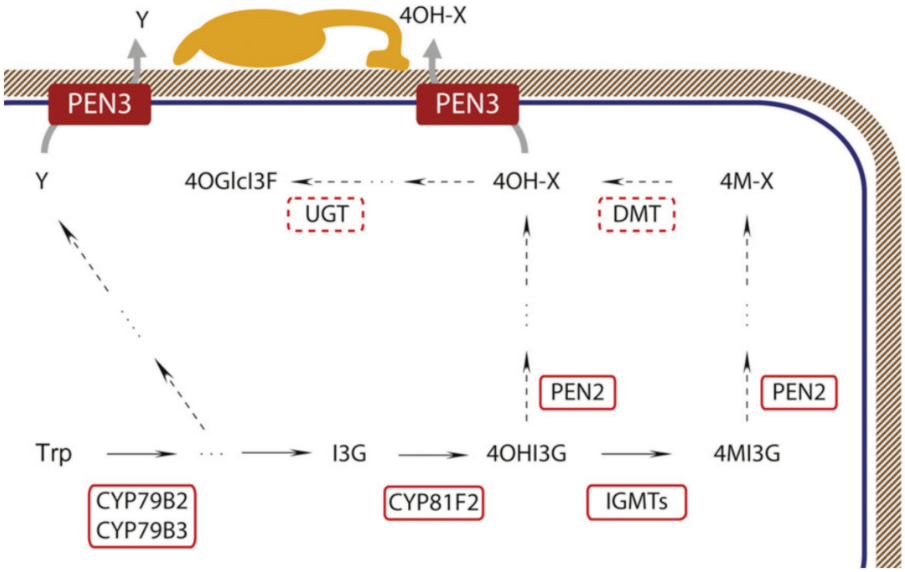

Figure 1: Proposed model for PEN2/PEN3 mediated nonhost resistance in *A. thaliana*. The tryptophan-derived compound I3G is converted to 4-OH-I3G by CYP81F2. 4-OH-I3G is then methylized by IGMTs to 4MI3G. Both, 4-OH-I3G and 4MI3G could be activated by PEN2. Possibly the 4MI3G-derived compound is again demethylized by O-demethyltransferase. The resulting active compounds might be exported by PEN3. In *pen3* mutant plants the compound 4OGlcI3F accumulated, which could result from detoxification of the bioactive PEN3-substrate through UDP-glycosoltransferase. The *pen2* mutant also exhibits PEN3-mediated resistance, which indicates that PEN3 might also export tryptophan-derived compounds independently of PEN2. The figure was taken from Lu et al. 2015.

1.1.3 ABC transporters take part in the adaption of plants to the sessile lifestyle

The sessile lifestyle of plants involves a defense mechanism that depends on secondary metabolites and the export of these. Plants produce a huge variety of secondary metabolites for fighting herbivores and pathogens but also for attraction of beneficial pollinators. More than 100,000 secondary metabolites were identified in plants (Rea, 2007). These metabolites often need to be transported across membranes to the site of action. The autotrophic lifestyle requires the *de novo* synthesis of many compounds and the transport of intermediates and products between the involved organelles as well as the export of toxic by-products (Sanchez-Fernandez et al., 2001a, Rea, 2007). Plants acquire nutrients from the soil. Thereby they often take-up toxic compounds from the soil like heavy metals or xenobiotics, which then have to be exported or transferred to storage organs. Physiological processes are organized on the whole plant-level, which involve plant hormones as signaling molecules. Phytohormones often have to be transported from one plant organ to another. They regulate plant development and also the response to biotic and abiotic stressors (Hwang et al., 2016, Kretzschmar et al., 2011). In all these processes ABC transporters are involved (Rea, 2007).

Compared to other organisms, plants are enriched in genes coding for ABC proteins (two to four times more) (Figure 2). For example, 48 ABC proteins were identified in humans and 29 in yeast, 128 and 129 were identified in *A. thaliana* or rice (Kang et al., 2011, Nuruzzaman et al., 2014, Rea, 2007). The number of genes was thereby not simply multiplied in relation to the genome size, as the comparison with the number of human ABC proteins elucidated (Sanchez-Fernandez et al., 2001b). The enrichment does not apply for microalgae, the ancestor of plants. This implies that during evolution of plants from microalgae the genes coding for ABC proteins got multiplied and in this process also diversified to obtain new functions. The increased capability to transport compounds and thereby interact with the environment may have been crucial for the adaption of plants to the sessile lifestyle (Hwang et al., 2016).

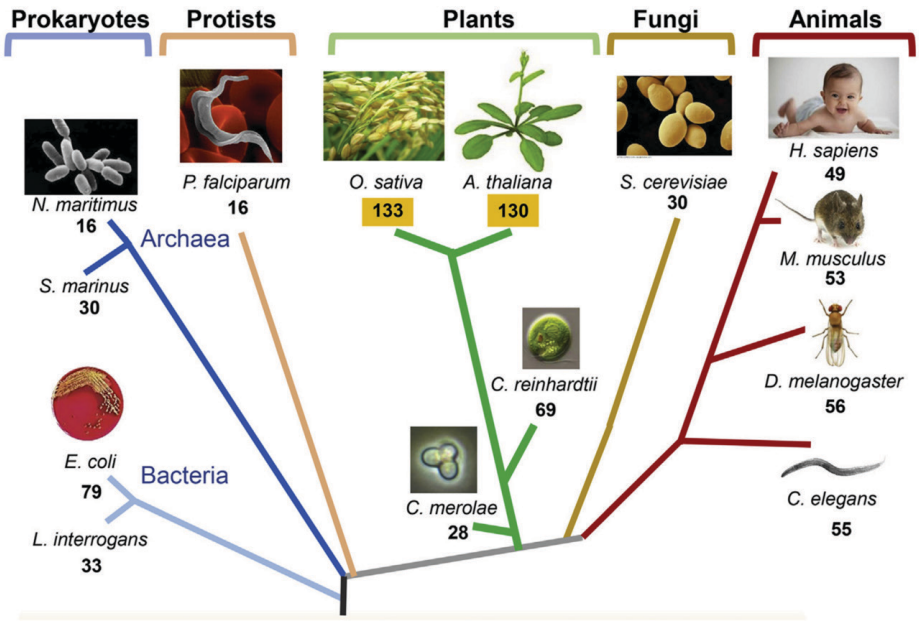

Figure 2: ABC proteins are enriched in plants. The phylogenetic tree displays species from all kingdoms of life. Numbers below the species names stand for the numbers of ABC proteins present in the respective species. The figure was taken and modified from Hwang et al. (2016).

1.2 ABC transporters: the organization of domains and transport mechanism

1.2.1 Domain organization in ABC transporters

ABC transporters are built in a modular fashion of four core domains (Figure 3). These include two nucleotide-binding domains (NBD) and two transmembrane domains (TMD) (Rea, 2007). Some ABC transporters comprise additional domains with proposed regulatory functions (Biemans-Oldehinkel et al., 2006). Some transporters, e.g. C-subfamily members or human TAP1, comprise an additional TMD (TMD0), which in humans and yeast is important for correct targeting but seems to have no function in the transport of compounds (Mason and Michaelis, 2002, Westlake et al., 2005, Procko et al., 2005).

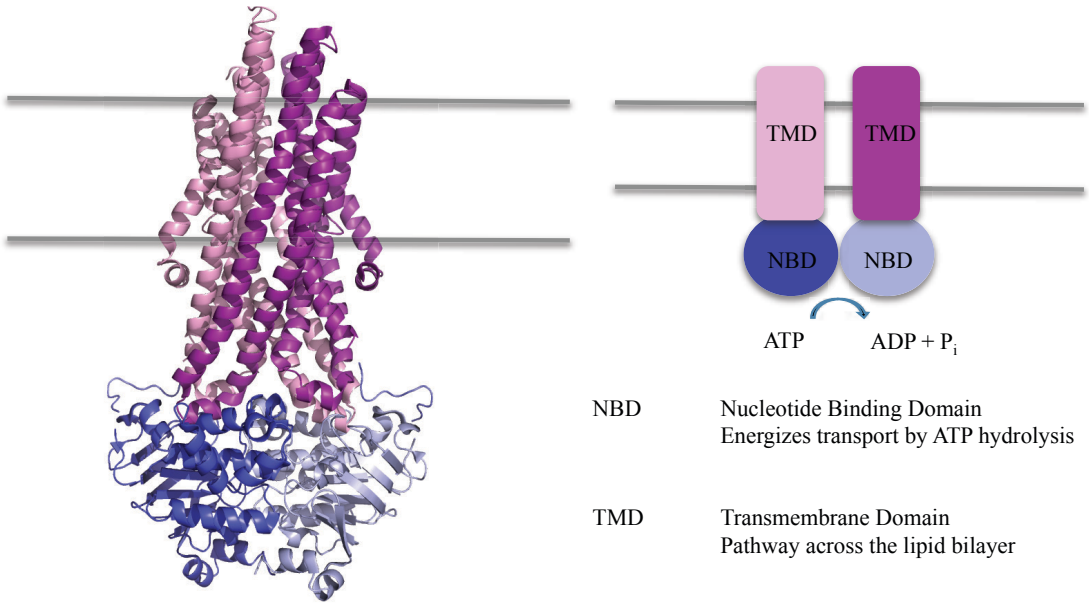

Figure 3: Organization of domains in ABC transporters. The crystal structure of the exporter Sav1866 from *Staphylococcus aureus* (PDB entry 2HYD) determined by Dawson and Locher (2006) is shown in cartoon style on the left side. The schematic representation of the four domains of ABC transporters is depicted on the right side. The two NBDs and TMDs are shown in shades of blue and purple, respectively. The membrane is indicated in grey.

While in prokaryotes different genes often encode the four domains, it was widely accepted that in eukaryotes two or four domains are fused in one polypeptide chain. Thereby the NBDs and TMDs are alternating meaning a full size transporter has the following order of domains: NH_3^+-TMD-NBD-TMD-NBD-COO^-. In case that the transporter is a half-size transporter the order of domains would be: NH_3^+-TMD-NBD-COO^-. Two half-size transporters dimerize to form a functional transporter. Some half- and full-size transporters are encoded by genes with

a reversed order of domains. In that case the NBD is N-terminal und the TMD is C-terminal: NH_3^+-NBD-TMD-[NBD-TMD]-COO^- (van den Brule and Smart, 2002, Verrier et al., 2008, Rea, 2007). However, there is evidence that in plants functional ABC transporters also assemble from individual protein domains. The bacterial-like ABC proteins *Os*STAR1 and *Os*STAR2 transcribe an NBD and a TMD and were shown to form a functional ABC transporter complex that acts in aluminum resistance (Huang et al., 2009). The ABC proteins *At*ABCI14 (Trigalactosyldiacylglycerol 1, TGD1) *At*ABCI15 (TGD2) and *At*ABCI (TGD3) are involved lipid transport in *A. thaliana* chloroplasts (Lu et al., 2007, Awai et al., 2006, Xu et al., 2003). The three proteins assemble to form a functional ABC transporter where TGD1 is the TMD, TGD3 the NBD and TGD2 the substrate binding protein (Roston et al., 2012). The ABC transporter complex is located in in the inner envelope of the chloroplasts. Another protein involved in lipid translocation is TGD4, which is located in the outer envelope of the chloroplasts and does not belong to the ABC protein family. Studies demonstrate that the contact between TGD4 and the ABC transporter complex TGD1/TGD2/TGD3 is mediated by TGD5, which is located in the chloroplast envelope (Fan et al., 2015). These findings indicate that in plants transport mechanisms exist that are similar to those found in bacteria (Symmons et al., 2009, Malinverni and Silhavy, 2009).

1.2.2 The nucleotide binding domains

The transport is energized by ATP hydrolysis. During ATP hydrolysis a hydroxyl group derived from water attacks the γ-phosphate group of the ATP molecule. The high-energy electrons relocate and form new bonds, which releases energy. The ATP molecule breaks into the products ADP and orthophosphate, which are lower in energy than ATP due to multiple resonance structures of the orthophosphate and less electrostatic repulsion in the ADP molecule (Hill and Morales, 1951). In the enzymatic reaction, divalent cations can act as cofactors by interacting with the oxygen atoms of the phosphate groups (Mildvan, 1979). The NBDs of ABC transporters, which catalyze the ATP hydrolysis, are highly conserved among all organisms and are approximately 220 – 240 amino acids in size (Ambudkar et al., 2006, Rea, 2007). They contain several conserved motifs (Figure 4 and Figure 5).

The Walker A (phosphate-binding loop or P-Loop) and Walker B motifs are important for nucleotide binding and are present in many enzymes that hydrolyze ATP (Vetter and Wittinghofer, 1999, Schmitt and Tampe, 2000). The Walker A motif is glycine–rich with the

consensus sequence GXXGXGK[ST] (X can be any residue). The amino acid residues interact with the phosphate groups of the nucleotide and the cofactor Mg^{2+}. The lysine of the Walker A motif is highly conserved and interacts with the β- and γ-phosphate of ATP, which fixes the ligand in a defined position (Zaitseva et al., 2005). The Walker B motif has the consensus sequence hhhhD (h is any hydrophobic residue). The highly conserved aspartate coordinates the magnesium ion in the binding pocket (Schneider and Hunke, 1998, Zaitseva et al., 2005). The Walker B motif is directly followed by a glutamate (the catalytic base), which activates the water molecule for nucleophilic attack of the γ-phosphate of the nucleotide (Orelle et al., 2003).

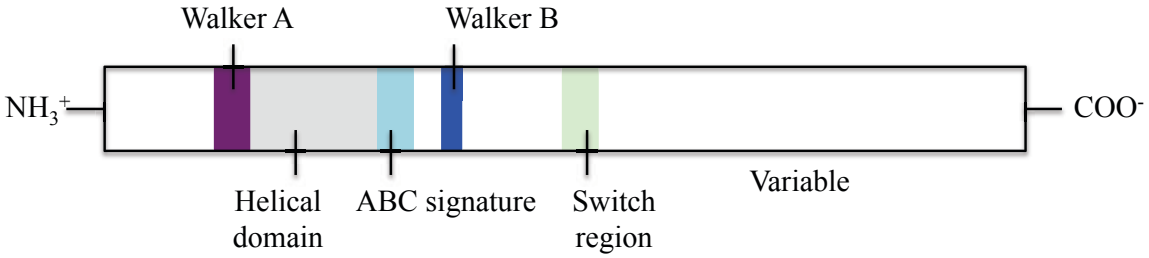

Figure 4: Scheme of the nucleotide binding domain of ABC proteins. The consensus sequences of the respective motifs are listed. h stands for any hydrophobic residue and X can be any residue. The Figure was adapted from Schneider and Hunke (1998).

Studies involving mutations of the Walker A and B motifs could show that exchanging the important amino acids can completely abolish ATPase activity of ABC proteins (Koronakis et al., 1995, Schneider et al., 1994, Loo and Clarke, 1995, Henriksen et al., 2005, Moody et al., 2002). The A-loop is located upstream of the Walker A motif (Ambudkar et al., 2006). It is an aromatic residue that contacts the adenosine ring of ATP via π-π interactions (Gaudet and Wiley, 2001, Yuan et al., 2001). Another important motif is the ABC signature motif (C-loop or peptide linker), which has the consensus sequence [LIVMFY]S[SG]GXXX[RKA][LIVMYA]X[LIVFM][AG] and is typical for ABC proteins. It is located between the Walker A and B motif and mutations in this sequence severely affect ATP hydrolysis (Panagiotidis et al., 1993, Koronakis et al., 1995, Schneider et al., 1994, Loo and Clarke, 1995, Aparicio et al., 1996). Crystal structures of several NBDs showed that the ABC signature motif is involved in forming the nucleotide-binding pocket. The two NBDs are thereby located in a head-to-tail arrangement, which means that the Walker A motif of one NBD pairs with the ABC signature motif of the other NBD (Chen et al., 2003, Smith et al., 2002, Zaitseva et al., 2005). The Walker B motif is followed by a switch region (H-loop),

which assists in signal transduction between the domains (Schneider and Hunke, 1998), but was also shown to be involved in catalytic activity (Zaitseva et al., 2005). The D-loop is the contact area of the two NBDs. The D-loop of one NBD interacts with the H-loop of the other NBD and thereby enables monomer-monomer communication (Zaitseva et al., 2005). The Q-loop is located at the surface of the NBD. Its residues interact with the coupling helices of the TMDs. The Q-loop and the coupling helices thereby build the contact area between NBD and TMD (Hollenstein et al., 2007). In some full-size transporters and some heterodimeric half-size transporters certain motifs are degenerated by amino acid substitutions in the binding sites. For example the hydrophobic Walker B motif is interrupted by a hydrophilic residue or the signature motif contains other residues than the consensus sequence (Gupta et al., 2014, Rea, 2007).

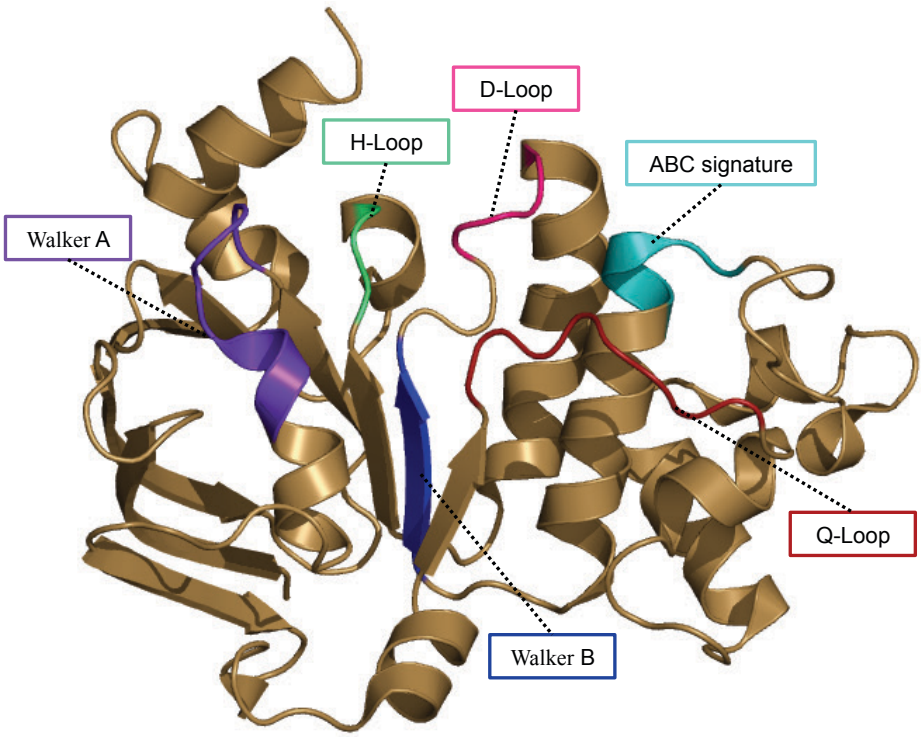

Figure 5: Crystal structure of the nucleotide binding domain of the *E. coli* ABC transporter haemolysin B. The structure was published by Schmitt et al. in 2003 (PDB entry 1MT0). The NBD monomer is depicted in cartoon style and the conserved motifs are listed: Walker A (magenta), Walker B (blue), ABC signature (cyan), D-loop (pink), H-loop (green) and the Q-loop (red).

1.2.3 The transmembrane domains

The TMDs build the pathway across the biological membrane. They consist of 5 – 10 α-helices per domain meaning a complete transporter consist of 10 – 20 α-helices, depending on the transporter class (Locher et al., 2002, Kadaba et al., 2008). The majority of exporters however follows the 6 + 6 paradigm and consists of 12 α-helices in two TMDs (Dawson and Locher, 2006, Ward et al., 2007). The TMDs are arranged in a way that they form a tunnel for the substrate translocation. Unlike the NBDs the TMDs are hardly conserved, although they can display a similar topology within the same transporter class (Rees et al., 2009). The TMDs have short cytoplasmic helices in the cytoplasmic loops, which are in contact with the NBDs (via the Q-loop) and are therefore named coupling helices (Locher et al., 2002). They transfer the conformational change induced by ATP binding and hydrolysis from the NBDs to the TMDs (Locher, 2016, Rees et al., 2009). Through the conformational change the TMDs switch between the inward and the outward facing conformations (Figure 6). The TMDs are considered as being important for substrate binding and specificity, which might reflect the heterogeneity of the primary sequence since the transported substrates are very diverse (Yazaki, 2006). For some transporters specific residues were identified, which are important for substrate binding and therefore form a binding site (Chen, 2013, Oldham and Chen, 2011). Other ABC transporters do not seem to have a specific binding site, but rather a hydrophobic cavity (Korkhov et al., 2014) and again others have more than one binding site (Aller et al., 2014).

A) Outward-facing confirmation B) Inward-facing confirmation

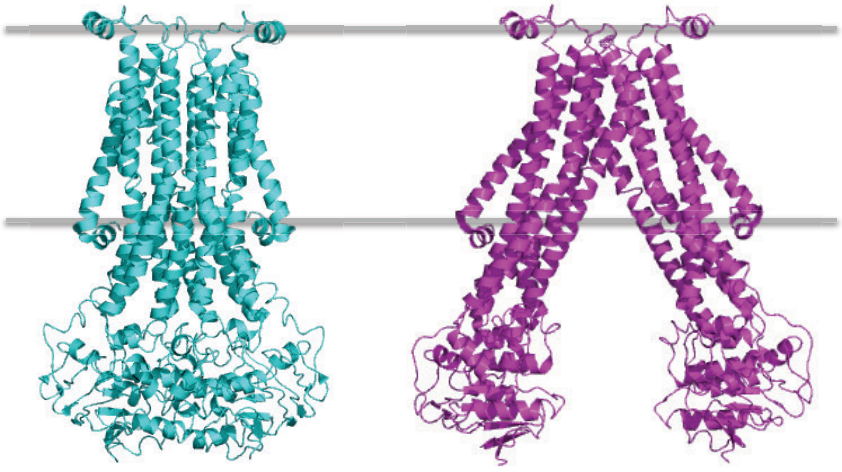

Figure 6: Crystal structure of the flippase PglK from *Campylobacter jejuni* determined by Perez et al., 2015. During the conformational change the transporter changes between the outward-facing confirmation (A) and the inward-facing (B) confirmation.

1.2.4 The transport mechanism

Different models exist that explain the conformational changes of the domains upon binding and hydrolysis of ATP. The models thereby rely on biochemical and structural data reported for different ABC transporters (Senior et al., 1995, Janas et al., 2003, Chen et al., 2003). It is unclear in which way ATP hydrolysis is coupled to the transport (Jones and George, 2004). One model supports the idea that two ATP molecules are simultaneously bound at the NBDs. After the substrate binding the conformational change of the NBDs in induced by ATP binding and thereby also the conformational change of the TMDs, which releases the substrate from the transporter. After sequential hydrolysis of ATP the NBDs open and ADP and orthophosphate are released. The TMD configuration also changes so that another substrate can bind (Hopfner et al., 2000, Smith et al., 2002, Verdon et al., 2003). Another model suggests that the NBDs are always close to each other and that ATP hydrolysis of the two binding site takes place as alternating cycle. That means when one binding site hydrolyses ATP the products are released at the other binding site and *vice versa* (Janas et al., 2003, Qu et al., 2003, Druley et al., 2001). Since the motifs of the NBDs are highly conserved in a lot of species one could assume that the mechanism of ATP hydrolysis is also conserved, however, at which step during ATP binding and hydrolysis the conformation of TMDs is still under debate.

1.3 The role of ABC transporters in plants

ATP binding cassette (ABC) proteins comprise one of the largest and diverse protein superfamily and are uniquely present in all kingdoms of life (Kang et al., 2011, Theodoulou, 2000). The protein family comprises ABC proteins without any TMD and membrane proteins, the ABC transporters. Soluble ABC proteins have regulatory functions in the cell, like regulation of translation or expression (Chakraburtty, 2001, Marton et al., 1997), mRNA trafficking and DNA repair (Kozak et al., 2002, Goosen and Moolenaar, 2001, Hopfner et al., 2000). The ABC transporters, which represent the larger part of the ABC family, are primary pumps using energy derived from ATP hydrolysis to drive active transport of various substrates across biological membranes. Their substrates range from small peptides, sugars, lipids, heavy metals, and polysaccharides to steroids, inorganic acids and even intact proteins (Rea, 2007, Theodoulou et al., 2006, Biemans-Oldehinkel et al., 2006). ABC transporters catalyze the substrate translocation in different cell compartments.

ABC transporters can be divided into importers and exporters. Importers are for example involved in nutrient uptake while exporters for example confer resistance to cells by exporting xenobiotics or by participating in pathogen defense. They often have substrate binding proteins that are located in the periplasm and transmit the substrate to the TMDs (Oldham et al., 2008). Classically, it was believed that importers only exist in prokaryotes and archaea, however, more and more evidence arises that plants, as the only eukaryotes until now, have ABC transporters that function as importers (Lee et al., 2008, Kang et al., 2010, Terasaka et al., 2005, Kang et al., 2015).

In plants, ABC transporters are located in plasma membranes, mitochondrial membranes, vacuolar membranes, the chloroplasts and the peroxisome (Choi et al., 2014, Jaquinod et al., 2007, Hayashi et al., 2004, Fan et al., 2015, Kushnir et al., 2001). They are expressed in all organs of plants (figure 2). While some are uniquely expressed others are only expressed in certain organs such as for example roots or seeds. The first described plant ABC transporters were thought to be involved in detoxification. Today it is known that plant ABC transporters are involved in many more processes. They are important in plant hormone transport, biotic and abiotic stress response and for plant nutrition. All these processes indicate that ABC transporters are critical for the plant's interaction with the environment (Kang et al., 2011, Martinoia et al., 2002).

1.3.1 Organization of the plant ABC protein family

According to their phylogenetic relationship plant ABC transporters can be divided into eight subfamilies A – G and I (H does not exist in plants) (Verrier et al., 2008). The phylogenetic tree of the NBDs from *A. thaliana* is shown in Figure 7. The ABCA subfamily comprises the full-size transporter ABCA1 (AOH) and 11 half-size transporters ABCA2 – 12 (ATHs). In *A. thaliana* AOH is the largest ABC protein. The protein has a large linker domain and is orthologous to the human ABC1 (Sanchez-Fernandez et al., 2001a, Verrier et al., 2008, Kang et al., 2011). The ABCB subfamily consists of 21 full-size transporters (ABCB1 – 7, 9 – 22), which are also named Pgps or MDRs. Characterized full-size transporters were shown to localize to the plasma membrane. The seven half-size transporters (ABCB23 – 29) of the ABCB subfamily are *inter alia* located in the mitochondria, the chloroplasts und the vacuole (Sanchez-Fernandez et al., 2001a, Verrier et al., 2008, Kang et al., 2011). The ABCC subfamily comprises only full-size transporters (MRPs), which have an additional

transmembrane domain (TMD0) compared to the core structure of two NBDs and two TMDs (Sanchez-Fernandez et al., 2001a, Verrier et al., 2008, Kang et al., 2011). The smallest subfamily is the ABCD subfamily, which consist of one half-size transporter and one full-size transporter, which localizes to the peroxisome (Sanchez-Fernandez et al., 2001a, Verrier et al., 2008, Kang et al., 2011). Soluble ABC proteins are represented by the ABCE (ABCE1 – 3) and ABCF subfamily (ABCF1 – 5). These proteins have no transmembrane domain and therefore have no transport function (Sanchez-Fernandez et al., 2001a, Verrier et al., 2008, Kang et al., 2011). Of all subfamilies the ABCG family is by far the largest containing 29 half-size (ABCG1 – 29, also named WBCs) and 15 full-size transporters (ABCG30 – 43, also named PDRs) (Sanchez-Fernandez et al., 2001a, Verrier et al., 2008, Kang et al., 2011). Many proteins of the ABCG subfamily were shown to localize to the plasma membrane (Ruzicka et al., 2010, Stein et al., 2006, Kang et al., 2010, Yim et al., 2016, McFarlane et al., 2010, Yadav et al., 2014, Choi et al., 2014). Compared to the other subfamilies, the members of the ABCG subfamily have a reverse orientation of domains, meaning that the NBD is located at the N-terminus of the protein. The ABCH subfamily is the only other subfamily with reverse domain orientation, but this subfamily is not present in plants (Sanchez-Fernandez et al., 2001a, Verrier et al., 2008, Kang et al., 2011). Members of the ABCI subfamily form a heterogeneous group with no phylogenetic relationship. They encode for single NBDs, TMDs or potential substrate binding proteins (Sanchez-Fernandez et al., 2001a, Verrier et al., 2008, Kang et al., 2011).

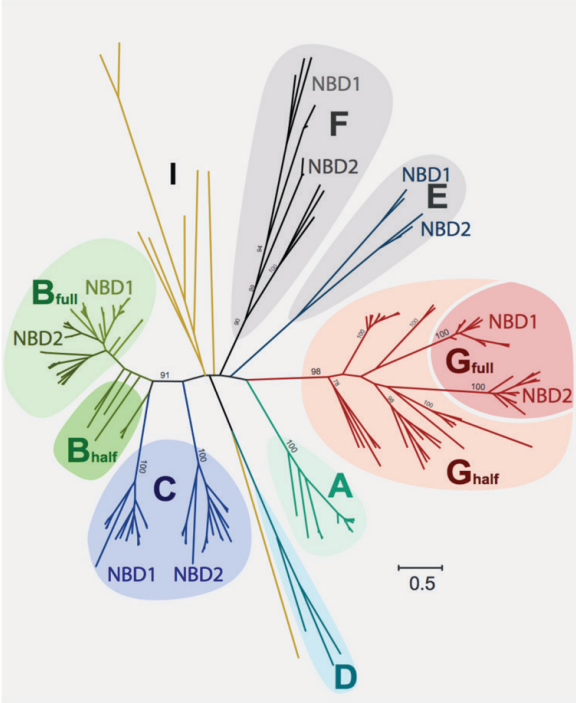

Figure 7: Phylogenetic tree of all nucleotide binding domains of *A. thaliana* ABC proteins. The letters stand for the respective ABC subfamilies. The figure was taken and modified from Kang et al. 2011.

1.3.2 The Pleiotropic Drug Resistance ABC transporter subfamily

The pleiotropic drug resistance (PDR) proteins are the full-size transporters of the ABCG subfamily. Proteins of the ABCG subfamily have a reverse orientation of domains. Due to sequence analysis it is hypothesized that the PDR transporters originate from duplication of a half-size transporter gene of the same subfamily, the *WBCs* (Kang et al., 2011, Verrier et al., 2008). Crouzet et al. (2006) performed a sequence comparison and created a phylogenetic tree of plant and fungi PDR and WBC genes (Figure 8). In the phylogenetic tree the WBCs of plants and fungi cluster together, but separately from the PDRs. That indicates that the WBCs from plants and fungi have a common ancestor. The PDRs might result from duplication of a half-size transporter and this happened before plants and fungi separated during evolution. The PDRs of fungi and plants again cluster in separate groups, which shows that, after the separation of plants and fungi, the PDRs evolved individually in the respective groups. It is therefore unlikely to find functionally comparable orthologs of plant and fungi PDRs. By comparing ABC genes of different plant species it becomes obvious that the genes do not cluster according to their species affiliation. For example *At*MRP3 clusters with *Os*MRP1 and *At*MDR5 clusters with *Os*MDR5 and *Os*MDR14. That illustrates that the differentiation of the ABCs happened before the plants separated into monocots and dicots (Crouzet et al., 2006).

The genomic structure of plant PDRs displays high conversation. This is reflected in the exon/intron boundaries, which are at similar positions as well as in the number of exons (19 – 24). The only exceptions are *AtPDR7* and *AtPDR8*, which have 9 and 7 exons, respectively. Those *PDR* genes that cluster together in the phylogenetic tree also display similar genomic structures. Only the linker region of the two half-molecules of each *PDR* gene displays high variability (van den Brule and Smart, 2002). The fungal PDR genes display highly degenerated Walker A, Walker B, H-loop and ABC signature motifs (Gupta et al., 2014). The Walker A motifs of the plant *PDR* genes are highly conserved, but the N-terminal Walker B motifs do not strictly follow the consensus sequence. For example in eight of the 15 *PDR* genes in *A. thaliana* the second residue of the N-terminal Walker B motif is not hydrophobic. Both of the ABC signature motifs vary from the consensus sequence. The second last residue of the N-terminal motif does not correspond to the consensus sequence as well as the second, third and fourth residues of the C-terminal ABC signature motif (van den Brule and Smart, 2002). The plant PDR genes contain four regions with identical residues, which are the plant PDR signature motifs. PDR signature motif one (LLLGPP) precedes the N-terminal Walker A

motif and PDR signature motif two (GLDSST) follows the N-terminal Walker B motif. The third PDR signature motif (GLDARAAAIVMR) is downstream of the Walker B motif of the C-terminal NBD followed by the fourth PDR signature motif (VCTIHQPSI) (van den Brule and Smart, 2002).

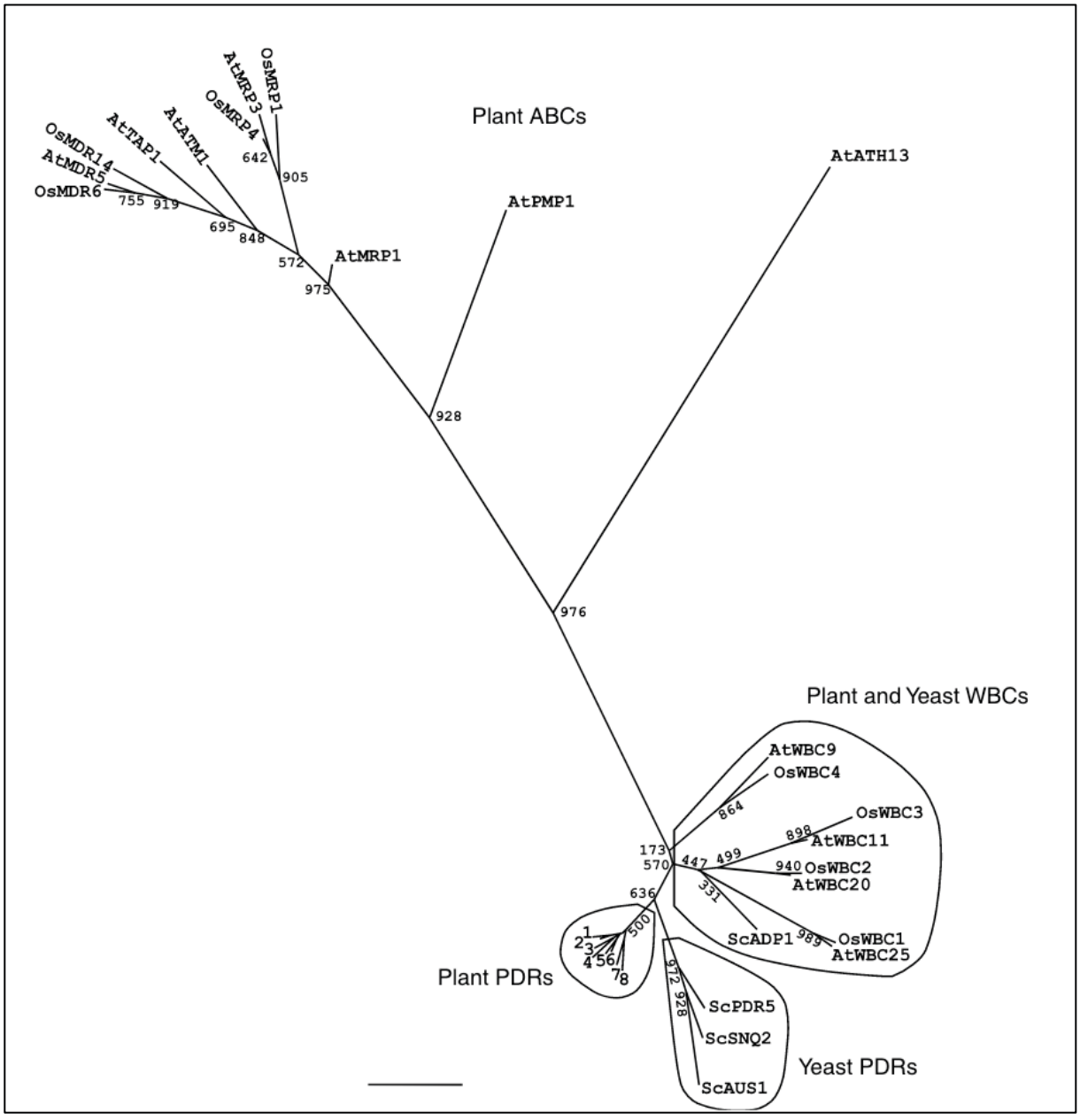

Figure 8: Phylogenetic analysis of half- and full-size members of the ABCG subfamily. Randomly selected genes of the full-size transporters (PDRs) and the half-size transporters (WBC) of *A. thaliana*, *O. sativa* and *S. cerevisiae* were analysed and compared to other members of the plant ABC family. The numbers in the Plant PDR cluster stand for the following proteins: *At*PDR1 (1), OsPDR12 (2), *At*PDR6 (3), *Os*PDR5 (4), *At*PDR12 (5), *Os*PDR9 (6), *At*PDR9 (7), *Os*PDR8 (8). The figure was taken from Crouzet et al. (2006). For details see the publication.

The first PDR was characterized in the yeast *Saccharomyces cerevisiae*. With a total number of 29 ABC proteins the yeast contains nine PDR transporters. Out of these *Sc*Pdr5 has been studied best and is thereby considered as the prototype for the PDR family. It was shown to mediate resistance to various drugs, among these antifungal and anticancer drugs (Ernst et al., 2005). Since it exports a broad range of structurally unrelated compounds it is considered a functional homolog to the mammalian Multi Drug Resistance (MDR) group of ABC transporters. However, the sequence identity between the mammalian MDRs and *Sc*Pdr5 is low and the domain orientation is different (Rea, 2007, Nuruzzaman et al., 2014). In fact there is no *Sc*Pdr5 homolog identified in prokaryotes or animals; the PDR subfamily only exist in plants, fungi, brown algae, slime molds and oomycetes (Huala et al., 2001, Cock et al., 2010, Tyler et al., 2006, Anjard et al., 2002, Cherry et al., 2012).

1.3.3 PDRs are involved in many physiolocical processes by secondary metabolite transport

The first identified PDR in plants was *Sp*TUR2 from the water plant *Spirodela polyrrhiza* (Smart and Fleming, 1996). The expression of *Sp*TUR2 in *A. thaliana* conferred resistance to the diterpene sclareol, therefore it was described as a sclareol exporter. The transcription of *SpTUR2* is activated by absicic acid (ABA) and abiotic stress factors such as cold or salinity (van den Brule et al., 2002). Another PDR transporter potentially involved in sclareol export is *Np*PDR1 from *Nicotiana plumbaginifolia. Np*PDR1 expression is elevated by sclareolide, the lactone of sclareol and in suspension culture the export of radiolabeled sclareol was monitored after induction of *Np*PDR1 expression The *NpPDR1* promoter sequence furthermore includes the *cis*-regulatory sequence sclareol box 3, which is important for induction by sclareol and methyl jasmonate (Grec et al., 2003, Jasinski et al., 2001).

Apart from sclareol plant PDRs are involved in the transport of many different secondary metabolites, as summarized in Figure 9. For example *Cr*TPT2 expression is induced by the alkaloid catharanthine; the PDR is supposed to transport this anticancer drug to the leaf surface in *Catharanthus roseus* (Yu and De Luca, 2013). *Mt*ABCG10 from *Medicago truncatula* was shown to be involved in phenylpropanpoid metabolism by likely exporting 4-coumarate and liquiritigenin, two intermediates of the medicarpin pathway (Biala et al., 2017). *Vm*TPT2 from *Vinca minor* could export monoterpene indole alkaloids, especially vincamine (Demessie et al., 2017). These functions are interesting from a pharmacological

point of view since the phenylpropanoids and monoterpene indole alkaloids were shown to have therapeutical relevance (Demessie et al., 2017, Biala et al., 2017).

*At*PDR9 expression was induced upon iron deficiency. The protein is involved in the secretion of highly oxygenated coumarin compounds. Coumarins are known to be secreted under iron deficiency. The *At*PDR9 promoter sequence contains putative WRKY transcription factor binding sites, which implies a role in pathogen response, too (Ziegler et al., 2017, Fourcroy et al., 2014, Ito and Gray, 2006, Rushton et al., 2010). Transport experiments in a heterologous system confirmed that the auxin precursor indole-3-butyric acid (IBA) was transported by *At*PDR9 (Ruzicka et al., 2010). Another PDR involved in plant hormone transport is *Ph*PDR1 from *Petinua hybrida*. It was postulated to export strigulactone and thereby regulate the axillary branching and the cultivation of arbuscular mycorrhizae (Kretzschmar et al., 2012). The expression of *Nt*PDR3 from *Nicotiana tabacum* was upregulated under iron deficiency, too. Furthermore the promoter sequence comprises an iron deficiency responsive element 1 box, which is a common element in promoter regions (Kobayashi et al., 2003) of genes elevated under iron deficiency. It was speculated that the transporter acts in iron homeostasis. The expression of *Nt*PDR3 was induced by the diterpene cembrene, salicylic acid, jasmonate and 1-naphthalene acetic acid (NAA) (Ducos et al., 2005).

*At*PDR2 was shown to shape the microbiome of the rhyziosphere. The knock-out mutation of *At*PDR2 changed the secretion levels of a variety of root exudates (e.g. phenolics, indolics, organic acids sugars, flavonols), which possibly altered the microbial community. This does not necessarily mean that *At*PDR2 transports such a large set of compounds; it is likely that this pleiotropic phenotype resulted from other metabolic interactions (Badri et al., 2009).

*At*PDR3 is involved in steryl glucoside deposition at the pollen surface, which is important for pollen coat maturation. The transporter therefore contributes to the protection of the pollen against abiotic factors like drought and cold (Choi et al., 2014). Plant PDR transporters were furthermore shown to be involved in cuticle and cell wall formation and thereby adding to the physical barrier of the plant. *Hv*ABCG31 from *Hordeum vulgare* might contribute to cuticle formation since mutating *Hv*ABCG31 resulted in water loss in leafs (Chen et al., 2011). *At*PDR4 could fulfill a similar function in *A. thaliana* (Bessire et al., 2011). *At*PDR1 was shown to play a role in monolignol transport to the cell wall, which is important for lignin synthesis. Another study could not find any difference in lignin contents in *AtPDR1* knockout

plants compared to the wild-type and thereby concludes that *At*PDR1 is not solely involved in monolignol transport (Alejandro et al., 2012). Next to *At*PDR1, *At*PDR2 *At*PDR4, *At*PDR5 and *At*PDR6 were co-expressed with lignin synthesis related genes. Analysis of the expression levels in mutants resulted in upregulation of *At*PDR2 in the *atpdr6* and of *At*PDR6 in the *atpdr2* mutant, respectively (Takeuchi et al., 2018). These results suggest that several PDRs are involved in monolignol transport and thereby in lignin synthesis. Because the cuticle and the cell wall build physical barriers transporters involved in the formation of these indirectly also play a role in plant defense.

Another strategy for plant defense is the secretion of secondary metabolites that are repelling or toxic for plant enemies. *PDR* genes were upregulated under pathogen or herbivore attack, which implies that PDR transporters are involved in biotic stress response. *Nt*PDR1 was expressed in response to fungal and bacterial elicitors, methyl jasmonate and cembrene (Sasabe et al., 2002, Crouzet et al., 2013). Activity of the purified protein was stimulated by diterpenes and sesquiterpenes, which are involved in plant defense (Pierman et al., 2017). *Np*PDR1 was upregulated upon pathogen infection (Stukkens et al., 2005, Bultreys et al., 2009) and *Nt*PDR5 was upregulated upon wounding, herbivore attack, pathogen infection and methyl jasmonate treatment (Bienert et al., 2012). In a mutant screening *atpdr6* plants showed hypersensitivity for sclareol. *At*PDR6 expression was induced by methyl jasmonate and pathogen infection. It was proposed that the indole alkaloid camalexin is exported in response to pathogen infection (Khare et al., 2017). In petunia *Ph*PDR2 confers resistance against herbivores, likely by extruding petuniasterone and petuniolide (Sasse et al., 2016). *Ta*PDR1 from wheat was induced after treatment with the mycotoxin deoxynivalenol and aluminium and calcium ions. It was suggested that *Ta*PDR1 takes part in defense as well as detoxification (Shang et al., 2009). *TaLr34*, a gene mediating resistance to fungal pathogens in wheat, was shown to code for a PDR transporter as well (Krattinger et al., 2009).

Stimulus	Gene/Protein	Transport	Physiological role	Reference
p-coumaryl	*At*PDR1	Monolignols (p-coumaryl)	Cell wall formation	Alejandro et al., 2012 Takeuchi et al., 2018
	*At*PDR2	Root exudates? ABA	Shaping soil microbiome Hormone transport Cell wall formation?	Badri et al., 2009 Kang et al., 2015 Takeuchi et al., 2018
	*At*PDR3	Steryl glucoside? ABA	Pollen coat maturation Hormone transport	Choi et al., 2014 Kang et al., 2015
	*At*PDR4		Cuticle formation Cell wall formation?	Bessire et al., 2011 Takeuchi et al., 2018
Pathogen infection MeJA, SA, Auxin	*At*PDR5		Cell wall formation?	Takeuchi et al., 2018 Crouzet et al., 2006
MeJA Pathogen infection	*At*PDR6	Camalexin, Sclareol?	Pathogen response Cell wall formation?	Khare et al., 2017 Takeuchi et al., 2018
Fungal elicitors Bacterial elicitors Pathogen infection Lead Copper Cadmium	*At*PDR8	Indole-derived compounds Product(s) of PEN2 pathway Cadmium IBA	Pathogen response Detoxification Auxin homeostasis Drought resistance Salt resistance	Stein et al., 2006 Kobae et al., 2006 Under wood and Somerville, 2013 Kim et al., 2007 Strader and Bartel, 2009 Kim et al., 2010
Iron deficiency Pathogen infection, JA, SA, Auxin	*At*PDR9	Coumarins? IBA 2,4-D? NPA?	Iron homeostasis Pathogen response? Hormone transport	Ziegler et al., 2017 Fourcroy et al., 2014 Ito and Gray 2006 Ruzicka et al., 2010 Crouzet et al., 2006
Lead Sclareol Pathogen infection SA, MeJA, ET	*At*PDR12	Lead? ABA	Detoxification Hormone transport Pathogen response	Campbell et al., 2003 Lee et al., 2005 Kang et al., 2010 Kang et al., 2015b Crouzet et al., 2006
Catharanthine	*Cr*TPT2	Catharanthine?	Secretion of monoterpene indole alkaloids	Yu and De Luca, 2013
	*Hv*ABCG31	Cutin?	Cuticle formation	Chen et al., 2011
Fungal elicitors 4-coumarate	MtABCG10	4-coumarate liquiritigenin	Part of phenylpropanoid pathway	Biala et al., 2017
Sclareolide Larixol Pathogen infection MeJA Abietic acid	*Np*PDR1	Sclareol?	Pathogen response Constitutive defense?	Stukkens et al., 2005 Bultreys et al., 2009 Jasinski et al., 2001 Crouzet et al., 2006
Fungal elicitors Bacterial elicitors Cembrene MeJA	*Nt*PDR1	Diterpenes Sesquiterpenes	Defense?	Sasabe t al., 2010 Crouzet et al., 2012 Pierman et al., 2017
Iron deficiency Cembrene SA, JA, NAA	*Nt*PDR3		Iron homeostasis Diterpene transport?	Ducos etal., 2005
Herbivore attack Pathogen infection Wounding MeJA	*Nt*PDR5		Defense? Herbivore resistance	Bienert et al., 2012
GR24 NAA	*Ph*PDR1	Strigulactone?	Hormone transport Axillary branching Mycorrhizae cultivation	Kretzschmar et al., 2012
MeJa	*Ph*PDR2	Petuniasterone? Petuniolide?	Herbivore resistance	Sasse et al., 2016
Temperature Salinity ABA Sclareol Rhodamine 6G Cycloheximide	*Sp*TUR2	Sclareol?	Pathogen response?	Smart and Fleming, 1996 Van den Brule et al., 2002
Pathogen infection	*Ta*Lr34		Pathogen response	Krattinger et al., 2009
Mycotoxin DON Aluminium Calcium	*Ta*PDR1		Defense? Detoxification?	Shang et al., 2009
	*Vm*TPT2	Vincamine	Secretion of monoterpene indole alkaloids	Demessie et al., 2017

Figure 9: Overview about the functions fulfilled by plant PDRs. The list shows the environmental stimuli that induced expression of the respective genes as well as the suggested substrates and functions of the protein. For details see text.

1.3.4 Plant PDRs: several phenotypes – several substrates?

Many PDR transporters seem to be involved in diverse physiological processes, which always leaves the question whether one substrate is transported or several, maybe structurally unrelated, substrates. The expression of *At*PDR12 was induced by sclareol and the transporter was show to be involved in pathogen response, which implies a role in plant defense (Campbell et al., 2003, Lee et al., 2005). On the other hand, growth experiments could show that plants expressing *At*PDR12 displayed increased resistance against lead ions. It was hypothesized that the lead ions are detoxified via glutathione conjugation (Lee et al., 2005). Another study showed abscisic acid (ABA) transport by *At*PDR12 (Kang et al., 2010). It was reported that together with *At*PDR2, *At*PDR3 and *At*WBC25, *At*PDR12 mediates the transport of ABA from the endosperm to the seeds. ABA is produced in the endosperm, which surrounds the seed embryo, and is exported by *At*WBC25 and *At*PDR3. The uptake of ABA into the embryo is then mediated by *At*PDR12 and *At*PDR2, which both are postulated to have an importer function (Kang et al., 2015).

These data raise the question if *At*PDR12 is able to transport several structurally unrelated compounds, as some yeast and mammalian ABC transporters do (Kolaczkowski et al., 1996b, Ambudkar et al., 1999), or if only one stress inducible compound is transported. In fact only ABA transport was demonstrated applying transportomic approaches (Kang et al., 2010), the other findings result from mutant studies with *AtPDR12* knock-out plants or plants expressing *AtPDR12* constitutively. In addition, the transport experiments point to ABA as the only substrate of *At*PDR12. ABA is a phytohormone that is involved in several physiological events. In rice it was shown to be involved in cadmium response and in *A. thaliana* overproduction of ABA causes increased susceptibility to pathogens (Mohr and Cahill, 2003). A reason could be that ABA inhibits ethylene production, a signaling molecule involved pathogen response (LeNoble et al., 2004, Guo and Ecker, 2004). The diverse roles of ABA support the possibility that *At*PDR12 maybe transports a single compound and that knocking out the transporter results in different phenotypes regarding biotic and abiotic stress.

The PDRs have gained more and more interest in recent years. While in 2002 only 21 PDRs were identified in plants (van den Brule and Smart, 2002) the number increased to 43 in 2006. This number comprises PDRs from the species *Oryza sativa*, *A. thaliana*, *S. polyrrhiza*, *N. tabacum* and *N. plumbanigifolia* (Crouzet et al., 2006). Until now additional PDRs have been

analyzed, for example in cucumber, wheat, petunia and barley (Nuruzzaman et al., 2014, Krattinger et al., 2011, Chen et al., 2011, Sasse et al., 2016), which underlines the increasing interest in PDR transporters from crops. The studies demonstrate that PDRs are involved in vital processes of plants and understanding the function of the PDRs will greatly improve our understanding of these processes. Especially the function of PDR transporters in crops could be of valuable knowledge for future perspectives. However, considering the number of PDRs in each plant species and the fact that in most reports the substrates could not be clearly identified we are still at the beginning of understanding these processes.

1.4 *At*PDR8 – a key player in stress response

*At*PDR8/*At*ABCG36/PEN3 is an ABC transporter belonging to the Pleiotropic Drug Resistance family of *A. thaliana*. The 5.7 kbp large gene was identified in the Arabidopsis genome-sequencing project (Arabidopsis Genome, 2000, Huala et al., 2001) and annotated according to its homology to *Sc*Pdr5 from *S. cerevisiae* (Sanchez-Fernandez et al., 2001a). It comprises seven introns and eight exons that code for a 1469 aa protein (van den Brule and Smart, 2002, Huala et al., 2001). It was predicted to have 13 (Stein et al., 2006, Strader and Bartel, 2009, Sazuka et al., 2004) or 14 transmembrane helices (Tsirigos et al., 2015). *At*PDR8 is expressed in all organs of *A. thaliana* (van den Brule and Smart, 2002). Promoter analysis revealed that the *At*PDR8 promoter is most active in leafs, root tips, around stomata and in the root hair (Kobae et al., 2006, Kim et al., 2007). Several studies proof the localization of *At*PDR8 in the plasma membranes of *A. thaliana* cells (Stein et al., 2006, Xin et al., 2013, Underwood and Somerville, 2013, Kobae et al., 2006, Campe et al., 2016).

1.4.1 *At*PDR8 is involved in biotic stress response

In 2006 Stein and colleagues performed a mutant screening of *A. thaliana* plants for susceptibility to non-adapted powdery mildew pathogens. Plants grown from ethyl methanesulfonate-mutagenized seeds were screened for elevated penetration of the barley powdery mildew *Blumeria graminis* f. sp *hordei*. In that screening the *penetration 3* (*pen3*) mutants *pen3-1* and *pen3-2* were discovered and mapped to the *AtPDR8* locus on the *A. thaliana* chromosome one (Stein et al., 2006). The *pen3-1* mutation is a single amino acid substitution at position 354 that replaces a glycine by aspartic acid in the Walker A motif of the N-terminal NBD. The *pen3-2* mutation substitutes a glycine to a serine at position 915 in the C-terminal Walker A motif. Both alleles transcribe the gene but seem to result in non-

functional proteins (Lu et al., 2015, Stein et al., 2006). On the other hand the *pen3-3* (SALK_110926) and *pen3-4* (SALK_000578) mutants contain T-DNA insertions in the first exon of the gene, which result in no expression of the protein (Stein et al., 2006). All *pen3* mutants exhibited similar infection phenotypes. Upon inoculation with the non-adapted pathogens *B. g. hordei*, the pea powdery mildew *Erysiphe pisi,* the potato late blight *Phytophthora infestans* (an oomycete) and *Alternaria alternate*, which causes Alternaria stem canker in tomato, penetration, hyphae formation and elongation of the pathogens were increased in *pen3* mutants suggesting a function of *At*PDR8 in nonhost resistance to inappropriate pathogens (Sanchez-Vallet et al., 2010, Stein et al., 2006, Egusa et al., 2013). Inoculation with the broad host range necrotrophic pathogen *Plectosphaerella cucumerina* resulted in severe leaf damage of *pen3* plants compared to wild-type plants and *At*PDR8 was also shown to accumulate at fungal penetration sites, which implies that the protein exports an antifungal compound (Stein et al., 2006). In contrast to these results the *pen3* mutation mediated enhanced resistance towards the adapted *A. thaliana* pathogen *Erysiphe cichoracearum*. Leafs of *E. cichoracearum*-infected *pen3* plants showed chlorosis and necrosis, which are defense mechanisms against biotrophs. This *pen3*-associated resistance phenotype was likely SA-dependent since microarray data suggested an upregulation of the SA pathway in *pen3* plants (Stein et al., 2006). Similar observations were obtained by Kobae et al. (2006), who also studied *P. infestans* infections in *pen3* plants. Loss of *At*PDR8/PEN3 resulted in a loss of penetration resistance towards *P. infestans*. They further inoculated with the biotrophic bacterial strain *Pseudomonas syringae* pv. *tomato* DC3000. They report enhanced cell death of infected *pen3* plants compared to wild-type plants and suppressed growth of the bacteria, which is comparable to the results after *E. cichoracearum* infection. Contrary to this, Xin et al. (2013) reported decreased resistance towards *P. syringae* pv. *tomato* DC3000 in *pen3* plants. They also did not observe chlorosis or cell death of infected *pen3* plants, which might be the reason of the contradictory phenotypes. They argue that additive biotic and abiotic stressors might result in the unspecific upregulation of defense pathways. In line with this where the observations made by Sanchez-Vallet et al. (2010), where functional *At*PDR8 was important for the resistance against the adapted pathogen *P. cucumerina BMM.*

*At*PDR8 was shown to accumulate at fungal penetration sites, however, after a certain time the accumulation was suppressed by *P. syringae* pv. *tomato* DC3000 in a type III secretion-dependent manner (Xin et al., 2013). Expression of the *P. syringae* pv. *tomato* DC3000

effector AvrPto, which interferes with the *A. thaliana* FLS2 receptor (Xian et al. 2008), together with *At*PDR8 in *A. thaliana* resulted in reduced accumulation of *At*PDR8. These results cold not be confirmed by bacterial infection experiments, which implies more complex effector interactions between plants and bacteria (Xin et al., 2013)

Johanson et al. (2014) infiltrated leaves of the *pen* mutants with *P. syringae* pv. *tomato* DC3000 expressing the effectors AvrRps4 and AvrRpm1 and monitored the programmed cell death. The hypersensitive response was reduced up to 50 % for the *pen3-1* plants compared to the wild-type. In order to test the influence of other effectors they also inoculated with the oomycete *Hyaloperonospora arabidopsidis* isolate Cala2, which produces the effector ATR2. While the wild-type was able to restrict pathogen growth by rapid host cell death *pen3* plants exhibited extended necrosis and hyphae formation that was outgrowing cell death (Johansson et al., 2014). These results are contrary to that obtained by Kobae et al. (2006), who reported that *pen3* plants displayed enhanced resistance towards *P. syringae* expressing AvrRpt2 due to the hypersensitive response. The results suggest a role for *At*PDR8 in effector-triggered immunity, too.

Lu et al. (2015) isolated an additional *pdr8* mutant. The *pen3-5* mutation, which displays an amino acid substitution (L704F) in the 4th transmembrane helix of *At*PDR8, still results in protein production. Aligning all *A. thalina* PDRs showed that this position contains aliphatic amino acids in all *At*PDRs. After pathogen inoculation Lu at al., performed metabolite profiling of compounds from PEN3 wild-type and mutant plants. They observed the accumulation of 4-*O*-β-D-glucosyl-1-H-indole-3-yl formamide (4OGGlcI3F) in *pen3* mutants, which might be a product of the PEN2 pathway. The authors speculated that 4OGGlcI3F was not the bioactive compound transported by *At*PDR8 but rather a detoxified derivative form of the potentially toxic *At*PDR8 substrate. Interestingly, *pen3-5* plants did not display the IBA-sensitive phenotypes of the other *pen3* mutants in response to IBA treatment (chapter 1.4.3). The authors thereby concluded that the *pen3-5* mutation did not abolish potential IBA transport as the *pdr8-115* mutation (chapter 1.4.3) or the *pen3*-null mutants did (Lu et al., 2015).

1.4.2 *At*PDR8 is involved in abiotic stress response

Abiotic stresses are important factors in plant growth, productivity and immunity (Pandey et al., 2017). Heavy metals are common pollutants and can have severe effect for plants by causing cellular damage, protein denaturation and supporting the creation of reactive oxygen species. The detoxification involves the transport of heavy metal ions or conjugates and ABC transporters were shown to be involved in heavy metal resistance (Kim et al., 2006, Lee et al., 2005). *At*PDR8 was suggested to be involved in heavy metal detoxification through extrusion of metal ions from the plant cell. The expression of *At*PDR8 was increased by lead, copper and cadmium treatment. *AtPDR8* knock-out and RNAi plants exhibited diminished growth on media containing cadmium and lead ions while *At*PDR8 overexpressing lines grew better compared to wild-type plants. The metal ions Cu^{2+}, Fe^{3+}, Zn^{2+} and Al^{3+} had no influence on growth behavior. The same result was obtained for sclareol ABA, H_2O_2 and cycloheximide, which all did not alter growth behavior of *At*PDR8 RNAi and wild-type plants. The cadmium and lead contents were measured in wild-type plants, *atpdr8* mutant and overexpressing plants. Mutant plants contained higher cadmium levels than wild-type plants and the overexpressing plants exhibited lower cadmium levels than wild-type plants. No difference was detected for the lead content. The cadmium transport was confirmed by monitoring radiolabeled ^{109}Cd transport across the plasma membrane in *A. thaliana* protoplasts. The uptake of cadmium was less in protoplasts from *At*PDR8-overexpressing plants compared to protoplasts from wild-type plants. The uptake was highest in protoplasts from *At*PDR8 RNAi plants. The same pattern was observed for the cadmium release, which was fastest in *At*PDR8-overexpressing protoplasts und slowest in *At*PDR8 RNAi protoplasts. The transport was unaffected by pH changes but could be abolished by vanadate and glibenclamide. These results suggest that the resistance to cadmium was mediated by an ABC-transporter, potentially *At*PDR8 (Kim et al., 2007).

Kim et al. (2010) further investigated the role of *At*PDR8 in drought and salt resistance. They observed that *At*PDR8-overexpressing plants were more resistant to drought and salt while *At*PDR8 mutant plants showed decreased resistance compared to the wild-type. They could further show that the sodium content in the *At*PDR8-overexpressing plants was reduced, and the plants grew better on sodium-containing media. That implies that the drought and salt resistance phenotypes were linked to sodium reduction. Interestingly, the *At*PDR8 expression was not elevated under drought and salt stress conditions (Kim et al., 2010). It remains to be

clarified whether the *At*PDR8-mediated drought and salt resistance relies on direct export of sodium by *At*PDR8 or depends on the influence of other mechanisms.

1.4.3 The role of *At*PDR8 in phytohormone transport

The phytohormone auxin is important for plant growth and development because it regulates cell division and elongation and thereby controls stem and root elongation, leaf expansion and patterning and lateral root initiation. The auxin precursor indole-3-butyric acid (IBA) has an elongated side chain compared to the active auxin indole-3-acetic acid (IAA). IBA is transformed into IAA by shortening of the carbon carboxyl side chain that takes place in the peroxisomes. Plants store IAA *inter alia* in the precursor version IBA (Woodward and Bartel, 2005). Strader and Bartel (2009) used mutant studies to analyze the auxin transport in plant cells and the resulting developmental effects. They identified the *pdr8-115* mutation, which results in an amino acid substitution from alanine to valine at position 1357 in the 11th transmembrane helix. Using this and other published mutants (Stein et al., 2006) they observed impaired [^{3}H]-IBA-efflux in the mutants but normal [^{3}H]-IAA accumulation. Furthermore the *atpdr8* plants showed increased lateral root production and lengthened root hairs as well as larger cotyledon areas compared to wild-type plants. These phenotypes pointed to an excessive auxin production that resulted from prior IBA accumulation. This finding was supported by the blocking of the IBA to IAA conversion, which resulted in suppression of the *atpdr8* phenotypes. The authors proposed a model for the function of *At*PDR8 in auxin homeostasis. Active auxin is produced by the β–oxidation of IBA to IAA in the peroxisomes. IAA then regulates lateral root formation, root hair elongation and cotyledon expansion. In that model *At*PDR8 regulates the IBA accumulation in the cell by exporting excessive IBA into the apoplast. The IBA levels then influences IAA production levels, which is why *At*PDR8 acts in auxin homeostasis (Strader and Bartel, 2009). Several mechanisms involve IBA and IAA transport and accumulation (Blakeslee et al., 2005, Woodward and Bartel, 2005). Thereby the question will always remain if the phenotypes observed by Stader and Bartel could as well be due to other redundant processes in the cell.

1.4.4 Recruitment and regulation of *At*PDR8

*At*PDR8 is constitutively expressed in *A. thaliana,* however, expression was enhanced by pathogen inoculation and elicitor treatment (Kobae et al., 2006, Stein et al., 2006, Johansson et al., 2014). *At*PDR8 is equally distributed in the plasma membrane, but it relocates and accumulates at bacterial infections sites and in response to flg22 (Underwood and Somerville, 2013). The bacterial effector binds the FLS2 receptor (Chinchilla et al., 2006) and thereby possibly activates *At*PDR8 expression. FLS2 forms a complex with BRI1-associated receptor kinase 1 (BAK1) (Sun et al., 2013) and *bak1* mutants fail to induce several responses to flg22 (Chinchilla et al., 2007). The *bak1-4* null mutant seems to have no influence on the accumulation of *At*PDR8 to fungal penetration sites, but the *bak1-5* allele seems to have a dominant negative effect on *At*PDR8 recruitment since a reduction in accumulation was observed (Underwood and Somerville, 2013). That implies that the accumulation of *At*PDR8 at penetration sites is FLS2-dependen but does not require the functional FLS2-BAK1 complex. The accumulation of *AT*PDR8 was further investigated using pharmacological inhibitors in order to disrupt specific cellular functions. Disruption of microtubules, secretory trafficking, vesicle trafficking and protein biosynthesis did not affect *At*PDR8 accumulation. Only disruption of the actin cytoskeleton resulted in impaired localization of *At*PDR8 at pathogen penetration sites. These data suggest that accumulation of *At*PDR8 at penetration sites does not depend on secretory trafficking or synthesis of new protein and vesicle-dependent transport to the site of action. It seems that protein synthesized prior to pathogen attack is relocated and this process depends on actin microfilaments (Underwood and Somerville, 2013).

Campe et al. (2015) performed an *A. thaliana* protein array (*At*PMA-500) screening in order to identify potential interaction partners of the N-terminal cytosolic domain of *At*PDR8. Most of the identified interaction partners were calcium-sensing proteins, as well as proteins involved in biotic stress response. The authors then created an *At*PDR8 network with calcium-sensing proteins, which it included mainly calmodulines (CaMs) or calmodulin-like (CMLs) proteins. CaMs and CMLs are catalytically inactive, but calcium binding induces conformational changes, which influences the interaction with other proteins. Plants contain several *CaM* genes that encode multiple CaM isoforms. Additional database research revealed that *At*PDR8 is co-expressed with *At*CaM7. Fluorescence microscopy revealed that *At*PDR8-GFP and *At*CaM7-mRFP co-localized *in planta*. Binding of *At*CaM7 to the N-terminal

cytosolic domain of *At*PDR8 was proven *in vitro* by CaM overlay assays and pull-down assays. The binding was enhanced in the presence of calcium ions. However, mutant studies revealed that *At*CaM7 was not important for the role of *At*PDR8 in defense resistance. In addition, microarray data of pathogen-infected plants indicated that *At*CaM7 was not co-expressed with *At*PDR8. Furthermore none of the *At*CaM isoforms showed differential expression upon pathogen attack. It could be that the different CaM isoforms have overlapping functions in *A. thaliana* (Campe et al., 2016).

*At*PDR8 was differentially phosphorylated after induction with fungal and bacterial elicitors (Benschop et al., 2007, Nuhse et al., 2007) The identified phosphorylation sites of *At*PDR8 are located in the N-terminal NBD, which implies that this domain is important for *At*PDR8 regulation. The screening for *At*PDR8 interaction partners furthermore identified several kinases, among these MAP3Ks, MAP3K-like integrin kinases, RLKs and CDPKs. In the network for calcium-sensing proteins CDPK10 was connected to *At*PDR8 via CML9 (Campe et al., 2016). CDPK10 was shown to phosphorylate an *At*PDR8 peptide *in vitro* (Curran et al., 2011) and CML9 is involved in plant defense likely through flagellin-dependent signaling pathways (Leba et al., 2012). Calcium ion influx is one of the first responses to elicitor perception (Zhao et al., 2005). A potential scenario in plant pathogen response could be that after elicitor recognition calcium binds to CaM (possibly CML9 or CaM7), which then recruits a kinase (possibly CDPK10) to phosphorylate and thereby activate *At*PDR8. *At*PDR8 then exports an antimicrobial compound, which was prior activated by the myrosinase PEN2.

1.5 *In vivo* versus *in vitro* – why an additional system is needed

Several *in vivo* studies with *At*PDR8 knock-out mutant and overexpressing lines were conducted, which show that the protein is involved in biotic as well as abiotic stress response and plant hormone homeostasis. These different roles imply that *At*PDR8 transports a variety of diverse substrates. Potential substrates, according to the *in vivo* and mutant studies, could be for example heavy metal ions, heavy metal conjugates, phytochelatines, the auxin precursor IBA, indoles, terpenoids and products of the PEN2 pathway. But is this really the case? *Sc*Pdr5, the PDR prototype was shown to transport structurally unrelated compounds (Kolaczkowski et al., 1996b). However, this concept was not biochemically proven for any plant ABC transporter so far. Another example for a PDR transporter with pleiotropic mutant phenotypes is *At*PDR12. As described above, the transporter is supposed to be involved in

pathogen resistance, in ABA transport and in lead resistance. Only the ABA transport could be proven by a transport assay and in that assay *At*PDR12 was highly specific for this substrate. This raised the assumption that *At*PDR12 possibly only transports one stress-inducible compound and the other observed phenotypes were the result of the deficiency of this compound (Lefevre et al., 2015). The same could apply for *At*PDR8. The various *At*PDR8 mutant studies give an idea in what general processes the protein is involved. Concerning pathogen response, *At*PDR8 seems to be involved in PAMP-triggered immunity as well as in effector-triggered immunity. However, several contradictory studies exist, which complicate the understanding of *At*PDR8 function in plant immunity. Insights about the transported substrate(s) could help to clarify the exact physiological role of the transporter. The approach of reverse genetics and mutant studies seems to be insufficient to characterize *At*PDR8 in regard to the transported substrates. There is always the possibility that effects of different pathways mask each other. In addition, the plant ABC protein family is very large, which brings the potential of functional redundancy among the proteins, especially when they are involved in important processes that are linked to plant survival. An example for the insufficiency of *in vivo* studies is *Np*PDR2. The protein was shown to be expressed in roots and inflorescences, however, knocking-out *Np*PDR2 by RNA interference showed no phenotypical difference compared to the wild-type. The expression was furthermore not affected by pathogens nor by phytohormones involved in stress response (Trombik et al., 2008). In that particular case knocking-out the transporter gave no insights about the potential function of the protein.

In order to better understand the plant PDR proteins and the transport processes further studies are required. These involve biochemical approaches as well as an *in vitro* system to ensure that interfering processes do not mask the roles of the PDR transporters. To date, biochemical studies are rather limited. One reason is the necessity for purified protein in adequate quantities for biochemical and/or structural studies. Suitable overexpression that provides sufficient amounts of the protein in reasonable time is still a main issue concerning eukaryotic membrane proteins (Gräfe et al., in preparation). Heterologous overexpression of membrane proteins is often challenging due to the size and hydrophobic nature of membrane proteins, toxicity of the protein to the host, misfolding, incorrect localization or the lack of the proper post-translational modification(s) (Gräfe et al., in preparation, Bernaudat et al., 2011, Ahmad et al., 2014, Crouzet et al., 2013, Lefevre et al., 2015, Gul et al., 2014). It furthermore emerged that not only expression, but also cloning of membrane proteins, especially ABC

transporters, can be difficult because the sequences are unstable in *E. coli* (Gräfe et al., in preparation, Sami et al., 1997, Covic and Lew, 1996, Stindt et al., 2011, Ellinger et al., 2013, Crouzet et al., 2013).

Members of the plant PDR family were heterologously overexpressed in eukaryotic systems (Gräfe et al., in preparation, Choi et al., 2014, Ruzicka et al., 2010, Biala et al., 2017, Yu and De Luca, 2013, Demessie et al., 2017). However, other studies also showed that expression of PDRs is not always easily achieved. For example *Np*PDR5 from *N. plumbaginifolia* could neither be expressed in *S. cerevisiae* nor in *S. pombe* (Pierman et al., 2017, Gräfe et al., in preparation). *At*PDR9 was expressed in *S. cerevisiae* but did not localize to the correct membranes. It localized correctly when it was expressed in HeLa cells and in *Schizosaccharomyces pombe* (Gräfe et al., in preparation, Ruzicka et al., 2010). Heterologous expression of *Nt*PDR1 completely failed, only the expression in the homologous system worked. For *Np*PDR1, even cloning was not successful (Gräfe et al., in preparation, Crouzet et al., 2013). Despite these challenges, heterologous overexpression is for some subsequent applications, like protein purification, essential, because heterologous systems, like bacterial or yeast based systems, have the advantage of fast protein production with higher yields compared to homologous (plant) systems (Gräfe et al., in preparation, Lefevre et al., 2015).

This work aimed the establishment of an *in vitro* system for the biochemical characterization of *At*PDR8. This included the overexpression of full-length *At*PDR8 in an appropriate heterologous system. Therefore the gene needed to be cloned into suitable expression vectors for the respective systems. Another important step was the establishment of a purification protocol for *At*PDR8 in order to prevent cross-interactions with other transport proteins during the *in vitro* characterization. In order to perform transport studies, *A*tPDR8 should be reconstituted into liposomes; this also required the establishing of the reconstitution protocol as well as the transport assay protocol. The resulting proteoliposomes represent a helpful tool to analyze the binding properties, kinetic parameters and the substrate spectrum of the ABC transporter.

2 Materials and Methods

2.1 Materials

2.1.1 Chemicals and Reagents

Chemicals and reagents that were used in this study are listed in Table 1.

Table 1: Chemicals and reagents

Chemical/reagent	Purity	Manufacturer
Acetic acid	Analytical reagent grade	VWR
Acetone	For analysis	VWR
D-Adenine	≥ 99 %	Fluka
Agar Agar (Agar)	Research grade	Serva
Agarose, GTQ	For gelextraction	Carl Roth
L-Alanine	≥ 99 %	Carl Roth
4-Aminobenzoic acid	≥ 99 %	Sigma-Aldrich
6-Aminohexanoic acid	≥ 98.5 %	Sigma-Aldrich
Ammonium hydroxide, 25 % solution	Not specified	VWR
Ammonium-^{15}N chloride	98 atom % ^{15}N	Sigma-Aldrich
Ammonium iron(III) citrate	Pharma grade	Sigma-Aldrich
Ammonium peroxodisulfate (APS)	For analysis	Carl Roth
Antifoam 204, mixture of organic polyether dispersions	Not specified	Sigma-Aldrich
L-Arginine	pure	AppliChem
L-Asparagine	≥ 98 %	Sigma-Aldrich
L-Aspartic acid	≥ 98.5 %	Carl Roth
Biobeads® SM-2 Adsorbent 20 – 50 mesh	Not specified	BioRad
Biotin	≥ 99 %	Sigma-Aldrich
Boric acid	≥ 99.8 %	Carl Roth
Bromphenol blue	Not specified	Merck
Calcium chloride dihydrate	≥ 99,5 %	Fluka
Calcium sulfate	99 %	Acros Organics
Chemiluminescence substrate Western Lightning® Ultra	Not specified	PerkingElmer Inc.
Chloroform	Analytical reagent grade	Fluka
Coomassie® Briliant blue R-250	Not specified	Serva
Cobalt(II) chloride x 6 H_2O	For analysis	Acros Organics
Complete™ protease inhibitor cocktail tablets, EDTA-free	-	Roche Diagnostics
Copper(II) chloride x 5 H_2O	For analysis	Merck
Cysteine	> 99 %	Fluka

Diethyl ether	≥ 99.8 %	Carl Roth
Dimethylsulfoxid (DMSO)	99.9 %	Acros Organics
1,2-dioleoyl-*sn*-glycero-3-phosphocholine (DOPC)	> 99 %	Avanti polar lipids
1,2-dioleoyl-*sn*-glycero-3-phosphoethanolamine (DOPE)	> 99 %	Avanti polar lipids
1,2-dioleoyl-*sn*-glycero-3-phospho-(1'-*rac*-glycerol) (sodium salt) (DOPG)	> 99 %	Avanti polar lipids
Dipotassium hydrogen phosphate	For analysis	Merck
Disodium hydrogen phosphate	≥ 99.5 %	Carl Roth
Dithiotreitol (DTT)	≥ 99 %	Carl Roth
DNA loading dye (6 x)	Not specified	Thermo Scientific
n-Dodecyl-β-D-maltopyranoside (β-DDM)	> 99 %	Glycon
Deoxynucleotides mix: 10 mM dATP, 10 mM dCTP, 10 mM dGTP, 10 mM dTTP (dNTPs)	For molecular biology	New England BioLabs
Ethanol	technical	Carl Roth
Ethidium bromide	For molecular biology	Carl Roth
Ethylenediamine tetraacetic acid (EDTA)	For analysis	AppliChem
Ethylene glycol-bis(β-aminoethyl ether)-N,N,N',N'-tetraacetic acid (EGTA)	≥ 99 %	Carl Roth
Fos-choline 14 (FOS-14)	Sol-grade	Anatrace
D-(+)-Glucose monohydrate	For analysis	Sigma-Aldrich
Glycerol	Analytical reagent grade	Fisher Scientific
Glutamine	≥ 99.5 %	Sigma-Aldrich
Glutamic acid	99 – 100 %	Sigma-Aldrich
Glycine	≥ 99.5 %	Sigma-Aldrich
Histidine	≥ 99 %	Sigma-Aldrich
Hydrochloric acid, 37% (w/v)	pure	Sigma-Aldrich
2-(4-(2-Hydroxyethyl)-1-piperazinyl)-ethansulfonsäure (HEPES)	For molecular biology	Fisher Scientific
Imidazole	≥ 99.5 %	Sigma-Aldrich
Iodixanol solution OptiPrep™ Density Gradient Medium		Sigma-Aldrich
Iron(II) sulfate x 7 H_2O	≥ 99.5 %	Fluka
L-Isoleucine	≥ 98 %	Sigma-Aldrich
Isopropanol	99.6 %	VWR
Isopropyl β-D-1-thiogalactopyranoside (IPTG)	≥ 99 %	Carl Roth
Ketoconazole	≥ 98 %	Sigma-Aldrich
Lauryl maltose neopentyl glycol (LMNG)	Sol-grade	Anatrace
L-Leucine	≥ 98 %	Sigma-Aldrich
Lithium acetate x 2 H_2O	For analysis	AppliChem

L-Lysine	≥ 98 %	Sigma-Aldrich
Magnesium chloride	≥ 98.5 %	Carl Roth
Magnesium sulfate heptahydrate	≥ 99,5 %	Sigma-Aldrich
Manganese sulfate x H_2O	Pure	Merck
2-Mercaptoethanol	≥ 99 %	Carl Roth
Methanol	Analytical reagent grade	Fisher Scientific
L-Methionine	≥ 99 %	Carl Roth
Myo-Inositol	> 97 %	Duchefa Biochemie
Nickel(II) chloride hexahydrate	≥ 98,0 %	Carl Roth
N,N,N',N'-Tetramethyl-1,2-ethylendiamin (TEMED)	For analysis	Merck
Non-fat dried milk powder	Blotting Grade	Carl Roth
Polyethylene glycol 400 (PEG 400)	Pure	AppliChem
L-Phenylalanine	For biochemistry	Carl Roth
Phosphoric acid 85 %	For analysis	Fisher Scientific
Potassium dihydrogen phosphate	Analytical regent grade	Fisher Scientific
Potassium hydroxide, pellets	85 %, for analysis	AppliChem
Potassium sulfate	Laboratory reagent grade	Fisher Scientific
L-Proline	For biochemistry	Merck
Rhodamine 6G chloride	99 %	Sigma-Aldrich
Rotiphorese® Gel: 30 % Acrylamide solution and 0.8 % bisacrylamide solution (37.5:1) (Acrylamide)	-	Carl Roth
L-Serine	For biochemistry	Merck
Sodium acetate x 3 H_2O	Not specified	Acros Organics
Sodium azide	99 %	Acros Organics
Sodium chloride	For analysis	Fisher Scientific
Sodium dodecylsulfate (SDS)	≥ 99,0 %	Serva
Sodium hydroxyde	For analysis	AppliChem
Sodium iodide	Pure	Merck
Sodium molybdate(VI) x 2 H_2O	99+ %	Acros Organics
Sodium dihydrogen phosphate	For analysis	AppliChem
D-Sorbitol	≥ 98 %	Carl Roth
D(+)-Saccharose (Sucrose)	≥ 99.5 %	Carl Roth
Sulfuric acid	95 %	VWR
Tetramethylethylendiamin (TEMED)	Not specified	Merck
Thiamin hydrochloride	> 98.5 %	Duchefa Biochemie
D-Threonine	≥ 98 %	Sigma-Aldrich
Trans-PCC α-maltoside	Not specified	Glycon
Trichloroacetic acid (TCA)	For analysis	AppliChem
Tris-(hydroxymethyl)-aminomethan (Tris)	For analysis	VWR

Triton X-100	-	Anatrace
Tryptone/peptone from caseine	For microbiology	Carl Roth
L-Tryptophan	≥ 98 %	Sigma-Aldrich
Tween 20	Pure, pharma grade	AppliChem
L-Tyrosine	≥ 98 %	Sigma-Aldrich
L-Valine	≥ 98.5 %	Carl Roth
Yeast extract	For bacteriology	Carl Roth
Yeastmaker™ Carrier DNA	-	Takara Bio USA
Yeast nitrogen base (YNB)	Not specified	Difco
Zinc chloride	Molecular biology grade	AppliChem

2.1.2 Devices

The (technical) devices used in this study are summarized in Table 2.

Table 2: Devices

Device	**Manufacturer**
ÄKTA™ liquid chromatography system, contains UV-900, P-900, Frac-920, PV908 and INV-907	GE Healthcare, Boston, MA, USA
ÄKTAprime plus system	GE Healthcare, Boston, MA, USA
Autoklav Systec VX-120 und VX-150	Systec GmbH, Linden, DE
Balance EW 2200-2NM (max: 2200 g ± 0,01 g)	Kern & Sohn GmbH, Balingen-Frommern, DE
Balance ABT I20-5DM (42 g; 120 g ± 0,00002 g; 0,0001 g)	Kern & Sohn GmbH, Balingen-Frommern, DE
BeadBeater	Bio Spec Products Inc., Bartlesville, OK, USA
Benchtop UV Transillluminator	UVP, LLC, Upland, CA, USA
Bioreactor (15 L), glass, autoclavable	Applikon Biotechnology, Delft, NL
Cell disruption system	Constant Systems Limited, Daventry, UK
Centrifuge 5415D for 1.5 and 2.0 mL tubes	Eppendorf AG, Hamburg, DE
Centrifuge AvantiRJ-26xP	Beckman Coulter, Brea, CA, USA
Centrifuge Heraeus Megafuge 1.0R for 50 and 15 mL tubes	Thermo Fisher Scientific, Waltham, MA, USA
Centrifuge Sorvall Evolution RC	Thermo Fisher Scientific, Waltham, MA, USA
Centrifuge rotor Sorvall SLC-6000	Thermo Fisher Scientific, Waltham, MA, USA
Centrifuge rotor Sorvall SS-34	Thermo Fisher Scientific, Waltham, MA, USA
Centrifuge rotor JA-10, 10,000 rpm	Beckman Coulter, Brea, CA, USA
Confocal microscope Zeiss LSM 880 with Airyscan, 63 x NA 1.4 objective	Carl Zeiss Microscopy GmbH, Jena, DE
Cooling unit NESLAB RTE 740	Thermo Fisher Scientific, Waltham, MA, USA
Disruptor-Genie™	Scientific Industries, Bohemie, NY, USA

Electroporation system Multiporator®	Eppendorf AG, Hamburg, DE
ez-Control for autoclavable bioreactors	Applikon Biotechnology, Delft, NL
Fluorolog	Horiba Jobin Yvon GmbH, Bensheim, DE
Heating and cooling block Thermomixer comfort	Eppendorf AG, Hamburg, DE
Incubator	Heraeus GmbH, Hanau, DE
Lumia Imaging System: Chemi Genius2 Bio Imaging System	Synoptics (Syngene), Cambridge, UK
Microplate reader FUOstar OPTIMA	**BMG LABTECH GmbH**, Ortenberg, DE
Milli-Q water filtration unit	Merck (Millipore) KgaA, Darmstadt, DE
PCR cycler Gradient Thermocycler	Analytic Jena AG (Biometra), Jena, DE
Peristaltic pump Masterflex® console drive	Cole-Parmer GmbH, Wertheim, DE
Peristaltic pump Minipuls®3	Gilson, Middleton, WI, USA
pH-Meter pHenomenal pH1000L	VWR, Radnor, PA, USA
Pipettes Pipetman Classic® with variable volumes: 1000 µL, 200 µL, 100 µL, 20 µL, 10 µL and 2 µL	Gibson, Middleton, WI, USA
Power supply Consort EV215	Cleaver Scientific, Warwickshire, UK
Power supply EPS 500/400	GE Healthcare, Boston, MA, USA
Rotary evaporator	Heidolph Instruments GmbH & Co. KG, Schwabach, DE
SDS-PAGE chamber	Bio-Rad Laboratories GmbH, München, DE
Shaking incubators Multitron Standard and Ecotron	Infors AG, Bottmingen, CH
Sonorex ultrasonic water bath	Bandelin electronic GmbH & Co. KG, Berlin, DE
Spectrophotometer NanoDrop™ ND-1000	PEQLAB Biotechnologie GmbH, Erlangen, DE
Spectrophotometer Ultrospec10	GE Healthcare, Boston, MA, USA
Sterile cleanbench Lamin Air LB-48-C	Heraeus GmbH, Hanau, DE
Swing out ultra centrifuge rotor Kontron TST 41.14	tresser instruments, Rossdorf, DE
Swing out ultra centrifuge rotor Kontron TST 60.4	tresser instruments, Rossdorf, DE
Tank blotting system Criterion™ Blotter	Bio-Rad Laboratories GmbH, München, DE
Ultra centrifuge Optima™ L-90K	Beckman Coulter, Brea, CA, USA
Ultra centrifuge rotor S100AT6	Hitachi-Koki, Chiyoda, Tokyo, JP
Ultra centrifuge rotor S120AT3	Hitachi-Koki, Chiyoda, Tokyo, JP
Ultra centrifuge rotor Ti-45	Beckman Coulter, Brea, CA, USA
Ultra centrifuge rotor Ti-70	Beckman Coulter, Brea, CA, USA
Ultra centrifuge Sorvall Discovery M120 SE	Hitachi-Koki, Chiyoda, Tokyo, JP
Tube rotator Stuart SB2	Cole-Parmer, Staffordshire, UK
Vacuum concentrator plus	Eppendorf AG, Hamburg, DE
Vacuum pump MZ2C NT 2AK	Vacuubrand GmbH + CO KG, Wertheim, DE
Vortex-Genie 2	Scientific Industries, Bohemie, NY, USA
Wavin platform shaker Polymax 1040	Heidolph Instruments GmbH & Co. KG, Schwabach, DE

2.1.3 Enzymes

Polymerases, restriction enzymes and other enzymes that were used in this study are listed in Table 3. All enzymes were used in their corresponding buffers, which are also named.

Table 3: Enzymes

Enzymes	**Manufacturer**
*Bam*HI restriction enzyme (20 U/µL) with NEBuffer™ 3.1 (10 x)	New England BioLabs
BglII restriction enzyme (10 U/µL) with buffer	Thermo Fisher Scientific
Deoxyribonuclease I from bovine (≥ 400 kunits/mg protein)	Sigma-Aldrich
*Dpn*I restriction enzyme (20 U/µL) with CutSmart® buffer (10 x)	New England BioLabs
*Eco*RI-HF restriction enzyme (20 U/µL) with CutSmart® buffer (10 x)	New England BioLabs
Lysing enzymes from *Trichoderma harzianum*	Sigma-Aldrich
*Mss*I restriction enzyme (5 U/µL) with buffer Tango (10 x)	Thermo Fisher Scientific
*Nhe*I-HF restriction enzyme (20 U/µL) with CutSmart® buffer (10 x)	New England BioLabs
*Not*I restriction enzyme (10 U/µL) with NEBuffer™ 3.1 (10 x)	New England BioLabs
*Pac*I restriction enzyme (10 U/µL) with CutSmart® buffer (10 x)	New England BioLabs
Pfu DNA polymerase (2.5 U/µL) with *Pfu* buffer with $MgSO_4$ (10 x)	Thermo Fisher Scientific
Phusion® High-Fidelity DNA Polymerase (2 U/µL) with Phusion® HF buffer (5 x)	New England BioLabs
PrimeSTAR® GXL DNA Polymerase (1.25 U/µL) with PrimeSTAR® GXL buffer (5 x)	Takara Bio USA
*Spe*I restriction enzyme (10 U/µL) with CutSmart® buffer (10 x)	New England BioLabs
*Sph*I restriction enzyme (10 U/µL) with CutSmart® buffer (10 x)	New England BioLabs
T4 DNA Ligase (5 U/µL) with T4 DNA Ligase buffer (10 x)	Thermo Fisher Scientific
Taq DNA Polymerase with ThermoPol® buffer (10 x)	New England BioLabs
Xho restriction enzyme (20 U/µL) with CutSmart® buffer (10 x)	New England BioLabs
*Xma*I restriction enzyme (10 U/µL) with CutSmart® buffer (10 x)	New England BioLabs

2.1.4 Antibodies

The antibodies that were used to detect proteins in this study are listed in Table 4.

Table 4: Antibodies

Antibody	**Referrence**
Anti-rabbit IgG HRP conjugated	Sigma-Aldrich
Anti-mouse IgG HRP conjugated	Jackson ImmunoResearch
Penta His™ antibody	Qiagen
Anti-Pdr5 antibody	Davids Biotechnologie

2.1.5 Kits and electrophoresis markers

Table 5 lists the kits and electrophoresis markers used in this study.

Table 5: Kits and electrophoresis markers

Kits	**Manufacturer**
Plasmid Midiprep Kit NucleoBond® Xtra Midi/Maxi	Macherey-Nagel
CloneJET PCR Cloning Kit	Thermo Fisher Scientific
Plasmid Miniprep Kit NucleoSpin® Plasmid	Macherey-Nagel
Gel/PCR purification Kit NucleoSpin® Gel and PCR clean-up	Macherey-Nagel
Gibson Assembly mastermix	New England Biolabs
Quick Blunting™ Kit	New England Biolabs
Detergent Solution Master Kit, 10 % solutions	Anantrace
In-Fusion® HD cloning Kit	Takara Bio USA
Electrophoresis markers	**Manufacturer**
GeneRuler™ 1 kb DNA ladder, 0,5 µg/µl	Thermo Fisher Scientific
PageRuler™ unstained protein ladder 10 – 200 kDa	Thermo Fisher Scientific
PageRuler™ prestained protein ladder 10 – 170 kDa	Thermo Fisher Scientific

2.1.6 Antibiotics

Antibiotics used in this study are shown in Table 6. Ampicillin and kanamycin were prepared as aqueous stock solutions. Chloramphenicol was dissolved in 100 % ethanol and zeocin was purchased as solution. All antibiotic solutions were filter sterilized (0.2 µm). The final working concentrations in medium are also listed.

Table 6: List of antibiotics and the used working concentrations.

Antibiotic	Purity	Manufacturer	Working concentration
Ampicillin sodium salt	≥ 97 %	Carl Roth	100 µg/mL
Chloramphenicol	≥ 98 %	Sigma-Aldrich	30 µg/mL
Kanamycin sulfate	≥ 750 I.E./mg	Carl Roth	50 µg/mL
Zeocin™	Not specified	InvivoGen	25 µg/mL for *E. coli*, 0.5 – 1 mg/mL for *P. pastoris*

2.1.7 Strains

Strains that were used for cloning and expression are listed in Table 7. In addition the genotype and the origin of the strain are mentioned.

Table 7: Strains for cloning and expression with genotypes

Strains	***Organism***	**Genotype**	**Origin**
DH5alpha	*Escherichia coli*	F$^-$ *endA1 glnV44 thi-1 recA1 relA1 gyrA96 deoR nupG purB20* φ80d*lacZ*ΔM15 Δ(*lacZYA-argF*)U169, hsdR17($r_K^- m_K^+$), λ$^-$	Thermo Fisher Scientific (Invitrogen^{TM})
XL1-Blue	*Escherichia coli*	*endA1 gyrA96(nal^R) thi-1 recA1 relA1 lac glnV44 F'[::Tn10 proAB$^+$ lacI^q Δ(lacZ)M15] hsdR17(r_K^- m_K^+)*	Stratagene
XL10-Gold	*Escherichia coli*	*endA1 glnV44 recA1 thi-1 gyrA96 relA1 lac Hte Δ(mcrA)183 Δ(mcrCB-hsdSMR-mrr)173 tet^R F'[proAB lacI^{q}ZΔM15 Tn10(Tet^R Amy Cm^R)]*	Stratagene
SURE2	*Escherichia coli*	*endA1 glnV44 thi-1 gyrA96 relA1 lac recB recJ sbcC umuC::Tn5 uvrC e14- Δ(mcrCB-hsdSMR-mrr)171 F'[proAB$^+$ lacI^q lacZΔM15 Tn10 Amy Cm^R]*	Stratagene
ABLE K	*Escherichia coli*	*E. coli C lac(LacZω$^-$) [Kan^{R}McrA$^-$McrCB$^-$ McrF$^-$Mrr$^-$HsdR($r_K^- m_K^-$)] [F′ proAB lacI^{q}ZΔM15Tn10 (Tet^R)]*	Agilent Technologies
BL21(DE3)	*Escherichia coli*	*E. coli* str. B F$^-$ *ompT gal dcm lon hsdS$_B$*($r_B^- m_B^-$) λ(DE3 [*lacI lacUV5-T7p07 ind1 sam7 nin5*]) [*malB*$^+$]$_{K-12}$(λ^S) pLysS[*T7p20 ori*$_{p15A}$](Cm^R)	Stratagene
X33	*Pichia pastoris*	Wild type	Thermo Fisher Scientific (Invitrogen^{TM})
YRE1001 (ΔPP)	*Saccharomyces cerevisiae*	*MAT*a;*ura3–52;trp1-1;leu2–3,112;his311,15;ade2-1; PDR1–3; ΔPDR5prom,ΔPDR5::TRP*	Ernst et al., 2008
YPH500	*Saccharomyces cerevisiae*	*MAT*α *ura3-52 lys2-801_amber ade2-101_ochre trp1-Δ63 his3-Δ200 leu2-Δ1*	Sikorski anf Hieter, 1989

2.1.8 Plasmids

Table 8 lists the used plasmids with encoded resistances and signaling peptides.

Table 8: Plasmids with encoded references and signaling peptides.

Plasmid	Promoter	Selection	Signaling peptide	Reference
pSGP18-2µ	AOX1	Zeocin	6xHis, CBP (C-term.)	Ellinger et al., 2013
pSGP18-Ntag	AOX1	Zeocin	10xHis, CBP (N-term.)	Based on pSGP18 (Chloupkova et al., 2007) Kindly provided by Dr. Diana Kleinschrodt
pET16b	T7	Ampicillin	10xHis (N-term.)	Merck
pET24a	T7	Kanamycin	T7 (N-term.) 6xHis (C-term.)	Merck
p426GPD	GPD	Ampicillin	-	Mumberg et al., 1995
pNZ-SV-Entero-His	PNisA	Kanamycin, erythromycin	6xHis (C-term.)	Kindly provided by Dr. Diana Kleinschrodt
pIL-SV	PNisA	Ampicillin, chloramphenicol	-	AlKhatib et al., 2014
pJET1.2/blunt	T7	Ampicillin	-	Thermo Fisher Scientific

2.1.9 Chromatography media and columns

Table 9 lists the columns and resins used for protein purification.

Table 9: Chromatography media and columns

Column or resin	Manufacturer
Calmodulin affinity resin	Agilent Technologies
HiTrap Chelating HP column (5 mL)	GE Healthcare
Ni-NTA resin	Thermo Fischer
Superdex^{TM} 200 10/300 GL column	GE Healthcare

2.1.10 Oligonucleotides

Table 10 shows the primers that were used for cloning, site directed mutagenesis and sequencing. All primers were purchased at MWG-Biotech AG (Ebersberg, DE) and diluted in sterile water to a final concentration of 100 pmol/µL.

Table 10: PCR and sequencing primers. The Annealing temperature of all sequencing primers was 55 °C

PCR primer	Sequence 5'→3'	$\vartheta_{annealing}$	Description
Hom.Rek.PDR8FWD	ACT TAG TTT CGA CGG ATT TTC GAA CTA GTG GAT CCC CCG GGA TGG	59 °C	Primers include overhangs for homologous recombination in *S. cerevisiae*. Amplification of PDR8 with C-terminal tags from pSGP18-2µ-PDR8.
Hom.Rek.PDR8REV	TGT AAG CGT GAC ATA ACT AAT TAC ATG ACT CGA GGT CGA CGG GTC	59 °C	
Lin.p426GPDFWD	CGT CGA CCT CGA GTC ATG TAA TTA G	65 °C	Linearization of vector p426GPD for homologous recombination in *S. cerevisiae*.
Lin.p426GPDREV	CCC GGG GGA TCC ACT AGT TC	65 °C	
PDR8InFuspNZFWD	CGA CGA CGA CAA GAT GAT CCA TGG CAG CAG ATG GAT TAC AAT CCA AAT	59 °C	Amplification of PDR8 from pSGP18-2µ-PDR8 with or without C-terminal tags for cloning in pNZ via In-Fusion® reaction. Primers include respective overhangs.
PDR8InFusTagsRE	CGG ATC TCA GTG GTG GTG GTG GTG GTG GGG TCG AAG AAT TCA GTG	59 °C	
Lin.pNZ-FWD	CCA CCA CCA CCA CTG AGA	65 °C	Linearization of vector pNZ for In-Fusion® reaction.
Lin.pNZ-REV	CTG CTG CCA TGG ATC TTG T	65 °C	
PDR8 BamHI FWD	AGC TGA GGA TCC ATG GAT TAC AAT CCA AAT CTT	59 °C	Amplification of PDR8 with C-terminal tags. Primers include overhangs for restriction sites *Bam*HI and *Xho*I.
PDR8 XhoI REV	AGC TGA CTC GAG GGT CGA AGA ATT CAG TGA	59 °C	
PDR8FWD	ATG GAT TAC AAT CCA AAT CTT C	59 °C	Amplification of PDR8 with tags from pSGP18-2µ-PDR8 for blunt end ligation in pIL-SV.
TagsPDR8REV	GGT CGA AGA ATT CAG TGA TG	59 °C	
PDR8_PacI-fwd	TCA GAC TTA ATT AAA TGG ATT ACA ATC CAA ATC TTC CTC CTT TAG	65 °C	Amplification of PDR8 from pJET and addition of restriction sites for *Pac*I and *Sph*I.
PDR8_SphI_rev	TGC ACG GCA TGC TCT GGT CTG GAA GTT GAG AGT TCT G	65 °C	
pSGP18-2µ.SphI.fw	AGT TCT GCA TGC CGT CTC GCC TCC AAC TCC TTA GAA GTC	68 °C	Linearization of the vector pSGP18-2µ and addition of restriction sites for *Pac*I and
pSGP18-2µ_PacI-2	TCG ACG TTA ATT AAG CTG CAG CGT CTC GAA CCC ATT CTT TTA C	68 °C	

			*Sph*I.
PDR8 XhoI FWD	AGC TGA CTC GAG ATG GAT TAC AAT CCA AAT	59 °C	Amplification of PDR8 without tags and addition of restricton sites for *Xho*I and *Bam*HI.
PDR8 BamHI REV	AGC TGA GGA TCC CTA TCT GGT CTG GAA GTT GAG	59 °C	
PDR8_1_FWD	GGA TTA CAA TCC AAA TCT TCC TCC TTT AGG	60 °C	Amplification of the PDR8 coding sequence from cDNA.
PDR8_2_REV	TTA TCT GGT CTG GAA GTT GAG AGT TCT G	60 °C	
EcoRIPDR8pNZFWD	AGC TGA GAA TTC ATG GAT TAC AAT CCA AAT CTT C	60 °C	Amplification of PDR8 without tags from pSGP18-2µ. Primers include overhangs with restrictions sites for *Eco*RI and *Not*I.
NotIPDR8pNZREV	TGC AGC GCG GCC GCT CTG GTC TGG AAG TTG	60 °C	
Mutagenesis primer	**Sequence 5'→3'**		
PDR8 SiDiMu FWD	GTT CCA CTA CTT TCC AAA TCG TCA AGT G		
PDR8 SiDiMu REV	CAC TTG ACG ATT TGG AAA GTA GTG CAA C		
Sequencing primer	**Sequence 5'→3'**		
3'AOX	GCA AAT GGC ATT CTG ACA TCC		
5'AOX	GAC TGG TTC CAA TTG ACA AGC		
PDR8_2	TCA ATG GTT ACC AAC TCG		
PDR8_3	AAC CCG AAC AGA CCT TAT C		
PDR8_4	ACT TCT TGT GTT CTT GCT C		
PDR8_5	ATT GTG ATG AGG GCG GTA AGG		
PDR8_6	AGC GTT GGT AAA AGA AC		
PDR8_7	TGG ACC GTG TAT GGA TTG		

2.1.11 Other materials

Additional materials that do not belong to the categories named before are listed in Table 11.

Table 11: List of other materials that were used.

Material	Manufacturer
Beakers Duran® 500 ml, 100 ml, 50 ml	Schott AG, Mainz, DE
Bottle-top filter unit Nalgene®	Thermo Fisher Scientific, Waltham, MA, USA
Cannula	Henke Sass Wolf GmbH, Tuttlingen, DE
Centrifuge beakers 1 L	Hitachi-Koki, Chiyoda, Tokyo, JP
Centrifuge beakers 500 mL	Hitachi-Koki, Chiyoda, Tokyo, JP
Centrifuge tubes Clear' PPCO, 50 ml	Laborgeräte Beranek GmbH, Nußloch, DE
Ultra centrifuge tubes, polyallomer, thin wall, 14 mL	Laborgeräte Beranek GmbH, Nußloch, DE
Concentrator Vivaspin® 6 MWCO 100 kDa, 6 mL	Satorius AG, Göttingen, DE
Cuvettes, polystyrol, 1 cm pathlength	Sarstedt AG & Co, Nümbrecht, DE
Cuvettes QS High Precision Cell Quartz Suprasil®	Hellma GmbH & Co. KG, Müllheim, DE
Disposable sterile plastic pipettes 5 mL, 10 mL and 25 mL	Sarstedt AG & Co, Nümbrecht, DE
Disposable petri dishes	Sarstedt AG & Co, Nümbrecht, DE
Disposable pipette tips	Sarstedt AG & Co, Nümbrecht, DE
Electroporation cuvette, 2 mm, short electrode	Bio-Budget Technologies GmbH, Krefeld, DE
Erlenmeyer flask Duran® 5 L, 2 L, 300 mL and 100 mL (with or without baffles)	Schott AG, Mainz, DE
Filter membrane Supor®-200 0,2 µm	Sarstedt AG & Co, Nümbrecht, DE
Filter paper for Western blotting	Bio-Rad, Hercules, CA, USA
Forceps, 18/10, stainless steel	VWR, Radnor, PA, USA
Glass beads 0.5 mm diameter	Carl Roth GmbH + Co. KG, Karlsruhe, DE
Glass bottle Duran® 1 L, 0,5 L, 250 ml, 100 mL and 50 mL	Schott AG, Mainz, DE
Glass syringe Hamilton™, 50 µl	Hamilton Company, Reno, NV, USA
Measuring cylinder 500 mL, 250 mL, 100 mL, 50 mL	VITLAB GmbH, Grossostheim, DE
Nitrocellulose blotting membrane BioTrace™ NT	Pall Life Sciences, Pensacola, FL, USA
Parafilm® M	Bemis Company, WI, Neenah, USA
PVDF blotting membrane Amershan™Hybond™ 0.45 µm	GE Healthcare, Boston, MA, USA
Reaction tubes 1.5 mL, 2 mL, 15 mL and 50 mL	Sarstedt AG & Co, Nümbrecht, DE
Scalpel	B. Braun Melsungen AG, Melsungen, DE
Sterile filter Filtropur S 0,2 µm	Sarstedt AG & Co, Nümbrecht, DE
Syringe Injekt®-F 1 mL	B. Braun Melsungen AG, Melsungen, DE
Syringe 10 mL	BD DiscarditTM, Beckton Dickinson S.A., Fraga,

	Huesca, ES
Syringe 50 mL	Henke Sass Wolf GmbH, Tuttlingen, DE
Test tubes 10 mL, glass	
Ultra centrifuge tubes, polyallomer, thin wall, 4.4 mL	Laborgeräte Beranek GmbH, Nußloch, DE
Ultra centrifuge tubes polycarbonate, thick wall, 3.2 mL	Laborgeräte Beranek GmbH, Nußloch, DE
Ultra centrifuge tubes polycarbonate, thick wall, 0.5 mL	Laborgeräte Beranek GmbH, Nußloch, DE
Ultra centrifuge tubes with lids 60 mL and 25 mL	Beckman Coulter, Brea, CA, USA
Zirconium/glass pellets 0.5 mm diameter	Carl Roth GmbH + Co. KG, Karlsruhe, DE

2.1.12 Buffers, solutions and culture media

Tables 12 to 14 list the buffers, solutions and media used in this study. If not stated otherwise, all solutions were prepared in filtered water. Buffers were filtered (0.2 µm) and all media were autoclaved at 121 °C for 20 min.

Table 12: List of buffers and their composition.

Buffers	**Composition**		
Extraction buffer	Tris-HCl pH 8 (4 °C)	50	mM
	NaCl	200	mM
	Sucrose	330	mM
	EDTA	1	mM
	EGTA	1	mM
	Aminohexanoic acid	100	mM
	Protease inhibitor cocktail	1	tablet
Membrane buffer	Tris-HCl pH 7.2 (4 °C)	50	mM
	NaCl	200	mM
	Glycerol	10	% (v/v)
10 x membrane buffer	Tris-HCl pH 7.2 (4 °C)	500	mM
	NaCl	2	M
	Glycerol	50	%
Hypo-osmotic buffer	Tris-HCl pH 7.5 (4 °C)	50	mM
	Sorbitol	200	mM
	EDTA	1	mM
	Protease inhibitor cocktail	1	tablet
IMAC wash buffer	Tris-HCl pH 8 (4 °C)	50	mM
	NaCl	150	mM
	Glycerol	20	mM
	Imidazole	10	mM

	Respective detergent	3	x cmc
IMAC elution buffer	Tris-HCl pH 8 (4 °C)	50	mM
	NaCl	150	mM
	Glycerol	20	mM
	Imidazole	200	mM
	Respective detergent	3	x cmc
LP-mix	PEG 400	40	%
	Lithium acetate	100	mM
	Tris-HCl pH 7.5 (RT)	10	mM
	EDTA	1	mM
Pdr5 re-suspension buffer	Tris-acetic acid pH 7.5 (4 °C)	50	mM
	EDTA	5	mM
	Protease inhibitor cocktail	1	tablet
Pdr5 transport buffer	Hepes pH 7	50	mM
	$MgCl_2$	10	mM
	Sodium azide	10	mM
	Rhodamine 6G	150	nM
Protein buffer	Tris-HCl pH7.2 (4 °C)	50	mM
	NaCl	200	mM
	Glycerol	10	% (v/v)
	Respective detergent	3	x cmc
Resolving gel buffer	Tris-HCl pH 8.85 (RT)	1.5	M
	SDS	0.4	% (w/v)
SDS-PAGE electrophoresis buffer (10 x)	Glycin	1.9	M
	Tris-HCl pH 8.3 (RT)	0.25	M
	SDS	1	% (w/v)
Stacking gel buffer	Tris-HCl pH 6.8 (RT)	0.5	M
	SDS	0.4	% (w/v)
Sucrose gradient buffer	Tris-HCl, pH 7.5	10	mM
	EDTA	1	mM
	Sorbitol	800	mM
TAE buffer	Tris-acetic acid pH 8.4 (RT)	40	mM
	EDTA	1	mM
TAE buffer for Pdr5	Tris-acetic acid pH 7.5 (4 °C)	10	mM
	EDTA	0.2	mM
TAEG buffer for Pdr5	Tris-acetic acid pH 7.5 (4 °C)	10	mM
	EDTA	0.2	mM
	Glycerol	20	%
Tank blotting buffer	Glycin	11.2	g/L
	Tris	2.42	g/L

	Methanol	10	% (v/v)
TE buffer	Tris-HCl pH 8 (RT)	50	mM
	EDTA	1	mM
TBS buffer	Tris-HCl pH 8 (RT)	20	mM
	NaCl	250	mM
TBS-T buffer	Tris-HCl pH 8 (RT)	20	mM
	NaCl	250	mM
	Tween 20	0.1	% (v/v)

Table 13: List of solutions and their composition.

Solutions	**Composition**		
Blocking solution	Milk powder in TBS-T buffer	10	% (w/v)
Colloidal coomassie staining solution	Aluminium sulfate	5	% (w/v)
	Ethanol	10	% (v/v)
	Coomassie brillant blue-R250	0.02	% (w/v)
	Phosphoric acid	2.35	% (v/v)
Lysing enzymes solution	Lysing enzymes	10	mg/mL
	Na_3PO_4 pH 7.4	100	mM
	DTT	1	mM
Primary antibody solution	Penta-His antibody	1	µL/mL
	BSA	3	%
	→ in TBS-T		
PTM_1 Trace salts	Copper(II) sulfate x 5 H_2O	6	g/L
	Sodium iodide	0.08	g/L
	Manganese sulfate x H_2O	3	g/L
	Sodium molybdate x 2 H_2O	0.2	g/L
	Boric acid	0.02	g/L
	Colbalt chloride	0.5	g/L
	Zinc chloride	20	g/L
	Iron(II) sulfate x 7 H_2O	65	g/L
	Biotin	0.2	g/L
	Sulfuric acid	5	mL/L
SDS-PAGE loading dye for membrane proteins (5 x)	SDS-PAGE stacking gel buffer	10	mL
	SDS (16 % in H_2O)	10	mL
	Urea	1.5	M
	Glycerol	20	mL
	H_2O	10	mL
	Bromphenol blue	40	mg

Secondary antibody solution	Anti-mouse/rabbit-HRP	0.1	µL/mL
	Milk powder	10	%
	→ in TBS		
TCA solution, 100 %	TCA	2.2	g/mL
TCA solution, 10 %	TCA solution 100 %	1	mL
	H_2O	9	mL

Table 14: Composition of culture media for *E. coli*, *P. pastoris* and *S. cerevisiae.*

Culture media	Composition					
Basal salt medium	Phosphoric acid 85 %	26.7	mL/L			
	Calcium sulfate	0.93	g/L			
	Potassium sulfate	18.2	g/L			
	Magnesium sulfate x 7 H_2O	14.9	g/L			
	Potassium hydroxide	4.13	g/L			
	Glycerol	40	g/L			
Boost medium	Yeast extract	50	g/L			
	Tryptone/peptone	100	g/L			
Buffered complex glycerol medium (BMGY)	100 mM potassium phosphate	100	mM			
	Yeast extract	10	g/L			
	Tryptone/peptone	20	g/L			
	Yeast nitrogen base	13.4	g/L			
	Biotin	0.4	g/L			
	Glycerol	1	% (v/v)			
Buffered complex methanol medium (BMMY)	100 mM potassium phosphate	100	mM			
	Yeast extract	10	g/L			
	Tryptone/peptone	20	g/L			
	Yeast nitrogen base	13.4	g/L			
	Biotin	0.4	g/L			
	Methanol	0.5	% (v/v)			
Drop out mix minus uracil	Adenine	0.5	g	Leucine	10	g
	Alanine	2	g	Lysine	2	g
	Arginine	2	g	Methionine	2	g
	Asparagine	2	g	p-aminobenzoic		
	Aspartic acid	2	g	acid	2	g
	Cysteine	2	g	Phenylalanine	2	g
	Glutamine	2	g	Proline	2	g
	Glutamic acid	2	g	Serine	2	g
	Glycine	2	g	Threonine	2	g
	Histidine	2	g	Tryptophan	2	g
	Inositol	2	g	Tyrosine	2	g

	Isoleucine	2 g	Valine	2 g
LB medium	Yeast extract	5	g/L	
	Tryptone/peptone	10	g/L	
	NaCl	5	g/L	
	(Agar for plates)	15	g/L	
Minimal glycerol medium (MGY)	Yeast nitrogen base	13.4	g/L	
	Biotin	0.4	g/L	
	Glycerol	1	% (v/v)	
Minimal methanol medium (MM)	Yeast nitrogen base	13.4	g/L	
	Biotin	0.4	g/L	
	Methanol	0.5	% (v/v)	
Synthetic complete (SC) medium minus uracil	Yeast nitrogen base	6.7	g/L	
	Glucose	20	g/L	
	Drop out mix	2	g/L	
	Agar	20	g/L	
YPD	Yeast extract	10	g/L	
	Tryptone/peptone	20	g/L	
	Glucose	2	% (w/v)	
	(Agar for plates)	20	g/L	

2.2 Methods

2.2.1 Cultivation of strains

2.2.1.1 Cultivation of *E. coli*

E. coli strains were grown on LB medium supplemented with the respective antibiotics, depending on the resistance gene encoded on the plasmid and on the strain used for transformation. Plates were incubated at 37 °C. Liquid cultures were shaken at 37 °C and 180 rpm.

2.2.1.2 Cultivation of *P. pastoris*

P. pastoris strain X33 was grown on YPD plates at 30 °C. *L*iquid cultures were grown in either minimal glycerol medium (MGY) or buffered glycerol medium at 30 °C and 200 rpm. For induction of protein expression, glycerol was substituted by 0.5 % methanol in minimal as well as in complex media.

2.2.1.3 Cultivation of *S. cerevisiae*

S. cerevisiae strain YPH500 was grown on YPD medium at 30 °C, liquid cultures were shaken at 200 rpm.

2.2.2 Electrophoresis and immunoblotting

2.2.2.1 Agarose gel electrophoresis

DNA fragments were separated using an agarose gel (1 % in TAE buffer). Samples were prepared as follows: For plasmid preparations from *E. coli* 2 µL were added to 10 µL water and mixed with 5 x DNA loading dye to a final concentration of 1 x loading dye. For PCR products 5 µL were used. DNA fragments were separated for 60 min at 100 V. The gel was stained in ethidium bromide aqueous solution (1 µg/mL) for 30 min and visualized with the Lumi Imaging system. DNA fragment sizes were determined by comparing band sizes to a DNA marker.

2.2.2.2 SDS-PAGE

For SDS-polyacrylamide gel electrophoresis SDS gels were prepared according to Table 15. The content of acrylamide of the resolving gel depends on the molecular weight of the target protein. For detecting PDR8 gels with 7.5 % acrylamide were used. All PDR8 samples were mixed with SDS-PAGE loading dye for membrane proteins to a final concentration of 1 x loading dye. 30 µL of the mixture were loaded onto the gel. For determination of protein sizes a protein marker was used. Samples were separated at 100 V for 2 – 3 h. Gels were either subjected to Western Blotting (see below) or stained with colloidal coomassie staining solution overnight. Gels were de-stained in water for two days, while the water was replaced several times.

Table 15: Compositions of stacking and resolving gel for SDS-PAGE.

Chemical	4.5 % stacking gel	7.5 % resolving gel
Stacking gel buffer	8.75 mL	-
Resolving gel buffer	-	18.75 mL
H_2O	21 mL	38 mL
Acrylamide	6 mL	17.5 mL
TEMED	70 µL	70 µL
APS	210 µL	300 µL

2.2.2.3 Western blotting

Immunoblotting was performed in order to detect the protein and to proof the identity. After SDS-PAGE protein content of the gel was transferred to a PVDF membrane using wet/tank blotting. The membrane was incubated in methanol, the filter paper was incubated in tank blotting buffer. The SDS-gel was stacked on top of three layers of filter paper followed by the PVDF membrane and another three layers of filter paper. Proteins were transferred for 90 min at 80 V. The membrane was incubated 1 – 12 h in blocking solution in order to saturate the surface and to prevent unspecific binding of antibodies. The membrane was washed three times for 10 min in TBS-T buffer and incubated with primary antibody for 1 – 12 h. The membrane was washed again three times in TBS-T and incubated with the secondary HRP-conjugated antibody for one our. The membrane was washed three times for 10 min in TBS-T and once in TBS buffer. Afterwards the chemiluminescent substrate was spread onto the

membrane and proteins were detected with the Lumi Imager System: 5 min for expression tests of PDR8, 1 min for purified PDR8.

2.2.3 DNA amplification and purification methods

2.2.3.1 cDNA

First strand cDNA was generated by reverse transcription of *A. thaliana* Columbia-0 extracted RNA and was kindly provided by the laboratory of Prof. Andreas Weber, Institute for Plant Biochemistry, Heinrich-Heine University Düsseldorf.

2.2.3.2 Primer Design

The Clone Manager Suite (Sci-ED Software) was used for primer design. If required for cloning, overhangs were fused to the primers adding, for example, restriction sites to the sequence. Primers used for side directed mutagenesis PCR were designed using the web-based program PrimerX (http://bioinformatics.org/primerx/). All oligonucleotides were synthesized by MWG Eurofins.

2.2.3.3 Polymerase Chain Reaction (PCR) from cDNA

The PCR reagents were pipetted according to table 16 to a total volume of 50 µL. 396 ng cDNA were used as template for the reaction. The used PCR program is displayed in Table 16.

Table 16: Pipetting protocol and program for the PCR from cDNA. Denaturation, annealing and elongation were repeated for 32 cycles.

PCR reagent	[µL]	Program step	[°C]	[min]	
PrimeSTAR® GXL buffer (5x)	5	Initial denaturation	98	1	
dNTPs (10 mM each)	1	Denaturation	98	0.15	↺ 32 cycles
Primer PDR8_1_FWD	1	Annealing	60	0.15	
Primer PDR8_2_REV	1	Elongation	68	2	
PrimeSTAR® GXL Polymerase (1.25 U/µL)	1	Final elongation	68	5	
cDNA (197 ng/µL)	2	Pause	12	∞	
H_2O	34				

2.2.3.4 Polymerase Chain Reaction (PCR) from plasmid template

Depending on the polymerase, the PCR reagents were pipetted according to Tables 17 and 18. The total volume of 50 µL was used for one reaction or was divided into 15 µL aliquots to test different annealing temperature in a temperature gradient. If needed the total volume was scaled up keeping the ratio of the ingredients. The volume of the template complied with the concentration of the isolated plasmids. The used PCR programs are displayed in Tables 17 and 18. The annealing temperatures depended on the used primer pair, the elongation time on the performance of the respective polymerase and the size of the amplified DNA fragment. PCR products were gel purified.

Table 17: Pipetting protocol and program for the PCR with GXL polymerase. Denaturation, annealing and elongation were repeated for 32 cycles.

PCR reagent	[µL]	Program step	[°C]	[min]	
PrimeSTAR® GXL buffer (5x)	5	Initial denaturation	98	1	
dNTPs (10 mM each)	1	Denaturation	98	0.25	32 cycles
Primer FWD	1	Annealing	Variable	0.25	
Primer REV	1	Elongation	68	1/kpb	
PrimeSTAR® GXL Polymerase (1.25 U/µL)	1	Final elongation	68	5	
Plasmid DNA (app. 300 – 500 ng)	Variable	Pause	12	∞	
H_2O	Fill up to 50				

Table 18: Pipetting protocol and program for the PCR with Phusion polymerase. Denaturation, annealing and elongation were repeated for 32 cycles.

PCR reagent	[µL]	Program step	[°C]	[min]	
Phusion® buffer (5x)	5	Initial denaturation	98	0.5	
dNTPs (10 mM each)	1	Denaturation	98	0.15	32 cycles
Primer FWD	1	Annealing	Variable	0.5	
Primer REV	1	Elongation	72	0.5/kbp	
Phusion® Polymerae	0.5	Final elongation	72	5	
Plasmid DNA (app. 3 ng)	Variable	Pause	12	∞	
H_2O	Fill up to 50				

2.2.3.5 Side directed mutagenesis PCR

To integrate mutations into the DNA sequence of a plasmid the site directed mutagenesis PCR was used. Primers contained one or two mismatching base pairs integrating a mutation that resulted in an amino acid change of the protein sequence. The PCR mix was pipetted as listed in Table 19. If required different annealing temperatures were screened in a temperature gradient. The template was a circular plasmid, which needed to be removed from the PCR product by digestion with the restriction enzyme *Dpn*I. Because the enzyme was active in the PCR buffer 1 µL of *Dpn*I was directly added to 50 µL of PCR product and incubated at 37 °C overnight. The PCR product was transformed into *E. coli* as described in chapter 2.2.4.7.

Table 19: Pipetting protocol and program for the side directed mutagenesis PCR. Denaturation, annealing and elongation were repeated for 32 cycles.

PCR reagent	[µL]	Program step	[°C]	[min]	
Pfu buffer with $MgSO_4$ (10 x)	5	Initial denaturation	95	3	
dNTPs (10 mM each)	1	Denaturation	95	0.5	32 cycles
Primer FWD	0.5	Annealing	Variable	0.5	
Primer REV	0.5	Elongation	72	2/kbp	
Pfu Polymerae (2.5 U/µL)	1	Final elongation	72	15	
Plasmid DNA (app. 25 – 65 ng)	Variable	Pause	12	∞	
H_2O	Fill up to 50				

2.2.3.6 Purification of PCR products and DNA fragments

PCR products were separated by agarose gel electrophoresis (chapter 2.2.2.1). Under UV light the DNA bands at the correct fragment size were cut out of the gel. The selected DNA was purified from the gel with the Gel/PCR purification kit according to the user manual. Alternatively, DNA fragments (for example after restriction digestion) were purified without prior gel extraction using the same kit. The DNA was eluted with 20 µL 50 °C water. The concentration was determined with the NanoDrop™ spectrophotometer.

2.2.3.7 Isolation of plasmids from *E. coli* cultures

The respective *E. coli* culture was grown overnight in a 3 mL LB medium with the respective antibiotics (see Tables 8 and 6) at 37 °C and 180 rpm. The culture pas pelleted (2 min 11,000 x g) and the plasmids were isolated with the Plasmid Miniprep kit. The plasmid DNA was eluted with 20 µL 50 °C water. If a larger quantity of plasmid material was needed the

E. coli culture volume was increased to 100 mL and the Plasmid Midiprep kit was used. The concentration was determined with the NanoDrop™ spectrophotometer. The DNA was sequenced by GATC Biotech AG.

2.2.3.8 Colony PCR of *E. coli* clones

One transformed *E. coli* colony was transferred into 6.35 µL water. The remaining PCR ingredients (Table 20) were added and the DNA was amplified using the PCR program listed in Table 20. The PCR products were analyzed by agarose gel electrophoresis.

Table 20: Pipetting protocol and program for the *E. coli* colony PCR. Denaturation, annealing and elongation were repeated in for cycles.

PCR reagent	[µL]	Program step	[°C]	[min]	
Taq buffer (10 x)	1	Initial denaturation	95	0.5	
dNTPs (10 mM each)	0.2	Denaturation	95	0.5	30 cycles
Primer FWD	0.2	Annealing	Variable	0.5	
Primer REV	0.2	Elongation	68	1/kbp	
Taq Polymerae (5 U/µL)	0.05	Final elongation	68	15	
H_2O	6.35	Pause	12	∞	

2.2.4 Cloning and transformation

2.2.4.1 Blunt end ligation into pJET1.2/blunt

PCR products amplified from cDNA were cloned into pJET1.2/blunt from the CloneJET PCR Cloning kit. The ligation reaction was pipetted as listed in Table 21. The reaction was incubated for 15 min at 22 °C and immediately used for transformation into XL1-Blue cells.

Table 21: Pipetting protocol for the blunt end ligation into pJET1.2/blunt.

Reagent	[µL]
Reaction buffer (10 x)	2
Purified PCR product	10
pJET1.2/blunt (50 ng/µL)	2
T4 DNA ligase (5 U/µL)	1
H_2O	7

2.2.4.2 Cloning by restriction digestion and ligation

Purified plasmids/PCR products (PDR8 gene and expression vector) were digested in a single reaction mixture that includes all the required endonuclease enzymes (Table 22). If the two enzymes were not active in the same buffer (Table 3) two subsequent digestion reactions were set up with a DNA purification step in between. The reaction was incubated for 1 h at 37 °C. Digested fragments were always gel purified using the Gel/PCR purification kit.

Table 22: Pipetting protocol for the restriction digestion with two endonucleases.

Reagent	[µL]
Buffer (10 x), depends on the enzymes	6
Purified DNA	50
Enzyme 1	1.5
Enzyme 2	1.5

The ligation reaction was set up according to Table 23. The digested PDR8 gene (insert) and the expression vector were combined in a molar ration of 3:1. Formulas 1 and 2 were used to calculate the volumes of insert and vector, taking the concentration and the number of base pairs (bp) into account. The combined volume of both insert and vector was set to 8 µL. The ligation mix was incubated at 4 °C overnight, alternatively at 22 °C for 30 min. After transformation into *E. coli* clones were screened by plasmid isolation, restriction digestion and agarose gel electrophoresis.

Table 23: pipetting protocol for the ligation into expression vectors.

Reagent	[µL]
Buffer (10 x)	2
Vector, digested and purified	X
PDR8 gene, digested and purified	Y
T4 DNA Ligase	1
H_2O	Fill up to 20 µL

$$V(insert) = Y = \frac{bp\ (insert)}{bp\ (vector)} \cdot \frac{c(vector)}{c(insert)} \cdot n \qquad [1]$$

$$V(vector) = X = 8 - V(insert) \qquad [2]$$

with

$V = volume\ [\mu L]$

$c = concentration\ [ng/\mu L]$

$n = factor\ of\ the\ insert\ to\ vector\ ratio$

$bp = number\ of\ base\ pairs$

2.2.4.3 In-Fusion® cloning

In-Fusion® cloning was performed using the In-Fusion® HD Cloning kit. Following the manual, expression vector was linearized by PCR reaction. The insert was amplified by PCR. Primers included 15 bp overhangs that were complementary to the ends of the linearized vector. Both amplified insert and vector were purified using the Gel/PCR purification kit. The In-Fusion reaction mix was set up as shown in Table 24 and incubated for 15 min at 50 °C. The reaction mix was then transformed into *E. coli.* Clones were screened by restriction digestion of the isolated plasmids and agarose gel electrophoresis.

Table 24: Pipetting protocol for In-Fusion cloning.

Reagent	**[µL]**
In-Fusion® HD enzyme premix (5 x)	2
Vector, linearized and purified (200 ng)	Variable
Insert gene, purified (200 ng)	Variable
H_2O	Fill up to 10

2.2.4.4 Gibson Assembly Cloning

The insert was mixed with the vector in a ratio of 3:1 and added to 8 µL Gibson mastrmix in a total volume of 10.4 µL. The reacrion was incubated at 50 °C for 1 h and subsequently used for transformation into *E. coli*.

2.2.4.5 Blunting

After restriction digestion the following was added directly into the restriction digestion mixture: 5 mM DTT, 2 µL Blunt enzyme mix and 10 mM dNTPs. The blunting reacrion was incubated at room temperature for 30 min followed by heat inactivation at 70 °C for 10 min. The mixture was subsequently used for ligation.

2.2.4.6 Homologous recombination in *S. cerevisiae*

Homologous recombination *in S. cerevisiae* was performed similarly as described in Schiestl and Gietz (1989). A 3 mL *S. cerevisiae* YPH500 overnight culture was pelleted (5,000 x g, 1 min) and the reaction mixture was pipetted as listed in Table 25. The mixture was incubated at 25 °C for 30 min followed by a heat shock at 42 °C for 15 min. After addition of 500 µL TE-buffer the cells were pelleted (5,000 x g, 1 min) and washed with 1 mL TE-buffer (10,000 x g, 30 sec.). The cells were re-suspended in 500 µL YPD medium and incubated for 1 h at 30 °C, 180 rpm. For selection, cells were plated on SC minus uracil medium and incubated at 30 °C until appearance of colonies (2-3 days).

Table 25: Protocol for homologous recombination *in S. cerevisiae*.

Reagent	**[µL]**
Carrier DNA	10
Insert gene, purified (500 ng)	Variable
Vector, linearized and purified (100 ng)	Variable
LP-mix	500
DMSO	55

2.2.4.7 Transformation of *E. coli*

Plasmids were transformed into *E. coli* strains using heat shock transformation. 100 µL chemically competent *E. coli* cells were thawed on ice, mixed and added to 5 µL of ligation reaction or 20 ng of isolated plasmid DNA. The mix was first incubated on ice for 20 min and then shocked at 42 °C for 1 min. After 2 min incubation on ice 1 mL LB medium was added. Cells were shaken at 37 °C for 90 min, spun down (11,000 x g, 2 min) and plated on LB plates containing the respective antibiotics. Colonies formed overnight at 37 °C.

2.2.4.8 Transformation of *P. pastoris*

The expression vectors were transformed into *P. pastoris* by electroporation according to the guidelines of Invitrogen. Electro-competent *P. pastoris* X33 cells were prepared by inoculating a 50 mL pre-culture with one colony of X33 cells and growing overnight. The main culture was inoculated to a final OD_{600} of 0.2 and grown until an OD_{600} of 1.3 was reached. Cells were then pelleted (1,500 x g for 5 min) and re-suspended in 400 mL ice-cold sterile water. Cells were centrifuged three more times and re-suspended first in 250 mL water, second in 50 mL ice-cold 1 M sorbitol and finally in 1 mL sorbitol. 40 µg of plasmid were linearized with the restriction enzyme *Mss*I overnight and purified with the Gel/PCR purification kit. 20 µg linearized plasmid were mixed with 80 µL electro-competent *P. pastoris* cells and incubated on ice for 5 min. Electroporation cuvettes were pre-chilled on ice. Cells were transformed by pulsing the cells with 1,500 V for 5 ms. Immediately, 1 mL of ice-cold 1 M sorbitol was added. Cells were incubated at 30 °C for 1 h without shaking. After addition of 1 mL YPD medium cells were shaken for another 2 h at 200 rpm. 200 µL of cell suspension were plated on YPD-agar supplemented with 0.5 and 1 mg/mL zeocin. Single clones were re-stroked on separate YPD plates containing 0.5 mg/mL zeocin.

2.2.5 Protein expression and subcellular localization

2.2.5.1 Expression test of *P. pastoris* clones

Expression screenings were performed similarly to the protocol described in Ellinger *et al.* (2013). 50 mL minimal glycerol medium was inoculated with ¼ fully grown plate and shaken at 220 rpm and 30 °C for 24 h. Expression was induced by exchanging to minimal methanol

medium Therefore the culture was pelleted (3,000 x g, 10 min, 4 °C) and re-suspended in MM medium. After another 24 h, 10 mL of cells were harvested by centrifugation and re-suspended in 4 mL ice-cold extraction buffer. The cells were centrifuged again and re-suspended in 0.5 mL extraction buffer. Zirconia beads according to 1/3 of the total volume were added. Cells were disrupted by mixing 6 times for 1 min and chilling on ice between the disruption cycles. Cell debris was removed by centrifugation (12,000 x g, 5 min, 4 °C) and $MgCl_2$ was added to the supernatant to a final concentration of 10 mM. After incubation for 15 min on ice, the membranes were pelleted by centrifugation (90 min at 20,000 x g, 4 °C). The supernatant was removed and the membranes were re-suspended in extraction buffer. Protein expression was analyzed by SDS-PAGE and Western blotting.

2.2.5.2 Expression test of *E. coli* clones

The cloned constructs were transformed into the respective *E. coli* expression strain as described above. A 3 mL pre-culture containing the respective antibiotics was inoculated with a single *E. coli* colony and grown at 37 °C and 180 rpm overnight. 10 mL main culture in a 50 mL flask was inoculated to an OD_{600} of 0.2 and incubated at 37 °C and 180 rpm. When the OD_{600} had reached 0.7 the expression was induced by addition of 1 mM IPTG. Cells were grown for another 4 – 5 h. Every 60 min the OD_{600} was determined and a 1 mL sample was pelleted and stored at –20 °C. Expression was analyzed by SDS-PAGE and Western blotting.

2.2.5.3 Fermentation of *P. pastoris*

Cells were fermented in a 15 L glass bioreactor according to the Invitrogen Pichia Fermentation Process Guidelines. The bioreactor was connected to the steering unit, which automatically fed antifoam and ammonium hydroxide solution according to the data reported by the sensor technology. The carbon source (glycerol or methanol) was fed manually by a separate pump system. As preliminary work the bioreactor containing 6 L basal salt medium was autoclaved and run overnight without culture in order to saturate the medium with dissolved oxygen and to adjust the pH to 5.2 and the temperature to 30 °C. In addition two YPD plates fully grown with the *P. pastoris* expression clone were used to inoculate a 1 L MGY pre-culture. After incubation at 30 °C and 200 rpm overnight the complete pre-culture was used to inoculate the basal salt medium. 4.35 mL/L PTM_1 trace salts were added. During the whole fermentation process the dissolved oxygen is kept ≥ 20 %. If required, the feeding was reduced. In the glycerol batch phase the glycerol in the medium is consumed by the cells,

which can be monitored by a decrease in dissolved oxygen. When all glycerol is consumed the dissolved oxygen value rises to 100 %. Then 50 % glycerol, supplemented with 4.35 mL/L PTM_1 trace salts, was fed with a rate of 13 mL/h/L. After 5 h glycerol fed-batch phase the feeding was stopped. When the dissolved oxygen value had increased to 100 % expression was induced by feeding methanol with 3.6 mL/h/L for 48 h. Cells were harvested by centrifugation (5,000 x g, 10 min, 4 °C), frozen in liquid nitrogen and stored at -80 °C for subsequent use.

2.2.5.4 Sucrose gradient centrifugation

The localization of proteins expressed in *P. pastoris* was analyzed using a sucrose gradient. The gradient was created with the ÄKTAprime plus pump system generating a linear gradient ranging from 22 to 60 % sucrose in sucrose gradient buffer. The total volume of one gradient was 10 mL. 1 mL of crude membranes diluted to 2 mg/mL in 1 mL ice-cold hypo-osmotic buffer and was layered on the top of the sucrose gradient. Ultracentrifugation in a swing-out rotor (130,000 x g, 22 h, 4 °C, TST 41.14 rotor) was used to separate the different membrane species. The gradients were separated into 500 µL aliquots and analyzed by SDS-PAGE and Western blotting.

2.2.5.5 Confocal fluorescence microscopy

The construct pGSP18-eGFP-Ntag-*At*PDR8 was transformed in to *P. pastoris* and expressed as described above. A 50 mL MGY culture was inoculated with ¼ of a fully grown plate and incubated at 30 °C, 200 rpm for 24 h. The medium was exchanged by centrifugation (4,000 rpm, 5 min) and re-suspension of the cells in MM medium. Thereby protein expression was induced. After 24 h cells were harvested and mixed with 0.1 % (v/v) of the fluorescence stain SCRI Renaissance 2200 (SR2200) (Musielak et al., 2015). The mixture was pipetted onto a poly-L-lysine coated slide (Thermo Scientific) and covered with a coverslip. Images were taken on a Zeiss LSM880 microscope with Airyscan and a 63 x NA 1.4 objective. The SR-Airyscan mode (pixel size of 40 nm) was used for image acquisition and the ZEN software was used for automatic procession of the images. Figures were created using OMERO.figure (Allan et al., 2012). eGFP excitation was performed at 488 nm and SR2200 excitation at 404 nm. Images were taken with kind support of the Center for Advanced Imaging, Heinrich Heine University Düsseldorf.

2.2.6 Protein purification

2.2.6.1 Membrane preparation of *P. pastoris* cells for protein purification

100 g of *P. pastoris* were thawed on ice and re-suspended in 200 mL extraction buffer. The cells were passed twice with 2.5 kbar through a pre-cooled cell disruptor. The disrupted cells were centrifuged two times (15,000 x g, 30 min, 4 °C) in order to get rid of the cell debris. The supernatant was centrifuged at 125,000 x g and 4 °C for 90 min to pellet the membrane vesicles, which were then re-suspended in membrane buffer. The concentration was determined by measuring a dilution series with the NanoDrop™ spectrophotometer. Crude membrane vesicles were frozen in liquid nitrogen and stored at – 80 °C. In order to prepare plasma membrane vesicles, crude membrane vesicles were thawed on ice and diluted to 5 mg/mL. The mitochondria were precipitated by titrating the crude membranes to pH 5.2 with 18.5 % HCl. After 1 min the pH was titrated back to 7.2 with 5 M NaOH. Mitochondria were pelleted by centrifugation (7,000 x g for 10 min, 4 °C). The plasma membrane vesicles were collected by centrifugation at 125,000 x g and 4 °C for 90 min. Plasma membrane vesicles were frozen in liquid nitrogen and stored at – 80 °C. The concentration was determined as described above in this chapter.

2.2.6.2 Solubilization screening for PDR8

Detergents that possibly solubilize PDR8 were screened using the Dot Blot technique (Ellinger et al., 2013) in combination with the Detergent Solution Master Kit. All included detergents were dissolved in water to a concentration of 10 %. The solubilization screening was set up as follows: In a total volume of 200 µL membrane buffer the protein concentration was adjusted to 5 mg/mL. The respective detergent was added to a final concentration of either 1 % or higher, depending on the critical micellar concentration of the respective detergent (Appendix A1). In total 88 detergents were tested. All reactions were incubated at 4 °C for 1 h in a tube rotator. After centrifugation at 168,000 x g the supernatant was mixed in a ratio of 5:1 with SDS-PAGE loading dye. 5 µL were spotted on a nitrocellulose blotting membrane. After drying the membrane was blocked in 10 % milk powder in TBS-T followed by incubation in primary and secondary antibodies as described in chapter 2.2.2.3.

2.2.6.3 Solubilization for protein purification

Membrane vesicles were diluted to a final protein concentration of 5 – 7 mg/mL. For solubilization of crude membranes 1 % Fos-Choline-14 was added, for solubilization of plasma membranes 2 – 3 % of Fos-choline-14 were added. Solubilization either happened on a tube rotator at 4 °C or at 12 °C without shaking. The progress of solubilization was determined by the turbidity of the sample. When the solution was optically clear, insolubilized protein was removed by centrifugation at 125,000 x g and 4 °C for 45 min. When solubilization took more than 2 – 3 h additional detergent was added. The supernatant was used for purification.

2.2.6.4 Immobilized metal ion affinity chromatography of PDR8

A 5 mL HiTrap Chelating HP column was prepared as follows: Using a peristaltic pump, the column was rinsed with 5 column volumes water, then it was loaded with Ni^{2+} ions by rinsing with 100 mM $NiCl_2$, the column was washed again 5 column volumes water and then it was equilibrated with 5 column volumes of IMAC wash buffer. The Äkta™ liquid chromatography system was washed with water and equilibrated in IMAC wash buffer. Membrane vesicles were solubilized as described in chapter 2.2.6.3. Imidazole was added to a final concentration of 10 mM to the supernatant. The supernatant was loaded onto the HiTrap Chelating HP column with a flow rate of 1 mL/min. The column was washed with IMAC wash buffer (2 mL/min) until a stable baseline was reached. During loading and washing the flow-through was collected in 10 mL fractions. The protein was eluted with a gradient from 0 – 100 % elution buffer or the percentage of the elution buffer was increased in steps. The flow rate was 2 mL/min and 2 mL fractions were collected. Fractions were analyzed by SDS-PAGE and Western blotting.

2.2.6.5 Calmodulin affinity chromatography

Membrane vesicles were solubilized as described in chapter 2.2.6.3. After centrifugation the supernatant was rotated overnight at 4 °C with 1.5 mL calmodulin affinity resin and 2 mM $CaCl_2$. The resin was collected with a filter and washed with twenty volumes of protein buffer, supplemented with 2 mM $CaCl_2$. The protein was then eluted with 2 mM EGTA in five column volumes of protein buffer. 500 µL fractions were collected and protein

concentration was determined using the NanoDrop™ spectrophotometer. If the detergent was exchanged during purification the wash buffer and the elution buffer contained the new detergent. Fractions were analyzed by SDS-PAGE and Western blotting.

2.2.6.6 Size exclusion chromatography of PDR8

For size exclusion chromatography of PDR8 a Superdex™ 200 10/300 GL column was used. It has a base volume of 23.562 mL. The buffer and water used were filtered (0.2 µm) and degased. The protein sample was centrifuged at 100,000 x g for 30 min to remove precipitated protein. The Äkta™ liquid chromatography system was washed with H_2O, and then the column was connected and rinsed with 30 mL water. The flow rate was 0.3 mL/min. After equilibrating the column with 28 mL protein buffer the protein sample was injected. During sample separation 400 µL fractions were collected. Fractions were analyzed by SDS-PAGE and Western blotting.

2.2.6.7 TCA precipitation of proteins

25 % of ice-cold 100 % TCA solution was added to the volume of each protein sample. Samples were incubated on ice for 10 min. 500 µL of an ice-cold 10 % TCA solution were added and samples were incubated on ice for 20 min. After centrifugation (20,000 x g, 30 min, 4 °C) the supernatant was removed. The pellets were washed twice with 500 µL ice-cold acetone (20,000 x g, 10 min, 4 °C) and dried in a vacuum evaporator. Pellets were re-suspended in SDS-PAGE loading dye for SDS-PAGE analysis.

2.2.7 Reconstitution into liposomes

2.2.7.1 Preparation of liposomes

Liposomes were prepared similarly as described in Geertsma et al. (2008). 100 mg of lipids were dissolved in chloroform and dried in a rotary evaporator for at least 1 h at room temperature. 1 mL of diethyl ether was added and removed in a rotary evaporator for 3 h. For hydration of lipids 5 mL of membrane buffer was added and rotated overnight without vacuum. Liposomes were aliquoted and ultrasonicated for 10 min to form small, unilamellar vesicles. The aliquots were flash-frozen in liquid nitrogen and allowed to thaw at room

temperature. This was repeated another two times to generate large, multilamellar vesicles. Vesicles were stored at – 80 °C.

2.2.7.2 Destabilization screening of liposomes

Liposomes were thawed at room temperature and extruded eleven times through a 400 nm polycarbonate membrane in order to form large, unilamellar vesicles. Vesicles were diluted to 4 mg/mL with membrane buffer. In a 96 well plate 100 µL aliquots were destabilized with different detergent concentrations ranging from 0.25 to 20 mM of the respective detergent. After 90 min incubation at room temperature the plate was measured in a plate reader at wavelengths ranging from 330 to 595 nm. By plotting the absorption against the detergent concentration, the optimal detergent concentration for later reconstitution was determined, as described in Geertsma et al. (2008).

2.2.7.3 Reconstitution of PDR8 into liposomes

Liposomes were extruded as described above and diluted to 4 mg/mL with membrane buffer in a volume of 5 mL. The respective detergent was added to the concentration that was determined in the destabilization screening. After 90 min incubation at room temperature the purified and concentrated protein was added to the lipids in a ratio of 1:100. The mixture was incubated at 4 °C under rotation. After 1 h 200 mg biobeads were added to the reconstitution mixture. Another 200 mg were added after 30 min, after 1 h, the next day and after another 2 h the next day. In total 800 mg biobeads were added. The biobeads were removed with a filter and washed with 1 mL membrane buffer. Proteoliposomes were pelleted by centrifugation (30 min, 267,000 x g, 4 °C) and re-suspended in 500µL 50 mM Tris-HCl pH 7.2 (30 °C).

2.2.7.4 Floating Centrifugation

The success of the reconstitution was validated by floating centrifugation through an iodixanol gradient. First the 60 % iodixanol solution was diluted in 10 x membrane buffer to a concentration of 54 % iodixanol. The proteoliposomes were then mixed with the 54 % iodixanol solution to a final concentration of 30 % iodixanol in a volume of 900 µL. This solution was pipetted to the bottom of a centrifugation tube. Successively 900 µL of 25, 10

and 5 % iodixanol dilutions (in membrane buffer) were pipetted on top of the proteoliposomes. The last layer consisted of only buffer. The gradient was centrifuged at 20,000 rpm and 4 °C in TST 60.4 rotor for 8 h. By pipetting from the top to the bottom the gradient was divided in 4 fractions. The proteins in the fractions were precipitated with TCA and analyzed by SDS-PAGE and Western blotting.

2.2.8 TNP-ATP binding assay

Fluorescence measurements were preformed as described previously (Ernst et al., 2006). In a 2 mL quartz cuvette, 0.5 µM purified protein in protein buffer supplemented with 10 mM $MgCl_2$ was constantly kept at 30 °C. Fluorescence was monitored using a Fluorolog with slit widths set to 4 nm. TNP-ATP was excited at 409 nm and emission was detected from 520 to 580 nm. The fluorescence titration was performed by successively adding 1 µM TNP-ATP from a 1 mM stock solution. The measured total fluorescence upon TNP-ATP binding is described by equation 4. Parameters describing the binding are the dissociation constant (K_D) and the ligand number (N). F_{max} is the maximum fluorescence intensity upon binding of TNP-ATP to *At*PDR8. K_D and N were determined by nonlinear fitting of equation 4 to the experimental data. Q_1 and Q_2 are fluorescence constants and were determined by titration of TNP-ATP to buffer alone and fitting the data to the polynomial equation 3. With increasing TNP-ATP amounts the fluorescence does not remain proportional to the ligand concentration. The emitted fluorescence is partly absorbed, which is corrected by equation 3.

$$F_{buffer} = Q_1 L_0 + Q_2 L_0^2 \quad [3]$$

$$F_{total} = Q_1 L_0 + Q_2 L_0^2 + F_{max} \cdot \left(A - \sqrt{A^2 - 4 L_0 N P_0}\right) \quad [4]$$

with

$$A = \left(K_{D_L} + L_0 + N P_0\right) \quad [5]$$

and

L_0: *nucleotide concentration* Q_1, Q_2: *fluorescence constants*

F: *fluorescence* P_0: *protein concentration*

c_0: *protein concentration* N: *ligand number*

F_{max}: *maximal fluorescence upon TNP − ATP binding*

2.2.9 Transport assay

2.2.9.1 Expression of *S. cerevisiae* Pdr5

Two 100 mL pre-cultures were inoculated with the *S. cerevisiae* strain YRE1001 overexpressing wild-type *Sc*Pdr5 or the *Sc*Pdr5 E1036Q mutant, respectively. Both pre-cultures were shaken at 30 °C and 200 rpm overnight. The pre-cultures were used to inoculate a 2 L main culture (in a 5 L baffled flask) to an OD_{600} of 0.05. The cultures were incubated overnight at 25 °C and 200 rpm. When the OD_{600} had reached 1.5 200 mL boost medium were added to each flask. Cells were harvested at an OD_{600} of 3.6 by centrifugation at 8,000 x g and 4 °C for 10 min. Cells were re-suspended with 30 mL water, transferred into a 50 mL reaction tube and pelleted again. Cells were stored at -80 °C.

2.2.9.2 Plasma membrane preparation of *S. cerevisiae* Pdr5

All steps were performed on ice; centrifuges, glass beads and buffers were pre-chilled. Frozen cells from 4 L cell culture were re-suspended in 80 mL Pdr5 re-suspension buffer and filled into the container of the bead beater together with 200 mL glass beads. To minimize air space the container was filled to the top with buffer. The container was placed on the bead beater and covered with ice. Cells were disrupted in 5 cycles for 1 min with 1 min pause in between. The glass beads were removed with a glass filter; the beads were rinsed with 160 mL TAEG buffer. The cell suspension was centrifuged twice at 1000 x g for 5 min and once at 3000 x g for 5 min in order to remove un-cracked cells. Membranes were pelleted by centrifuging the supernatant at 20,000 x g for 40 min. The pellet was re-suspended in 20 mL TAE buffer for Pdr5. The concentrations of a dilution series were determined with the NanoDrop™ spectrophotometer. The mitochondria were precipitated by titrating the pH to 5.2 with 1 M sodium acetate. Mitochondria were removed by centrifugation at 7000 x g for 5 min. Immediately the pH was neutralized to 7.5 with 2.5 M Tris-acetic acid pH 7.5. Plasma membranes were pelleted at 26,500 x g for 30 min and re-suspended in 10 mL 50 mM Hepes pH 7. Plasma membranes were frozen in liquid nitrogen and stored at -80 °C.

2.2.9.3 *Sc*Pdr5 transport measurements

Different dilutions of the drug ketoconazole in DMSO were prepared. For each measurement 970 µL Pdr5 transport buffer were mixed with 30 µL *Sc*Pdr5 plasma membrane vesicles (protein concentration 1 mg/mL, either the wild type or the E1036Q mutant) in a quartz cuvette. To keep the influence of DMSO comparable, equal amounts of the dilutions were added to achieve the respective concentration of the drug. In addition, the maximal added volume of drug in DMSO was 0.2 %. The final concentrations of the drugs were 20, 50, 100, 200, 300, 400, 500, 600, 700 and 800 nM. Cuvettes were equilibrated at 35 °C for 10 min with stirring. In order to start the transport 50 µL of 200 mM ATP pH 7 were added to the cuvette. Rhodamine 6G transport was monitored with a Fluorolog III. The fluorescence was detected over time; the excitation wavelength was 529 nm, the emission wavelength 553 nm.

2.2.9.4 Membrane vesicle disruption tests

The transport reaction was set up similarly as described above. In a 1.5 mL reaction tube 970 µL Pdr5 transport buffer were mixed with 30 µL Pdr5 plasma membranes (protein concentration 1 mg/mL, either the wild type or the Pdr5 E1036Q mutant) and supplemented with 200 nM ketoconazole. After 5 min incubation at 35 °C the transport was started with addition of 50 µL of 200 mM ATP pH 7. After 60 min reaction the membrane vesicles were pelleted at 60,000 rpm in the rotor S100AT6. The supernatant was discarded and the pellet was washed twice wish Pdr5 transport buffer without ketoconazole. For vesicle disruption, the pellets were treated as described in Table 26. Samples were centrifuged at 60,000 rpm in the rotor S120AT3 and the supernatant was transferred to a new reaction tube for mass spectrometry analysis.

Table 26: Methods for disrupting the membrane vesicles.

Disruption method		**Pellets were resuspended in:**
Physical	Osmotic pressure	100 µL H_2O.
	Ultrasonication	100 µL H_2O and ultrasonicated for 1 h.
Chemical	Methanol	100 µL of 80 % methanol.

3 Results

3.1 Strategy for the *in vitro* characterization of the ABC transporter *At*PDR8

In vivo protein studies often involve the problem of different processes interfering with each other and thereby masking the effects caused by the target protein. This could complicate the interpretation of results and leave doubts about the reliability of data. In order to circumvent this, an *in vitro* approach was chosen for the characterization of the ABC transporter *At*PDR8. This approach in turn requires homogenous protein that can be produced in sufficient quantities in reasonable time. To meet these requirements, it was decided to overexpress *At*PDR8 in a heterologous system. Choosing the appropriate expression host is thereby not of minor importance. Heterologous overexpression of plant membrane proteins is often challenging because of the size of membrane proteins, their hydrophobicity, possible toxicity of the protein to the expression host, wrong localization, misfolding and/or lack of the proper post-translational modification(s) (Bernaudat et al., 2011, Gul et al., 2014, Crouzet et al., 2013, Lefevre et al., 2015). Since *At*PDR8 is a plant membrane protein a bacterial host seemed less suitable. Therefore the expression system *Pichia pastoris* was chosen. The methylotrophic yeast is a eukaryotic system with the ability to perform post-translational modifications and it was used before for successful overexpression of human full-size ABC transporters (Chloupkova et al., 2007, Ellinger et al., 2013). The complete strategy for the *in vitro* characterization is outlined in Figure 10. It involved first the cloning of the *AtPDR8* coding sequence into the expression vector. In this step affinity tags for later purification were fused to the protein. Overexpression was performed in a bioreactor, which allowed the production of the protein in larger amounts compared to shaking flask cultures. Overexpression was followed by protein purification. The purification protocols were established in this thesis. This included the choice of a detergent that was able to solubilize *At*PDR8 out of the membrane and the set up of an affinity chromatography protocol. Pure protein can be used for various *in vitro* approaches. In order to determine the substrates that are translocated by *At*PDR8 an approach was needed that not only gives information about the activity of the NBDs in presence of certain compounds, but also provides data about the actual transport process. Furthermore, *AtPDR8* mutant studies (Lu et al., 2015, Kim et al., 2010, Kim et al., 2007, Strader and Bartel, 2009) imply that not a single compound is transported, but several compounds. In addition to this, it is very likely, that some potential substrates have not been identified yet, since there are *AtPDR8* mutant phenotypes that cannot

be connected with the currently proposed substrates. Because of these reasons, an *in vitro* approach was needed that contained the determination of the transport characteristics as well as the screening of a large set of potential substrates. Reconstitution of the protein into liposomes followed by a vesicular transport assay could meet these requirements. The reconstitution of membrane proteins gives the advantage, that the protein is located in a lipid environment without the influences of detergents, which can be necessary for proper activity. By reconstituting into inside-out vesicles, the direction of transport is from the outside to the inside of the vesicles. This offers the possibility to add a mixture of substrates to the liposomes. If a compound is a substrate to the transporter, it is transported to the inside of the vesicles in presence of ATP (Glavinas et al., 2008, Krumpochova et al., 2012). With this strategy, all potential substrates are transported to the inside of the vesicles and adding mixtures of unknown composition, like for example root or cytoplasm extracts, even unknown substrates could be identified. The liposomes need to be opened in order to analyze the content by mass spectrometry (Krumpochova et al., 2012). In theory every transported compound should give a peak in the mass spectrum and the identity of the compounds can be determined by tandem mass spectrometry.

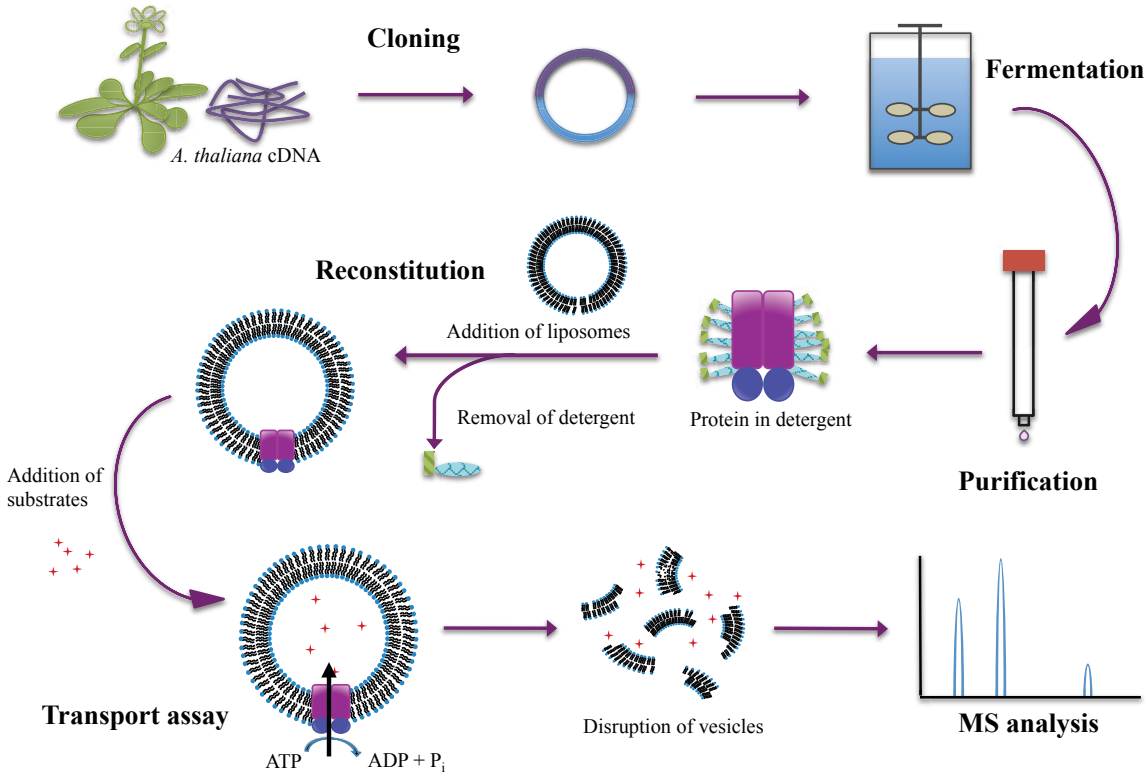

Figure 10: Strategy for the *in vitro* characterization of *At*PDR8. The gene is first amplified from *Arabidopsis thaliana* Col-0 cDNA and then cloned into an expression vector. The protein is expressed, purified and reconstituted into liposomes for the transport assay. After disruption of liposomes the transported compounds are analysed by mass spectrometry.

3.2 Cloning and expression of *At*PDR8

3.2.1 Overview of the cloning procedure and expression tests

In order to realize heterologous overexpression of *At*PDR8 the coding sequence had first to be cloned into an expression vector. Figure 11 depicts the strategy that was chosen. The gene was PCR-amplified from *A. thaliana* Col-0 cDNA and cloned into the pJET1.2/blunt vector for amplification in bacteria. The *AtPDR8* gene was then cloned into the *P. pastoris* expression vector pSGP18-2µ. Since there was no expression of *At*PDR8 in *P. pastoris,* the gene was also subjected to cloning for expression in other heterologous systems. This was only successful for the *E. coli* expression vector pET16b. For the other constructs different cloning strategies were applied but without success. Expression tests in *E. coli* showed the production of a truncated protein. This revealed that during transformation the *AtPDR8* coding sequence was spontaneously mutated and a stop codon was integrated. The same had happened in the pSGGP18-2µ-PDR8 construct. After correcting the sequence of both constructs by site directed mutagenesis still no expression was detected, neither in *P. pastoris* nor in *E. coli*. This lead to the idea to change the position of the affinity tags in the *P. pastoris* expression vector from the C-terminus to the N-terminus. The N-terminally tagged construct finally showed expression in *P. pastoris*. The process of cloning *AtPDR8* turned out to be complicated and several hurdles, like spontaneous mutations, had to be overcome. The cloning procedure and the expression tests are described in detail in the following chapters.

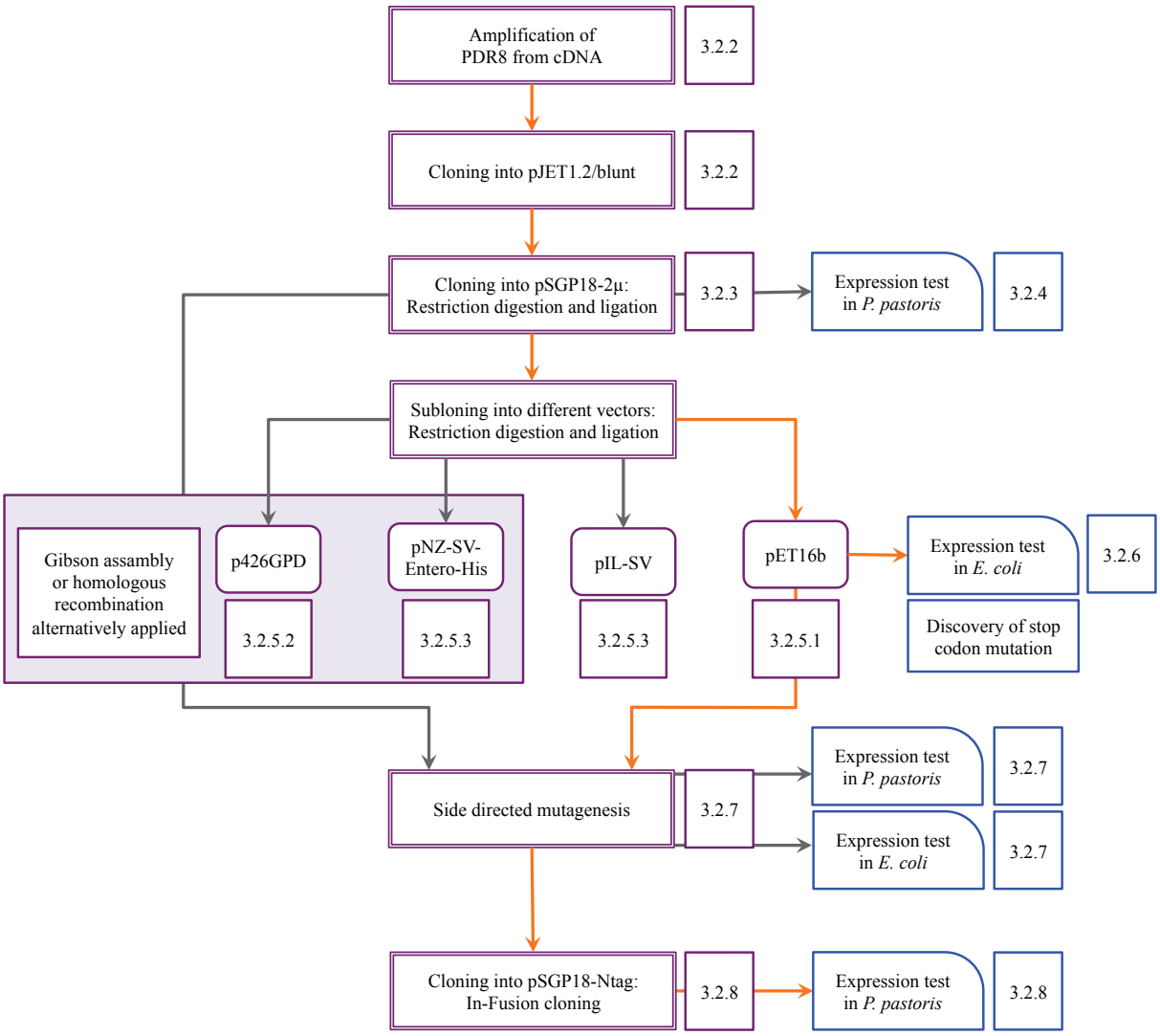

Figure 11: Strategy for cloning (purple boxes) and expression (blue boxes) of *At*PDR8. The numbers indicate the chapters in which the respective experiments are described. Successful steps are depicted in orange.

3.2.2 Amplification of *AtPDR8* from cDNA and cloning into pJET1.2/blunt

The *AtPDR8* coding sequence was amplified from *A. thaliana* Col-0 cDNA using PrimeStar GXL polymerase. The primers PDR8_1_FWD and PDR8_2_REV were used. The PCR product was purified by gel extraction and then blunt-end ligated into the vector pJET1.2/blunt. The ligation reaction was transformed into *E. coli* XL1-Blue cells and clones were selected on ampicillin. In order to check if the *AtPDR8* gene was integrated into the vector pJET1.2/blunt the isolated plasmids were digested with the restriction enzyme *Bgl*II. The enzyme cuts the insert out of the vector and the *AtPDR8* sequence itself is cut four times. That results in six fragments, which represent the pJET1.2/blunt vector of approximately 3,000 bp and five *AtPDR8* fragments of approximately 2,000 bp, 1,100 bp, 790 bp, 460 bp and 90 bp. Figure 12 shows the agarose gel electrophoresis of the fragments after *Bgl*II restriction digestion. The band pattern of sample MP 6 fits to the expected fragment sizes. The smallest fragment is not visible on the agarose gel. The plasmid sample MP 6 was positive, which was also confirmed by sequencing, and was therefore used for further cloning experiments.

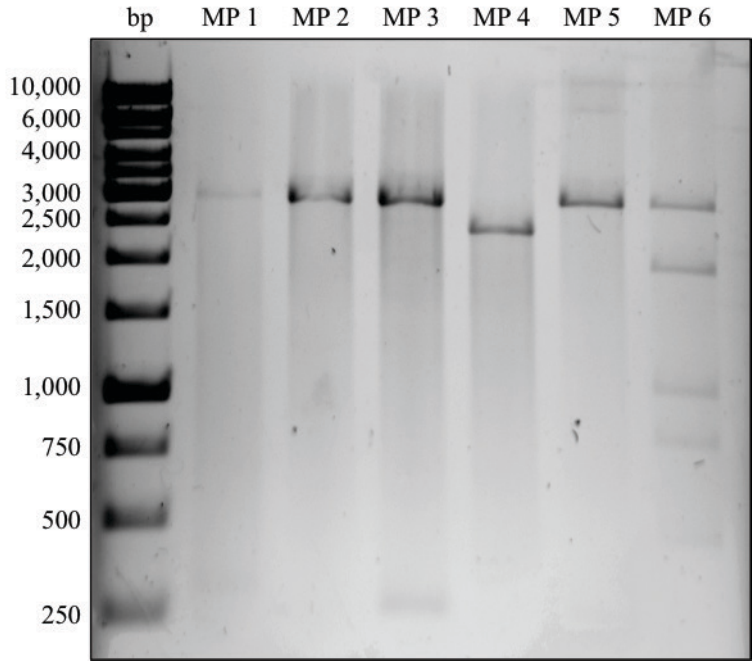

Figure 12: Agarose gel electrophoresis of isolated plasmids after *Bgl*II digestion. The cloning of *AtPDR8* into the vector pSGP18-2µ was successful for sample MP6. The left lane (bp) shows the loaded marker with the fragment sizes 10,000, 8,000, 6,000, 4,000, 3,500, 300, 2,500, 2000, 1,500, 1,000, 750, 500 and 250 bp. Lanes MP 1 to 6 display the loaded plasmid isolations 1 to 6. The band pattern of MP6 resembles the expected band pattern after *Bgl*II digestion.

3.2.3 Cloning of *AtPDR8* into the *P. pastoris* expression vector pSGP18-2µ

Figure 13 outlines the construct, which was supposed to be cloned, namely *AtPDR8* in the *P. pastoris* expression vector pSGP18-2µ. Genes integrated in this vector are controlled by the *alcohol oxidase I* (*AOX1*) promoter, which is a strong endogenous *P. pastoris* promoter. In *P. pastoris*, it controls the expression of the AOX protein, which is required for the methanol metabolism. The *AOX1* promoter is tightly regulated and inducible by methanol (Cregg et al., 2000). When *P. pastoris* is transformed with the expression vector, the target gene is integrated into the *P. pastoris* genome by homologous recombination of the *AOX1* promoter and terminator sequences. The vector contains furthermore the sequences of two affinity tags, which are the Calmodulin Binding Peptide (CBP) tag and the 6 x Histidin (6x His) tag, as well as a C3 cleavage site. Primers were designed to intergrade the *AtPDR8* coding sequence upstream and in frame with the tag sequences. With this strategy the tags were fused to the C-terminus of *At*PDR8.

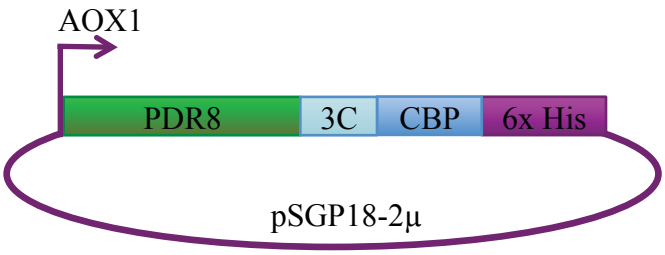

Figure 13: Schematic construct of *AtPDR8* (green) in the pSGP18-2µ vector backbone. The encoded protein is fused to a 6x His (purple box) and a CBP tag (dark blue) as well as a 3C cleavage site (light blue) at the C-terminus. The gene is controlled by the *AOX1* promoter (depicted by the arrow). The scale of the modules does not represent actual DNA-fragment sizes.

The *AtPDR8* gene was PCR-amplified from the construct pJET1.2/blunt-AtPDR8. The polymerase Phusion was used in combination with the primers PDR8_PacI-fwd and PDR8_SphI_rev. The primers included overhangs for fusing restriction sites for the enzymes *Pac*I and *Sph*I to the *AtPDR8* gene. The vector pSGP18-2µ was also PCR-amplified in order to linearize the plasmid and to add restriction sites to for *Pac*I and *Sph*I to the sequence (primers pSGP18-2µ.SphI.fw and pSGP18-2µ_PacI-2). The amplification of both fragments was successful (Figure 14). The *AtPDR8* gene has a size of approximately 4,420 bp and the linearized vector a size of 3,430 bp. Figure 14 indicates that the PCR product of the vector still contains the un-linearized template. Therefore the template was digested with the restriction enzyme *Dpn*I, which only cuts methylated DNA und thus not the PCR product.

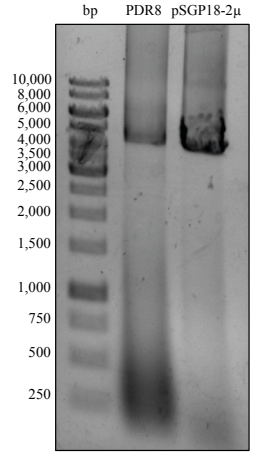

Figure 14: Agarose gel of the PCR products *AtPDR8* (middle lane) and the vector pSGP18-2µ (right lane) after amplification with Phusion polymerase. The left lane shows the marker with the fragment sizes 10,000, 8,000, 6,000, 4,000, 3,500, 300, 2,500, 2000, 1,500, 1,000, 750, 500 and 250 bp

Both PCR products were PCR purified and digested with the enzymes *Pac*I and *Sph*I. The digested fragments were gel purified and ligated. After transformation in *E. coli* XL1-Blue cells, plasmids were isolated from the respected clones, which were selected on zeocin. To check whether the insert was successfully ligated into the vector, the plasmids were digested with *Mss*I. In this reaction the plasmid was linearized by cutting the sequence once. This results in a fragment of approximately 9,000 bp. If only the vector was present, the fragment should be around 4,600 bp. Figure 15 shows the result of the cleavage after agarose gel electrophoresis. The sizes of the bands of the samples MP 3, 5, 6, 7, 9, 10, and 11 are in the expected range of 9,000 bp indicating that the insert *AtPDR8* was integrated into the vector pSGP18-2µ. The plasmid sample MP 11 was sent for sequencing, which confirmed the insertion of *AtPDR8*.

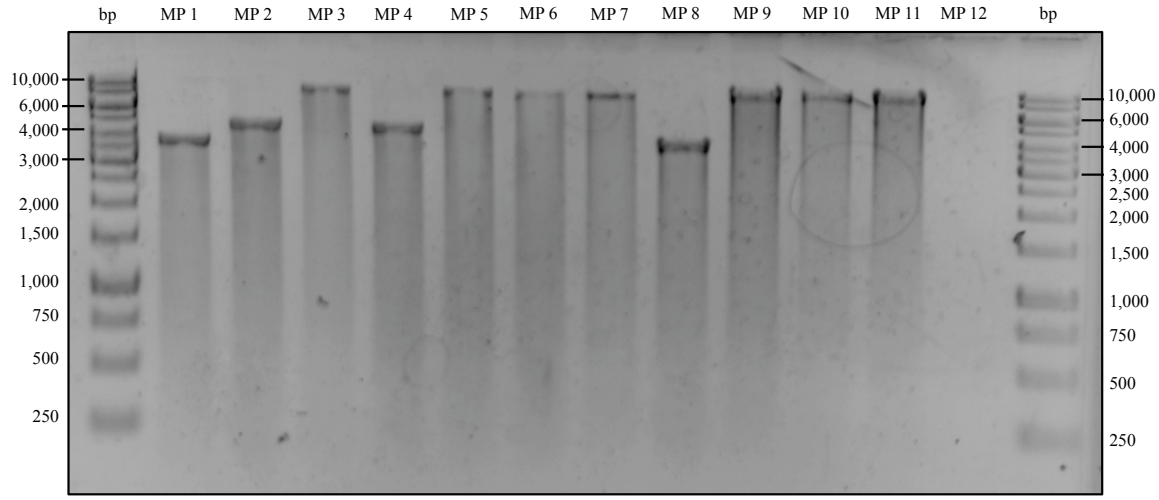

Figure 15: Agarose gel electrophoresis of the isolated plasmids pSGP18-2-*At*PDR8 digested with *Mss*I. Lanes MP 1 to 12 display the digested plasmid isolations 1 to 12.The samples MP3, 5, 6, 7, 9, 10 and 11 show the expected band size after successful integration of *AtPDR8* into the vector. The outer lanes (bp) show the loaded marker with the fragment sizes 10,000, 8,000, 6,000, 4,000, 3,500, 300, 2,500, 2000, 1,500, 1,000, 750, 500 and 250 bp.

3.2.4 Expression test of *At*PDR8 in *P. pastoris*

The positive plasmid pSGP18-2µ-*AtPDR8* was transformed into *P. pastoris*. Clones were selected on zeocin and screened in expression tests as described in Materials and Methods. None of the numerous tested clones showed expression. Figure 16 shows a typical Western Blot after an expression test. Membrane preparations of different time points after methanol induction were analyzed (lane M). As negative control samples of an un-induced culture (lane GY) were loaded for each time point, too. As positive control (+ ctrl) the human ABC transporter BSEP was expressed. The *At*PDR8 construct should display a signal at approximately 170 kDa. Only the positive control shows a band at its expected size. Expression conditions were altered by changing to buffered complex medium, screening for different expression temperatures and reducing the culture volume for better aeration. None of these methods resulted in expression of *At*PDR8.

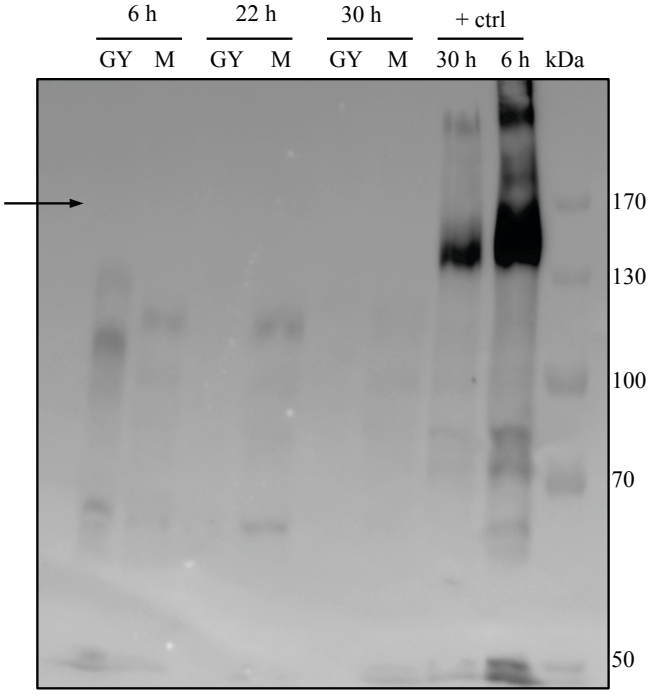

Figure 16: Western Blot analysis of the expression test of *At*PDR8 in *P. pastoris*. Expression was induced after 24 h with methanol (lanes M). At 6, 22 and 30 h after induction samples were analysed. Lanes GY shows the uninduced negative controls. + ctrl displays the expressed positive control BSEP at 6 and 30 h after induction. The right lane (kDa) shows the loaded marker with protein bands at 170, 130, 100, 70 and 50 kDa. Proteins were detected using anti-His antibody. The arrow marks the expected size of the *At*PDR8 protein band.

3.2.5 Cloning of *At*PDR8 for expression in *Saccharomyces cerevisiae*, *Lactococcus lactis* and *Escherichia coli*

Since the expression of *At*PDR8 in *P. pastoris* was not successful it was decided to clone *AtPDR8* into expression vectors for other heterologous overexpression systems, which were *S. cerevisiae*, *L. lactis* and *E. coli.* The respective constructs are shown in Figure 17.

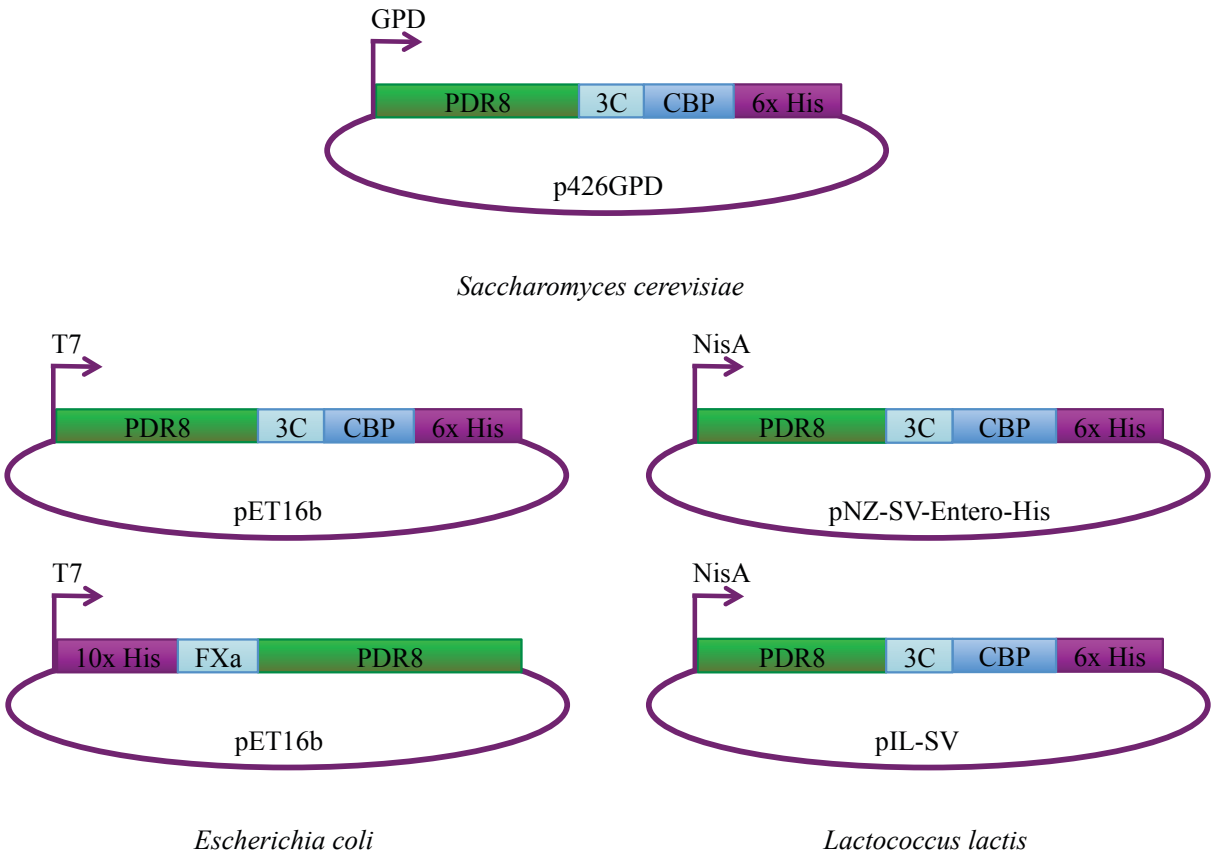

Figure 17: Scheme of the *AtPDR8*-constructs for the expression systems *E. coli*, *L. lactis* and *S. cerevisiae*. The *S. cerevisiae* construct comprises the p426GPD backbone and the *AtPDR8* sequence is integrated together with the 6x His (purple box), the CBP (dark blue) and the 3C (light blue) sequences from the pSGP18-2µ vector. The gene is controlled by the *GPD* promoter (depicted by the arrow). The same strategy was pursued for the *L. lactis* vectors pNZ-SV-Entero-His and pIL-SV and the *E. coli* vector pET16b, where again the *PDR8* coding sequence was integrated together with the sequences for the C-terminal tags. For the N-terminally tagged *E. coli* constructed the PDR8 gene was integrated without tag sequences and fused to the vector internal tags, which are a 10x His tag and a Factor Xa cleavage site. In the *L. lactis* plasmids the gene is controlled by the *NisA* promoter and in the *E. coli* vectors by the *T7* promoter. The scale of the modules does not represent actual DNA-fragment sizes.

3.2.6 Cloning into *E. coli* expression vectors

For expression in *E. coli*, two different constructs were planned. One construct with C-terminal tags and one with N-terminal tags. For the N-tagged construct the AtPDR8 coding sequence was PCR-amplified, gel purified and cloned into the pET16b expression vector so that the N-terminal 10 x His tag of the vector was in frame with the *AtPDR8* gene. Primers PDR8 XhoI FWD/PDR8 BamHI REV were used together with Phusion polymerase. The primers contained restrictions sites for *Xho*I and *BamH*I enabling cloning via restriction digestion and ligation. The vector already contained the respective restriction sites and was thereby directly digested. For the C-tagged construct the *At*PDR8 coding sequence was amplified together with the sequences of the affinity tags from the pSGP18-2µ-AtPDR8 construct. The primers PDR8 BamHI FWD and PDR8 XhoI REV contained restriction sites for *BamH*I and *Xho*I. The gene was then cloned into the pET16b expression vector not in frame with the vector tags. The fragments of the respective digestion reactions for the N-tagged and the C-tagged construct were ligated and transformed into XL1-Blue cells. The amplified plasmids were isolated and digested with *Xho*I and *BamH*I in order to check if the cloning was successful. The result of the cleavage for the two constructs is shown in Figure 18. If *AtPDR8* was integrated into the respective vector, two bands should be visible on the gel, representing the vector and the insert. For both ligations into pET16b, only one plasmid each shows a second band for the insert. These are the plasmids MP 6 (ligation into pET16b, N-terminal tags) and MP 4 (ligation into pET16b, C-terminal tags).

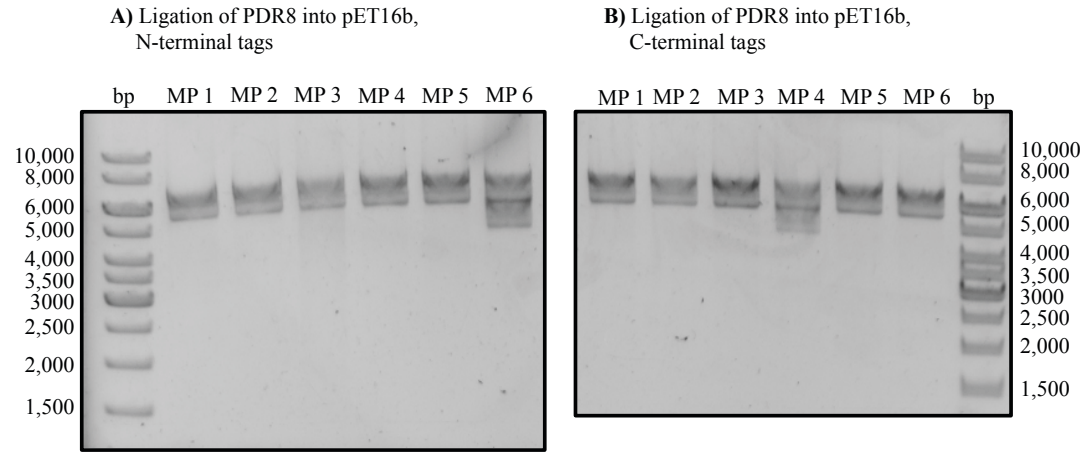

Figure 18: Agarose gels of the digested plasmids of *PDR8* ligated into pET16b. A) Ligation into pET16b with N-terminal tags. Only MP6 shows the expected band pattern after successful *PDR8* ligation. B) Ligation into pET16b with C-terminal tags. MP 4 shows the band pattern that confirms the PDR8 ligation. The lanes bp show the loaded marker with the fragment sizes 10,000, 8,000, 6,000, 4,000, 3,500, 300, 2,500, 2000, and 1,500 bp. Lanes MP 1 to 6 display the digested plasmid isolations 1 to 6 of the respective construct.

Sequencing the plasmids confirmed that the N-terminally tagged construct was indeed positive, but the sample with C-terminally tagged construct contained two plasmids. Additional clones of the transformation of the C-terminally tagged pET16b-*AtPDR8* construct were analyzed, but all isolated plasmids were lacking the *AtPDR8* insert (data not shown). The cloning experiment was therefore repeated for the C-terminally tagged construct. This time only one out of 12 clones had the *AtPDR8* gene integrated, however, the orientation of the gene in the vector was inverted (data not shown).

3.2.7 Cloning into the *S. cerevisiae* expression vector

The same strategy as for the C-terminal *E. coli* construct was applied for the *S. cerevisiae* vector p426GPD. The same primers were used as well as the same polymerase protocol. Figure 19 shows the agarose gel after digestion of the isolated plasmids with *Xho*I and *BamH*I. Since these enzymes remove the insert from the vector two bands should be visible on the gel if the integration of *AtPDR8* into p426GPD was successful. This is the case for the isolated plasmids MP 1, 2, 4, 5, and 6. Sequencing these plasmids revealed that the *AtPDR8* gene was integrated, but again the orientation was inverted.

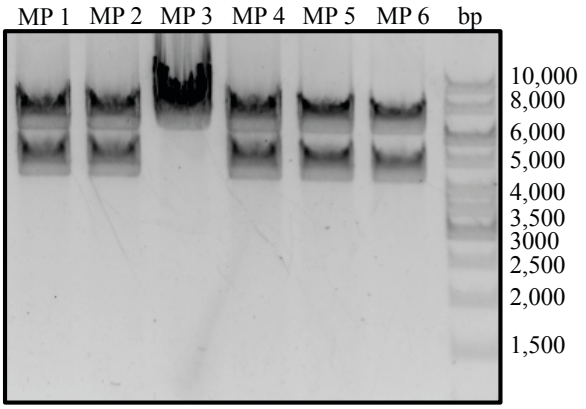

Figure 19: Agarose gel of the digested plasmids *PDR8* ligated into p426GPD. The most right lane (bp) displays the loaded marker with the fragment sizes 10,000, 8,000, 6,000, 4,000, 3,500, 300, 2,500, 2000 and 1,500 bp. Lanes MP 1 to 6 include the digested plasmid isolations 1 to 6.

Cloning of *AtPDR8* into p426GPD was therefore repeated, but was not successful as the insert *AtPDR8* was not present in any of the isolated plasmids (data not shown). Therefore the cloning strategy for the p426GPD construct was changed. In case of potential toxic effects that might prevent propagation of plasmids in *E. coli*, homologous recombination in *S. cerevisiae* was performed. This strategy has the advantages that it circumvents the amplification of plasmids in *E. coli* and the integration of the insert in the vector is performed *in vivo* in *S. cerevisiae*. *AtPDR8* was amplified together with the C-terminal tags from the pSGP18-2µ-*At*PDR8 template. The primers (Hom.Rek.PDR8FWD/REV) added overhangs to the sequence that were homologous to the flanking regions of insertion site in the p426GPD vector. The vector was linearized by PCR. The position of the primers (Lin.p426GPDFWD/REV) determined the insertion site of the *AtPDR8* gene. Agarose gel electrophoresis of the PCR products confirmed that the *AtPDR8* gene and the p426GPD vector were successfully amplified (Figure 20). Both samples were purified and heat shock transformed into *S. cerevisiae*. For selection the culture was plated on minus-uracil medium but no colonies formed. That indicates that the homologous recombination of the plasmid was not successful.

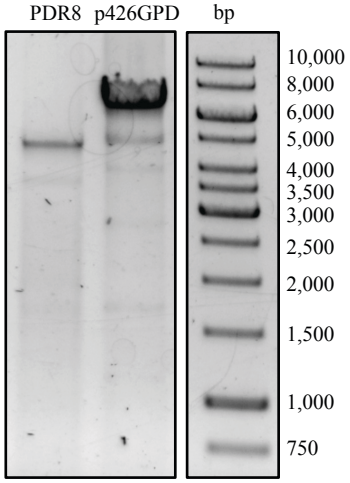

Figure 20: Agarose gel of the PCR products of PDR8 (left lane) and p426GPD (middle lane). The PCR primers fused overhangs to the sequences for homologous recombination. The right lane (bp) shows the DNA marker with the fragment sizes 10,000, 8,000, 6,000, 4,000, 3,500, 300, 2,500, 2000, 1,500, 1,000 and 750 bp.

3.2.8 Cloning into *L. lactis* expression vectors

For cloning *AtPDR8* into the *L. lactis* vector pIL-SV a blunt-end ligation was performed. Therefore the *AtPDR8* gene was PCR-amplified with the C-terminal tags from the pSGP18-2µ-*AtPDR8* construct. The primers PDR8FWD and TagsPDR8REV did not fuse any overhangs to the sequence. Figure 21 shows that the amplification of *AtPDR8* was successful; the agarose gel of the PCR product shows a band in a range that fits to the *AtPDR8* gene size (~ 4,400 bp).

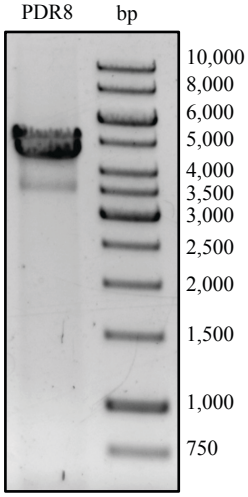

Figure 21: Agarose gel of the PCR product *PDR8* (left lane) amplified for cloning into pIL-SV. The right lane (bp) shows the DNA marker with the fragment sizes 10,000, 8,000, 6,000, 4,000, 3,500, 300, 2,500, 2000, 1,500, 1,000 and 750 bp.

The PCR product was purified. The expression vector pIL-SV was linearized by digestion with *Not*I. The resulting single-stranded overhangs were removed by blunting. The purified PCR product and the blunt-ended vector were ligated and transformed into *E. coli*. Plasmids were isolated and analyzed by *Nhe*I digestion and agarose gel electrophoresis. Both the AtPDR8 gene and the vector pIL-SV contain one restriction site for *Nhe*I. That means if the gene was integrated two bands should appear on the gel (7,233 and 3,936 bp). Figure 22 shows only one band between 6,000 and 8,000 bp on the agarose gel. The band represents the linearized vector (6,760 bp) meaning the insert was not present in all of the isolated plasmids. Repeating the whole experiment gave the same result (data not shown) showing that the background of non-cloned vectors is very high.

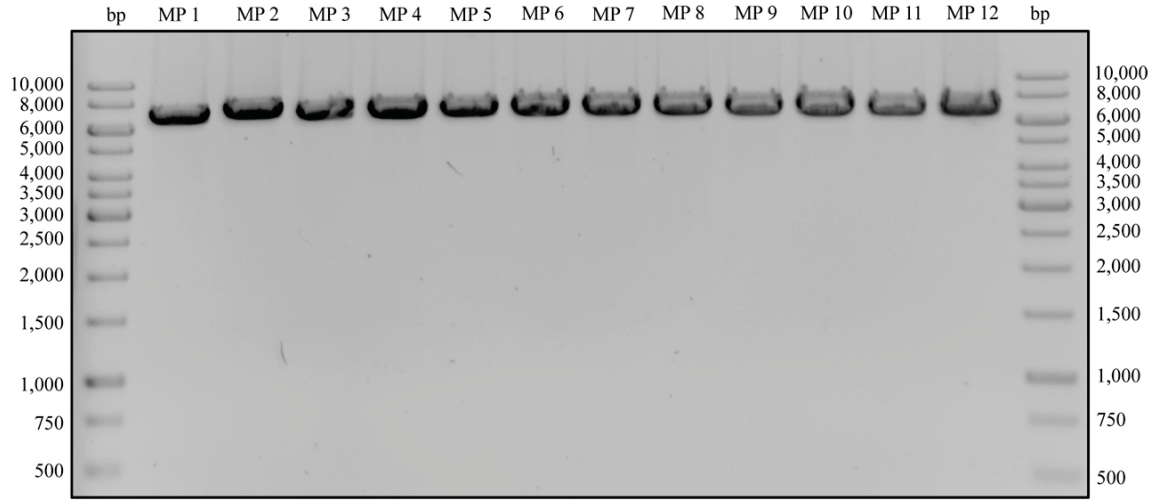

Figure 22: Agarose gel of the isolated plasmids of *PDR8* cloned into pIL-SV and digested with *Nhe*I. The lanes MP1 to 12 show the digested plasmid isolation 1 to 12. In all plasmid isolations the bands represent the vector without the *PDR8* insert. The two outer lanes (bp) show the DNA marker with the fragment sizes 10,000, 8,000, 6,000, 4,000, 3,500, 300, 2,500, 2000, 1,500, 1,000, 750 and 500 bp.

Alternatively, it was also tried to clone the *AtPDR8* gene into the *L. lactis* expression vector pNZ-SV-Entero-His. Here two cloning strategies were followed. On the one hand the cloning with restriction digestion and ligation and on the other hand the Gibson Assembly cloning. For restriction digestion and ligation, the *At*PDR8 gene plus the C-terminal tags were PCR-amplified by Phusion polymerase and with the primers EcoRIPDR8pNZFWD and NotIPDR8pNZREV, which added restrictions sites for the enzymes *Eco*RI and *Not*I to the *AtPDR8* sequence. The PCR was successful as Figure 23 proofs. The size of the PCR product conforms to the theoretical size of *AtPDR8* (~ 4,400 bp). After gel extraction the PCR product as well as the purified vector pNZ-SV-Entero-His were digested with *Eco*RI and *Not*I and ligated. The ligation reaction was transformed into XL10-Gold cells and the plasmids of the different clones were isolated. Agarose gel electrophoresis of the isolated plasmids shows that only the vector pNZ-SV-Entero-His was transformed (Figure 24). The insert *AtPDR8* is missing. The pNZ-SV-Entero-His-AtPDR8 construct would have a size of 10,425 bp. The vector alone has a size of 6015 bp, which fits to the band pattern seen on the gel. The gel shows the different forms of plasmids run on an agarose gel. These are the linearized plasmid, which runs exactly at its predicted size (~ 6,000 bp), the relaxed plasmid, which is kind of bulky and runs above its predicted size and the supercoiled plasmid, which is very compact and therefore runs faster than the linearized form and shows a band below 6,000 bp.

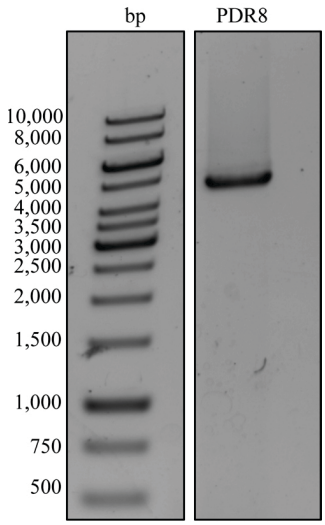

Figure 23: Agarose gel of *PDR8* PCR-amplified for the cloning into pNZ-SV-Entero-His. The right lane (PDR8) displays the *PDR8* PCR product. The left lane (bp) shows the DNA marker with the fragment sizes 10,000, 8,000, 6,000, 4,000, 3,500, 300, 2,500, 2000, 1,500, 1,000, 750 and 500 bp.

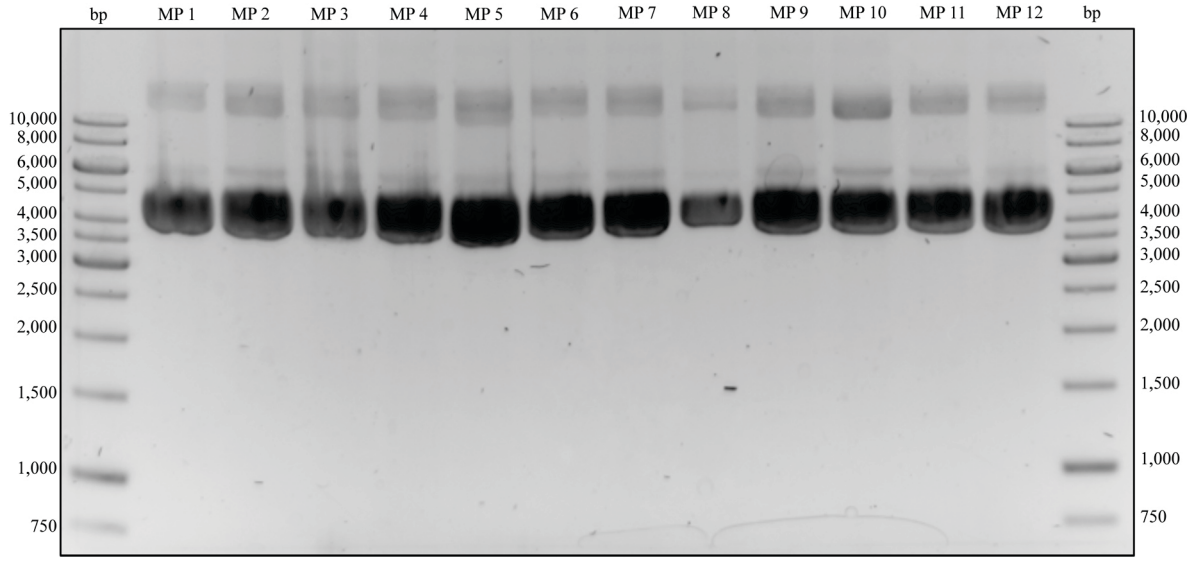

Figure 24: Agarose gel of the isolated plasmids after cloning of *PDR8* into the vector pNZ-SV-Entero-His. Lanes MP1 to 12 display the loaded plasmid isolations 1 to 12. The outer lanes show the DNA marker with the fragment sizes 10,000, 8,000, 6,000, 4,000, 3,500, 300, 2,500, 2000, 1,500, 1,000, and 750 bp.

Other than restriction digestion and ligation, Gibson Assembly allows the fusion of DNA fragments in a single, isothermal reaction by using a combination of an exonuclease, a polymerase and a ligase. The exonuclease digests the 5'-ends of two homologous sequences. The resulting sticky ends anneal and the polymerase fills in the remaining gaps. Finally a ligase closes the nicks.

The *AtPDR8* gene with the C-terminal tags was PCR-amplified with primers (PDR8InFuspNZFWD/PDR8InFusTagsRE) adding overhangs to the gene that were homologous to the pNZ-SV-Entero-His vector. The vector was linearized by PCR reaction with the primers Lin.pNZ-FWD/REV. Figure 25 shows the agarose gel of the PCR products. The *AtPDR8* sample as well as the vector sample shows a band at the expected fragment size of approximately 4,400 and 6,000 bp, respectively.

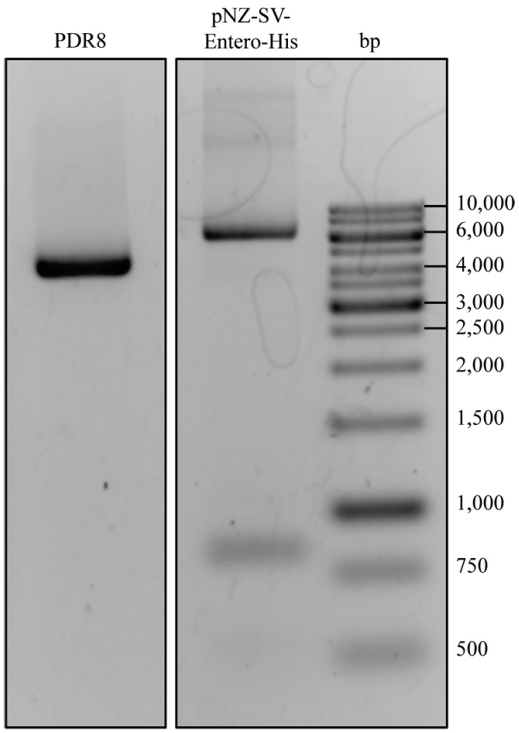

Figure 25: Agarose gel of the PCR products of *AtPDR8* (left lane) and the vector pNZ-SV-Entero-His (middle lane) for Gibson Assembly cloning. The right lane (bp) displays the DNA marker with the fragment sizes 10,000, 8,000, 6,000, 4,000, 3,500, 300, 2,500, 2000, 1,500, 1,000, 750 and 500 bp.

Because there was an additional band in the vector sample the PCR products were gel purified. Both fragments were incubated with the Gibson mastermix (see Materials and Methods) and transformed into DH5α cells. Clones were selected on kanamycin. A total of 19 colonies had formed, which were all checked for the integration of the *AtPDR8* gene by colony PCR. The PCR was performed with primers (PDR8FWD and TagsPDR8REV) that amplified the full-length *AtPDR8* sequence. If a clone is positive, the agarose gel should therefore show a band at approximately 4,400 bp. Figure 26 shows that the clones 6, 15, 17, 18 and 19 display bands at the expected size, however, additional bands appeared. That indicated that the primers did bind more than once. In fact, sequencing the isolated plasmids confirmed that wrong fragments were integrated into the expression vector, since none of the *AtPDR8* sequencing primers was able to bind to the plasmid sequences.

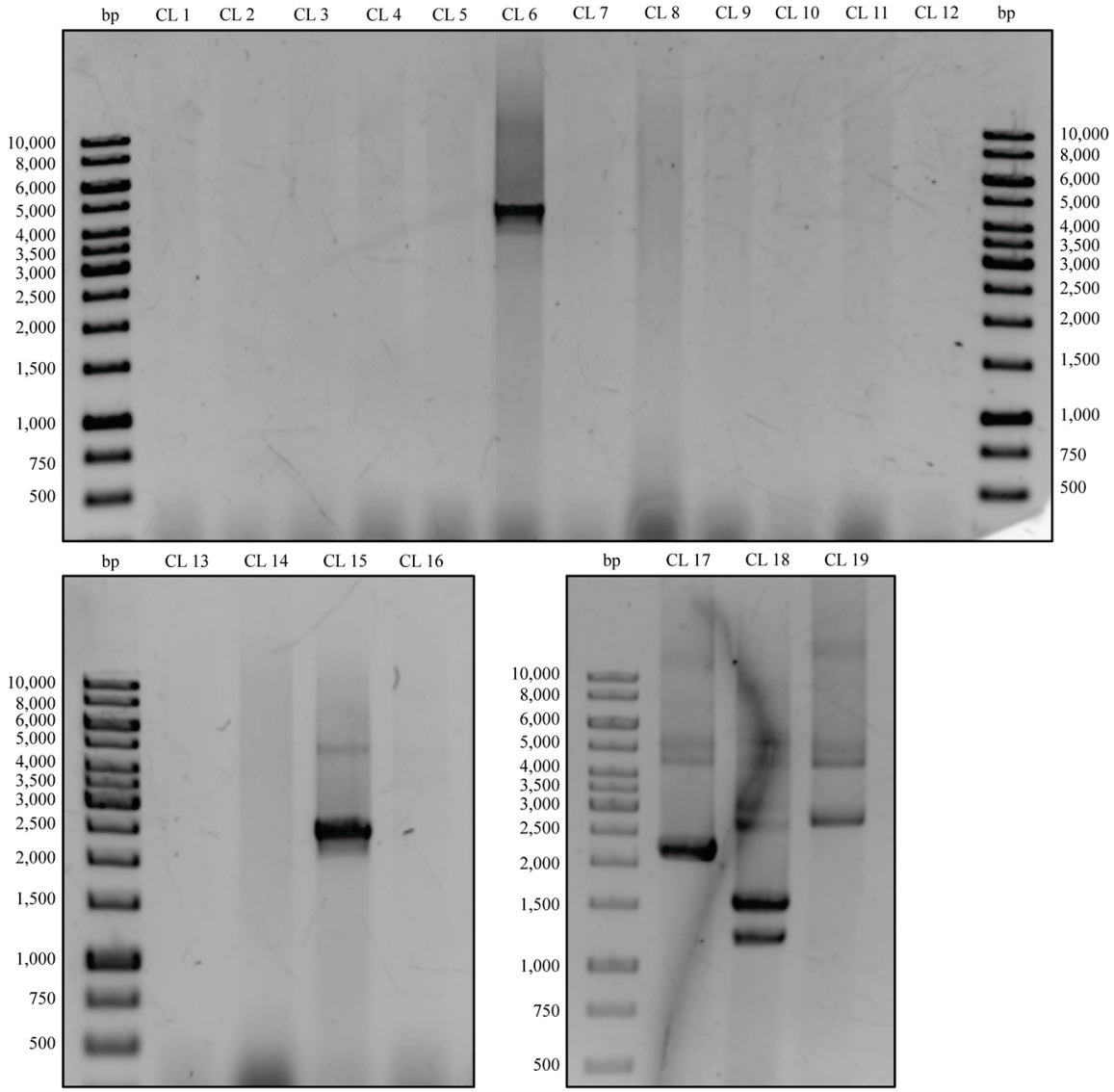

Figure 26: Agarose gel of the colony PCR products after Gibson Assembly cloning of *AtPDR8* into pNZ-SV-Entero-His. Lanes CL 1 to 19 show the PCR products of the *E. coli* clones 1 to 19. The respective lanes bp display the bands of the DNA marker with the fragment sizes 10,000, 8,000, 6,000, 4,000, 3,500, 300, 2,500, 2000, 1,500, 1,000, 750 and 500 bp.

3.2.9 Expression test of N-tagged *At*PDR8 in *E. coli* reveals spontaneous mutations

The positive plasmid pET16b-*AtPDR8* MP 6 was transformed into the *E. coli* BL21(DE3) expression strain. Expression was induced with IPTG and samples of different time points were analyzed by SDS-PAGE and Western Blotting. Figure 27 shows the Western Blot of the expression test of two different clones. Clone 1 shows protein bands of approximately 40 kDa at 1, 3 and 4 h after induction. The predicted size of the expressed *At*PDR8 construct is about 170 kDa. Testing additional clones did not provide successful expression of *At*PDR8 (data not shown). This raised the assumption that a truncated protein was expressed instead of the full-length *At*PDR8 construct. Sequencing the utilized plasmid again revealed that during a re-transformation step a stop codon was inserted into the *AtPDR8* codon sequence at 1,140 bp. Furthermore, mutations were discovered that result in four amino acid substitutions in the *At*PDR8 protein sequence compared to the reference sequence (Huala et al., 2001). This leads to the expression of the N-terminal 380 amino acids, which form a protein of approximately 40 kDa. The same had happened with the pSGP18-2µ-*AtPDR8* construct, but because of the C-terminal tagging the possible expression of a truncated protein was not detectable by Western Blotting.

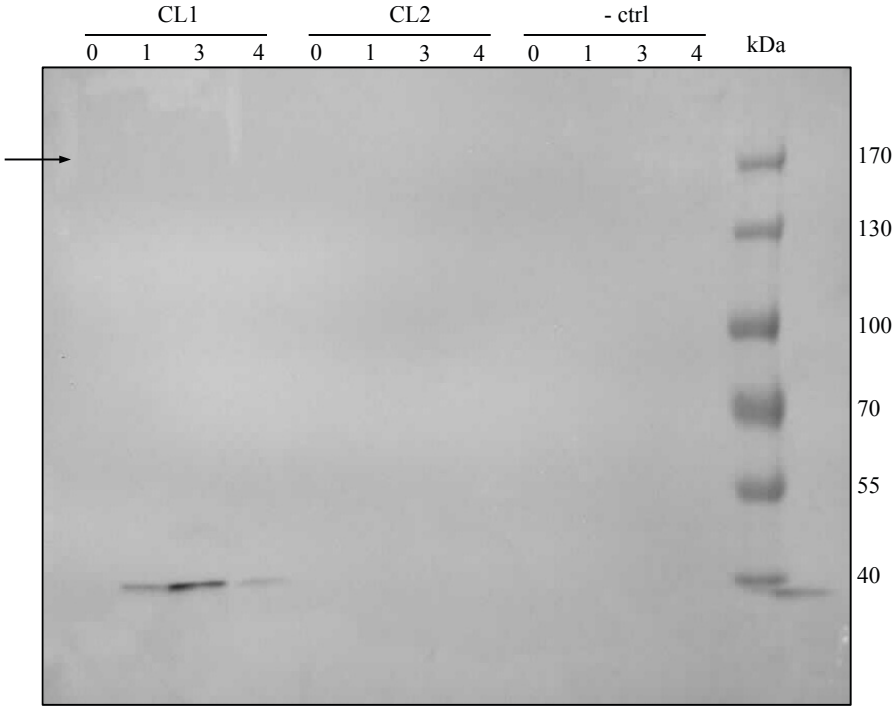

Figure 27: Western Blot analysis of the expression test of N-tagged *At*PDR8 in *E. coli* Bl21(DE3). Samples of two clones (CL1 and CL2) were analysed at 0, 1, 3 and 4 h after induction with IPTG (depicted by the respective numbers 0 - 4). Cells with the empty vector were grown as negative control (- ctrl). The most right lane shows the protein marker bands: 170, 130, 100, 70, 55 and 40 kDa. Proteins were detected using anti-His antibody. The arrow marks the expected size of the *At*PDR8 protein band.

3.2.10 Rectification of the stop codons by site directed mutagenesis

The *AtPDR8* coding sequence of the positive expression constructs pET16b-*AtPDR8* and pSGP18-2µ-*AtPDR8* was rectified by site directed mutagenesis PCR. Therefore the complete circular plasmid was PCR-amplified with primers (PDR8 SiDiMu FWD/REV) that contain mismatching bases and thereby insert mutations in the PCR product sequence. The PCR was performed at different annealing temperatures in order to screen for the optimal annealing temperature. Figure 28 A) shows the agarose gel of the PCR products. Most PCR product was produced at 62.0 °C. The PCR product was digested with *Dpn*I to remove the template and then transformed into XL1-Blue cells. Plasmids were isolated from different clones and linearized by digestion with *Bam*HI. Figure 28 B) shows the result of the agarose gel electrophoresis after the restriction digestion. Except for plasmid MP 3, all plasmid preparations contained fragments of the correct band size of ~ 10,100 bp (pET16b-*AtPDR8*). Plasmid preparations MP 1, 5, 6, 8 and 9 were sequenced. The preparations MP 1 and 9 contained several repetitions of the primers, but the other plasmid preparations, MP 5, 6 and 8, were positive as they contained the correct *AtPDR8* coding sequence without stop codons. The site directed mutagenesis was repeated with the pSGP18-2-µ-*AtPDR8* construct by using the same protocol with the same primers. Figure 28 C) proofs that the mutagenesis was successful; the agarose gel shows bands at the expected size of the construct (~ 9,000 bp). Both rectified constructs were tested for expression in the respective expression system, but no expression was detected in any system by Western Blotting (data not shown). That indicates that the expression of the truncated *At*PDR8 was successful, but not the one of the full-length protein.

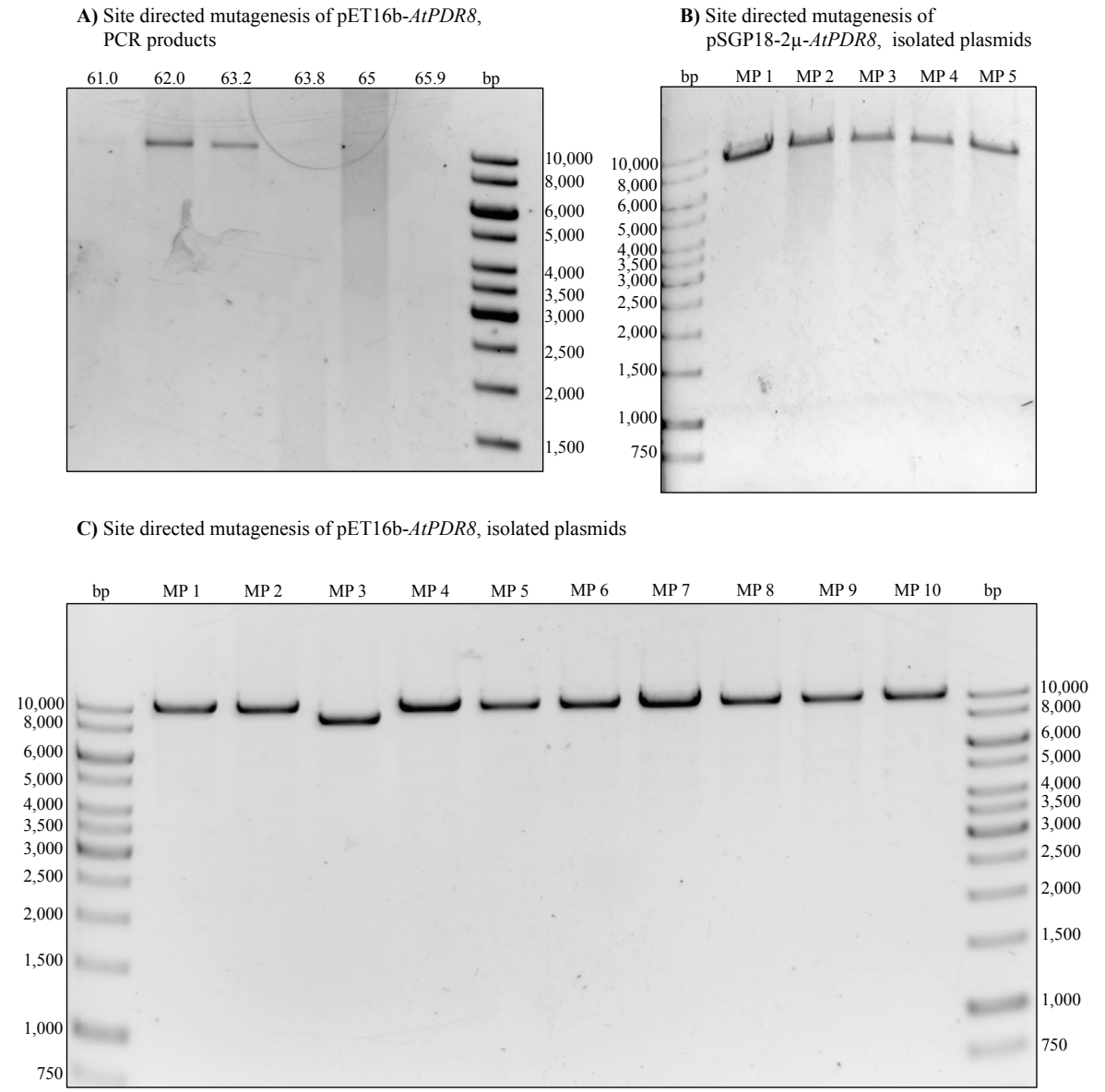

Figure 28: Site directed mutagenesis of *AtPDR8* in pET16b and in pSGP18-2µ. A) Agarose gel of the PCR product after side directed mutagenesis PCR of pET16b-*AtPDR8*. The numbers of the different lanes show the annealing temperatures at which the respective PCR was performed. B) Agarose gel of the isolated plasmids pSGP18-2µ-*AtPDR8* after linearization with *Mss*I. C) Agarose gel of the isolated plasmids pET16b-*AtPDR8* after digestion with *Bam*HI. Lanes labelled with MP 1 to 6 or 1 to 10, respectively, show the linearized plasmids of the respective constructs. Lanes labeled with bp display the DNA marker with the fragment sizes 10,000, 8,000, 6,000, 4,000, 3,500, 300, 2,500, 2000, 1,500, 1,000 and 750 bp.

3.2.11 Changing the position of the affinity tags enables expression in *P. pastoris*

Apart from changing to a different expression system, another strategy to realize *At*PDR8 expression was to change the tag position. Possibly, the position of the tag was important for detectable expression in *P. pastoris*. In order to check this hypothesis, expression was tested with the N-terminally tagged pSGP18-Ntag-AtPDR8 construct, which was kindly provided by Dr. Diana Kleinschrodt, Institute of Biochemistry, Heinrich-Heine University Düsseldorf. The pSGP18-Ntag vector contains a 10 x Histidin tag and a CBP tag as well as a C3 cleavage site. The *AtPDR8* sequence was integrated into the vector via In-Fusion reaction. The construct is depicted in Figure 29.

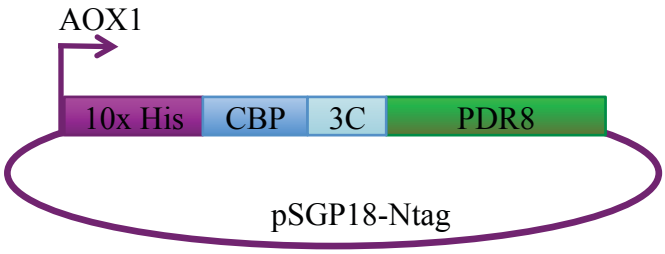

Figure 29: Scheme of the N-terminally tagged construct of *AtPDR8* in the vector pSGP18-Ntag. The *AtPDR8* gene (depicted in green) is fused to the sequences of a 10x His (purple box) and a CBP tag (dark blue) as well as a 3C cleavage site (light blue) at the N-terminus of the encoded protein. The scale of the modules does not represent actual DNA-fragment sizes.

The vector was transformed into *P. pastoris* and 10 clones were tested for expression. The measured OD_{600} values change marginally after induction with methanol (Table 27). The reason is the slow methanol metabolism of the transformed cells compared to non-transformed cells. In *P. pastoris*, methanol is metabolized by oxidation to formaldehyde, which is then further processed. The reaction is catalyzed by the alcohol oxidase. The *P. pastoris* genome comprises to genes that encode for AOX, the *AOX1* and the *AOX2* gene. The X33 strain is a Mut^S (methanol utilization sensitive) strain. Recombination of the plasmid DNA into the *AOX1* locus knocks out the *AOX1* gene. The cells then rely on the *AOX2* gene for the methanol metabolism. The *AOX2* promoter displays weaker expression compared to the strong *AOX1* promoter. This results in hardly any cell growth after induction with methanol.

Table 27: OD_{600} values of the different *P. pastoris* clones screened for *At*PDR8 expression. OD_{600} was determined 24 and 48 h after induction of expression with methanol. As positive control the human ABC transporter BSEP was expressed and as negative control cells transformed with the empty vector pSGP18-Ntag were grown.

Number of *At*PDR8 clone	OD_{600} 24 h after induction	OD_{600} 48 h after induction
1	14.1	14.6
2	12.9	14.4
3	11.1	12.1
4	12.1	12.2
5	12.4	12.5
6	13.2	14.4
7	12.8	13.5
8	11.7	11.8
9	12.8	12.4
10	10.2	10.7
Positive control BSEP	14.3	15.9
Negative control pSGP18-Ntag	12.6	14.1

Figure 30 shows the Western Blot of the isolated membranes of the clones 24 h after induction of expression. As positive control the human transporter BSEP was expressed (+ ctrl), the negative control was the transformed empty vector pSGP18-Ntag (- ctrl). All of the 10 tested clones displayed expression of N-terminally tagged *At*PDR8 as Figure 30 proofs. The results indicate that the position of the affinity tag is important for detectable *At*PDR8 protein expression in *P. pastoris*.

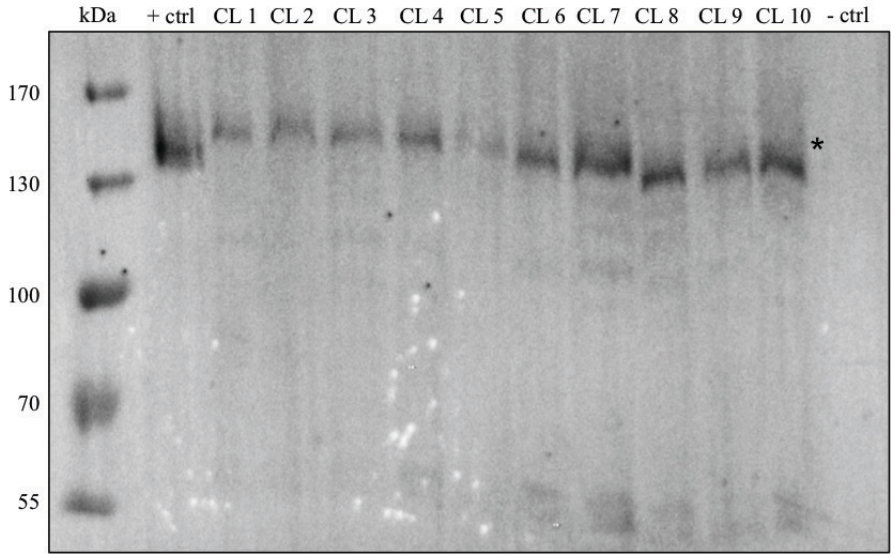

Figure 30: Western Blot analysis of the expression test of N-terminally tagged *At*PDR8 in *P. pastoris*. After 24 h glycerol feeding the expression was induced with methanol. 24 h after induction cells were harvested and the membranes were isolated. Membrane fractions of the different clones were run on SDS-PAGE and after Western Blotting *At*PDR8 was detected with anti-His antibody (marked with the asterisk). The outer left lane shows the protein marker bands: 170, 130, 100, 70, 55 and 40 kDa.

3.3 Subcellular localization of *At*PDR8 expressed in *P. pastoris*

In regard to functional studies, the correct localization of a heterologously overexpressed protein is important, since correct targeting implies correct folding. To check the localization of *At*PDR8 expressed in *P. pastoris*, centrifugation of the isolated crude membranes through a continuous sucrose gradient was performed. The different membrane species are thereby separated by retardation in different sucrose concentrations. Figure 31 shows the Western Blot of the different fractions of the linear sucrose gradient. The *At*PDR8 signal was detected in the fractions with higher sucrose concentrations. As marker proteins the plasma membrane proteins *Sc*Pdr5 in *S. cerevisiae* membranes (Egner et al., 1995) and the human MDR3 expressed in *P. pastoris* (Ellinger et al., 2013) were used. The three proteins co-localized in the same fractions indicating that *At*PDR8 is located in the plasma membrane in *P. pastoris*, which also implies that the protein is processed correctly in *P. pastoris*.

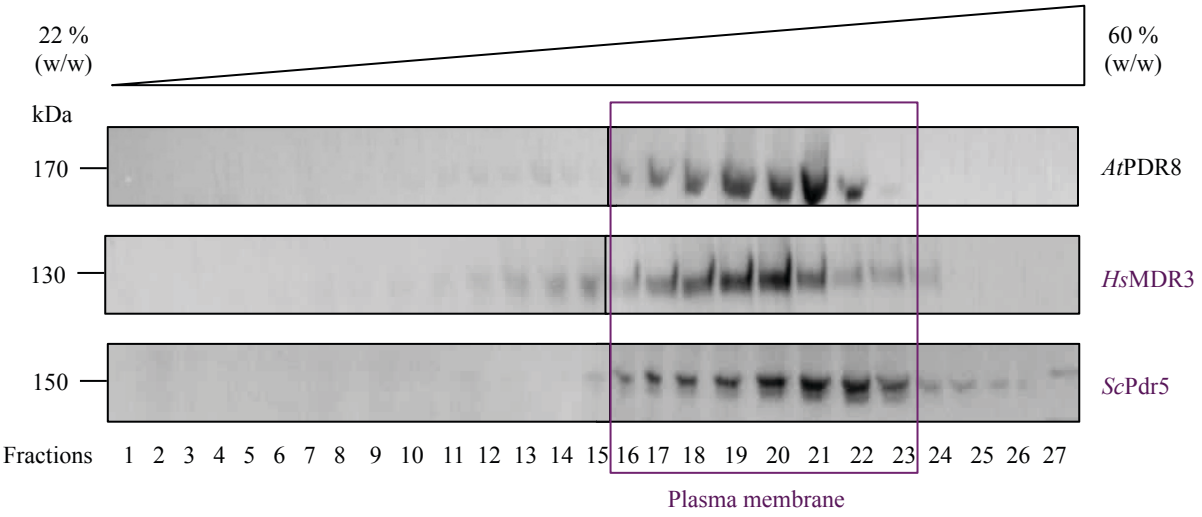

Figure 31: Subcellular localization of *At*PDR8 in *P. pastoris* determined by sucrose gradient centrifugation. The protein *At*PDR8 expressed in *P. pastoris* (top row) co-localizes with human MDR3 (middle row), which was also expressed in *P. pastoris* and with *Sc*Pdr5 (bottom row), which was expressed in *S. cerevisiae*. The sucrose concentration is indicated by the triangle. Numbers below the Western Blots display the fractions of the linear sucrose gradient. The position of the plasma membranes in the gradient is indicated by the rectangle. Proteins were detected with anti- His and anti-Pdr5 antibodies. See Appendix A2 for complete Western Blots.

As an alternative approach to determine the localization of *At*PDR8 in *P. pastoris* the eGFP-*At*PDR8 fusion protein was expressed and analyzed by confocal fluorescent microscopy. To mark the cell margin the cell walls of *P. pastoris* were stained with the cell wall marker SCRI Renaissance 2200 (SR2200). Upon excitation the eGFP gave a ring-like signal that was partially localized at the cell margin (Figure 32). In some areas the eGFP signal almost overlaps with the SR2200 signal. However the eGFP signal also appears in structures inside

the cells indicating the fusion protein was also located in other cell compartments. Cells that did not express the GFP fusion protein did not show any fluorescence signal (data not shown). The fluorescent microscopy only partially supports the result of the sucrose gradient.

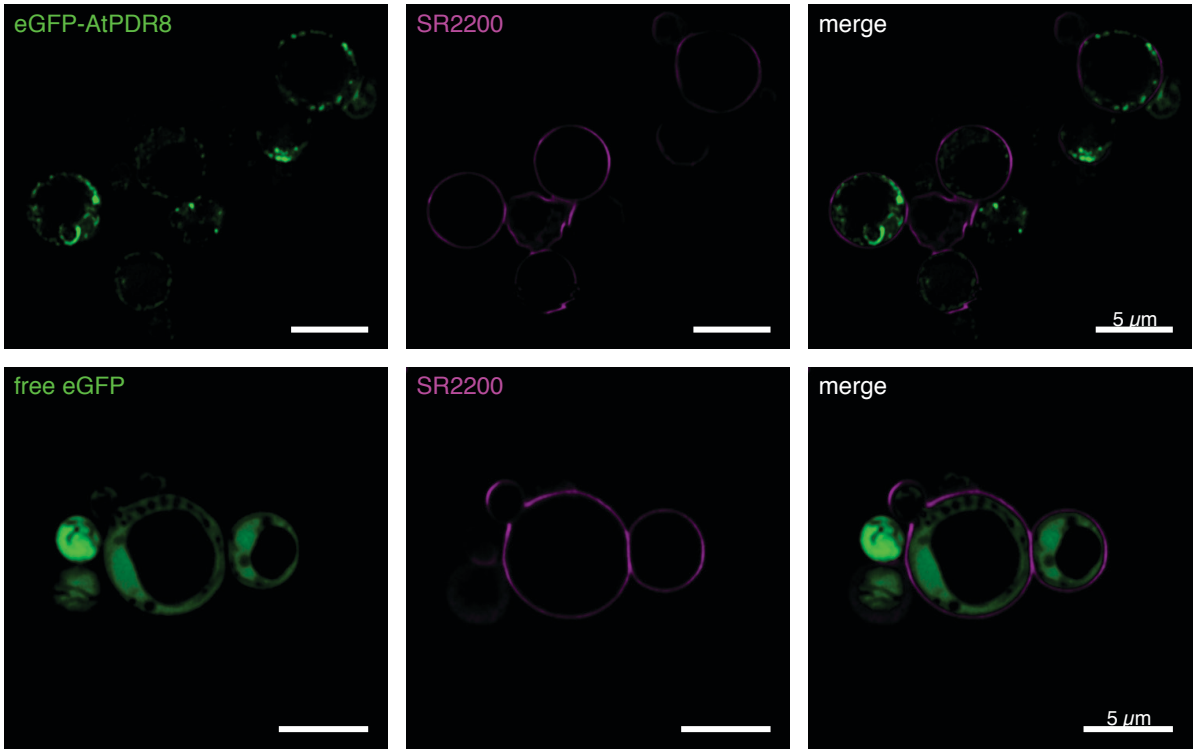

Figure 32: Confocal fluorescence microscopy of *P. pastoris* cells expressing GFP-*At*PDR8 (top) and free eGFP (bottom). The respective left pictures show the eGFP fluorescence signals while the pictures in the middle display the SR2200 signals of the cell wall marker. The left pictures show the merge of the eGFP and the SR2200 signals. The scale bars indicate 5 µm.

3.4 Purification of *At*PDR8

The purification of the membrane protein *At*PDR8 comprised several steps (Figure 33), whereby purification trials were inspired by previous purifications of ABC transporters expressed in *P. pastoris* cells (Ellinger et al., 2013, Wang et al., 2006). First the *P. pastoris* cells overexpressing the protein were fermented. The harvested cells were cracked to isolate the membranes. The membrane proteins were then solubilized out of the *P. pastoris* membrane; this required the screening for a detergent that was able to solubilize *At*PDR8. In order to separate *At*PDR8 from the co-solubilized proteins affinity chromatography was performed. The protocol was established by testing different approaches. *At*PDR8 was fused to two different affinity tags. This allowed the usage of immobilized metal ion affinity chromatography (IMAC) or calmodulin binding peptide affinity chromatography (CBP-AC), as well as a combination of both, the tandem affinity chromatography. Furthermore, it was tested whether the usage of a resin was preferable over the usage of a pre-packed column and if different detergents influence the purification result. Adding a subsequent size exclusion chromatography step was also analyzed.

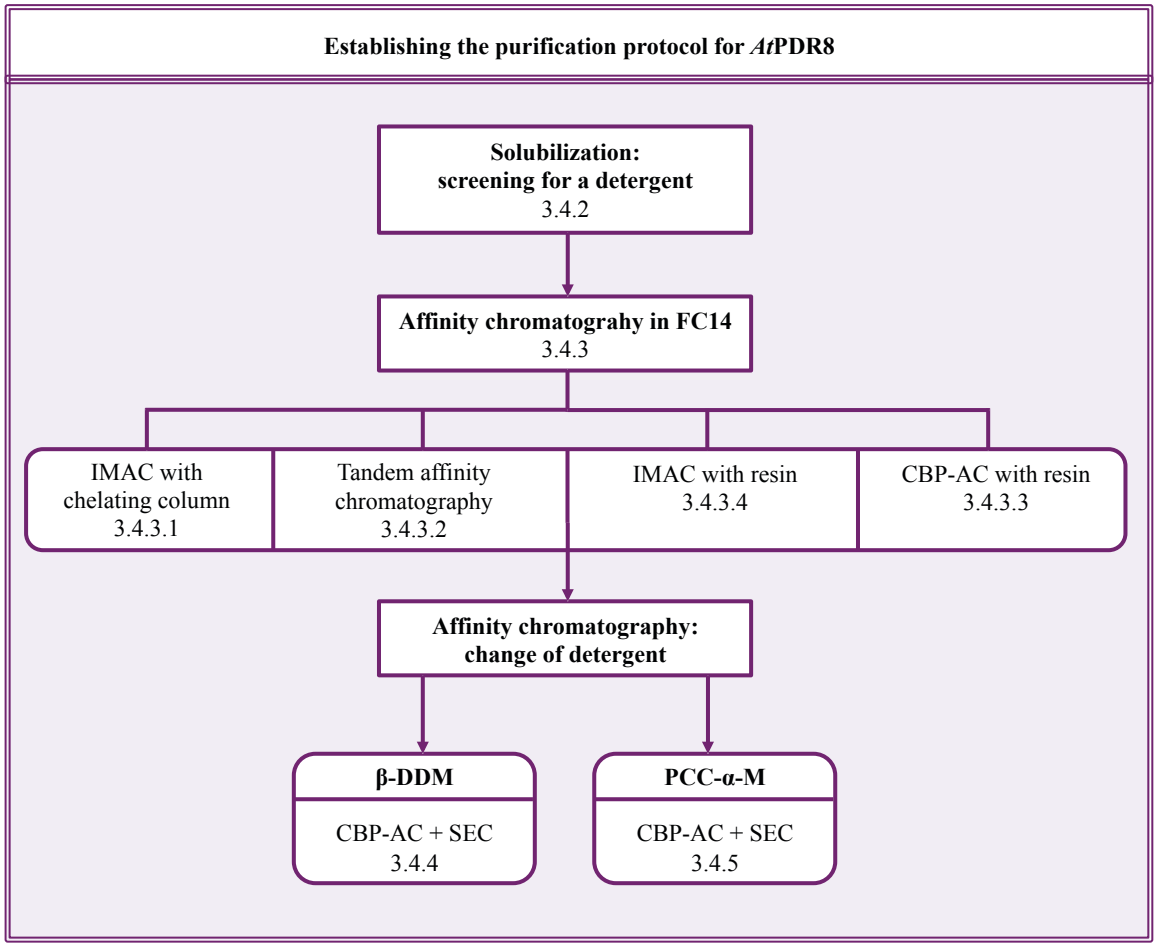

Figure 33: Scheme of the purification establishment of *At*PDR8.

3.4.1 Fermentation of *At*PDR8 and membrane preparation

Fermentation of *P. pastoris* cells overexpressing *At*PDR8 yielded approximately 1 kg wet cells from 6 L culture volume. The OD_{600} in the bioreactor had reached about 150. Membrane preparation of 100 g wet cells resulted in 45 mL volume with a protein concentration of about 50 mg/mL, depending on the respective preparation. *P. pastoris* plasma membranes were separated from the other membrane fractions, like mitochondrial membranes, by precipitation of the latter. Figure 34 shows a Western Blot after the preparation of crude and plasma membranes. The *At*PDR8 band runs at approximately 170 kDa, which corresponds to the size of the protein with the affinity tags (170 kDa). It seems that plasma membranes are enriched in *At*PDR8 compared to crude membranes since the immunoblot signal is stronger. Apparently, some protein was lost during the precipitation as lane MP (pellet after precipitation) shows a smeary signal on the Western Blot. The additional bands of higher molecular weight refer to protein that remained between the stacking and the resolving gel.

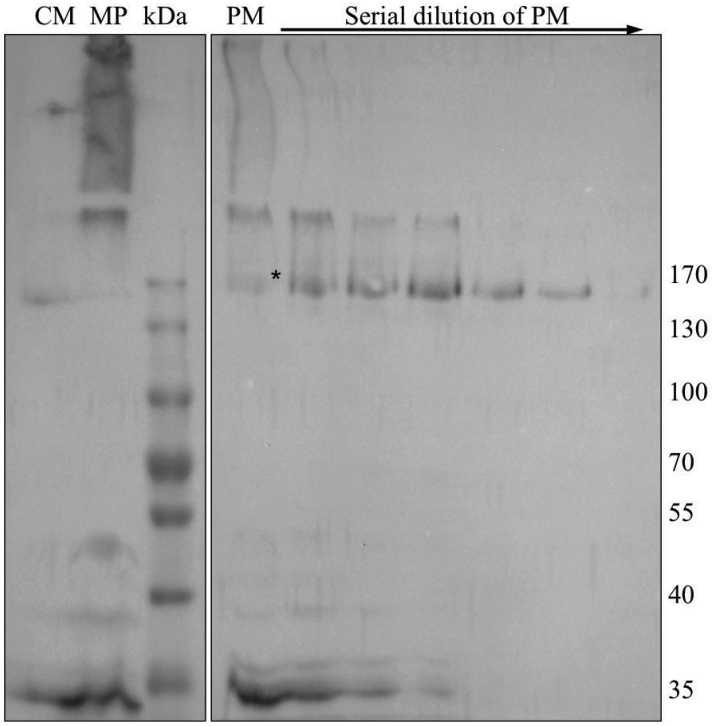

Figure 34: Membrane preparation after fermentation of *P. pastoris* cells expressing *At*PDR8. CM: preparation of whole cell membranes, MP: pellet after mitochondria precipitation, PM: plasma membranes, kDa: protein marker with the fragment sizes 170, 130, 100, 70, 55, 40 and 35 kDa. The asterisk marks the *At*PDR8 protein band.

3.4.2 Screening for a detergent that solubilizes *At*PDR8 out of the *P. pastoris* membrane

In order to identify a detergent that solubilizes *At*PDR8 out of the *P. pastoris* membranes the Dot Blot technique was used (Ellinger et al., 2013). Thereby 88 different detergents were tested (see Appendix A1 for a detailed list). After incubation of membranes with the respective detergent the insoluble fraction was separated and the solubilized proteins were spotted on a nitrocellulose membrane (Figure 35). Anti-His staining revealed in which soluble fraction *At*PDR8 was included. *At*PDR8 was mainly solubilized by Fos-Cholines (Figure 35, red boxes) while membranes solubilized with Fos-Choline-14 (Figure 35, E5) and Fos-Choline-15 (Figure 35, E6) displayed the strongest signals. The Fos-Cholines-11, -12, -13 and -16 solubilize *At*PDR8 more weakly compared to Fos-Choline-14 and -15. Furthermore *At*PDR8 was slightly solubilized by CHAPS and CHAPSO (green box), n-dodecyl-N,N-dimethylamine-N-oxide (DDAO) and sodium dodecanoyl sarcosine (Figure 35, dark blue and orange box). Very faint signals were observed for n-heptyl-β-D-thioglucopyranoside and n-heptyl-β-D-glucopyranoside (Figure 35, light blue box), and for Cyclofos-9 and -10 (Figure 35, purple box). As positive control sodium dodecyl sulfate (SDS) was used for solubilization (H5 in Figure 35). The signal on the Western Blot is weaker than the signal for the Fos-Cholines -14 and -16. This is due to partial precipitation of the SDS during the incubation at 4 °C. The negative control (buffer, H6 in Figure 35) does not show any protein signal on the Western Blot. Since sample E5 showed the strongest signal Fos-Choline-14 was used for further purification experiments.

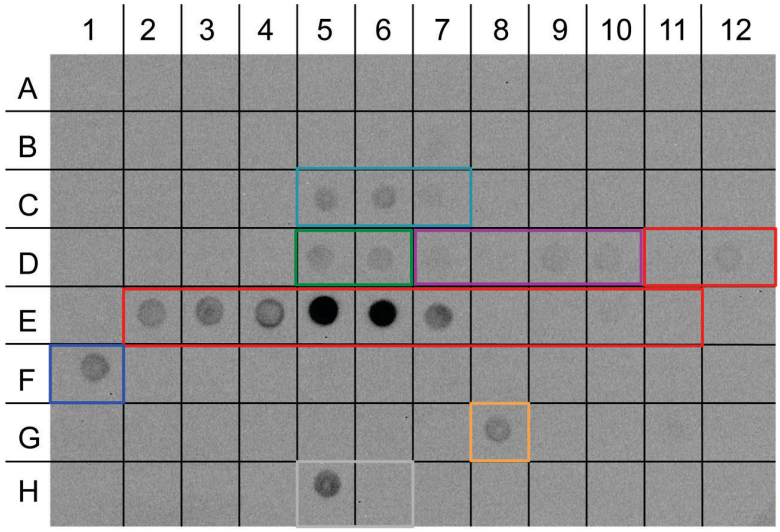

Figure 35: Detergent screening for the solubilization of *At*PDR8. 88 different detergents were incubated with *At*PDR8-containing *P. pastoris* membranes; the soluble fraction was spotted onto a nitrocellulose membrane. *At*PDR8 was detected by immune staining. Light blue box: glucopyranosides, green box: CHAPS and CHAPSO, purple box: Cyclofoses, red boxes: Fos-Cholines, dark blue box: DDAO, orange box: sodium dodecanoyl sarcosine, grey box: positive control SDS (H5) and negative control buffer (H6).

3.4.3 Purification of *At*PDR8 in the detergent Fos-Choline-14

3.4.3.1 Immobilized metal ion affinity chromatography (IMAC) in continuous flow process

Immobilized metal ion affinity chromatography (IMAC) was used to remove impurities that were co-solubilized with the target protein. The Ni^{2+} -saturated column was loaded with the solubilized protein mixture in a continuous flow process. Figure 36 shows the chromatogram of the absorption at 280 nm. After the loading (50 – 100 mL in Figure 36) the column was washed until the 280 nm signal had reached baseline level. The elution was started by mixing 30 % elution buffer with wash buffer (green line in Figure 36); the percentage of the elution buffer was then linearly increased until 100 %, which corresponds to a final imidazole concentration of 200 mM. The collected fractions were analyzed by SDS-PAGE and Western Blotting (Figure 37). The coomassie stained gel shows that the elution fractions contained a lot of impurities that were also present in the wash fractions. The protein *At*PDR8 is visible as a faint band in the elution fractions at approximately 150 kDa. The identity of *At*PDR8 band was confirmed by Western Blotting. Furthermore the Blot also shows bands at lower molecular weights in the elution fractions that were not present in the wash fractions. Since these bands were detected by immunoblotting there is a possibility that they correspond to degradation products of *At*PDR8. Most of the bands on the coomassie stained gel did not give a signal on the Blot and were therefore contaminant proteins.

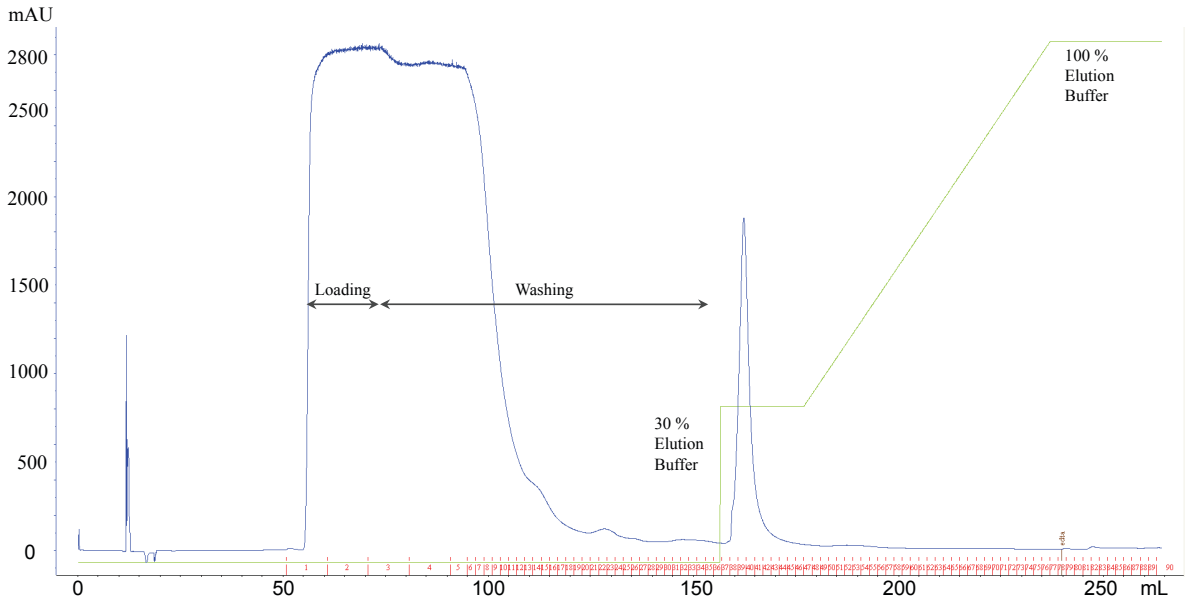

Figure 36: Chromatogram of the immobilized metal ion affinity chromatography of *At*PDR8. The absorption at 280 nm was monitored (blue line). The protein was eluted after 150 mL by adding 30 % elution buffer to the running buffer (green line).

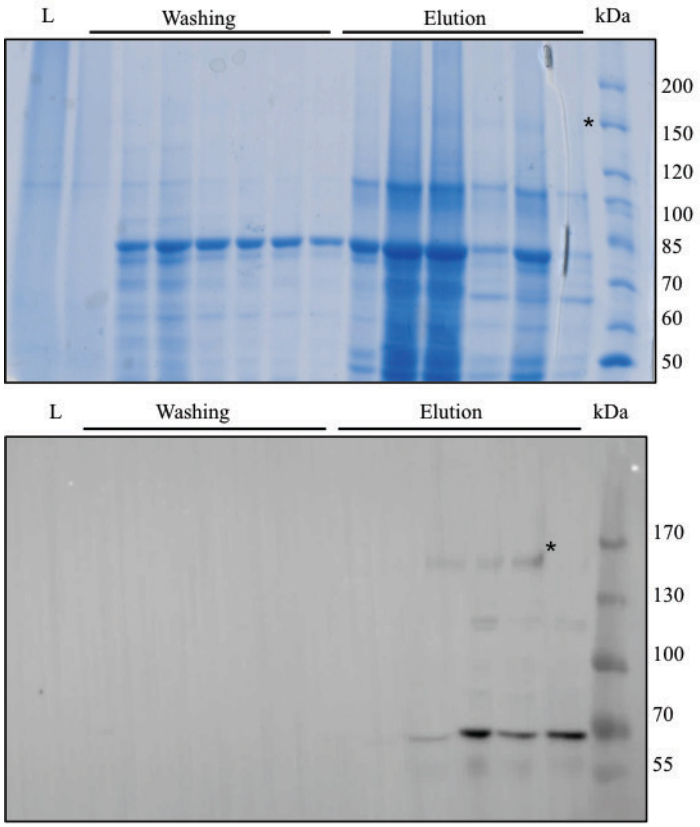

Figure 37: SDS-gel (top) and Western Blotting (bottom) of the IMAC fractions in Fos-Choline-14. The asterisk marks the *At*PDR8 protein band. L: load, kDa: protein marker with the fragment sizes 200, 150, 120, 100, 85, 70 60 and 50 kDa for the SDS-gel and 170, 130 100 70 and 55 kDa for the Western Blot.

3.4.3.2 Tandem affinity purification

After IMAC the elution fractions were not homogenous und *At*PDR8 was not the dominant protein in these fractions. The presence of two different affinity tags at the N-terminus of the protein enabled tandem affinity purification. The addition of another affinity chromatography step after the IMAC can improve protein purity. The calmodulin binding peptide affinity chromatography (CBP-AC) was performed after IMAC (Figure 38). The concentration of *At*PDR8 in the CBP elution fraction was increased compared to the IMAC elution fractions. Furthermore *At*PDR8 was the dominant protein band present in the fractions. Although there were fewer impurities as the comparison of the coomassie stained gel and the Western Blot shows, a lot of additional bands appeared in both detection methods. The extended purification time seemed to foster degradation of the target protein.

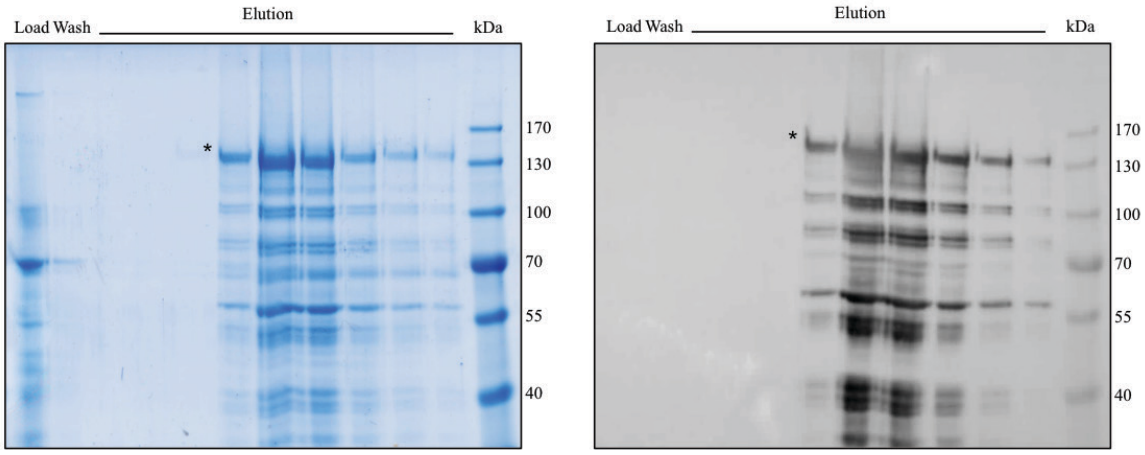

Figure 38: Tandem affinity purification of *At*PDR8. Coomassie stained SDS-gel (left) and Western Blot (right) of the CBP-AC, which was performed subsequently of the IMAC. The asterisk marks the *At*PDR8 protein band. kDa: protein marker with the fragment sizes 170, 130 100 70 and 55 kDa.

3.4.3.3 Calmodulin binding peptide affinity chromatography

The tandem affinity purification of *At*PDR8 resulted in higher concentrated target protein after the elution compared to the IMAC alone, although apparently a lot of the protein was degraded. This raised the question of the IMAC step was required at all or if a single CBP-AC step was also sufficient. Therefore after solubilization the CBP-AC was performed without a prior IMAC. The coomassie stained gel of the CBP-AC fractions shows a prominent band between the marker bands of 170 and 130 kDa, which is the *At*PDR8 band as confirmed by Western Blot (Figure 39). A lot of lower molecular weight bands were detected, which were probable degradation products. But compared to the other purification methods tested so far the lower molecular weight bands were less abundant in relation to the target protein, which was even higher concentrated than before. The concentrated elution fractions did not display ATPase activity in the detergent Fos-Choline-14.

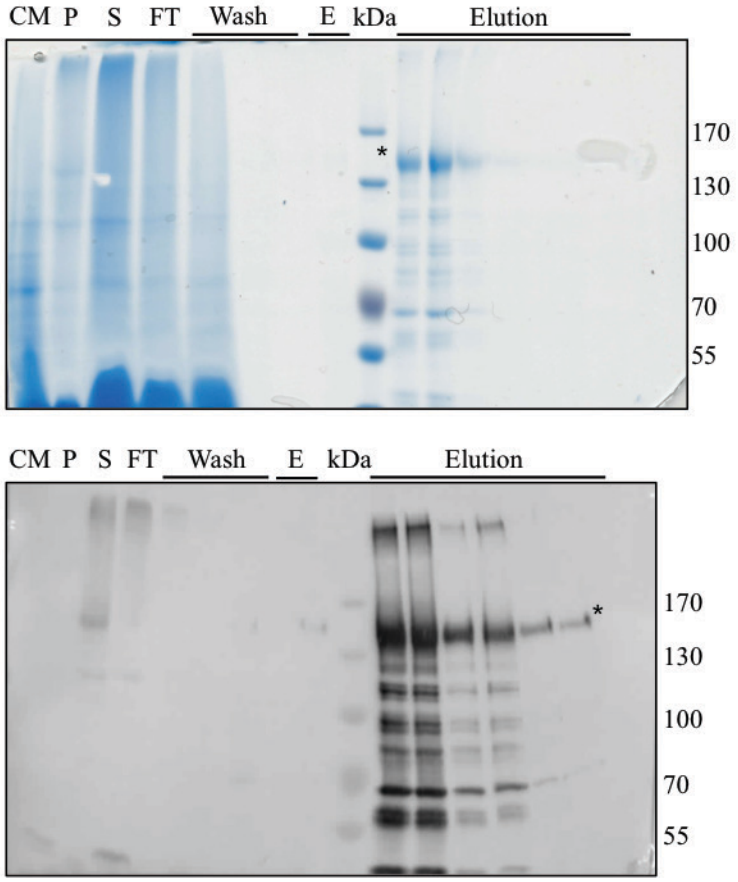

Figure 39: SDS gel (top) and Western Blotting (bottom) of the CBP-AC of *At*PDR8 in Fos-Choline-14. The arrows mark the *At*PDR8 protein bands. CM: *P. pastoris* whole-cell membranes, P: pellet after solubilisation, S: supernatant after solubilisation that was incubated with the calmodulin resin, FT: flow-through, E: elution, kDa: protein marker with the fragment sizes 170, 130 100 70 and 55 kDa.

3.4.3.4 Immobilized metal ion affinity chromatography in semi-batch process

For purification of *At*PDR8 the CBP-AC resulted in higher concentrated target protein and less impurities compared to the IMAC (Figure 39 and Figure 37). One difference between the two applications was the usage of a continuous flow-column for the IMAC and a resin for the CBP-AC. To test whether the process method or the different affinity tag resulted in higher concentrated *At*PDR8 the IMAC was performed using a Ni^{2+}-NTA resin. The binding of the protein to the resin was performed as batch incubation of the solubilisate and the resin. The washing and elution steps in turn were performed using continuous flow. Figure 40 shows the coomassie stained gel and the Western Blot of the IMAC with Ni^{2+}-NTA resin. The band pattern of the elution fraction is comparable to that of the CBP-AC elution fractions. The *At*PDR8 band is the most prominent band and a lot of lower molecular weight bands appeared that also showed up on the Western Blot. It can therefore be concluded that, regardless of the

affinity tag used for purification, the batch incubation results in higher concentration and purity of *At*PDR8 compared to the loading of the column in continuous flow.

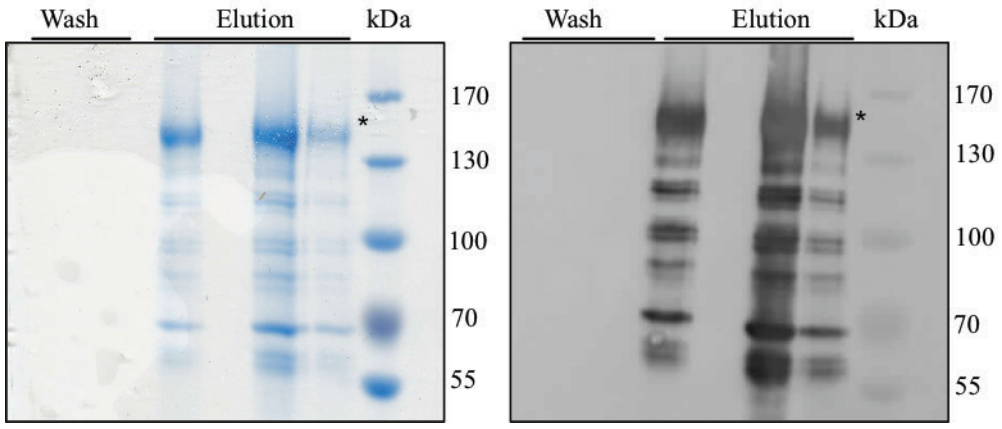

Figure 40: IMAC of *At*PDR8 in Fos-Choline-14 with Ni-NTA resin. SDS-gel (left) and Western Blot (right) of the IMAC fractions. The asterisk marks the *At*PDR8 protein band. kDa: protein marker with the fragment sizes 170, 130, 100, 70 and 55 kDa.

3.4.3.5 Size exclusion chromatography

Size exclusion chromatography (SEC) was performed in order to remove the lower molecular weight fragments that were present in the elution fractions after affinity chromatography. Figure 41 shows the chromatogram of the SEC run. The peak between 7 and 13 mL corresponds to *At*PDR8, as the coomassie stained gel and the Western Blot confirmed (Figure 42). The peak exhibits a shoulder starting at ~ 7 mL, which could represent aggregated protein. Some of the smaller fragments were separated from *At*PDR8, as the fragments of 70 and 100 kDa are less abundant in fractions 5 to 8, but more in fractions 9 to 11 (Figure 42). Furthermore an impurity of approximately 120 kDa appeared in fractions 10 to 13, which did not give a signal on the Western Blot. The SEC did not sufficiently separate the different fragments to obtain pure full-length *At*PDR8. The concentrated fractions did not show ATPase activity in Foc-Choline-14 (data not shown).

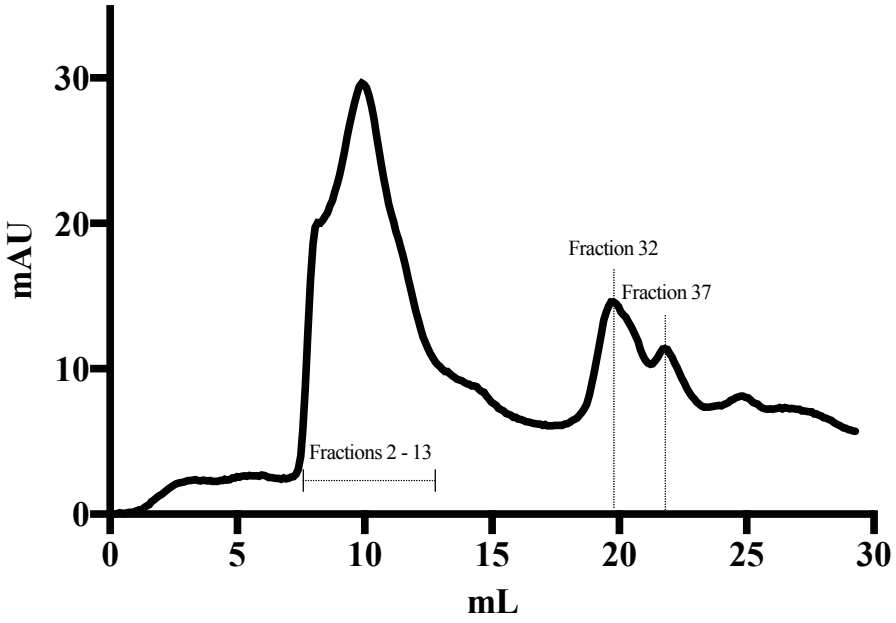

Figure 41: Chromatogram of the size exclusion chromatography of *At*PDR8 in Fos-Choline-14. The protein absorption at 280 nm was detected. The marked fractions were subjected to SDS-PAGE and Western Blotting.

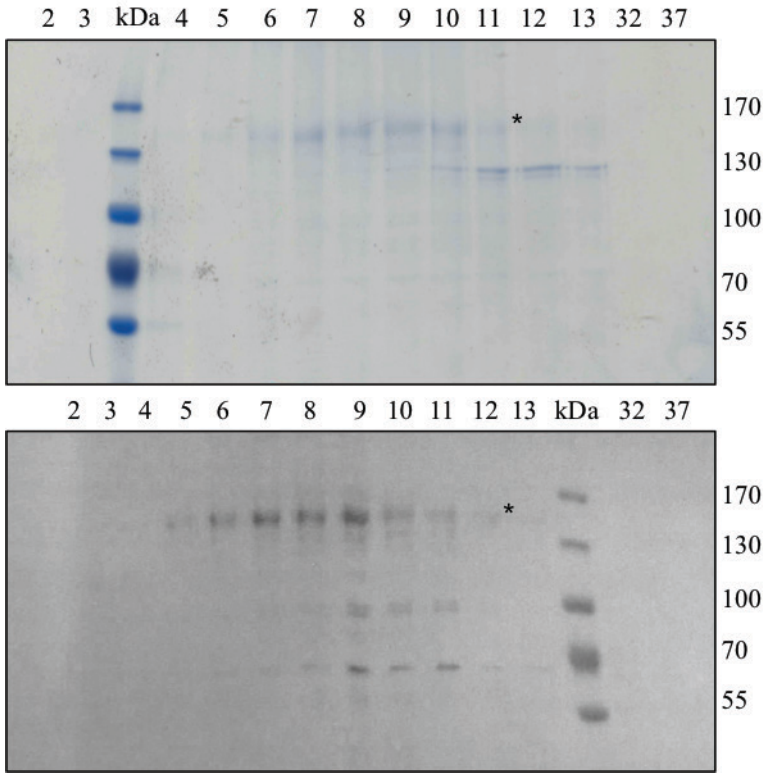

Figure 42: SDS-PAGE and Western Blotting of the SEC fractions of AtpDR8 in Fos-Choline-14. The asterisk mark the *At*PDR8 protein band. Two separate gels were run for Coomassie-blue staining and Western Blotting. kDa: protein marker with the fragment sizes 170, 130 100 70 and 55 kDa.

3.4.4 Purification of *At*PDR8 in the detergent *n*-Dodecyl-β-D-maltopyranoside

Because *At*PDR8 did not show ATPase activity in Fos-Choline-14 the detergent was exchanged to *n*-Dodecyl-β-D-maltopyranoside (β-DDM) during the washing step of the CBP-AC. Figure 43 shows the coomassie stained gels and the Western Blots of the CBP-AC and the SEC in β-DDM. The elution fraction (lane E in Figure 43 A) displays a weak *At*PDR8 band. Concentrating that fraction shows that also in β-DDM a lot of possible degradation products occurred (lane C in Figure 43 A). The SEC chromatogram did not show any protein peak (data not shown) but the SEC fractions on the gel show faint bands whose size corresponds to *At*PDR8. The Western Blotting revealed additional fragments of 70 and 100 kDa in the SEC fractions that could be degradation products of *At*PDR8.

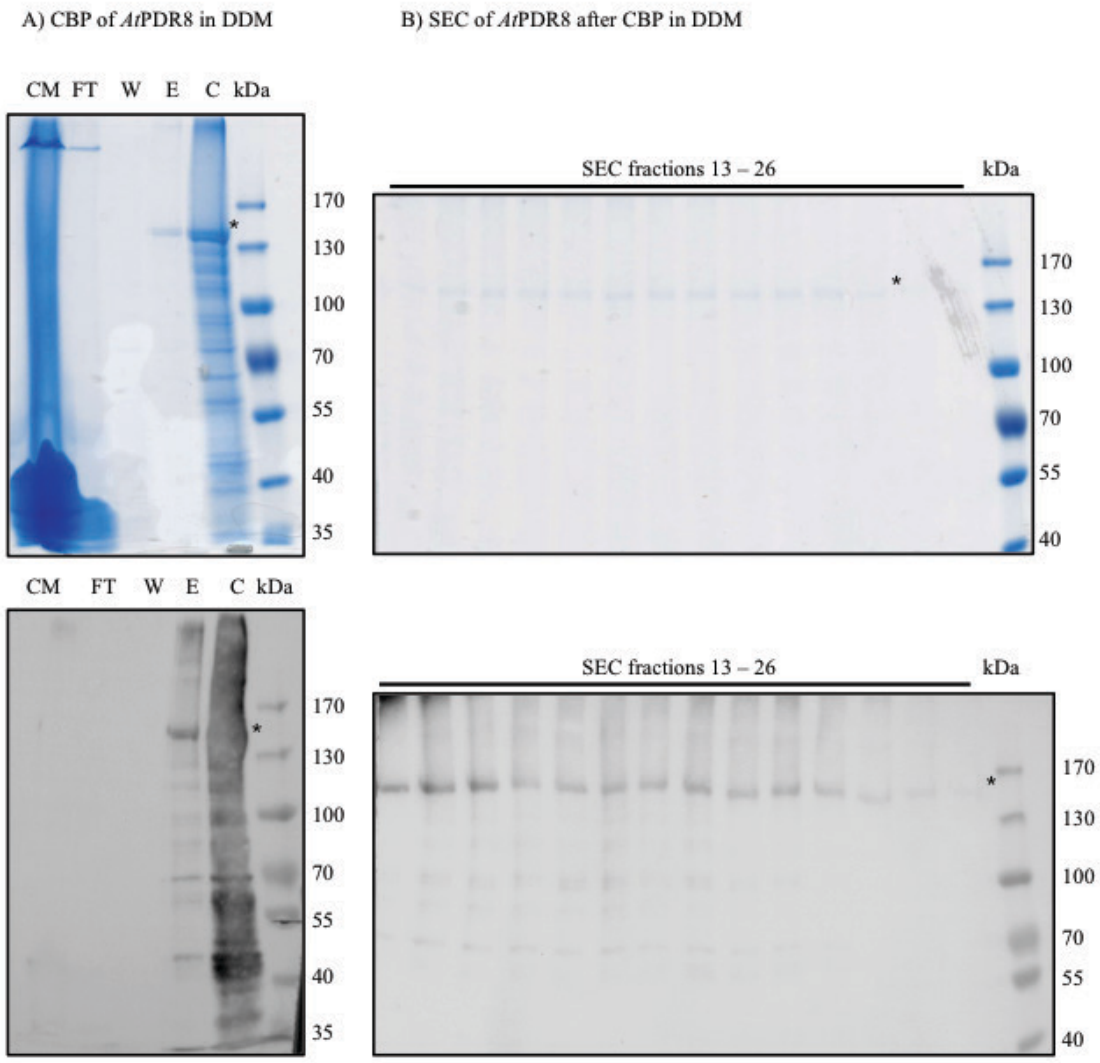

Figure 43: SDS-gels (upper row) and Western Blots (lower row) of the CBP-AC (A) and the SEC (B) of *At*PDR8 in β-DDM. The protein was solubilized in Fos-Cholone-14 from whole-cell membranes. CM: *P. pastoris* whole-cell membranes, FT: flow-through, W: washing, E: elution, C, concentrated elution fractions, kDa: protein marker with the fragment sizes 170, 130 100 70, 55 and 40 kDa. The asterisk marks the *At*PDR8 protein band.

In order elevate *At*PDR8 yield after CBP-AC in β-DDM plasma membranes were used instead of whole cell membranes as it was done before. Figure 44 shows that the elution fractions of the CBP-AC were enriched in *At*PDR8 and the impurities were less in relation to the target protein. In contrast to this no difference was observed between the usage of whole cell and plasma membranes when the CBP-AC was performed in Fos-Choline-14 (data not shown). Subsequently, a SEC was performed in β-DDM. The chromatogram shows two small peaks at approximately 8 and 11 mL and a higher peak at 19 mL (Figure 45 A). No protein was detected in the corresponding fractions neither with SDS-gel electrophoresis nor with Western Blotting (data not shown). The proteins in these fractions were therefore precipitated (Figure 45 B), which revealed that the second peak in the chromatogram contained *At*PDR8, the first peak may result from aggregates. As in Fos-Choline-14, the separation was not sufficient to remove the aggregate and the impurities from the target protein. Regarding purity and protein activity (data not shown), the purification in β-DDM shows no benefits compared with the purification in Fos-Choline-14.

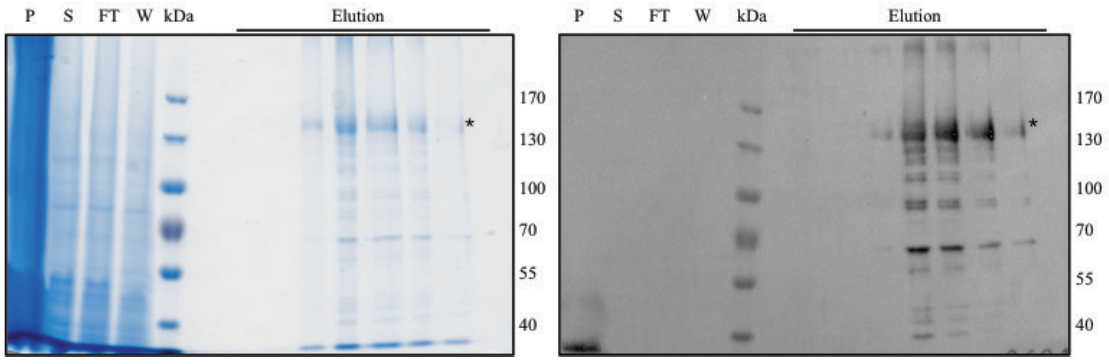

Figure 44: SDS-gel (left) and Western Blot (right) of the CBP-AC of *At*PDR8 in β-DDM. P: pellet after solubilization of plasma membranes, S: supernatant after solubilization that was incubated with the calmodulin resin, FT: flow-through, W: washing, kDa: protein marker with the fragment sizes 170, 130 100 70 and 55 kDa. The asterisk mark the *At*PDR8 protein band.

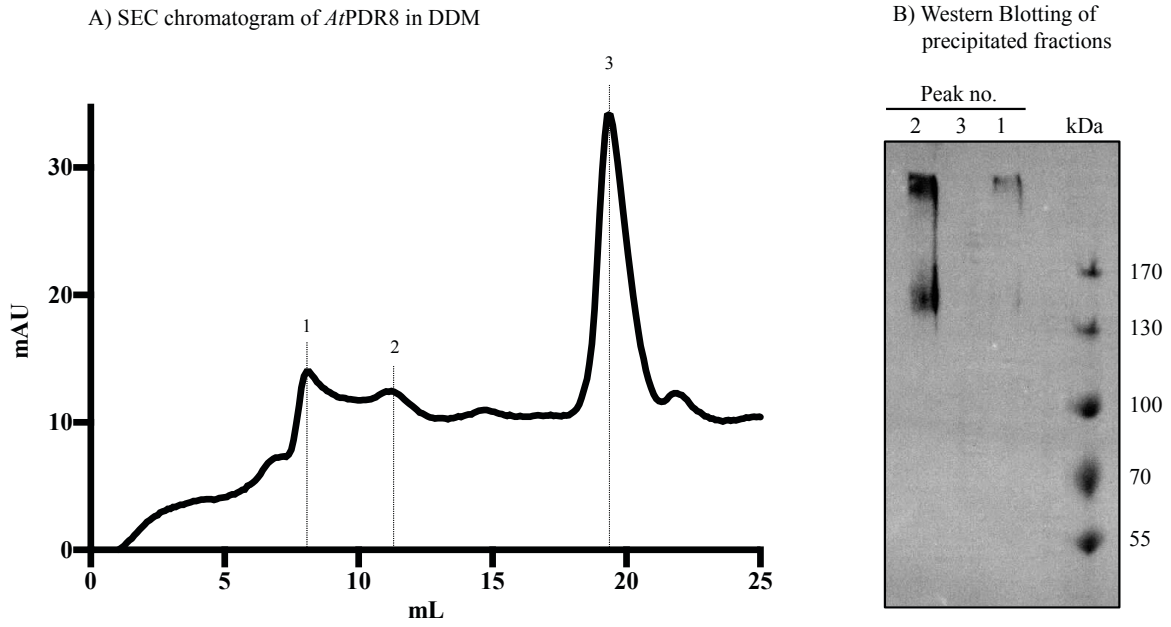

Figure 45: Size exclusion chromatography of *At*PDR8 in β-DDM purified from plasma membranes. A) SEC chromatogram of the absorption at 280 nm. B) Western Blotting of the in A) marked fractions after protein precipitation. kDa: protein marker with the fragment sizes 170, 130, 100, 70 and 55 kDa.

3.4.5 Purification of *At*PDR8 in the detergent *trans*-4-(*trans*-4′-propylcyclohexyl)-cyclohexyl-α-D-maltoside

Alternatively to β-DDM the detergent *trans*-4-(*trans*-4′-propylcyclohexyl)-cyclohexyl-α-D-maltoside (PCC-α-M) (Hovers et al., 2011a) was used for the purification of *At*PDR8. Figure 46 shows the results of the CBP-AC purification in PCC-α-M. The elution fraction displays a strong *At*PDR8 protein band on the coomassie stained gel, which was confirmed by Western Blotting (Figure 46 left and middle). In contrast to the purifications in Fos-Chline-14 and β-DDM, the abundance of potential breakdown products was significantly reduced. The CBP-AC in PCC-α-M resulted in almost homogenous protein. This result was successfully reproduced as Figure 46 (right) and Figure 48 demonstrate. *At*PDR8 protein concentrations up to 1 mg/mL were reached in a volume of 1 – 3 mL.

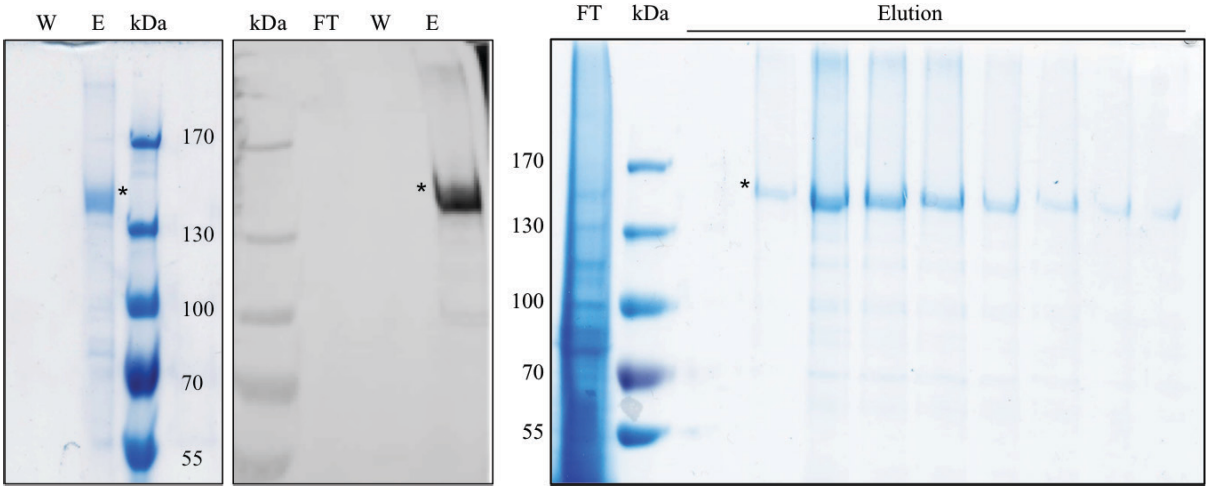

Figure 46: Calmodulin affinity chromatography of *At*PDR8 in the detergent PPC-α-M. The *At*PDR8 containing plasma membranes were solubilized with Fos-Choline-14. Left: SDS-gel of the CBP-AC with the corresponding Western Blot (middle). The CBP-AC was repeated to confirm the result (right). FT: flow-through, W: washing, E: elution, kDa: protein marker with the fragment sizes 170, 130 100 70 and 55 kDa. The asterisk mark the *At*PDR8 protein band.

Size exclusion chromatography in PCC-α-M after the CBP-AC shows an *At*PDR8 protein peak that eluted from the column between 7 and 13 mL (Figure 47). The coomassie stained gel and the Western Blot of these fractions demonstrate that *At*PDR8 was pure without any impurities or breakdown products (Figure 48). The high peak at 7 ml presents the aggregate peak; the resolution was therefore not sufficient to separate the aggregate (starting at 7 mL) from the protein. All peaks are quite dispersed and blend into each other. The other peaks of the SEC chromatogram did not show any protein signal neither on the coomassie stained gel nor on the Western Blot. SEC in PCC-α-M successfully removed the fragments of lower

molecular weight, which was not achieved in the other detergents. Although the purification was improved by exchanging the detergent, no ATPase activity was detected in PCC-α-M. For the SEC the protein must be concentrated after the CBP-AC to a final volume of 0.5 mL. This resulted in a loss of more than half of the eluted protein (compare lanes C and P in Figure 48). For further assays the SEC was therefore omitted.

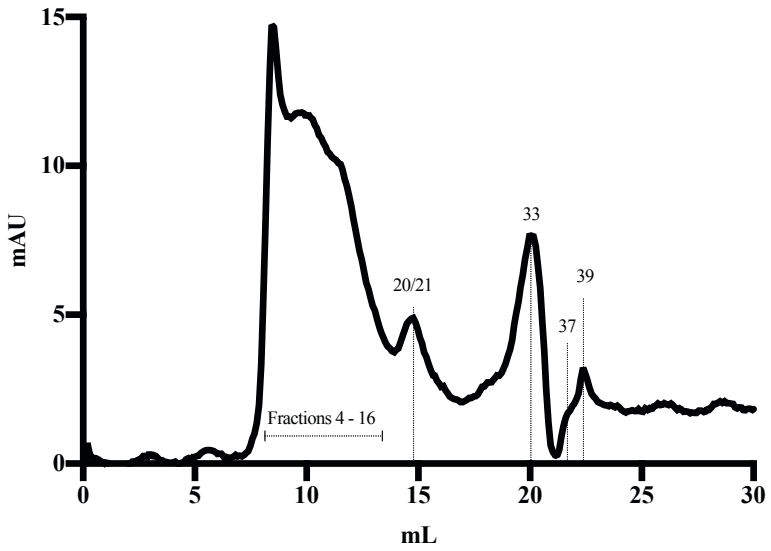

Figure 47: Size exclusion chromatography of *At*PDR8 in PCC-α-M purified from plasma membranes. The absorption signal at 280 nm is shown.

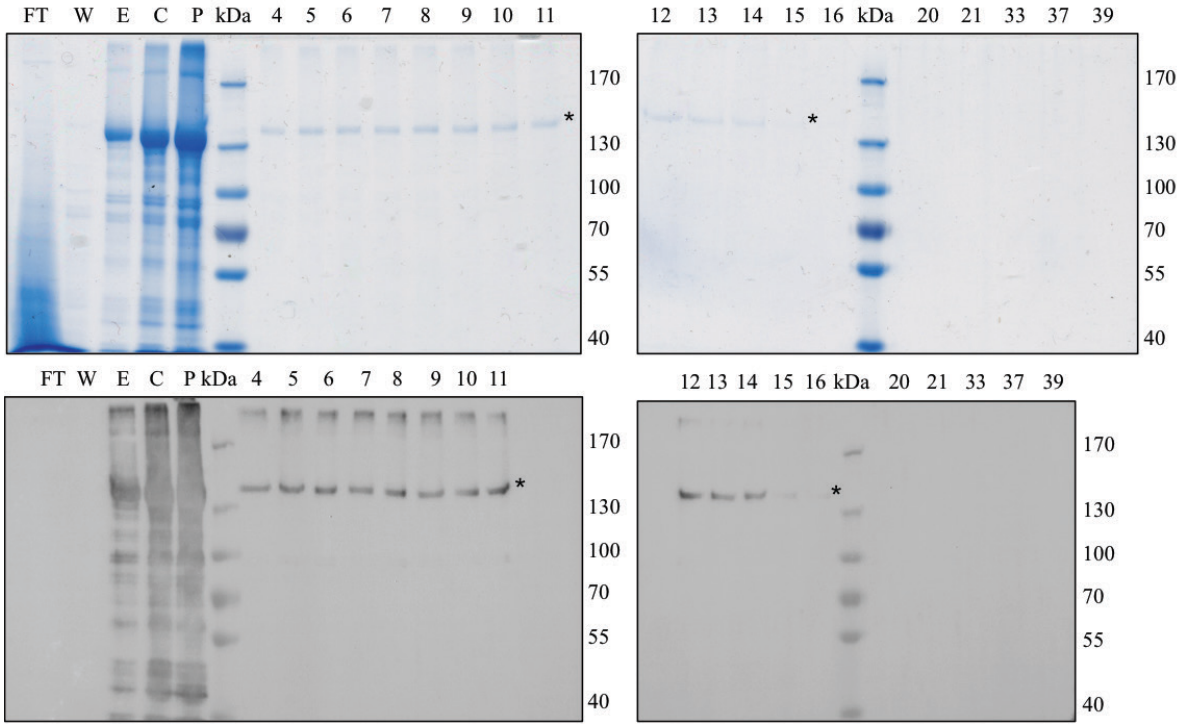

Figure 48: SDS-gels (upper row) and Western Blots (lower row) of the CBP-AC (A) and the SEC (B) of *At*PDR8 in PCC-α-M. The protein was solubilized in Fos-Cholone-14 from plasma membranes. Fractions of the CBP-AC: FT: flow-through (FT), washing (W), elution (E), concentrated elution fractions (C), pellet after centrifugation of the concentrated fractions (P). The numbers refer to the SEC fractions. kDa: protein marker with the fragment sizes 170, 130 100 70, 55 and 40 kDa. The asterisk mark the *At*PDR8 protein band.

3.4.6 Mass spectrometry analysis of *At*PDR8 after CBP-AC

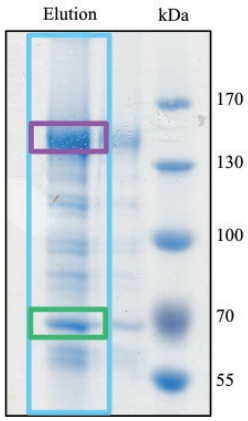

Figure 49: CBP-AC of *At*PDR8 in Fos-Choline-14. The boxes mark the samples that were analysed with MS: the *At*PDR8 protein band (purple), the impurity at 70 kDa (green) or the complete elution fraction (blue).

During purification, *At*PDR8 was detected by immunoblotting against the His-tag at the N-terminus of the protein. To confirm the identity of the protein the *At*PDR8 protein band (Figure 49 purple box) was analyzed by mass spectrometry. The proteins identified in the *At*PDR8 band are listed in Table 28. Most abundant in the sample was the *At*PDR8 construct with the N-terminal tag. 131 unique peptides were identified, which results in a sequence coverage of more than 50 %. Figure 50 displays the *At*PDR8 sequence coverage of the identified peptides. Noteworthy is the detection of the peptide TLNFQTR, which aligns to the C-terminus of *At*PDR8. That proofs that the full-length protein *At*PDR8 was present, although the protein band did not run exactly at 170 kDa in the SDS-gel. Next to the *At*PDR8-Ntag construct 13 other proteins were detected in the *At*PDR8 protein band-sample. Ubiquitin from *P. pastoris* was identified with 11 peptides, which cover the ubiquitin protein sequence by more than 90 %. Apart from ubiquitin some proteins were detected that are involved in protein biosynthesis, processing, folding and vesicular transport, such as for example the translation initiation factor EIF4F, Hsp90 or the coatomer subunit alpha. Furthermore, some membrane proteins were identified next to a transketolase and proteins that are in involved in synthesis of thiamin-related compounds.

Figure 50: Sequence coverage of the *At*PDR8 peptides that were identified by MS analysis of the *At*PDR8 protein band. Green areas illustrate the peptides that align to the *At*PDR8 protein sequence.

Additionally, the band at 70 kDa (green box in Figure 49) was also analyzed, because this impurity was present in many of the purifications. Furthermore, the complete elution fraction was analyzed in order to clarify whether the multiple bands of lower molecular weight, which were also detected by Western Blotting, were degradation products of *At*PDR8. In both samples the *At*PDR8-Ntag construct was the most abundant species with 103 unique peptides in the 70 kDa band-sample and 120 unique peptides in the complete elution fraction that align to the *At*PDR8-Ntag protein sequence (see Appendix A3 and A4). The sequence coverage was > 40 and > 50 %, respectively. In the 70 kDa band-sample ubiquitin was again identified. The list of other identified proteins is much longer for both samples (see Appendix A3 and A4) compared to the *At*PDR8-band sample and indicates that more impurities were present. However, most proteins whose peptides were identified in the *At*PDR8-sample were also detected in the two other samples.

Table 28: MS analysis of the *At*PDR8 protein band. The identified proteins of the detected fragments are listed as well as the respective coverage, the number of the unique peptides that were detected and the molecular weight.

***At*PDR8-Ntag protein band**						
UniProtKB Accession	**Description**	**Strain**	**Gene**	**Coverage [%]**	**# Unique Peptides**	**MW [kDa]**
	*At*PDR8 with N-terminal tags			52.04	131	170.7
C4R8V1	Ubiquitin from *P. pastoris*	GS115/ATCC 20864	*PAS_chr4_0762*	92.90	11	34.8
C4R5Q0	Transketolase, similar to Tkl2p from *P. pastoris*	GS115/ATCC 20864	*PAS_chr3_0834*	13.01	9	78.5
C4QVY8	Translation initiation factor eIF4G, subunit of the mRNA cap-binding protein complex (EIF4F) from *P. pastoris*	GS115/ATCC 20864	*PAS_chr1-1_0053*	7.65	7	121.4
C4R3X8	ATPase involved in protein folding and the response to stress from *P. pastoris*	GS115/ATCC 20864	*PAS_chr3_0230*	6.85	4	70.7
C4R9C8	ER membrane protein involved in regulation of OLE1 transcription, acts with homolog Spt23p from *P. pastoris*	GS115/ATCC 20864	*PAS_FragD_0002*	4.38	4	121.4
C4QWP7	Coatomer subunit alpha from *P. pastoris*	GS115/ATCC 20864	*PAS_chr1-1_0294*	4.06	4	136.7
C4R560	Thiazole synthase, catalyzes formation of the thiazole moiety of thiamin pyrophosphate from *P. pastoris*	GS115/ATCC 20864	*PAS_chr3_0648*	8.41	4	37.0
C4QZQ7	DNA-directed RNA polymerase from *P. pastoris*	GS115/ATCC 20864	*PAS_chr2-1_0125*	1.96	3	139.5
C4R6R6	Protein involved in synthesis of the thiamine hydroxymethylpyrimidine (HMP) from *P. pastoris*	GS115/ATCC 20864	*PAS_chr4_0065*	7.94	3	38.2
C4QVS9	Plasma membrane H+-ATPase, pumps protons out of the cell from *P. pastoris*	GS115/ATCC 20864	*PAS_chr1-1_0002*	2.57	2	97.8
C4R2D0	Putative magnesium transporter from *P. pastoris*	GS115/ATCC 20864	*PAS_chr2-2_0260*	3.19	2	91.8
C4R6M4	Ubiquitin carboxyl-terminal hydrolase from *P. pastoris*	GS115/ATCC 20864	*PAS_chr4_0022*	1.66	2	140.8
C4QXI5	Heat shock protein Hsp90 from *P. pastoris*	GS115/ATCC 20864	*PAS_chr1-4_0130*	3.40	2	80.9

Mass spectrometry also determined the post-translational modifications of the peptides. For the peptides of the *At*PDR8 protein band-sample three types of modifications were detected: the oxidations of methionines, the carbamidomethylation of cysteines and the ubiquination of lysins. The *At*PDR8 peptides of the 70 kDa band-sample contained only oxidations of methionines (data not shown) while the *At*PDR8 peptides of the complete elution fraction contained oxidations of methionines (data not shown) and ubiquibations of lysins. The number of the latter was larger compared to the number of ubiquinated lysins in the *At*PDR8 protein band-sample (Table 29). This supports the assumption that *At*PDR8 was partially degraded.

Table 29: List of *At*PDR8 peptides that were ubiquinated and detected by mass spectrometry. Modified lysines are indicated in italics.

Peptide sequence	Sample	Modification	Peptide sequence	Sample	Modification
AALVFD*k*YSVSK	Elution fraction	K7 (GlyGly)	ILT*k*LR	Elution fraction	K4 (GlyGly)
AQLTIL*k*DISGVIKPGR	Elution fraction	K7 (GlyGly)	*k*GTADFLQEVTSK	*At*PDR8 band	K1 (GlyGly)
ASAAQGV*k*NSLVTDYTLK	*At*PDR8 band	K8 (GlyGly)	*k*NFIAVSAANR	Elution fraction	K1 (GlyGly)
ASAAQGV*k*NSLVTDYTLK	Elution fraction	K8 (GlyGly)	*k*TGGYIEGDVR	Elution fraction	K1 (GlyGly)
DAGIFPEADVDLFM*k*ASAAQG VK	Elution fraction	K15 (GlyGly)	LD*k*SLQVSGDITYNGYQLDEF VPR	Elution fraction	K3 (GlyGly)
DISGVI*k*PGR	Elution fraction	K7 (GlyGly)	LPVFY*k*QR	*At*PDR8 band	K6 (GlyGly)
DNILEFFESFGF*k*CPER	Elution fraction	K13 (GlyGly)	MSNELAVPFD*k*SR	Elution fraction	K11 (GlyGly)
EVDVT*k*LDGEDR	Elution fraction	K6 (GlyGly)	VGI*k*LPTVEVR	Elution fraction	K4 (GlyGly)
FIDMVF*k*VAEQDNER	Elution fraction	K7 (GlyGly)	VVEYFESFPGVS*k*IPEK	Elution fraction	K13 (GlyGly)
GH*k*AALVFDK	Elution fraction	K3 (GlyGly)	WAAIE*k*LPTYSR	Elution fraction	K6 (GlyGly)
ILGLDIC*k*DTIVGDDMMR	Elution fraction	K8 (GlyGly)	YEHLTI*k*ADCYTGNR	Elution fraction	K7 (GlyGly)

3.4.7 TNP-ATP binding to *At*PDR8

Trinitro phenyl (TNP)-ATP is a fluorescent nucleotide analogue whose fluorescence ability is weak in buffer solutions but becomes enhanced upon binding to a hydrophobic environment such as a ligand binding side of a protein (Horn et al., 2003). TNP-ATP was therefore used to analyze the nucleotide binding ability and stoichiometry of purified *At*PDR8. The fluorescence emission spectrum (Figure 51) shows that the fluorescence intensity of TNP-ATP was enhanced in the presence of *At*PDR8, which indicates binding of the ligand to the protein. Furthermore the emission maximum was shifted to shorter wavelengths. In comparison, *At*PDR8 in buffer alone did not fluoresce. TNP-ATP was successively titrated to 0.5 µM *At*PDR8 (Figure 52). The fluorescence increased until the curve leveled off indicating that saturation of binding was reached. The TNP-ATP titration into buffer was used to determine the fluorescence constants Q1 and Q2 (equation 3 in Materials and Methods), which were calculated to be 60895 and -1678, respectively. The data points of the TNP-ATP titration to the protein were fitted to equation 4 (Materials and Methods). Thereby, the dissociation constant (K_D) was determined as 14.3 µM and the calculated ligand number (N) was 0.8.

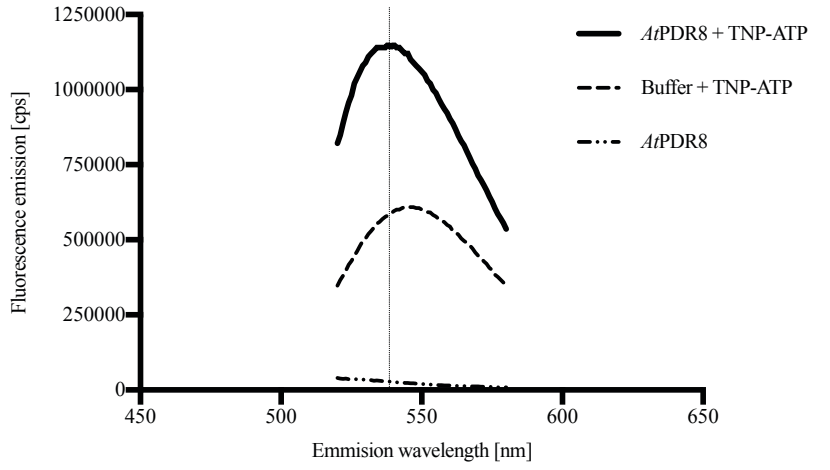

Figure 51: Emission spectrum of TNP-ATP in buffer with (solid line) and without (dashed line) *At*PDR8. In the absence of TNP-ATP *At*PDR8 showed almost no fluorescence (dot-dashed line).

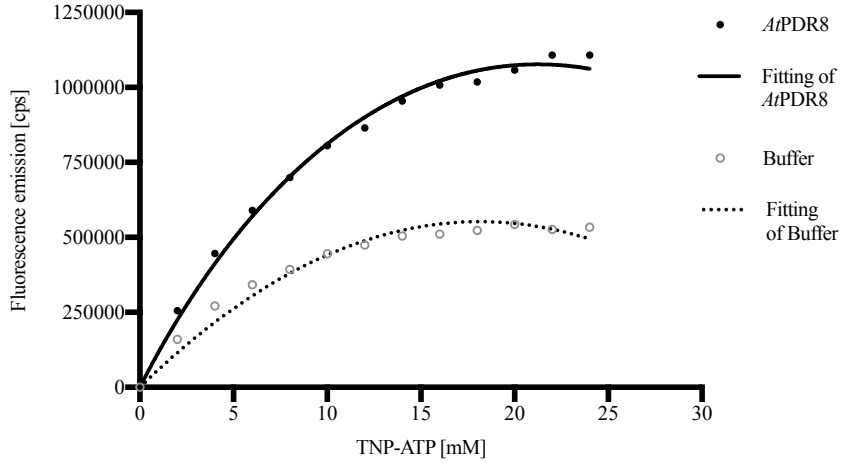

Figure 52: TNP-ATP binding to *At*PDR8. TNP-ATP was titrated to buffer (empty circles) and with 0.5 µM *At*PDR8 (filled circles). The data was analyzed and fitted according to equations 3 and 4 (Materials and Methods).

3.5 Reconstitution of *At*PDR8 into liposomes

Reconstitution is the *in vitro* process of integrating a membrane protein into an artificial lipid bilayer, which can be for example liposomes, giant vesicles or nanodiscs. The membrane protein is thereby situated in an *in vitro* lipid environment, which can influence activity or stability of the protein. The reconstitution of a protein into liposomes comprises three steps: 1) the liposome preparation, 2) the destabilization of liposomes with detergent and 3) the reconstitution of protein into liposomes by removing the detergent. A variety of reconstitution protocols exist (Rigaud et al., 1995), however, for establishing the reconstitution of *At*PDR8 the protocol published by Geertsma et al. (2008) was chosen as a starting point, because it describes the successful reconstitution of an ABC transporter.

Figure 53 shows the steps of the reconstitution process of *At*PDR8. For the liposome preparation the lipids were sonicated to form small unilamellar liposomes. By several cycles of freezing and thawing the small unilamellar liposomes were fused to form large multilamellar liposomes. By extruding these through a membrane of defined pore size large unilamellar liposomes of defined size were formed. In order to make the liposomes accessible for the membrane protein a detergent was added to penetrate the liposomes. The destabilization was monitored by measuring the optical density. After addition of the membrane protein the detergent was removed. In general, this can be done by various methods, for example by size exclusion chromatography, rapid dilution or dialysis. In this case *At*PDR8 was reconstituted by removing the detergent with polystyrene beads. Finally, floating gradient centrifugation was performed to check whether the reconstitution of *At*PDR8 into liposomes was successful.

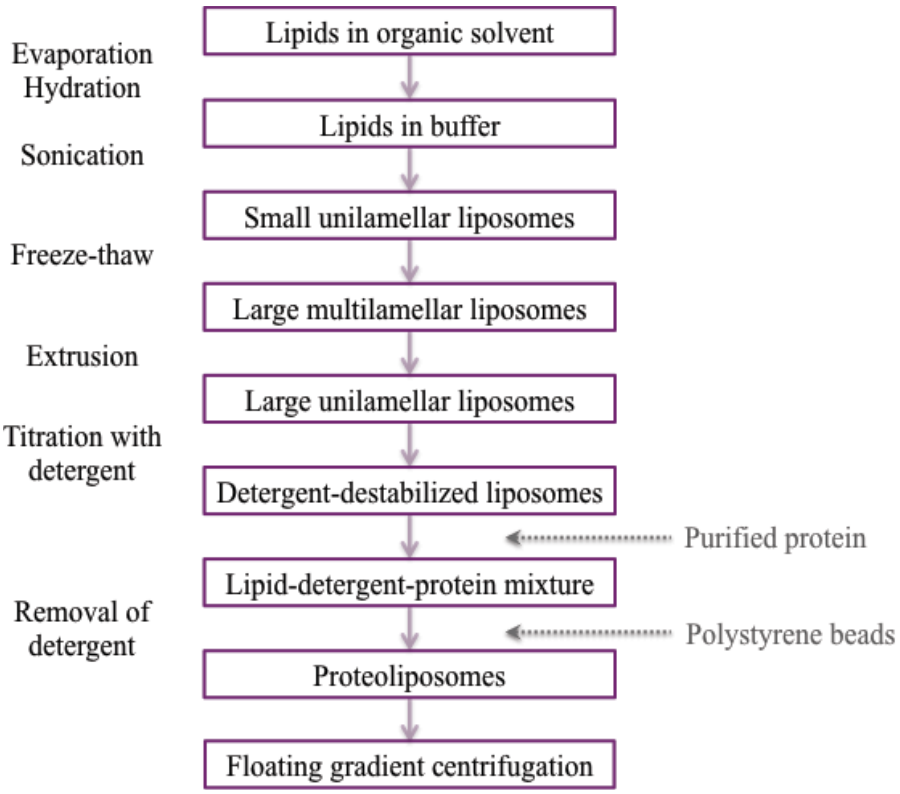

Figure 53: Flow-chart showing the different steps of *At*PDR8 reconstitution into liposomes. The steps include the preparation of liposomes, the destabilization and the formation of proteoliposomes by removing the detergent.

3.5.1 Preparation of liposomes

Liposomes were prepared as described in Materials and Methods. The lipids were dissolved in an organic solvent to prepare a homogeneous lipid film. This is especially important when mixtures of different lipids are used to ensure that the lipids are equally distributed. Differing from the protocol published by Geertsma *et al*. (2008) the rotary evaporation time of removing the solvent and the hydration were prolonged. By rotating the lipids overnight the formation of lipid vesicles was promoted since in this step the lipid film, which had formed after rotary evaporation, was hydrated in buffer. The lipid sheets swelled with buffer and because of the rotation they detach and close into vesicles. These can be very inhomogeneous with varying sizes. Freezing cycles fuse liposomes to larger structures while downsizing the liposomes needs energy input. Sonic energy was used to form very small unilamellar vesicles and mechanical energy (extrusion) was used to form unilamellar particles of defined sizes. Freezing and thawing cycles produced large multilamellar vesicles. These liposomes were used for the destabilization and reconstitution.

3.5.2 Optimization of the destabilization of liposomes with detergent

For destabilizing the liposomes aliquots of detergent were titrated to the liposomes and the optical density was monitored. Thus, the optimal detergent concentration for the reconstitution was determined. Figure 54 A shows a typical titration of liposomes with Triton X-100 (Geertsma et al., 2008). First the optical density increases because the detergent incorporates into the liposomes. At the maximum (R_{sat} in Figure 54 A) the liposomes are completely saturated with detergent. Then solubilization starts and the optical density decreases until the liposomes are fully solubilized (R_{sol} in Figure 54 A). At R_{sol} the optical density is almost zero. According to Geertsma et al. (2008) the optimal detergent concentration for reconstituting a membrane protein into liposomes is shortly after the saturation concentration (indicated by the red-boxed arrow in Figure 54). However, the first trials of *E. coli* total lipid extract liposomes destabilized with the detergent PCC-α-M, which was also used for *At*PDR8 purification, did not result in the typical titration curve (Figure 54 B). The data points did not show a maximum peak and at higher detergent concentrations the values did not reduce towards zero indicating that the solubilization was not achieved.

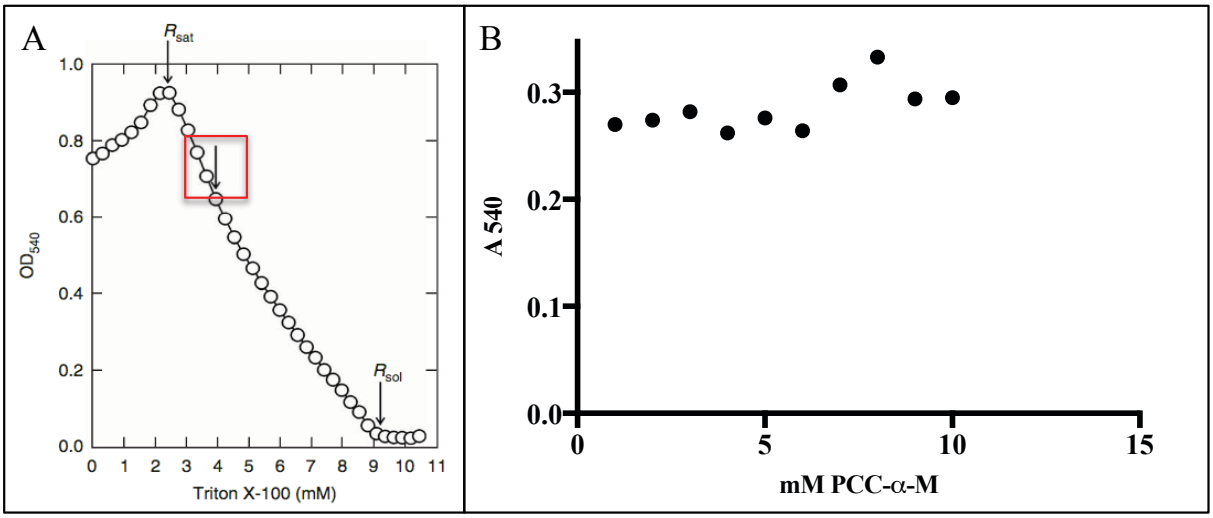

Figure 54: Titration of detergent to liposomes. A) Titration with Triton X-100 published by Geertsma et al. (2008). R_{sat} marks the concentration where liposomes are fully saturated with detergent and R_{sol} the concentration where the liposomes are fully solubilized. The red box marks the optimal concentration for the addition of the purified protein according to Geertsma et al. (2008). B) First titration trial of *E. coli* liposomes with the detergent PCC-α-M. The data points do not resemble the expected curve in A).

Factors influencing the destabilization in this experiment could have been the lipids, the wavelength, the incubation time and the used detergent. Not only the nature of the detergent and its concentration determine successful penetration of the lipids but also the reaction time. Furthermore, there is also the possibility that the conditions of measuring the optical density were not appropriate for the prepared liposomes. To take all these factors into account, the destabilization was optimized regarding the used lipids, the detergent, the wavelength for monitoring the destabilization and the incubation time. The tested conditions are listed in Figure 55 whereby the different possible combinations were tested. The resulting destabilization experiments are shown in the following chapters.

Optimization of destabilization - conditions that were tested:

→ Wavelengths:
- 330 nm
- 415 nm
- 544 nm
- 595 nm

→ Incubation time:
- 30 min
- 60 min
- 90 min

→ Lipids:
- *E. coli* total lipid extract
- DOPC

→ Detergents:
- β-DDM
- PCC-α-M
- LMNG

Figure 55: Optimization of the destabilization experiments. The conditions tested were different wavelengths, different incubation times, different detergents and different kinds of lipids.

3.5.2.1 The optimal wavelength for monitoring the destabilization

To exclude that the measurement set-up negatively influenced the destabilization experiments the first factor tested was the wavelength used for measuring the optical density. There is the possibility that depending on the wavelength the lipids absorb the light differently. The absorption of lipids could influence the values of the optical density. Liposomes from *E. coli* total lipid extract were prepared and incubated with different PCC-α-M concentrations. The absorption was determined at the wavelengths 330 nm, 415 nm, 540 nm and 595 nm. Figure 56 shows the results for 90 min incubation. It became evident that for these lipids the wavelength 415 nm worked best since during the titration the absorption values maximize to a peak and then reduce towards zero indicating the success of the solubilization. At 595 nm the values leveled out in a plateau but the minimal absorption was not tending to zero. At 540 nm the values had the tendency to form a maximum peak, but there was no clear reduction towards zero. For both wavelengths the difference between maximum and minimum was less compared to the values measured at 415 nm. This was not the case for the measurement at 330 nm, but the values were generally higher indicating the lipids itself absorbed more light at this wavelength. At 415 nm the lipids absorbed least and therefore this wavelength was chosen for the destabilization.

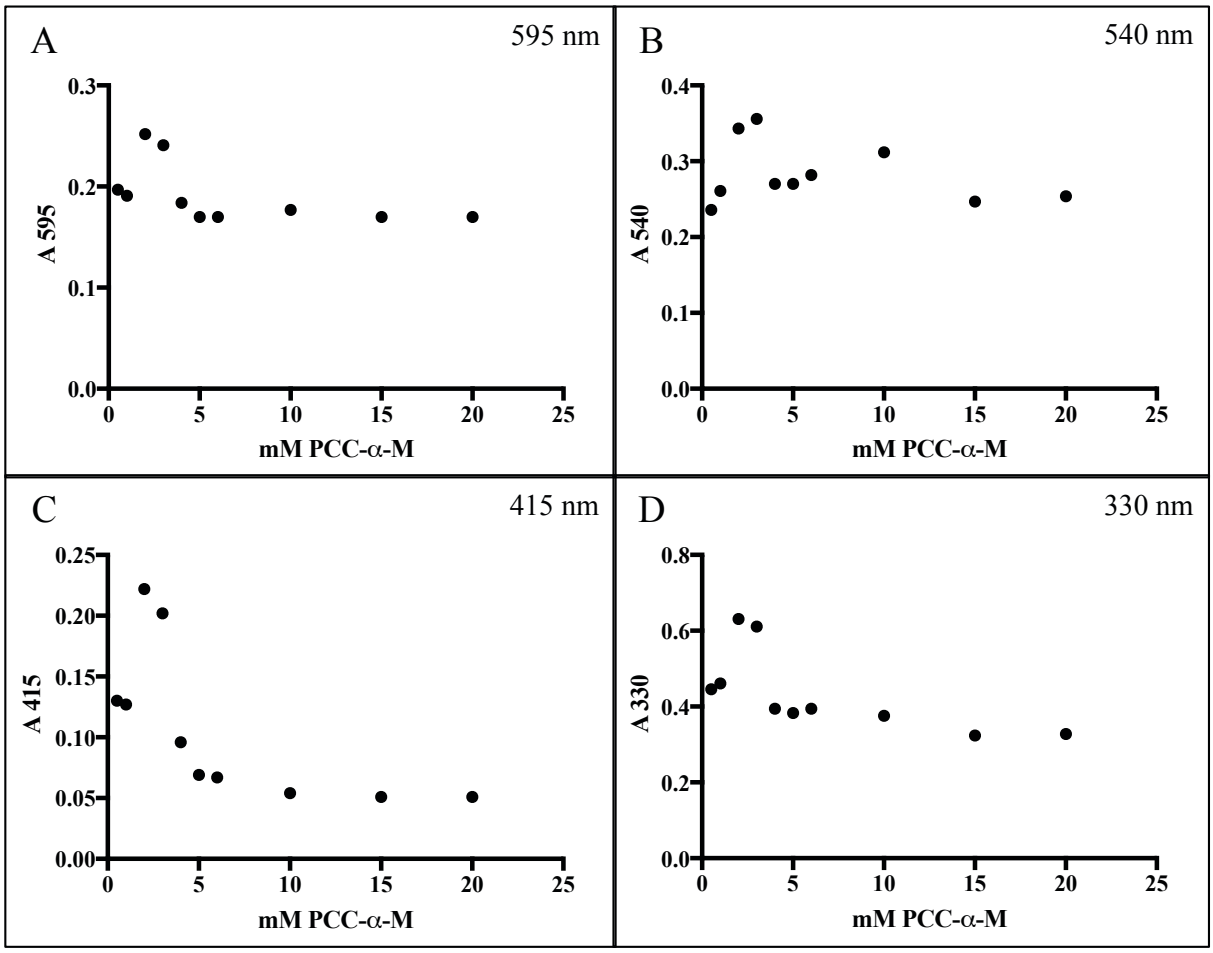

Figure 56: Destabilization of *E. coli* total lipids liposomes with PCC-α-M. The detergents was titrated to the liposomes and the absorption was monitored at different wavelengths: A) 595 nm, B) 540 nm. C) 415 nm and D) 330 nm.

3.5.2.2 Detergents need time for the destabilization of liposomes

To check whether different incubation times influence the destabilization process liposomes prepared from *E. coli* total lipid extract were titrated with PCC-α-M and incubated for 60 and 90 min. Figure 57 shows that the values at the titration start as well as at the end were similar, but the maximum increased with time. That indicates that at lower concentrations the detergent required time to penetrate the liposomes while at higher concentrations the solubilization was faster. Because of these results liposomes were generally incubated with detergent for 90 min.

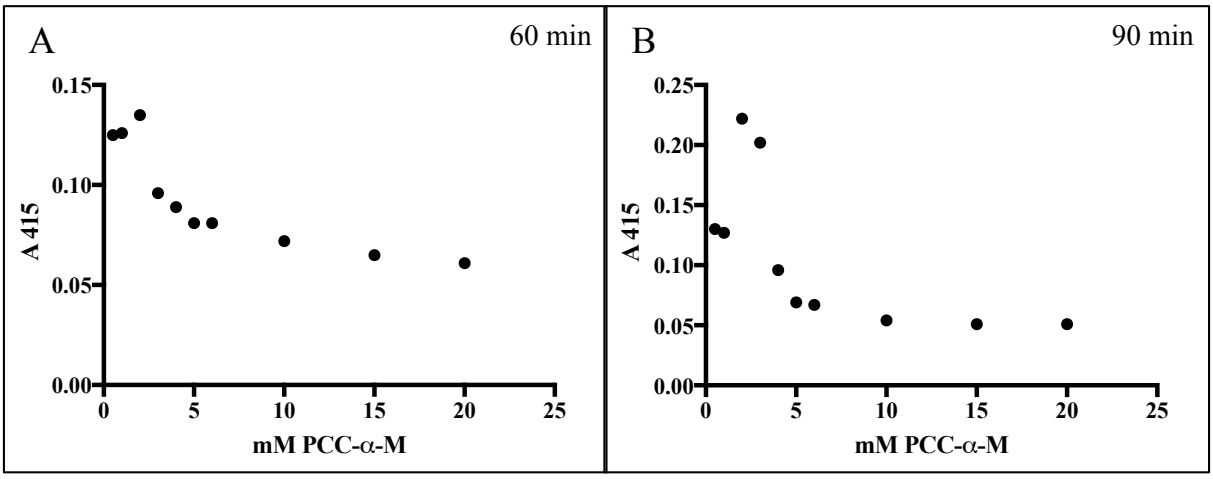

Figure 57: Comparison of different incubation times for the destabilization of liposomes. *E. coli* total lipids liposomes were titrated with PCC-α-M. The absorption was monitored at 415 nm after 60 min incubation (A) and 90 min incubation (B).

3.5.2.3 The influence of buffer conditions on the destabilization process

In order to assess whether buffer components influence the destabilization process four different buffer compositions were tested. Tris-HCl buffer was chosen because the *At*PDR8 purification was performed in Tris-HCl. The second buffer substance tested was phosphate since the destabilization and reconstitution in phosphate buffer had been published before (Geertsma et al., 2008). Both buffers were tested with and without glycerol. In all tested buffer conditions the destabilization curve resembled the theoretical curve with the increase of the absorption to a maximum followed by the leveling out towards zero with increasing detergent concentrations (Figure 58). During the 90 min incubation, the presence of glycerol slightly reduced the maximum absorption. In phosphate buffer, the absorption at the peaks was generally higher compared to Tris-HCl buffer. This indicates that the buffer substance itself as well as glycerol influences the absorption values. However, for the further reconstitution the buffer was not changed because the shape of the curves did not change with the different buffers. That means in all tested buffer conditions the optimal detergent concentration for the reconstitution was similar.

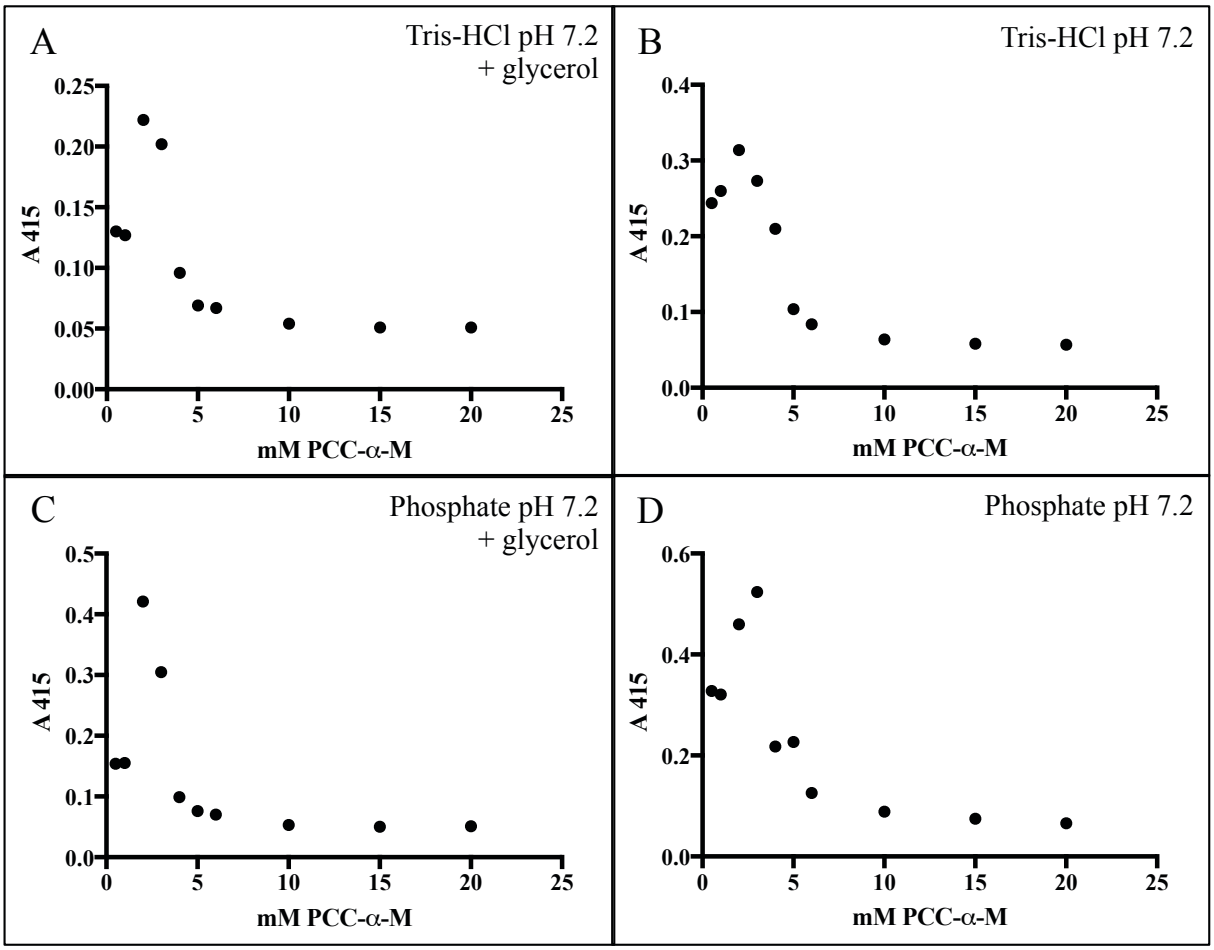

Figure 58: Comparison of different buffers during the destabilization. *E. coli* total lipids liposomes were prepared in either Tris-HCL with glycerol (A), without glycerol (B), or in phosphate buffer with (C) and without glycerol (D). Liposomes were titrated with PCC-α-M and the absorption was monitored after 90 min incubation.

3.5.2.4 Comparison of *E. coli* total lipid extract liposomes to DOPC liposomes

To examine how different lipids behave during the preparation of liposomes and the destabilization experiment two different types of lipids were tested. On the one hand a total lipid extract from *E. coli*, which is a complex mixture of lipids, and on the other hand the synthetic lipid DOPC, which is an unsaturated phosphatidylcholine.

During the extrusion a large proportion of the *E. coli* lipids was lost. This raised the assumption that during the freeze- and thaw-cycles the liposomes merged to big structures that could not pass the extrusion membrane. During the OD measurements this became evident since the maximum values were reduced pointing to a generally lower liposome concentration (Figure 59). Furthermore the complete solubilization of the *E. coli* lipids was achieved at lower detergent concentrations compared to DOPC. That indicated that the protocol for the liposome preparation needed to be further adapted for the *E. coli* total lipid extract.

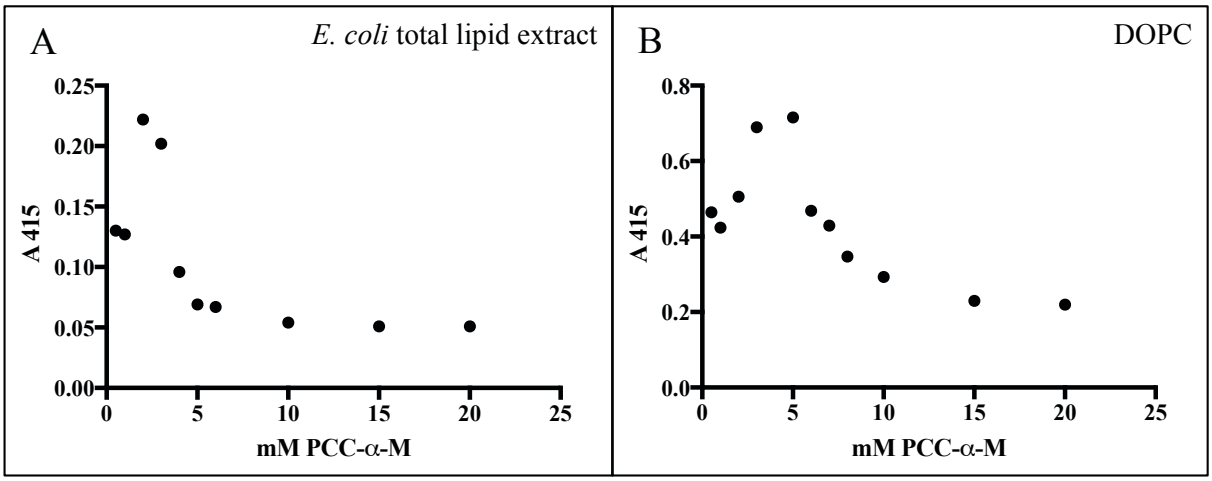

Figure 59: Destabilization of liposomes with different lipid compositions. A) Liposomes prepared from *E. coli* total lipid extract and B) liposomes prepared from DOPC were both destabilized with PCC-α-M.

3.5.2.5 Behavior of different detergents during the destabilization

The usage of polystyrene beads for removing the detergents enables the use of detergents with low cmc, which could be problematic in other applications like rapid dilution or dialysis. However, it also limits the choice to non-polar detergents as these adsorbed best to the non-polar beads. Mixing the protein with the destabilized liposomes exposes the protein to the detergent used for destabilization and dilutes the detergent used for purification. Thus it is desirable to use a detergent for destabilization that is mild and non-denaturing. Therefore the sugar-derivates β-DDM, LMNG and PCC-α-M were tested as well as Triton X-100. β-DDM, PCC-α-M and Triton X-100 showed the typical destabilization curve while LMNG displayed a one-point maximum but no curve progression (Figure 60 A, B and D). Furthermore all LMNG values except for the maximum were in the same absorption range (Figure 60 D). Measuring the samples at different wavelengths and with different buffer conditions gave the same result (data not shown). It is possible that LMNG could display a curve progression in the concentration range of 0 – 2 mM since the cmc of LMNG (0.01 mM) is more than 10 x lower compared to β-DDM and Triton X-100 (0.15 and 0.24 mM, respectively). However, PCC-α-M has a cmc of 0.036 mM and shows a similar behavior as β-DDM (Chae et al., 2010, Tiller et al., 1984, Hovers et al., 2011b). Both detergents displayed maxima at 4 mM detergent concentration, although β-DDM reached a higher maximal absorption than PCC-α-M. For both detergents the absorption values decreased to approximately 0.2. Triton X-100 has the highest cmc and the saturation was reached already at 1.5 mM. At higher detergent concentrations the absorption values decreased to almost zero (0.04 mM), which shows that not only the lipids but also the detergents absorb the light differentially. The destabilization

with Triton X-100 took place really fast compared to the other tested detergents. After 2 min incubation in Triton X-100 the destabilization of the lipids was visible and also measurable. The other detergents were incubated for 90 min as described earlier. This raised the assumption that different detergents also behave differentially concerning the incubation time. Therefore, the destabilization of lipids with PCC-α-M and β-DDM was compared after 30, 60 and 90 min. PCC-α-M needs at least 90 min to destabilize the liposome while for β-DDM the destabilization was achieved at 60 min. For both detergents 30 min were not enough to properly destabilize the liposomes (Figure 61). The detergents PCC-α-M, β-DDM and Triton X-100 successfully destabilized the liposomes under the elaborated conditions. LMNG was not considered as suitable for the destabilization without further optimization.

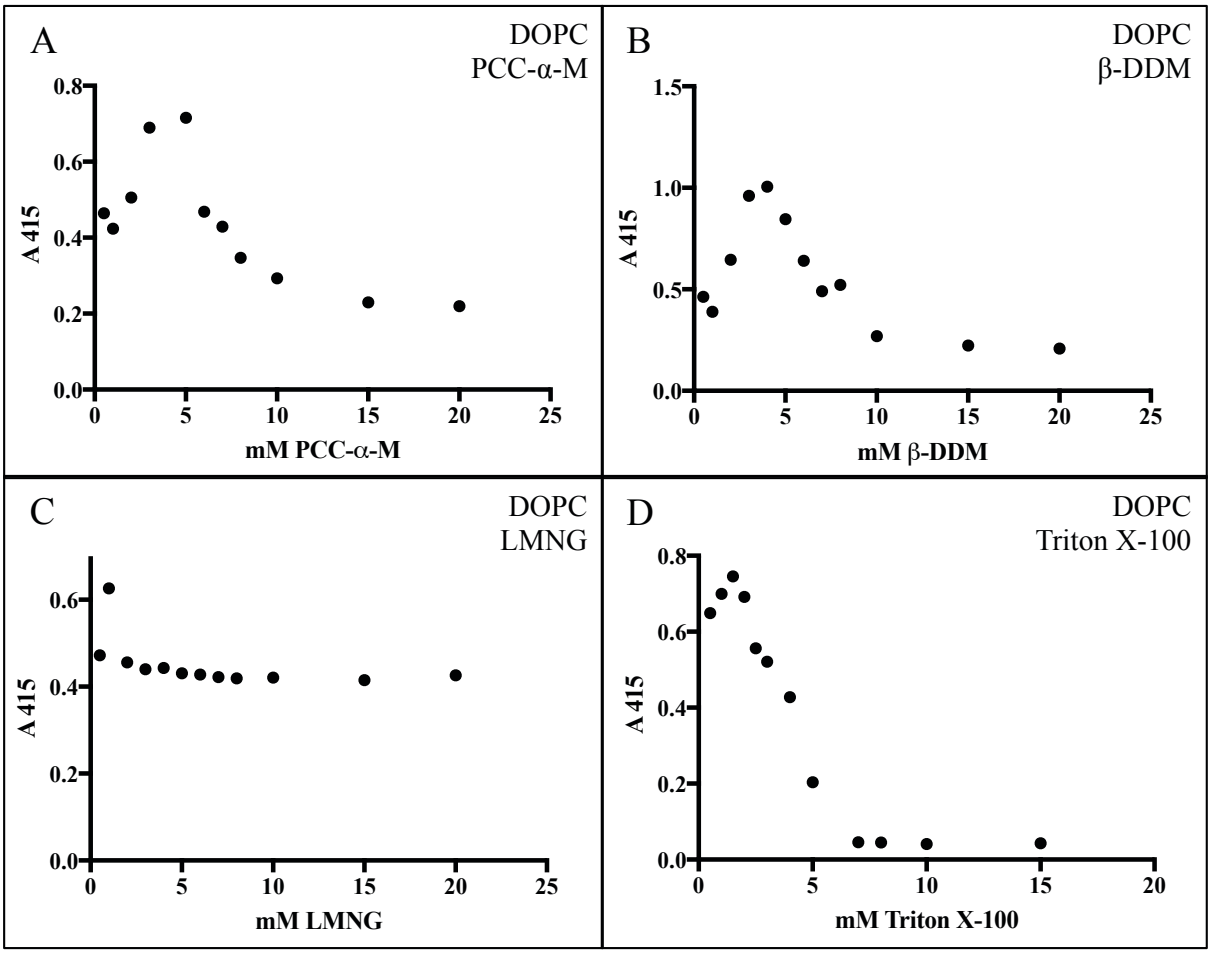

Figure 60: Comparison of different detergents for destabilization. DOPC liposomes were destabilized with PCC-α-M (A), β-DDM (B), LMNG (C) or Triton X-100 (D). PCC-α-M, β -DDM and LMNG were incubated for 90 min with the liposomes; Triton X-100 was incubated for 2 min.

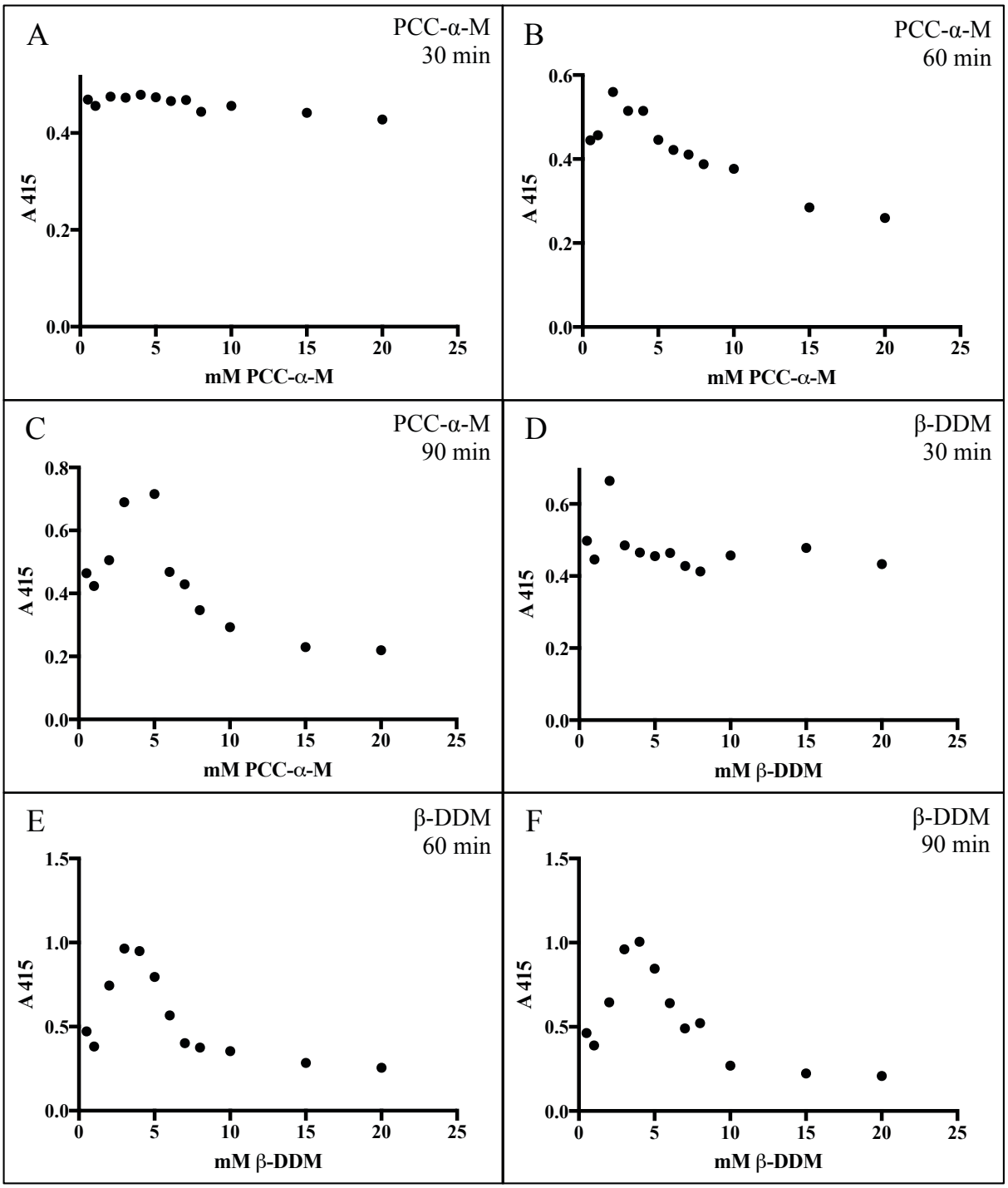

Figure 61: Comparison of the destabilization with PCC-α-M to the destabilization with β-DDM regarding the incubation time. PCC-α-M needs 90 min for the solubilisation process (A – C) compared to β-DDM (D – F), which needs 60 min.

3.5.2.6 Destabilization of DOPC/DOPE/DOPG liposomes with Triton X-100

For functionality, many membrane transporters require non-bilayer as well as anionic lipids. Therefore, the lipids DOPG and DOPE were added to DOPC in a ratio of 1:1:1 and liposomes were prepared. In order to test whether the differing lipid composition affects the destabilization the liposomes were titrated with Triton X-100 (Figure 62). The detergent concentration of the maximum absorption was similar, 2 mM (DOPC/DOPE/DOPG) and 1.5 mM (DOPC), though the absorption at the saturation point was less compared to the titration of the DOPC liposomes (0.32 compared to 0.75). The nature of the lipids therefore influenced the absorption values. The Triton X-100 concentration for the destabilization of DOPC/DOPE/DOPG liposomes was chosen to be 3 mM, which is in little excess of the saturation point.

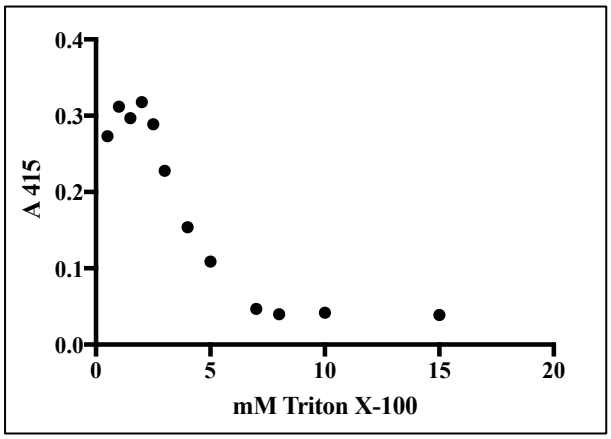

Figure 62: Titration of DOPC/DOPE/DOPG liposomes with Triton X-100.

3.5.3 Reconstitution of *At*PDR8 into DOPC/DOPE/DOPG liposomes and verification via floating gradient centrifugation

Liposomes containing the lipids DOPC, DOPE and DOPG were prepared and destabilized with Triton X-100 according to the optimized protocol described above. The protein was added to the detergent-destabilized liposomes in ratio of protein to lipids of 1:100. The detergent was successively removed by the step-wise addition of polystyrene beads. This step should force the insoluble protein into the destabilized liposomes otherwise it would precipitate. The complete absence of detergent should result in closed and intact proteoliposomes. Whether this process was successful was proven with a flotation gradient centrifugation (Hussain et al., 1981). In this method a gradient of the density medium

iodixanol was pipetted on top of the proteoliposomes starting with the highest concentration at the bottom (Figure 63, Density gradient). During centrifugation the lipids together with the proteoliposomes migrated to the top of the gradient. The gradient was separated into fractions and included proteins were TCA-precipitated and analyzed by Western Blotting. Figure 63 proofs that the reconstitution of *At*PDR8 into liposomes was successful as the protein was detected in the top fraction of the gradient. If the protein was not reconstituted it would have precipitated due to the absence of detergent. Precipitated protein would not float to the top together with the lipids but remain at the bottom of the gradient.

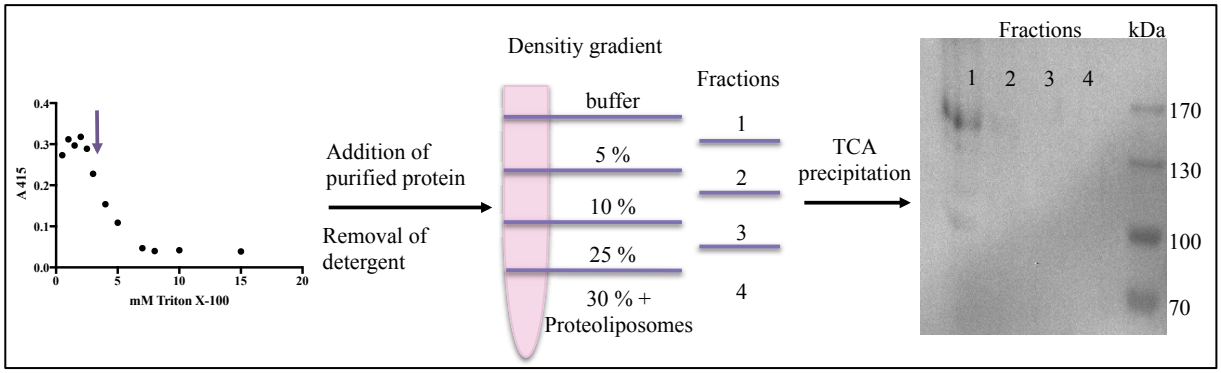

Figure 63: Reconstitution of AtPDR8 into DOPC/DOPE/DOPG liposomes. The liposomes were destabilized with Triton X-100 before the protein was added. The detergent was removed by successive addition of polystyrene beads. Flotation gradient centrifugation through a density gradient separated the proteoliposomes from not-reconstituted protein and liposomes. After precipitation of the fractions *At*PDR8 was detected by immunoblotting. kDa: protein marker with the fragment sizes 170, 130, 100 and 70 kDa.

3.6 Establishment of the vesicular transport assay with the *Sc*Pdr5 transport system

ABC transporters have the ability to transport several substrates that can be structurally unrelated compounds (Sakamoto et al., 2001, Kolaczkowski et al., 1996a). This can complicate an understanding of their physiological role. Especially when the mutant phenotypes are pleiotropic the identification of substrates and the characterization of the transporter may be difficult. In many cases vesicular transport assays with inside-out vesicles carrying ABC transporters were used to characterize these ABC transporters (Sharom et al., 1999, Zeng et al., 2000, Bakos et al., 1998). This requires expensive labeled substrates and, most importantly, the substrate must be somehow identified. Furthermore, this approach does not characterize the complete substrate spectrum. Krumpochova et al. (2012) combined the vesicular transport assay with liquid chromatography/mass spectrometry-based metabolomics to make an inventory of physiological substrates transported by human ABCC2. This chapter aimed the establishment of a transport assay for *At*PDR8 based on this method. This included first the transport of compounds into the vesicles, second the disruption of the vesicles after the transport and third the analysis of the vesicle content with mass spectrometry (Figure 64). In this case the transport step means the incubation of the vesicles with potential substrates in presence of ATP. To have a preferably large variety of compounds the vesicles could be incubated with plant cytosolic extracts or exudates. This allows a screening for substrates, which are transported to the inside of the vesicles. The obstacle is that natural compounds can occur in very low concentrations, which complicates subsequent analytics. Furthermore, a method must be found to get access to the vesicle content without interfering with the analytics. To address these points the transport assay was established with the *S. cerevisiae* ABC transporter Pdr5. It also belongs to the pleiotropic drug resistance family and the substrates have been studied before (Ernst et al., 2008, Gupta et al., 2014).

The establishment of the vesicular transport assay was performed in cooperation with Kalpana Shanmugarajah, Institute for Biochemistry, Heinrich-Heine University Düsseldorf, Germany. The mass spectrometry measurements were carried out by Dr. Sabine Metzger, CEPLAS Plant Metabolism and Metabolomics Facility, University of Cologne, Germany.

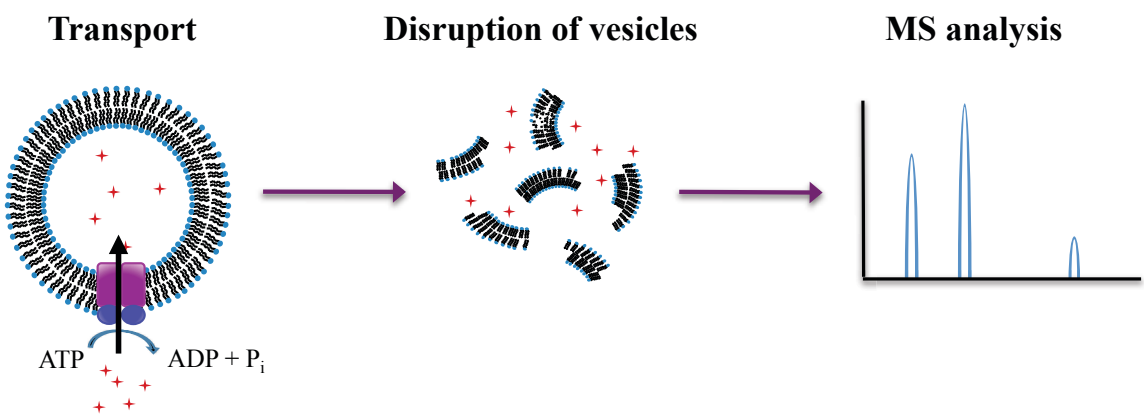

Figure 64: Scheme of the vesicular transport, the vesicle disruption and the mass spectrometry analysis.

3.6.1 Competitive *in vitro* transport of ketoconazole

Ketoconazole is an antifungal drug and a potential substrate to the ABC transporter *Sc*Pdr5. While *Sc*Pdr5 deficient yeast cells die at low ketoconazole concentrations, yeast cells expressing wild type *Sc*Pdr5 are more resistant to ketoconazole (Ernst et al., 2008, Gupta et al., 2014). This implies that *Sc*Pdr5 exports this cytotoxic compound. Thus, the ketoconazole transport by *Sc*Pdr5 has been proven *in vivo*, however, the proof for the *in vitro* transport is still missing. In comparison, the *Sc*Pdr5 mediated transport of the fluorescent compound rhodamine 6G was monitored *in vitro*. The transport into inside-out vesicles was detected by the fluorescence quenching of rhodamine 6G (Gupta et al., 2014). Figure 65 displays the quenching as the reduction of the monitored fluorescence after addition of ATP to the inside-out vesicles. In this study, the rhodamine 6G transport was used to indirectly demonstrate the *in vitro* ketoconazole transport. When both substrates are present they should compete for the *Sc*Pdr5 transporter. This should be detectable as it alters the monitored rhodamione 6G quenching. The fluorescence of rhodamine 6G together with the *Sc*Pdr5 wild type membrane vesicles was monitored over time (Figure 65 A). After 500 s the transport was activated by addition of ATP and the fluorescence decreased. When ketoconazole was present the fluorescence decreased less compared to the reaction with rhodamine 6G alone. However, the fluorescence decrease was not in linear dependence of the ketoconazole concentration. Up to 100 nM ketoconazole the fluorescence curves were similar displaying little rhodamine 6G transport compared to 0 nM ketoconazole. With higher ketoconazole concentrations the rhodamine 6G transport was also higher. When the experiment was repeated with the ATPase deficient *Sc*Pdr5 E1036Q mutant no rhodamine 6G transport was observed, independently of

the present ketoconazole (Figure 65 B). The reduced rhodamine 6G quenching in the presence of the non-fluorescent compound ketoconazole implies the transport of the same.

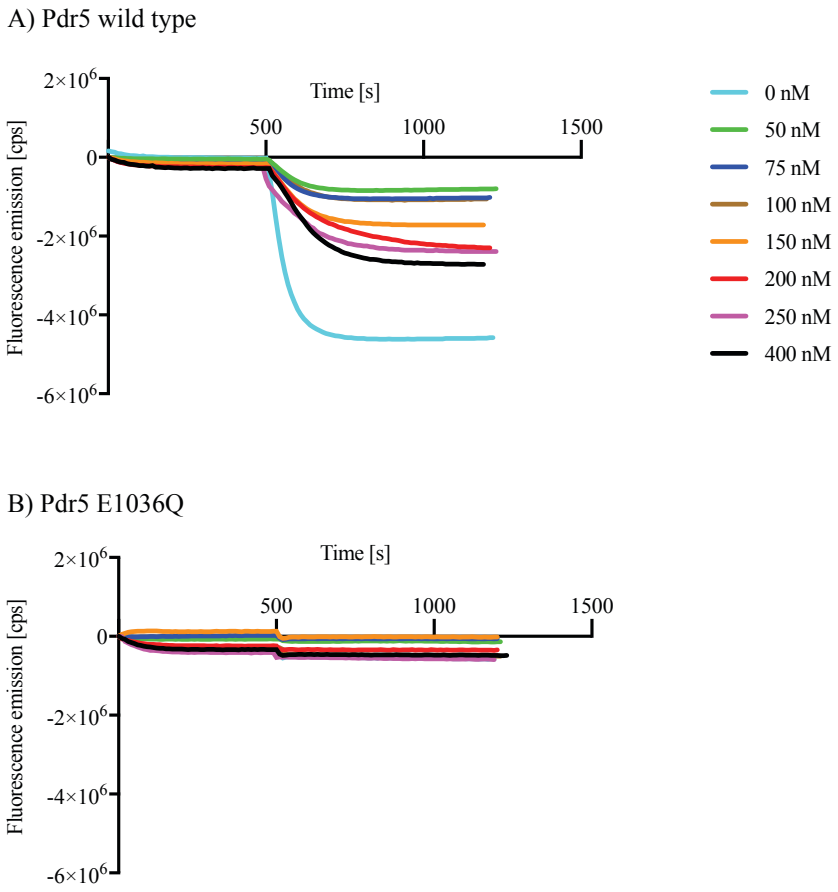

Figure 65: Competitive transport assay with *Sc*Pdr5. The rhodamine 6G transport was monitored as a quenching of the fluorescence signal after addition of ATP at 500 s. A) Transport assay with *S. cerevisiae* membranes containing the *Sc*Pdr5 wild type. B) Transport assay with *Sc*Pdr5E1036Q membranes. The colours represent the different ketoconazole concentrations that were added to the transport buffer next to rhodamine 6G. Turquoise: 0 nM, green: 50 nM, blue: 75 nM, brown: 100 nM, orange: 150 nM, red: 200 nM, pink: 250 nM and black: 400 nM ketoconazole.

3.6.2 Ketoconazole detection by mass spectrometry

Ketoconazole samples of different concentrations were analyzed with GC-ESI-TOF-MS. The theoretical mass of the protonated form is 531.16 g/mol. Figure 66 A shows the spectrum for the substance. The peak with a mass to charge ratio (m/z) of 531.14 belongs to ketoconazole. The other masses display the different isotope forms of ketoconazole. The chlorine isotopes ^{37}Cl and ^{35}Cl appear with a probability of app. 24.23 % and 75.77 %, respectively (Debievre and Taylor, 1993). Because the ketoconazole molecule has two chlorine atoms three isotope combinations are possible. Therefore the probability that two ^{35}Cl isotopes are present is 57.41 %, that one ^{35}Cl and one ^{37}Cl isotope is present is 36.72 % and that two ^{37}Cl isotopes are present is 5.86 %. This resembles the distribution of the ketoconazole isotope peak

intensities. The mass 531.14 is most abundant followed by the mass 533.14. The mass 535.14 was less abundant. The mass 532.14 could result from the ^{13}C isotope.

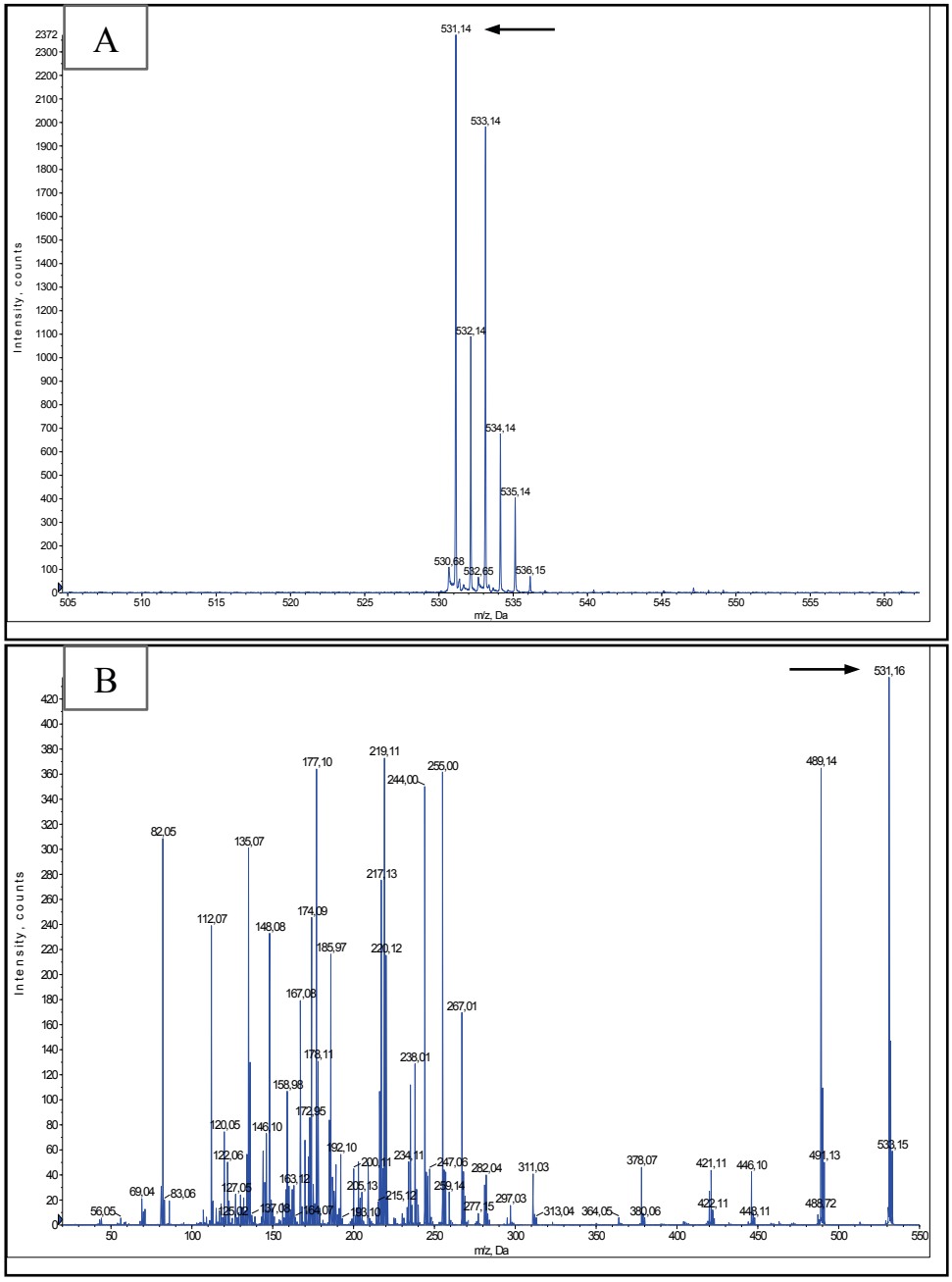

Figure 66: Mass spectrometry analysis of ketoconazole. A) ESI-TOF mass spectrum of ketoconazole analysed in positive-ion mode. B) ESI-TOF tandem mass spectrometric analysis of ketoconazole by scanning of m/z 531. The arrow marks the mass 531.

The tandem mass spectrometry spectrum (Figure 66 B) shows that the parent ion was most abundant. Smaller masses resulted from the fragmentation of the parent ion. The fragments with the higher intensities are listed in the table in Figure 67. Five possible fragmentation events of the ketoconazole molecule are schematically shown in Figure 67. For example fragmentation of the methylimidazole group creates the mass 82.05 (fragment 1 in Figure 67) and elimination of the methylcarbonyl radical creates the mass 489.14 of the remaining ion (fragment 3 in Figure 67). Similar fragmentation patterns of ketoconazole were also observed in other studies (Chen et al., 2002, Huang et al., 2007). This fragmentation pattern proofs that the mass 531 belongs to the substance ketoconazole.

m/z	Molecular formula
531.16	$C_{26}H_{29}Cl_2N_4O_4^+$
489.14	$C_{24}H_{27}Cl_2N_4O_3^+$
255.00	$C_{24}H_{27}Cl_2N_4O_3^+$
244.00	$C_{11}H_{10}Cl_2O_2^+$
219.11	$C_{12}H_{15}N_2O_2^+$
217.13	$C_{13}H_{17}N_2O^+$
177.10	$C_{10}H_{13}N_2O^+$
174.09	$C_{11}H_{12}NO^+$
135.07	$C_8H_9NO^+$
112.07	$C_6H_{10}NO^+$
82.05	$C_4H_6N_2^+$

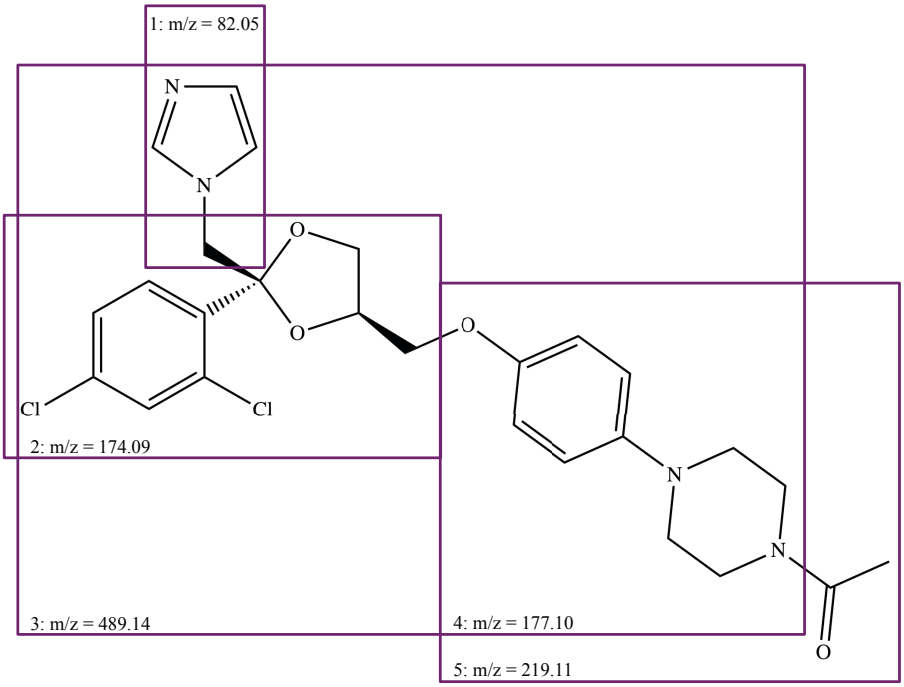

Figure 67: Fragmentation of the ketoconazole molecule. The corresponding molecular formulas to the masses that were detected in the tandem mass spectrum (Figure 66 B) are listed in the table on the left side. On the right side the ketoconazole molecule is shown. The boxes represent possible fragmentation events and the masses of the resulting fragments are stated inside the respective boxes.

The question whether the amount of transported ketoconazole in the transport assay is sufficient for detection by mass spectrometry was addressed by measuring very low concentrations down to 0.02 nM (Figure 68). The intensity of the 531.16 peak was in the range of 20,000 counts. This proofs that even substances of very low concentrations can be detected and makes mass spectrometry applicable for the detection of transported plant metabolites.

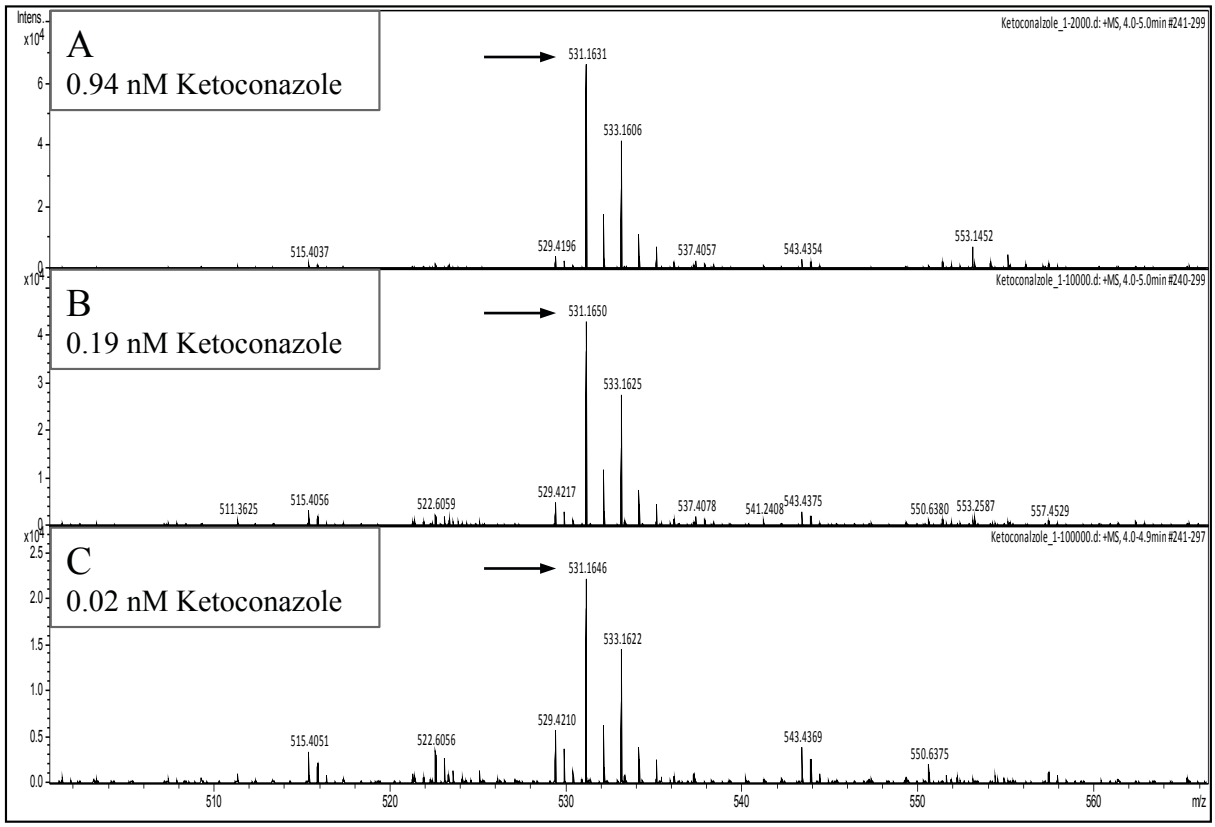

Figure 68: Detection of different ketoconazole concentrations by mass spectrometry analysis. Ketoconazole was diluted in water to A) 0.94 nM, B) 0.19 nM and C) to 0.02 nM. In all spectra the mas 531 (marked by the arrow) was clearly detectable.

3.6.3 Activity of *Sc*Pdr5 in Tris-HCl buffer

Previous studies used the buffering agent HEPES for *in vitro* assays with *Sc*Pdr5. However, when HEPES was present in the samples measured by mass spectrometry no ketoconazole was detectable (data not shown). The buffering agent was exchanged to Tris, which works better for mass spectrometry because the molecule is smaller and less complex than HEPES. The transport activity of *Sc*Pdr5 was confirmed by fluorescence measurement of rhodamoine 6G. Figure 69 shows the fluorescence curves of rhodamine 6G transported by *Sc*Pdr5 in different Tris-HCl buffer concentrations.

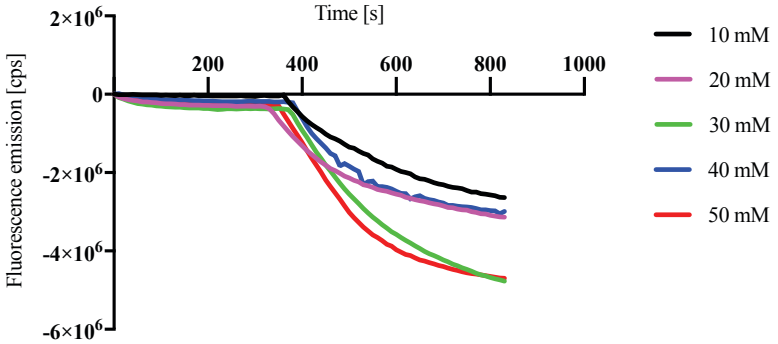

Figure 69: Transport of rhodamine 6G in Tris-HCl buffer. The transport was analysed in different Tris concentrations: 10 mM (black), 20 mM (pink), 30 mM (green), 40 mM (blue) and 50 mM (red).

3.6.4 Disruption of membrane vesicles

After the transport assay the vesicle content should be measured with mass spectrometry. This raises the challenge of opening the vesicles without interfering with the enclosed compounds or with the spectrometry analysis. Three different methods were tested to disrupt the membrane vesicles. These include chemical and physical approaches. Table 30 gives an overview about the different methods used and the obtained results.

Table 30: Overview about the tested vesicle disruption methods and results judged on the mass spectrometry spectry of ketoconazole (Figurejhsf and figure jhg).

Disruption method		**Result**	
Physical	Osmotic pressure	Inefficient	Small ketoconazole peak
	Ultrasonication	No disruption	No ketoconazole detectable
Chemical	Methanol	Disruption successful	WT displays higher ketoconazole peak than EQ

The physical disruption methods have the advantage that no additional substances are added to the vesicles that could interfere with the potential substrates or disturb the mass spectrometry measurements. Membrane vesicles were prepared in the presence of buffer and salt. Resuspension of the vesicles in water after transport should cause a swelling of the vesicles due to the increased osmotic pressure on the membrane and lead to the destruction of the vesicles. Figure 70 shows the mass spectrometry spectra of the disruption experiment with water. If the disruption was successful the spectra display the masses of the vesicles content after the transport assay. The spectrum of the disrupted *Sc*Pdr5 wild type membranes shows a ketoconazole peak (m/z = 531) with an intensity of appr. 16 counts. The spectrum of the *Sc*Pdr5 EQ mutant membranes shows no ketoconazole peak at all. This implies that the disruption was very inefficient since the peak intensity was hardly higher than the intensity of the background signals. Another physical disruption method tested was ultrasonication. This method was also applied for the generation of liposomes. It re-organizes the vesicle structures forming small unilamellar liposomes. This could free the enclosed substances. However, in this experiment the ketoconazole was not detected by mass spectrometry after the ultrasonication treatment (Figure 71 A and B). Neither the disruption test of the *Sc*Pdr5 wild type membrane nor of the EQ membranes lead to a detectable ketoconazole peak in the mass spectrometry spectrum.

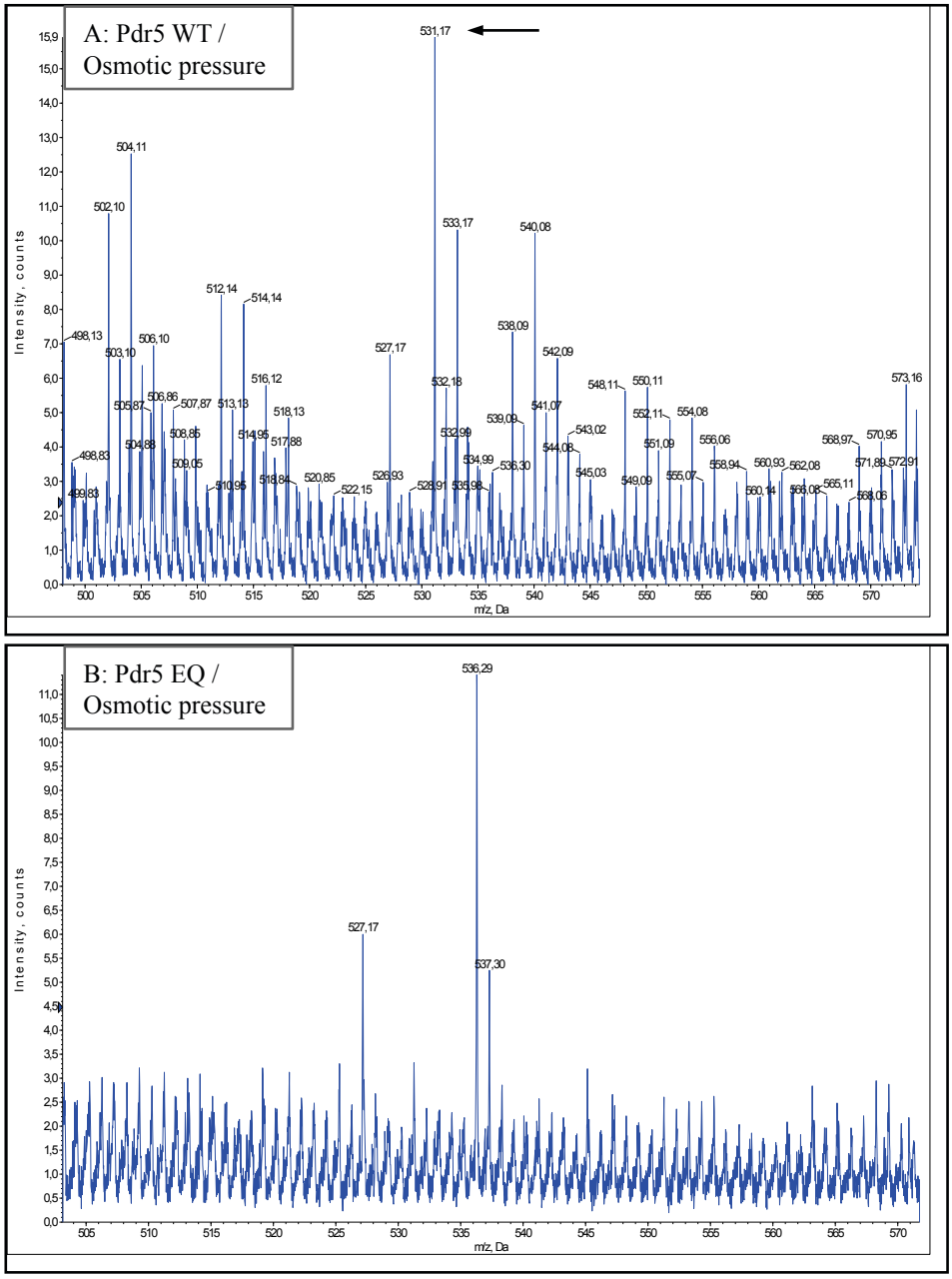

Figure 70: Disruption of membrane vesicles by changes in osmotic pressure. *Sc*Pdr5 wild type (A) and EQ (B) membrane vesicles were incubated in transport buffer with ketoconazole. For disruption the buffer was removed and the vesicles were resuspended in water. The insoluble membranes were separated by centrifugation and the supernatant was analysed by ESI-TOF mass spectrometry. The arrow marks the mass 531.

In the chemical disruption methods the lipids are dissolved by solvents or solubilized by detergents. The chemical method tested was the re-suspension of the vesicles in a methanol-water mix (80:20). Since most lipids dissolve in methanol the method should be able to destroy the vesicular structures. Figure 72 shows the MS spectra after the transport assay and the vesicle disruption with methanol.

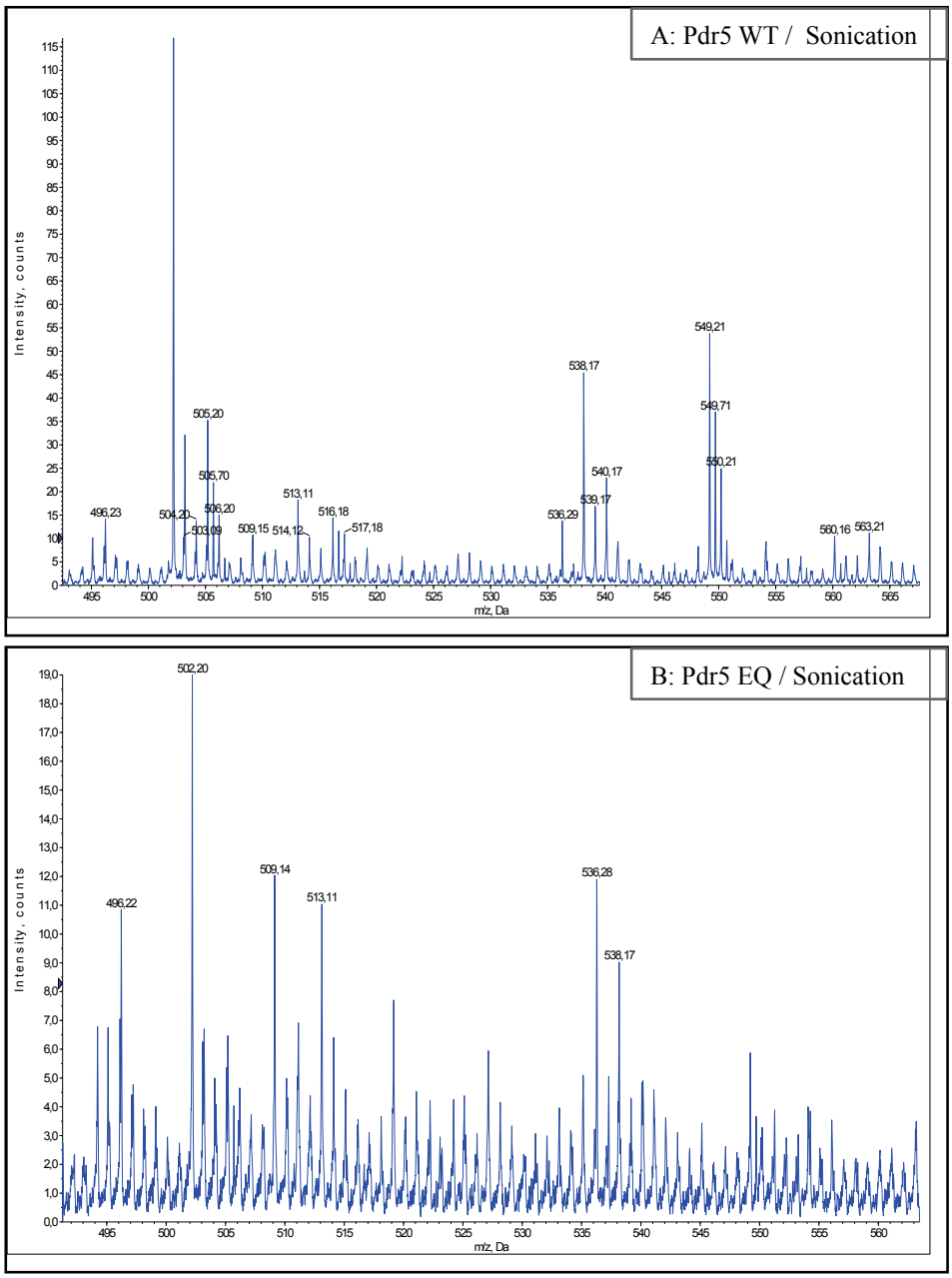

Figure 71: Disruption of membrane vesicles with ultrasonication. *Sc*Pdr5 wild type (A) and EQ (B) membrane vesicles were incubated in transport buffer with ketoconazole. For the disruption the buffer was removed and the vesicles were resuspended in water and sonicated. The insoluble membranes were separated by centrifugation and the supernatant was analysed by ESI-TOF mass spectrometry.

The spectrum for the *Sc*Pdr5 WT membranes displayed an appr. 2000 counts intense signal for the mass 531, which is the ketoconazole peak (Figure 72 A and C). The identity of the substance was confirmed by tandem mass spectrometry (Figure 72 B), where the MS/MS spectrum shows similar mass peaks as the MS/MS spectrum of ketoconazole in water (compare Figure 66 B). The spectrum for the *Sc*Pdr5 EQ membranes also displays a peak at the mass 531, but the intensity is with appr. 70 counts more than 25 times lower than the ketoconazole peak of the WT spectrum. The vesicle disruption with methanol was therefore successful.

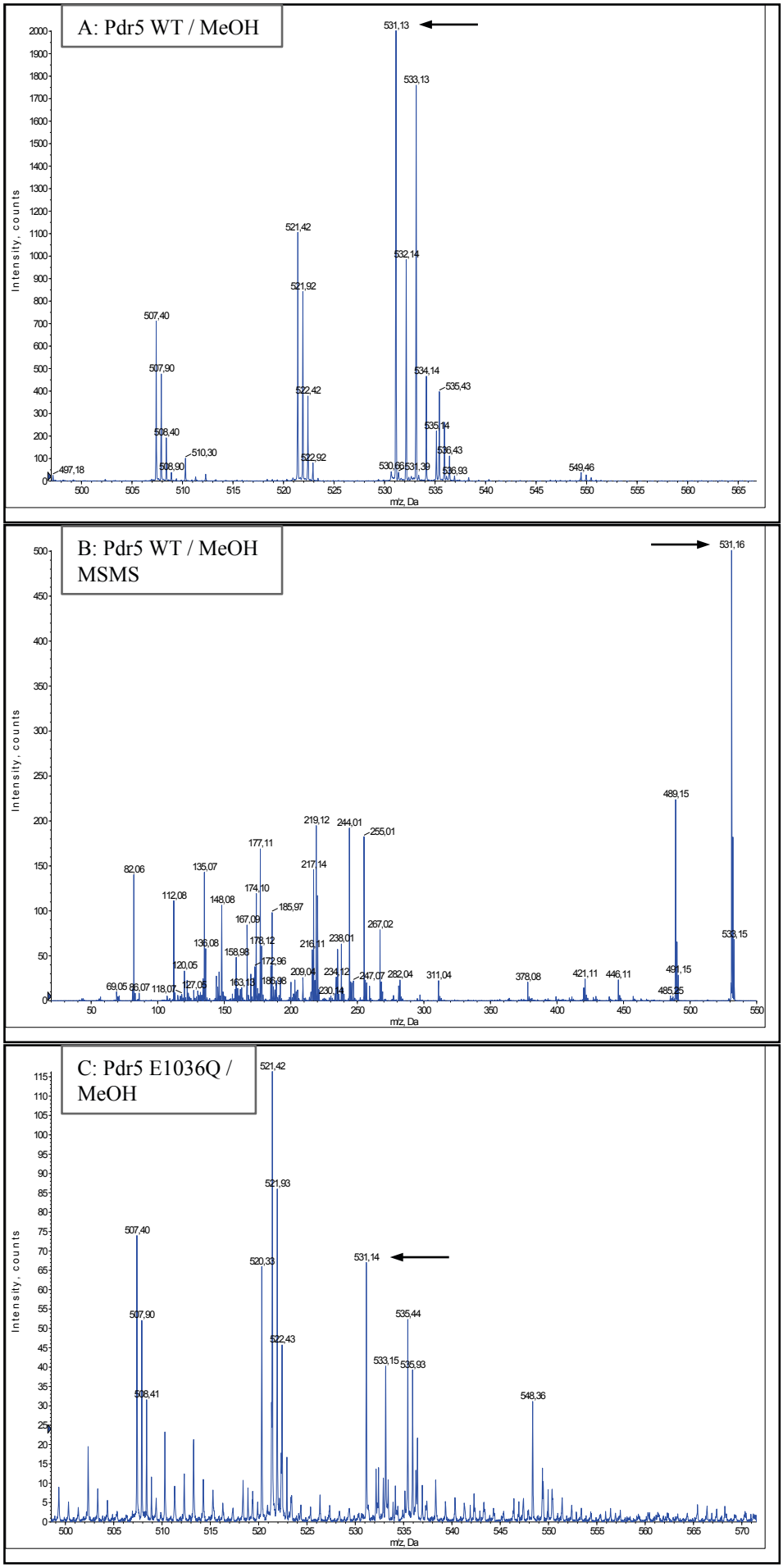

Figure 72: *Sc*Pdr5 wild type (A) and EQ (C) vesicles were disrupted with methanol. The vesicles were incubated in transport buffer with ketoconazole. For the disruption the buffer was removed and the vesicles were resuspended in 80 % methanol. The insoluble vesicles were separated by centrifugation and the supernatant was analysed by ESI-TOF mass spectrometry. The mass 531 was further analysed by tandem mass spectrometry to confirm the identity of the substance (B). The arrows mark the mass 531.

4 Discussion

4.1 Necessity of an *in vitro* system for the characterization of *At*PDR8

20 – 30 % of all genes code for membrane proteins, which applies for both prokaryotes and eukaryotes (Wallin and von Heijne, 1998). Membrane proteins fulfill essential physiological roles, which is demonstrated by the fact that many of membrane proteins are targets of drugs (Wagner et al., 2006). While animals have more ion channels plants exhibit elevated numbers of ABC transporters (Hwang et al., 2016). A possible explanation of the two – threefold higher numbers of ABC transporters in plants could be the sessile lifestyle of plants, which requires defense and detoxification mechanisms. In addition, plants produce a huge versatility of secondary metabolites, which often need to be transported across membranes since the productions sites may differ from the sites of action. ABC transporters were *inter alia* shown to be involved in detoxification mechanisms, plant defense, phytohormone transport and the transport of other secondary metabolites like terpenes, monolignols and coumarins (Alejandro et al., 2012, Kang et al., 2015, Kim et al., 2007, Demessie et al., 2017, Ziegler et al., 2017). In many cases the physiological role of the transporter was assessed from expression analysis as well as phenotypic and/or metabolite studies involving knockout and/or overexpressing plants and wild-type plants. However, plants are complex organisms and some mutants exhibit pleiotropic phenotypes. In such cases it remains to be clarified whether the diverse physiological roles are caused by a single compound or if several compounds are translocated. This also applies for *At*PDR8. The transporter is supposed to play a key role in nonhost resistance of *A. thaliana* to nonadapted pathogens. The protein is thought to export a bioactive compound produced by the PEN2 pathway. Additionally, *At*PDR8 seems to be involved in plant defense independent of the PEN2 pathway. This assigns *At*PDR8 an important role in plant defense. Apart from this, *At*PDR8 seems to further play a role in phytohormone transport, heavy metal transport and salt resistance. In order to shed light on the transported substrates of *At*PDR8 an *in vitro* system is required that allows the functional characterization of the transporter. The establishment of the *At*PDR8 *in vitro* system was therefore the subject of this work.

In order to perform functional *in vitro* studies proteins need to be cloned, overexpressed and purified, which remains a challenging task especially for eukaryotic membrane proteins. This is underlined by the fact that until today only two plant PDR proteins, *Nt*PDR1 and NpPDR5,

have been purified and characterized *in vitro* (Pierman et al., 2017, Toussaint et al., 2017). In the case of *Nt*PDR1 the heterologous overexpression in *S. cerevsisae* was not successful which is why *Nt*PDR1 was expressed in the homologous system (Crouzet et al., 2013). Expression trails of *Np*PDR5 in *S. cerevisiae* and *S. pombe* also resulted in misfolding and mistargeting of the protein so that *Np*PDR5 had to be expressed in tobacco cells as well (Toussaint et al., 2017).

4.2 Cloning of *At*PDR8 for heterologous expression

Cloning of *At*PDR8 comprised three steps: 1) the amplification of the coding sequence from cDNA, 2) the integration of the coding sequence into the pJET1.2/blunt vector and 3) the integration of the coding sequence into the expression vector for the respective expression system. For the amplification from cDNA it is very important to use cDNA obtained from plant material with a sufficient amount of transcripts. Some ABC transporters are only expressed in certain organs or tissues of the plant (Kang et al., 2011) and expression might be induced at certain conditions, like for example iron starvation (Ziegler et al., 2017). Low transcript levels of the respective ABC transporter gene in the plant material might complicate the amplification from cDNA since the relative abundance of the target sequence is low. *At*PDR8 was shown to be ubiquitously expressed in all plant organs of *A. thaliana* (van den Brule and Smart, 2002). Although *At*PDR8 expression is elevated by pathogen attack (Kobae et al., 2006), Underwood and Sommerville (2013) showed that the gene is constitutively expressed so that the protein can be recruited to infection sites in case of pathogen attack (Underwood and Somerville, 2013). The continuous abundance of *At*PDR8 transcripts in all plant organs could have facilitated the amplification from cDNA compared to the amplification of other *PDR* genes (data not shown). For further amplification of the *AtPDR8* gene in *E. coli* the PCR product was first cloned into the vector pJET1.2/blunt. The linearized vector contains the lethal gene *eco47IR,* which gets destroyed if the insert is integrated *(Hoseini and Sauer, 2015)*. This enabled efficient positives selection of *AtPDR8*-containing clones since all clones without any insert were non-viable. Figure 12 (chapter 3.2.2) shows that out of six tested clones one clone carried the *AtPDR8* gene. Compared to the first steps, cloning of *At*PDR8 into the respective expression vectors was complicated. Expression vectors for *E. coli*, *S. cerevisiae*, *L. lactis* and *P. pastoris* were used. Cloning was started using restriction digestion and ligation enzymes. DNA fragments were digested with two different restriction enzymes to reduce the probability of wrong fragments inserted into the

vectors. Still many tested clones did not contain the correct insert or only the empty vector. Several instances occurred were the *At*PDR8 sequence was integrated into the vectors but the orientation of the gene was inverted. To reduce the high background of empty vectors different cloning techniques were applied, which all did not result in positive *AtPDR8* clones. Homologous recombination in *S. cerevisiae* did not result in viable colonies. Positive *AtPDR8* clones were obtained for the *P. pastoris* vectors pSGP18-2µ and pSGP18-Ntag. During the expression studies it became evident that stop codons had been integrated into the *AtPDR8* coding sequence, which might have enabled cloning of *AtPDR8*. All these data point to toxicity of the *AtPDR8* gene product to the cloning host. It seems that positive *AtPDR8* clones were only propagated if the *AtPDR8* sequence was disrupted. This assumption is supported by the observation of reoccurring stop codons and mutations (e.g. deletion of the start codon) during different re-transformation steps of the *AtPDR8* constructs (data not shown). Toxicity could result from basal promoter activity, which can lead the accumulation of toxic gene products, especially in case of high-copy number plasmids. This in turn results in either cell death or evading the lethality by mutations (Lee, 2009).

Unstable DNA sequences and toxicity to the cloning host are phenomena observed for other membrane proteins as well. For example the fungal calcium channel Cch1 could only by cloned by homologous recombination in *S. cerevisiae* (Vu et al., 2009). Cloning of the housefly sodium channel *Vssc1* using conventional techniques involving a high-copy number plasmid was unsuccessful but could be realized by the utilization of a low-copy number plasmid in combination with an *E. coli* strain that reduces plasmid replication (Lee, 2009). Several studies reported toxicity problems and mutations when cloning the human bile salt export pump BSEP in *E. coli* (Byrne et al., 2002, Byrne et al., 2009, Noe et al., 2002). *Np*PDR1 could not be cloned at all because the coding sequence was rearranged in *E. coli* (Crouzet et al., 2013).

In some cases avoiding *E. coli* by performing homologous recombination in *S. cerevisiae* helped to solve the cloning issues (Stindt et al., 2011, Vu et al., 2009). However, when homologous recombination was performed for the *AtPDR8* constructs no *S. cerevisiae* colonies were obtained. This could have had two reasons. First the homologous recombination itself did not work, which could have been due to inefficient transformation of the DNA fragments or inefficient recombination events. Second, *At*PDR8 could also be toxic for *S. cerevisiae*. This would be quite extraordinary since other potentially toxic eukaryotic

sequences were successfully cloned in *S. cerevisiae* and *At*PDR8 was successfully overexpressed in the yeast *P. pastoris*. However, the used vector for yeast homologous recombination was p426GPD, which contains the constitutive GPD promoter for expression in yeast, meaning in case of successful recombination the gene was constitutively transcribed. Other plant PDRs were overexpressed in *S. cerevsisiae* (Kang et al., 2010, Demessie et al., 2017) and at least no stability problems were reported. Contrary to this, expression of *Nt*PDR1 in *S. cerevisiae* was low and unstable (Crouzet et al., 2013). Thus potential toxicity of *At*PDR8 to *S. cerevisiae* cannot be excluded.

Another strategy to circumvent DNA mutations and rearrangement is the usage of *E. coli* strains that were engineered for the propagation of unstable plasmids. The SURE 2 strain fails to produce certain proteins that are involved in the reorganization and deletion DNA fragments that build certain secondary and tertiary structures often found in eukaryotic DNA (Stratagene). However, in this study the usage of SURE 2 cells did not facilitate the cloning process as these cells were designed to prevent reorganization of DNA but not the toxicity of the gene products to the *E. coli* cells. On the other hand CopyCutter™ EPI400™ cells (epicentre) limit the number of plasmids in the cell and thereby reduce the accumulation of toxic gene products. Using these cells for the re-transformation steps of the successfully cloned *AtPDR8* constructs avoided the occurrence of mutations in the *AtPDR8* coding sequence. Reducing the copy number in *E. coli* cells thereby seems to be a helpful tool to accomplish propagation of plasmids containing plant *PDR* genes in *E. coli*.

4.3 Expression and localization of *At*PDR8 in *P. pastoris*

The intrinsic expression of membrane proteins is usually to low for isolation and subsequent biochemical studies (Wagner et al., 2006). This requires a suitable overexpression system. However, heterologous expression of helical membrane proteins is still a bottleneck (Wagner et al., 2006). This is mainly caused by the size and the hydrophobic nature of membrane proteins. Successful expression leading to functional protein comprises the correct translation, the correct folding and correct trafficking of the protein into the membrane. Extensive overexpression might result in overwhelming of the membrane protein insertion machinery and lead to misfolding and degradation of the target membrane protein (Vogl et al., 2014). Choosing the right host is therefore indispensible for successful overexpression of membrane proteins. The expression of *At*PDR8 in *E. coli* was not successful although different strains

and tag positions were tested. The translation elongation and folding rates of prokaryotes are higher than those of eukaryotes (Wagner et al., 2006, Grisshammer, 2006), which might have hampered the expression of *At*PDR8 in *E. coli*. Therefore the yeast *P. pastoris* was chosen for heterologous expression of *At*PDR8.

P. pastoris is one of the most commonly used systems for overexpression of membrane proteins and many structures were determined using *P. pastoris* for protein production (Vogl et al., 2014). The system does not require complex growth conditions and harbors the eukaryotic protein processing machinery (Macauley-Patrick et al., 2005). Unlike *S. cerevisiae*, *P. pastoris* is a Crabtree-negative yeast. Under aerobic conditions *P. pastoris* metabolizes glucose by respiration while in *S. cerevisiae* glucose is metabolized by fermentation to ethanol (Vogl et al., 2014). It is furthermore a methylotrophic yeast meaning it can use methanol as a sole carbon source. Most enzymes required for the methanol metabolism are only synthetized in presence of methanol, which makes the system applicable for the induction of heterologous protein production. The AOX1 promoter has therefore been used in most cases to drive heterologous expression in *P.pastoris*. Some proteins could not be functionally expressed in other systems like *S. cerevisiae*, bacteria, baculorvirus or insect cells but were successfully expressed in *P. poastoris* (Macauley-Patrick et al., 2005). Another feature of *P. pastoris* is the ability to grow to high cell densities. This is especially advantageous for the heterologous production of membrane proteins that might exhibit lower expression levels per cell, which can be compensated by high cell densities. The fermentation of *At*PDR8-expressing *P. pastoris* cells resulted in up to 20 g/L culture medium. However, as the example of *At*PDR8 also shows, heterologous expression of membrane proteins remains difficult. First trials of *At*PDR8 expression in *P. pastoris* were not successful since the protein was not detectable by immunoblotting.

Successful expression depends *inter alia* on the sequence properties of the heterologous protein, the cultivation conditions and the cellular environment of the expression host. Optimization of the heterologous overexpression of proteins comprises extrinsic and intrinsic parameters (Vogl et al., 2014). Extrinsic parameters that were changed during the establishment of the *At*PDR8 overexpression system were temperature, media compositions and aeration. All these changes did not result in successful expression of the C-tagged construct. Intrinsic parameters that influenced successful overexpression of *At*PDR8 in *P. pastoris* were the position of the affinity tag and the sequence properties.

Although numerous clones were tested at different culture conditions, the C-terminally tagged *At*PDR8 construct could not be expressed (chapter 3.2.4). When the affinity tag was cloned to the N-terminus of *At*PDR8 all tested *P. pastoris* clones expressed *At*PDR8, which was confirmed by immunoblotting (chapter 3.2.11). There are four possible explanations why the C-tagged constructs did not show detectable expression. One reason could be that the protein was expressed but the C-terminal tag was not accessible for the antibody. Because of the reverse domain orientation of *At*PDR8 the C-tag was fused to the second TMD. Depending on the topology of *At*PDR8 the C-terminus could either end at the cytoplasmic side of the membrane or at the apoplastic side. While the NBDs extend into the surrounding medium the cytoplasmic C-terminus is probably close to the lipid bilayer and might be shielded by the other domains. According to the domain model proposed by Stein et al. (2006) the 13th α-helix ends at the apoplastic side of the membrane. In such case the preparation of (mainly) inside-out membrane vesicles would make the C-terminus inaccessible for the antibody and the sensitivity could be too low for detecting the C-tagged protein only in membrane sheets. Low immunoblotting sensitivity could also be a problem if the expression was generally low. Analyzing the codon usage of the *At*PDR8 coding sequence by *P. pastoris* (Fuhrmann et al., 2004) shows that rare codons occur throughout the complete *At*PDR8 coding sequence; on average every fifth codon of *At*PDR8 displays a frequency of less than 20 % in *P. pastoris*. Rare codons sometimes hamper smooth protein expression (Bai et al., 2011). However, this reason does not explain why the expression of the N-terminally tagged construct worked. The tag sequence for the N-terminus was synthetically produced in a codon optimized version for *P. pastoris* and integrated into the pSGP18 expression vector while the C-terminal tags were deleted. Optimization of the codon usage at the beginning of the coding sequence can stabilize the initiation complex of the protein expression machinery (Chen and Inouye, 1990). This could explain why the N-terminally tagged construct was successfully expressed in contrast to the C-terminally tagged construct in regard of codon usage. A third reason why the C-tagged construct was not expressed could have been the formation of secondary mRNA structures that inhibited the formation of the translation initiation complex. Possibly the formation of hairpins or stem loops could have blocked the ribosome binding site of the C-tagged construct. The N-terminal tag could have prevented secondary structure formation near the ribosome binding site and thereby enable translation (Coleman et al., 1985, Griswold et al., 2003, Ramesh et al., 1994, Svensson et al., 2006, Busso et al., 2003). A fourth reason why the C-tagged construct was not expressed could have been misfolding of the protein. The C-terminal tag could have prevented proper folding of *At*PDR8, which might have caused

degradation of the protein. Indeed, it was reported that the position of the tag can influence protein production (Sachdev and Chirgwin, 1998).

The sequence stability was another parameter influencing *At*PDR8 expression in *P. pastoris*. During the cloning process four mutations were integrated into the *At*PDR8 coding sequence that resulted in amino acid substitutions. These mutations might have stabilized the molecule enabling expression in *P. pastoris*. The sequence was corrected by mutating the respective bases back to the published coding sequence (Huala et al., 2001). However, the corrected construct did not express any more in *P. pastoris* indicating that the amino acid substitutions were critical for successful expression. The substitution of amino acids is a common tool in order to enhance stability of heterologously expressed proteins and was used before (Yang et al., 2018, Warne et al., 2008).

Apart of the successful expression the correct targeting is also important for heterologous production of functional protein. Except for some peroxisomal and mitochondrial membrane proteins, most membrane proteins enter the secretory pathway, but instead of being secreted they localize to the ER, Golgi or the plasma membrane. In that pathway the ER is important for the correct folding, posttranslational modifications and membrane insertion (Vogl et al., 2014). The correct localization of the heterologously expressed membrane protein implies that folding and trafficking were correct. In *A. thaliana At*PDR8 was shown to be localized in the plasma membrane of leaf epidermal cells and epidermal and lateral root cap cells (Kim et al., 2007, Kobae et al., 2006). In order to check the localization of *At*PDR8 expressed in *P. pastoris* sucrose gradient centrifugation was performed. *At*PDR8 was detected in the same fractions as the controls *Sc*Pdr5 expressed in *S. cerevisiae* and *Hs*MDR3 expressed in *P. pastoris*. This result points to a plasma membrane localization of *At*PDR8 in *P. pastoris* and thus correct. In order to support this result a second technique to determine the subcellular localization of *At*PDR8 in *P. pastoris* was applied, fluorescence microscopy. Therefore the GFP coding sequence was fused to the N-terminus of the already N-tagged *At*PDR8 construct in the *P. pastoris* expression vector pSGP18. Expression of the GFP-fusion protein was not detectable by immunoblotting, only by fluorescence microscopy. This indicates that expression of GFP-*At*PDR8 was significantly lower compared to *At*PDR8 alone, which could be due to the increased size of the fusion protein. Bernaudat et al. (2001) analyzed the expression of different membrane proteins in different heterologous systems. They could show that with increasing molecular weight heterologous expression was less easily achieved

(Bernaudat et al., 2011). These results correspond to the reduced expression of the GFP-*At*PDR8 fusion protein. Fluorescence microscopy confirmed the plasma membrane localization of *At*PDR8 in *P. pastoris*; however, a considerable amount of the fusion protein was detected in other compartments. A possible explanation for this could be that the GFP fusion leads to mistargeting. Another explanation could be that the additional GFP sequence hampers the folding, which could be why the protein gets stuck in the protein control in the ER.

4.4 Purification of *At*PDR8

Biological membranes not only contain lipids, but also a substantial amount of proteins that are embedded in the lipid bilayers. The protein-lipid ratio ranges from 4:1 to 1:4 depending on the membrane of interest (Berg et al., 2007) This is why endogenous membrane proteins can bias *in vitro* studies of an overexpressed protein. Thus, biochemical characterization requires the purification of the protein of interest.

The first step of the purification of a membrane protein is the solubilization out of the membrane. This requires detergents, which are solubilizing agents consisting of a hydrophilic head group and a hydrophobic tail. Every detergent interacts differently with the membrane and the integral proteins, which depends on the lipid composition of the membrane and the chemical properties of the membrane proteins. Therefore extensive screening might be required to find a suitable detergent for the solubilization of the membrane protein of interest (le Maire et al., 2000). In order to determine which detergents are able to solubilize *At*PDR8 out of the *P. pastoris* membrane 88 different detergents were tested applying the DotBlot technique (Ellinger et al., 2013). The screening included nonionic, anionic, cationic and zwitterionic detergents. As Figure 35 (chapter 3.4.2) shows *At*PDR8 was solubilized best by zwitterionic detergents. The group of Fos-Cholines displayed the strongest signals in the DotBlot, out of which Fos-Choline-14 und -15 solubilized *At*PDR8 most efficient. Weaker signals were obtained by the solubilization with DDAO, which is also zwitterionic, and with sodium dodecanoyl sarcosine, which is an ionic detergent. Weak signals were also detected for the solubilization with CHAPS and CHAPSO, which are again zwitterionic but are steroid-based in comparison to the Fos-Cholines that contain an alkyl chain. The only nonionic detergents that slightly solubilized *At*PDR8 were n-heptyl-β-D-glucopyranoside and n-heptyl-β-D-thioglucopyranoside. These data demonstrate that ionic charges are required for

the solubilization of *At*PDR8 out of the *P. pastoris* membrane. The comparison of the Fos-Cholines with CHAPS and CHAPSO illustrates that the combination of the hydrohpilic haed group with an alkyl chain is more efficient than with a carbon ring. Solubilization furthermore improves with increasing number of carbon atoms in the carbon chain up to 14 and 15 (Fos-Choline-14 and -15), but is again reduced for 16 carbon atoms.

The solubilization comprises three stages. In stage I the detergent penetrates the lipid bilayer. Since the detergent concentration is below the critical micellar concentration (cmc) and below R_{sat} no micellar structures are formed. In stage II the lipid bilayer gets saturated with detergent and is bulging. With increasing detergent concentrations the detergent forms micelles that constantly deliver detergent molecules to the lipid bilayer. Lipids get extracted from the bilayer and incorporate into the micelles. Stage III displays the complete solubilization of the lipid bilayer resulting in detergent-lipid mixed micelles (le Maire et al., 2000, Lichtenberg et al., 2013). Removal of the lipids from the membrane exposes the hydrophobic parts of the membrane proteins, which in turn get engulfed by detergent molecules (le Maire et al., 2000). A possible explanation for the higher effectiveness of the Fos-Cholines might be that the structure of an ionic head group and an alkyl chain resembles the structure of membrane lipids and thereby facilitates the penetration into the *P. pastoris* membrane. Furthermore the Fos-Cholines exhibit low cmc, which enables the formation if micelles at lower detergent concentrations.

*At*PDR8 was purified using affinity chromatography. The *At*PDR8 construct comprised two affinity tags at the N-terminus of the protein sequence. The purification protocol was established in this thesis. Comparing a flow-though column with a resin revealed that binding was more efficient using the resin. The reason might be the batch incubation overnight, which allowed extensive interaction of the protein with the resin. This resulted in higher concentrated and more pure protein in the elution fractions after affinity chromatography. The positive effect of the batch incubation was independent of the used affinity tag; purification using the 10 x Histidine tag delivered similar results as the purification with the CBP tag. Tandem affinity chromatography, which comprises the combination of the IMAC and the CBP-AC, did not improve the purity of the eluted protein. In theory, the CBP tag binds specifically to calmodulin, which is more selective than the binding of the histidine tag to the metal ions, which is why the CBP tag was used for further purifications. The elution fractions of the affinity chromatography contained a lot of fragments of lower molecular weight, which

likely were degradation products of *At*PDR8. In order to remove these fragments a size exclusion chromatography was performed. The *At*PDR8 protein peak in the SEC chromatogram displayed a shoulder, which could be aggregated protein. SDS-PAGE of the fractions of the *At*PDR8 protein peak showed that the impurities were less abundant compared to the elution fractions of the CBP-AC, but not all impurities could be separated. *At*PDR8 purified in Fos-Choline-14 did not display ATPase activity.

Ionic and zwitterionic detergents are generally considered as harsh detergents meaning they are efficient solubilizers but often lead to the inactivation and denaturation of membrane proteins (le Maire et al., 2000). The detergent was therefore exchanged during the washing step of the affinity chromatography to β-DDM, which is a mild, non-ionic detergent. However, this did not restore ATPase activity. Furthermore, the CBP-AC elution fractions displayed a similar pattern of impurities and the result of the size exclusion chromatography showed that the protein was inhomogeneous and the yield was low. The detergent PCC-α-M was then used instead, which was synthesized by Hovers et al. (2011). The detergent contains a polar maltosyl head group connected to a propylbicyclohexyl group. The rigid and inflexible structure of the hydrophobic group increases the van-der-Waals contacts when the detergent molecules aggregate in the micelle, which resembles the surface tension in the lipid bilayer. This results in a mild detergent that improves the stability of membrane proteins in solution compared to the detergent β-DDM (Hovers et al., 2011b).

PCC-α-M forms micelles of similar molecular masses as β-DDM (63 and 66 kDa, respectively), but the maximal micellar radius of PCC-α-M is smaller than the radius of β-DDM with 11.2 Å compared to 13.7 Å. β-DDM has a higher cmc than PCC-α-M (0.17 and 0.036 mM, respectively), which results from the higher polarity of β-DDM compared to PCC-α-M (Hovers et al., 2011b). The two GPCRs, turkey β_1-adrenergic receptor and human Smo, displayed increased stability when purified in PCC-α-M compared to the purification in β-DDM. In addition, the cytochrome b6f complex, which is inactivated in high β-DDM concentrations, retains activity in a PCC-α-M solution of the same concentration (Hovers et al., 2011b). Because of these data purification of *At*PDR8 in PCC-α-M was analyzed. The elution fractions of the CBP-AC displayed significantly fewer impurities on the Coomassie blue stained gel and on the Western Blot compared to the purification in other detergents. Size exclusion chromatography resulted in pure protein. However, for the SEC the protein had to be concentrated, which resulted in the precipitation of almost half of the protein, which is

displayed by the big aggregate peak in the SEC chromatogram and the Coomassie blue-stained gel of the concentrated elution fraction (Figure 47 and Figure 48). No ATPase activity of *At*PDR8 was detected in PCC-α-M solution, however, the reduced degradation products of *At*PDR8 point to an increased stability of the protein in the detergent PCC-α-M, which is why this detergent was used in the final purification protocol.

4.5 Degradation of *At*PDR8

During the purification of *At*PDR8 additional bands of lower molecular weight than *At*PDR8 were observed on Coomassie blue-stained gels and Western Blots. The fact that these fragments were detected by both the anti-His antibody (chapter 3.4) and the anti-CBP antibody (data not shown) implied that they were degradation products of *At*PDR8. This assumption was confirmed by mass spectrometry, which identified the fragments *inter alia* as *At*PDR8 peptides (chapter 3.4.6). Degradation has caused difficulties when recombinant protein production was performed in *P. pastoris* (Ahmad et al., 2014).

But at which step did the degradation of *At*PDR8 occur? The degradation could take place *ex vivo* during the purification process. The cell disruption frees intrinsic proteases of *P. pastoris*, which can cleave the protein during downstream applications. The calmodulin affinity chromatography involved the overnight incubation of the protein slurry with the resin. This could have facilitated degradation although protease inhibitors were used. The presence of high concentrations of the detergent Fos-Choline-14 (up to 3 %) might have destabilized the protein as well. Alternatively, the degradation could occur *in vivo* during the heterologous overexpression, folding and targeting in *P. pastoris*.

Overexpression can overload the ER protein folding machinery, which results in misfolding. The accumulation of too many unfolded proteins induces the unfolded protein response (UPR). In order to eliminate stress, the UPR downregulates the expression of the heterologous protein and upregulates the expression of proteins that assist in folding. In addition, it also upregulates the ER-associated protein degradation system (ERAD). In the ERAD process the misfolded proteins get dislocated from the ER, ubiquinated and are finally degraded by the proteasome (Wagner et al., 2006).

The mass spectrometry analysis of purified *At*PDR8 also revealed the presence of ubiquitin in the samples. Furthermore the GlyGly modification, which points to the binding of ubiquitin, was detected at several *At*PDR8 peptides. These results indicate that *At*PDR8 was partially degraded in response to overload of the ER.

Degradation of the target protein can have several negative effects for downstream applications. The overall yield is reduced if a substantial amount of the overexpressed protein is degraded. Degradation can also affect protein activity if certain parts of the protein are cleaved. Degradation products have similar physical and chemical properties as the target protein and thereby can impair further applications and analyses, as it was the case for *At*PDR8 were the degradation products were co-purified. It is therefore desirable to reduce degradation of the heterologously expressed protein. In order to prevent proteolysis due to proteases from lysed cells protease-deficient strains can be used. Examples are the strains SMD1163 (*Δhis4 Δpep4 Δprb1*), SMD1165 (*Δhis4 Δpep4*) and SMD1168 (*Δhis4 Δpep4*) that contain mutations of three *P. pastoris* proteases (Ahmad et al., 2014, Sreekrishna et al., 1997). However, it was also reported that protease-deficient strains show reduced viability, growth rates and transformation efficiencies (Cereghino and Cregg, 2000). Another option to prevent proteolytic degradation during cultivation is the adjustment of the pH to a value that is reduces the activity of proteases. Adjustment of the pH can also be used to stabilize the target protein. Since *P. pastoris* is able to grow across a pH range from 3 to 7 changing the pH hardly affects cultivation (Macauley-Patrick et al., 2005). In order to avoid overload of the ER the cultivation temperature can be reduced. A temperature screening of *At*PDR8 expression in *P. pastoris* showed that most protein was produced at 30 °C (data not shown), which is why this temperature was chosen for further experiments, but it might be that the produced protein had partially poor quality. A further alternative to reduce the stress to the ER is attenuating the recombinant protein production by reducing the methanol concentration. However, these optimizations must be evaluated empirically, which is very laborious.

The overload of the ER is reflected in limited folding capacity and membrane space. The folding is catalyzed by chaperones, which might be limited if the overexpression reaches a certain threshold. The co-expression of chaperones can improve the folding capacity and thereby the yield of functional recombinant protein. The co-expression of the human serotonin transporter (SERT) with the ER chaperone calnexin in the baculovirus system resulted in a drastic increase of functional SERT compared to the expression of SERT alone

(Tate et al., 1999). Vogl et al. (2014) analyzed the co-expression of *Pp*Hac1 with several membrane proteins in *P. pastoris*. *Pp*Hac1 regulates the UPR by activating proteins involved in folding, trafficking and glycosylation. It furthermore increases the available membrane space in the ER by inducing the formation of additional ER membranes. The co-expression of *Pp*Hac1 had positive effects for the overexpression of heterologous ER-residing membrane proteins. However, no effect was observed for the overexpression of a heterologous plasma membrane protein (Vogl et al., 2014). If this is generally true for plasma membrane proteins needs to be evaluated.

4.6 Reconstitution of *At*PDR8 into liposomes

The establishment of the reconstitution of *At*PDR8 was performed following the protocol published by Geertsma et al. (2008). However, during the reconstitution process it became evident that several steps needed to be modified. The overall reconstitution involved the preparation of the liposomes, the destabilization of the liposomes and the insertion of the membrane protein into the liposomes. During the preparation of the liposomes the steps of the rotary evaporation were prolonged because the published evaporation times were insufficient to remove the solvents from the lipids quantitatively. Several factors had to be improved regarding the destabilization of the liposomes. First the optimal wavelength for monitoring the destabilization was figured out to be 450 nm. At this wavelength the minima and maxima of the destabilization curve were displayed best. Other wavelengths could either not completely detect the solubilization of the liposomes, which is represented by the almost complete reduction of the turbidity, or the values were in general elevated, which implies absorption of the detergent at the respective wavelength. Second, depending on the used detergent the solubiluzation process required significantly more time then stated in the published protocol. While Triton X-100 almost immediately destabilized the liposomes the detergent PCC-α-M needed a minimal incubation time of 90 min. This could be due to the nature of the detergents. Triton X-100 with its hydrophilic polyoxyethylene chain is a flexible detergent that flip-flops easily across the lipid bilayer. This results in detergent assemblies that form a toroidal ring and thereby in the rapid solubilization of the membrane. PCC-α-M contains a bulky hydrophilic maltosyl head group that leads to slow flip-flop rates. Thus, it is likely that the detergent rather extracts the lipids into preformed micelles, which is a slower process (Hovers et al., 2011b, le Maire et al., 2000). This is also the case for β-DDM, although destabilization was faster compared to PCC-α-M, which might be due to the more

flexible structure of the hydrophobic alkyl chain. Third, the used lipids influenced the destabilization process. The synthetic lipid DOPC was compared to the total lipid extract from *E. coli*. For the *E. coli* total lipids liposomes destabilization and solubilization were achieved at lower detergent concentrations compared to DOPC. This points to the fact that the concentration of the lipids was generally lower. It seemed that during extrusion a substantial amount of lipids was lost, which could result from the generation of bigger structures in the freeze- and thaw- cycles that could not pass the extrusion membrane. This did not happen when DOPC was used. A mixture of DOPC, DOPE and DOPG behaved similarly to DOPC alone in the destabilization experiments. Next to the lipids mentioned above yeast and soy total lipid extracts were also tested (data not shown), but the lipids exhibited comparable (or even worse) results as the *E. coli* total lipids. That indicates that this destabilization behavior is especially displayed by the lipid extracts. The preparation and the destabilization of total lipid extract liposomes would have required further optimization, which is why these liposomes were not used for the reconstitution trials. Furthermore different buffer conditions were assessed. The tested buffers resulted in the same shape of the destabilization curve. Only the total absorption values were changed in a way that phosphate buffer showed in general slightly higher absorption values compared to Tris buffer and the presence of glycerol slightly reduced the absorption values in both buffer substances. These effects were considered negligible.

In order to integrate *At*PDR8 into the destabilized liposomes the purified protein was added to the liposomes and the detergent was successively removed by several additions of polystyrene beads. The success of the reconstitution was confirmed by floating density centrifugation, however, the yield of reconstituted protein was low. The integration of *At*PDR8 into the liposomes was inefficient. This could be due to the procedure of removing the detergent. Possibly the detergent was removed to too slowly or too fast, which could have resulted in the aggregation of the protein before it could integrate into the liposomes. This could be due to the nature of the protein and its behavior in combination with the lipids and the detergent. The reconstitution could be reproduced regarding the qualitative integration of *At*PDR8 into the liposomes. However, the ATPase assay of the proteoliposomes delivered inconsistent results. Together with the low yield this points to the fact that the conditions of the detergent removal and protein integration are not optimal and would require further optimization.

4.7 The establishment of an *in vitro* transport assay

Mutant studies have shown that plant ABC transporters are involved in many diverse processes that are vital for the plant (Rea, 2007). However, the function of an ABC transporter cannot be fully characterized unless the substrates are identified. Different strategies exist for the identification of the substrates of plant ABC transporters. One approach involves the determination of uptake or release rates of labeled substrates into plant tissue or cells. Another approach is metabolic profiling of the plant tissues of wild-type plants and knock-out plants. Again another approach is the isolation of membrane vesicles including the respective transporter and the transport of compounds into the vesicles, which also requires labeled substrates. All the mentioned approaches have the disadvantages that endogenous processes could influence the outcome of the assay (Lefevre et al., 2015). In addition, the transport assays require expensive labeling of the compounds and one needs to have an idea about the potential substrates. To avoid these obstacles the approach by Krumpochova et al. (2012) was chosen. In that method the transport assay is combined with LC/MS metabolomics in order to identify unknown substrates of ABC transporters. Cytosolic extract or exudates could be used to provide potential substrates to the transporter. This circumvents the problems of labeling and the identification of potential substrates prior the transport assay. If reconstituted proteoliposomes are used instead of isolated membranes the effect of endogenous proteins interfering with the assay is also evaded.

The transport assay was established using the protein Pdr5 from *S. cerevisiae*. This protein has the advantage over *At*PDR8 that a lot of substrates have been identified and were analyzed. The substrate rhodamine 6G is a fluorescent compound, which is why transport could be easily detected by fluorescence quenching in *Sc*Pdr5-containing yeast plasma membranes (chapter 3.6.1). In contrast to this, transport of the substrate ketoconazole has only been studied *in vivo*. Because ketoconazole is not fluorescent, fluorescence transport analysis cannot be directly applied for the investigation of ketoconazole transport. To proof the *in vitro* transport of ketoconazole by *Sc*Pdr5 a competitive transport assay with rhodamine 6G was performed (chapter 3.6.1). In presence of ketoconazole a reduction of rhodamine 6G transport was observed, which indirectly proofs the ketoconazole transport by *Sc*Pdr5. This substrate was therefore used to establish the transport assay protocol for *At*PDR8.

First the substance ketoconazole was measured with mass spectrometry to get an idea about the isotope peak pattern and the fragmentation pattern of the MS/MS measurements (chapter 3.6.2). Ketoconazole has two chlorine atoms that can either be the ^{35}Cl or the ^{37}Cl isotope. These isotopes have different natural abundances, which were reflected by the intensities of the ketoconazole peaks in the MS spectrum. The MS/MS spectrum shows the typical fragmentation pattern of ketoconazole that was observed before (Chen et al., 2002, Huang et al., 2007). Five masses were exemplary assigned to the functional groups after possible fragmentation events. The use of plant extracts and exudates involves the difficulty that plant metabolites might occur in very low concentrations and the proportion that is transported in the assay could be even lower. To assess whether low concentrations of compounds could hamper the analytics of the transport assay different ketoconazole dilutions were detected with MS (chapter 3.6.2). The results show that concentrations down to 0.02 nM ketoconazole were detectable with MS. Analysis of ketoconazole diluted in the assay buffer showed that the buffer substance HEPES, which was until then used for *Sc*Pdr5 assays, was disturbing the MS detection of ketoconazole. The buffering agent was therefore changed to Tris, which is a smaller and less complex molecule than HEPES. The rhodamine 6G transport assay confirmed the *Sc*Pdr5 transport activity in Tris buffer (chapter 3.6.3).

During the transport assays the potential substrates are transported to the inside of membrane vesicles. MS analysis of the enclosed compounds requires the disruption of the vesicles, preferably without interfering with the subsequent analytics. To ascertain a way to open the vesicles different methods were tested. Therefore the ketoconazole transport experiment was performed with *S. cerevisiae* membranes containing either the *Sc*Pdr5 wild-type or EQ mutant. To determine the best disruption protocol three methods were tested including physical and chemical approaches. The success of the respective method was defined by MS detection of ketoconazole. Physical disruption methods have the advantage that no additional substances are added that could hamper the MS analytics. The methods tested were sonication and osmotic pressure. During the sonication the energy input leads to the reorganization of the membrane vesicles. Thereby small membrane vesicles are formed out of the larger vesicles and this could free enclosed compounds from the vesicles. The disruption by osmotic pressure was based on the assumption that resuspension of the membrane vesicles, which were previously prepared in buffer containing salt, would lead to a swelling of the vesicles until the lipid bilayer cannot sustain the resulting pressure and the vesicles burst. However, both physical approaches were not able to free the enclosed ketoconazole from the vesicles. The

chemical disruption represented the resuspension of the vesicle in methanol. The solvent dissolves the lipid, which destroys the lipid bilayer. This approach turned out to be the most efficient method. A possible explanation for the failure of the physical methods could be the hydrophobicity of ketoconazole. If the substrate attaches to the lipid bilayer simply opening the vesicles is not sufficient. In such case only the dissolution of the lipids would make the ketoconazole accessible for the detection by MS. This could also apply for potential hydrophobic substrates of *At*PD8.

4.8 Asymmetry of the nucleotide binding domains in *At*PDR8

The nucleotide binding domains contain the motifs that are necessary for binding and hydrolyzing ATP and thereby energize the substrate translocation in ABC transporters. The motifs are highly conserved in all species. However, some eukaryotic ABC transporters display discrepancies in their primary sequence so that the consensus sequence of certain motifs in not strictly followed. The prototype of the PDR family *Sc*Pdr5 has highly degenerated nucleotide binding domains (Figure 73). The NBDs are arranged head-to-tail meaning the Walker A, Walker B and the H-Loop of one NBD and the C-loop of the other NBD act together to bind and hydrolyze one ATP molecule. In case of *Sc*Pdr5 the Walker A and B motifs as well as the H-loop of the first NBD are degenerated and the C-loop of the second NBD. That results in one inactive nucleotide binding site (Figure 73blue boxes), which was proposed to bind but not hydrolyze ATP (Gupta et al., 2014). *At*PDR8 also shows degenerated motifs in one binding site, although to a much lesser extend compared to *Sc*Pdr5. In the first NBD the first amino acid of the Walker B motif is not hydrophobic as given by the consensus sequence. The Walker A motif as well as the C-loop and the H-loop follow the consensus sequence. The C-loop of the second NBD has two degenerated amino acids compared to the consensus sequence. For *Sc*Pdr5 the inactive binding site was proposed to structurally and functionally support the active binding site. Possibly the degeneration has evolved to optimize the communication between the two NBDs and between the TMDs and the NBDs (Gupta et al., 2014, Ananthaswamy et al., 2010). Since a lot of plant PDR proteins exhibit degenerations in the Walker B motif and the C-loop (van den Brule and Smart, 2002) a conserved role of the degenerated binding site could be possible. However, if these substitutions result in the complete inactivation of one binding site is questionable. In order to assess the binding stoichiometry of *At*PDR8 TNP-ATP binding studies were performed. The fluorescent nucleotide analogue TNP-ATP emits fluorescence when it binds to the

hydrophobic ligand binding side of a protein (Horn et al., 2003). In presence of purified *At*PDR8 the TNP-ATP fluorescence got enhanced compared to TNP-ATP in only buffer. This indicates the binding of TNP-ATP to *At*PDR8. Titration of TNP-ATP to purified *At*PDR8 and fitting of the fluorescence data was used to determine the K_D-value and the ligand binding number (chapter 3.4.7). The K_D-value was calculated to be 14.3 µM, which indicates a low affinity of TNP-ATP to the protein. The data support the assumption that *At*PDR8 is not functional in detergent and that ATP is not hydrolyzed. The ligand number was determined to be 0.8, which suggests that one TNP-ATP molecule was bound to *At*PDR8. This would support the possibility of one degenerated nucleotide binding site. However, these data require further verification.

	NBD1				NBD2			
Motif	Walker A	C-Loop	Walker B	H-Loop	Walker A	C-Loop	Walker B	H-Loop
Consensus	GXXGXGK[ST]	[IV]SGG	HHHHDE	XHX	GXXGXGK[ST]	LSGG	HHHHDE	XHX
*Sc*Pdr5	GRPGSGCT	VSGG	FQCWDN	QAD	GASGAGKT	LNVE	LVFLDE	IHQ
*At*PDR8	GPPSSGKT	ISGG	TLFMDE	VHL	GVSGAGKT	LSTE	IIFMDE	IHQ

Figure 73: Degeneration of motifs important for ATP binding. The consensus sequence of the motifs for each NBD is shown as well as the sequences of *Sc*Pdr5 and *At*PDR8. Degenerated amino acids are marked in magenta. The motifs that form the first nucleotide binding site are highlighted in blue and the motifs of the second nucleotide binding site in purple.

4.9 *At*PDR8 lacks *in vitro* ATPase activity

The nucleotide binding domains of ABC transporters bind and hydrolyze ATP to energize the transport of substrates across membranes. In order to perform *in vitro* assays the purified ABC transporter must therefore display activity. Activity can be monitored by the phosphate release resulting from ATP hydrolysis. Purified *At*PDR8 did not show ATPase activity in comparison to the negative controls (data not shown). Possible reasons why purified *At*PDR8 lacks detectable ATPase activity are discussed below. One reason could be that the detergent environment impairs *At*PDR8 activity. The protein was solubilized in Fos-Choline-14, which is a harsh zwitterionic detergent. However, in case of *At*PDR8 ATPase activity could not be restored by replacing the detergent by a milder detergent during purification (data not shown). Another reason could be that the presence of a substrate was required for *At*PDR8 to exhibit detectable ATPase activity. The presence of the potential substrates IBA and cadmium in the ATPase assay did not stimulate activity, neither of the purified nor of the reconstituted protein (data not shown).

The data obtained from TNP-ATP-binding studies (chapter 3.4.7) show that *At*PDR8 is likely able to bind TNP-ATP. In consequence, purified *At*PDR8 is able to bind but not hydrolyse ATP. This raises the suspicion that the protein was not functionally produced in *P. pastoris.*

The mass spectrometry data showed that none of the identified *At*PDR8 peptides was phosphorylated. Benschop et al. (2007) showed that *At*PDR8 is phosphorylated in response to elicitor treatment, which was not the case in samples from untreated plant material. Some of the differentially phosphorylated peptides from that study were also identified in the MS data in this work, however they were not phosphorylated. Campe et al. (2016) suggested that *At*PDR8 is phosphotylated by CDPK10 kinase. Furthermore the protein was shown to bind calmodulin *in vitro* and an *At*PDR8 peptide was phosphorylated *in vitro* (Benschop et al., 2007, Campe et al., 2016, Curran et al., 2011). These data suggest that after pathogen perception calmodulin possibly binds *At*PDR8 and recruits a kinase to phosphorylate *At*PDR8. Thus, *At*PDR8 would be activated by phosphorylation and the absence of phosphorylated groups in the purified *At*PDR8 could be a reason for the lacking ATPase activity of the protein.

Another reason that impairs activity of *At*PDR8 could be the amino acid substitutions that were introduced into the protein sequence during the cloning process. The expression tests of the mutated and the wild-type constructs indicated that the amino acid substitutions possibly facilitated the expression of the protein in *P. pastroris*. Analysis of the primary sequence showed that the mutations were not located in the motifs important for ATP binding and hydrolysis. Still, a potential inhibitive effect of the mutations on ATP hydrolysis cannot be excluded.

Another factor potentially influencing membrane protein activity are lipids. In their natural environment membrane proteins are embedded in the lipid bilayer, thus it is conclusive that these proteins form complexes with lipids. Lipids can be important for protein function or assist in folding and stability (Opekarova and Tanner, 2003). Crystal structures of membrane proteins obtained in the presence of lipids show that the lipids interact with the proteins. Amino acid substitutions of the lipid contact sites in the yeast cytochrome *bc1* complex lead to instability of the complex (Lange et al., 2001). The *in vitro* activity of human MDR1 was shown to depend on the presence of phosphatidyl choline and phosphatidyl ethanolamine

(Sharom, 1997). Different lipid compositions of the membrane in the heterologous expression host compared to the native environment might also affect the production of functional protein. The *E. coli* lactose permease *Ec*LacY requires phosphatidyl ethanolamine for the uptake of lactose into the cell. Phosphatidyl ethanolamine assists in folding of the *E. coli* permease LacY and the topology of *Ec*LacY in the membrane changes depending on the presence of phosphatidyl ethanolamine (Chen and Wilson, 1984, Bogdanov and Dowhan, 1998, Bogdanov et al., 2002). When expressed in *S. cerevisiae*, human MDR1 displayed decreased substrate binding ability compared to homologous expression (Saeki et al., 1991). The lipid composition of the expression host might have also affected the overexpression of *At*PDR8 in *P. pastoris*. The main difference between yeast and plant membranes is the high ergosterol content in yeasts while plant membranes contain of stigmasterol, sitosterol and campesterol. Functionality of plant membrane proteins expressed in yeast systems might *inter alia* depend on the ability of ergosterol to replace the plant-specific sterols. Of those plant membrane proteins that were heterologously overexpressed and purified from yeast systems, *in vitro* data regarding the effect of lipid compositions from yeast systems on plant membrane proteins is limited (Opekarova and Tanner, 2003). HUP1 from Chlorella was analyzed after homologous expression and expression in *S. pombe* and the *A. thaliana* plasma H^+-ATPase was after expression in *S. cerevisiae.* In both cases the *in vitro* data did not vary between proteins obtained from the homologous and the heterologous systems (Sauer et al., 1990, Lanfermeijer et al., 1998). This indicates that lipid compositions of yeasts do not necessarily impair functionality of plant proteins. If the *P. pastoris* lipid composition was not impairing *At*PDR8 activity it could have been the purification conditions. The exchange of the detergent required extensive washing of the protein in order to remove the Fos-Choline-14. This might have also removed all the lipids from the micelles together with the Fos-Choline-14. The complete delipidation of a membrane protein might lead to the loss of functionality (Opekarova and Tanner, 2003, le Maire et al., 2000). The reconstitution of *At*PDR8 did not restore functionality. During the reconstitution the detergents were removed and the protein was transferred into a lipid environment. However, ATPase activity of *At*PDR8 proteoliposomes was inconsistent. Whether this resulted from non-functional protein or the generally low reconstitution efficiency requires further clarification.

4.10 Establishment of the *At*PDR8 *in vitro* system – lessons learned and future perspectives

The *At*PDR8 mutant studies suggested that the protein is involved in diverse physiological processes, which implies multifunctionality of *At*PDR8. However, this hypothesis lacks direct evidence. Furthermore, contradictory studies exist that assign *At*PDR8 different roles in nonhost resistance (Kobae et al., 2006, Stein et al., 2006, Xin et al., 2013). The *in vitro* system is therefore required to determine the transported substrates and to clarify the role of *At*PDR8. The establishment of an *in vitro* system for a membrane protein can be a complicated process. This was demonstrated by several studies that reported problems with the cloning (Crouzet et al., 2013, Ellinger et al., 2013), the overexpression (Toussaint et al., 2017), the correct localization (Ruzicka et al., 2010) and the *in vitro* activity (Ellinger et al., 2013) of ABC transporters. Until today no 3D structure of a plant ABC transporter has been solved, which might *inter alia* result from the difficulties in producing sufficient amounts of functional protein. Regarding the plant PDR family, only two transporters have been successfully purified and analyzed *in vitro*. Also in these cases the authors reported complications concerning the heterologous overexpression of the protein in yeast (Pierman et al., 2017, Toussaint et al., 2017).

Also the establishment of the *At*PDR8 *in vitro* system comprised several difficulties. However, the gained knowledge might facilitate the establishment of *in vitro* systems of other plant full-size ABC transporters. The first hurdle that had to be overcome was the toxicity of the foreign gene or protein to the cloning host *E. coli*. Mutations were frequently introduced into the coding sequence of *At*PDR8 during the propagation in *E. coli*. This problem was solved using a strain that drastically reduces the copy number of plasmids in the cell, e.g. CoppyCutter™ EPI400™ cells (epicentre). During the heterologous expression instability of the protein in the expression host seemed to be another issue. For the heterologous overexpression it is advisable to keep options broad regarding the used expression vectors, promoters and tag positions. To facilitate expression, the gene of interest should be synthesized in a codon-optimized version for the respective expression host. In addition, different tag positions might influence success of expression. The screening of promoters of varying strength could prevent an overload of the folding machinery.
Screening different promoters in combination with different tags and tag positions can easily result in a huge workload. Especially the expression tests of membrane proteins in yeasts and

plant cells require the laborious preparation of cell lysates and membranes in combination with gelelectrophoresis and Western Blotting methods to detect the heterologous proteins. To facilitate the screening process the system published by Vogl et al. (2014) could be used. In this approach the GFP sequence was fused to the target protein and expression of different clones was analyzed in a 96-well plate by simply screening for fluorescence signals during the cultivation. Positive clones can be further analyzed by fluorescence microscopy to determine the localization in the cell (Vogl et al., 2014). In such approach different cultivation conditions could also be easily tested.

Degradation was a problem during the expression and potentially also in the downstreaming applications. To reduce degradation in response to folding stress in the ER the co-expression of chaperones can be useful. In case of *P. pastoris* the co-expression of Hac1, which induces the UPR, could be tested. In order to avoid proteolytic degradation the usage of engineered strains, like protease-deficient strains, can be helpful. However, regarding functionality it can be reasonable to use a plant system preferably over a yeast expression system, although this might affect the yield of the produced protein. The facts that the non-mutated *At*PDR8 could not be expressed in *P. pastoris*, the cloning of *At*PDR8 in *S. cerevisiae* did not result in viable clones and that *At*PDR9, *Nt*PDR1 and *Np*PDR5 could not be successfully produced in yeast systems (Toussaint et al., 2017, Pierman et al., 2017, Ruzicka et al., 2010) indicate that for certain plant ABC transporters yeast expression systems are not the ideal choice. The BY2 tobacco suspension cell culture could be an alternative system. It combines the advantage of being a plant system with the relatively easy handling of a liquid culture. Regarding the problems in protein stability and activity of *At*PDR8 produced in *P. pastoris* the BY2 system represents an alternative expression system worth testing in the future. The purification conditions could have been another factor that potentially impaired the functionality of *At*PDR8. *At*PDR8 had to be solubilized with a harsh zwitterionic detergent that very often inactivates membrane proteins (le Maire et al., 2000). The exchange to a mild detergent required extensive washing with probably resulted in the delipidation of the protein. Delipidation is one factor causing inactivity of membrane proteins (le Maire et al., 2000). To avoid delipidation in future purifications the washing buffer could be supplemented with solubilized lipids during the purification so that the removed lipids are replaced. This could contribute to the stability and thereby to the activity of the protein.

For the reconstitution of *At*PDR8 in to liposomes the protocol published by Geertsma et al. was used, which especially refers to the reconstitution of ABC transporters. In this work this reconstitution protocol was already optimized to a large extend regarding the preparation and destabilization of liposomes. However, the final integration of *At*PDR8 into the liposomes remained ineffective. Further optimization of the protocol could involve different approaches to remove the detergent, for example size exclusion chromatography. Apart from this, additional protocols for the reconstitution exist, which could be more efficient for the particular reconstitution of *At*PDR8.

Several eukaryotic ABC transporters display a broad substrate spectrum of structurally unrelated compounds. Examples are human MDR1 and yeast *Sc*Pdr5, which were shown to export a huge variety of compounds. Mutant studies implied that also several plant ABC transporter transport a structurally unrelated compounds. For *At*PDR8 several possible substrates (e.g. cadmium ions, IBA, indolic compounds) were proposed. *At*PDR9 is thought to transport coumarins as well as auxinic compounds. However, direct evidence for the multifunctionality of plant ABC transporters is still missing. In contrast, there is rather evidence that plant ABC transporters display high substrate specify (Kang et al., 2010, Kuromori et al., 2010, Geisler et al., 2005). *At*PDR12 was first thought to function in different, unrelated processes, which are plant defense through diterpene export, detoxification through lead export as well as the import the phytohormone ABA. Except for the multifunctionality, these data hence propose that *At*PDR12 performs transport in both directions, meaning import and export of compounds. More recent data involving transport studies suggest that *At*PDR12 has indeed only one substrate, which is ABA.

All these contradictory observations call for the establishment of *in vitro* systems of the respective transporters. As reported for other transporters, the establishment of the *At*PDR8 *in vitro* system comprised several difficulties. However, the gained knowledge might facilitate the establishment of *in vitro* systems of other plant full-size ABC transporters in the future. These systems will be required to biochemically characterize the transporters regarding the 3D structure, the substrate spectrum and the transport characteristics. *In vitro* systems are indispensible for clarification of the function of ABC transporters in plants.

5 References

AHMAD, M., HIRZ, M., PICHLER, H. & SCHWAB, H. 2014. Protein expression in Pichia pastoris: recent achievements and perspectives for heterologous protein production. *Applied Microbiology and Biotechnology,* 98**,** 5301-5317.

ALEJANDRO, S., LEE, Y., TOHGE, T., SUDRE, D., OSORIO, S., PARK, J., BOVET, L., LEE, Y., GELDNER, N., FERNIE, A. R. & MARTINOIA, E. 2012. AtABCG29 Is a Monolignol Transporter Involved in Lignin Biosynthesis. *Current Biology,* 22**,** 1207-1212.

ALKHATIB, Z., LAGEDROSTE, M., ZASCHKE, J., WAGNER, M., ABTS, A., FEY, I., KLEINSCHRODT, D. & SMITS, S. H. J. 2014. The C-terminus of nisin is important for the ABC transporter NisFEG to confer immunity in Lactococcus lactis. *Microbiologyopen,* 3**,** 752-763.

ALLAN, C., BUREL, J. M., MOORE, J., BLACKBURN, C., LINKERT, M., LOYNTON, S., MACDONALD, D., MOORE, W. J., NEVES, C., PATTERSON, A., PORTER, M., TARKOWSKA, A., LORANGER, B., AVONDO, J., LAGERSTEDT, I., LIANAS, L., LEO, S., HANDS, K., HAY, R. T., PATWARDHAN, A., BEST, C., KLEYWEGT, G. J., ZANETTI, G. & SWEDLOW, J. R. 2012. OMERO: flexible, model-driven data management for experimental biology. *Nature Methods,* 9**,** 245-253.

ALLER, S. G., LI, J. Z. & JAIMES, K. 2014. Refined Structures of Mouse P-Glycoprotein. *Biophysical Journal,* 106**,** 790a-790a.

AMBUDKAR, S. V., DEY, S., HRYCYNA, C. A., RAMACHANDRA, M., PASTAN, I. & GOTTESMAN, M. M. 1999. Biochemical, cellular, and pharmacological aspects of the multidrug transporter. *Annual Review of Pharmacology and Toxicology,* 39**,** 361-398.

AMBUDKAR, S. V., KIM, I. W., XIA, D. & SAUNA, Z. E. 2006. The A-loop, a novel conserved aromatic acid subdomain upstream of the Walker A motif in ABC transporters, is critical for ATP binding. *Febs Letters,* 580**,** 1049-1055.

ANANTHASWAMY, N., RUTLEDGE, R., SAUNA, Z. E., AMBUDKAR, S. V., DINE, E., NELSON, E., XIA, D. & GOLIN, J. 2010. The Signaling Interface of the Yeast Multidrug Transporter Pdr5 Adopts a Cis Conformation, and There Are Functional Overlap and Equivalence of the Deviant and Canonical Q-Loop Residues. *Biochemistry,* 49**,** 4440-4449.

ANJARD, C., LOOMIS, W. F. & CONSORTIU, D. S. 2002. Evolutionary analyses of ABC transporters of Dictyostelium discoideum. *Eukaryotic Cell,* 1**,** 643-652.

APARICIO, G., BUCHE, A., MENDEZ, C. & SALAS, J. A. 1996. Characterization of the ATPase activity of the N-terminal nucleotide binding domain of an ABC transporter involved in oleandomycin secretion by Streptomyces antibioticus. *Fems Microbiology Letters,* 141**,** 157-162.

ARABIDOPSIS GENOME, I. 2000. Analysis of the genome sequence of the flowering plant Arabidopsis thaliana. *Nature,* 408**,** 796-815.

AWAI, K., XU, C. C., TAMOT, B. & BENNING, C. 2006. A phosphatidic acid-binding protein of the chloroplast inner envelope membrane involved in lipid trafficking. *Proceedings of the National Academy of Sciences of the United States of America,* 103**,** 10817-10822.

BADRI, D. V., QUINTANA, N., EL KASSIS, E. G., KIM, H. K., CHOI, Y. H., SUGIYAMA, A., VERPOORTE, R., MARTINOIA, E., MANTER, D. K. &

VIVANCO, J. M. 2009. An ABC transporter mutation alters root exudation of phytochemicals that provoke an overhaul of natural soil microbiota. *Plant Physiol,* 151**,** 2006-17.

BAI, J. P., SWARTZ, D. J., PROTASEVICH, I. I., BROUILLETTE, C. G., HARRELL, P. M., HILDEBRANDT, E., GASSER, B., MATTANOVICH, D., WARD, A., CHANG, G. & URBATSCH, I. L. 2011. A Gene Optimization Strategy that Enhances Production of Fully Functional P-Glycoprotein in Pichia pastoris. *Plos One,* 6.

BAKOS, E., EVERS, R., SZAKACS, G., TUSNADY, G. E., WELKER, E., SZABO, K., DE HAAS, M., VAN DEEMTER, L., BORST, P., VARADI, A. & SARKADI, B. 1998. Functional multidrug resistance protein (MRP1) lacking the N-terminal transmembrane domain. *Journal of Biological Chemistry,* 273**,** 32167-32175.

BEDNAREK, P., PISLEWSKA-BEDNAREK, M., SVATOS, A., SCHNEIDER, B., DOUBSKY, J., MANSUROVA, M., HUMPHRY, M., CONSONNI, C., PANSTRUGA, R., SANCHEZ-VALLET, A., MOLINA, A. & SCHULZE-LEFERT, P. 2009. A Glucosinolate Metabolism Pathway in Living Plant Cells Mediates Broad-Spectrum Antifungal Defense. *Science,* 323**,** 101-106.

BENSCHOP, J. J., MOHAMMED, S., O'FLAHERTY, M., HECK, A. J. R., SLIJPER, M. & MENKE, F. L. H. 2007. Quantitative phosphoproteomics of early elicitor signaling in Arabidopsis. *Molecular & Cellular Proteomics,* 6**,** 1198-1214.

BERG, J. M., TYMOCZKO, J. L. & STRYER, L. 2007. *Biochemistry*, W. H. Freeman.

BERNAUDAT, F., FRELET-BARRAND, A., POCHON, N., DEMENTIN, S., HIVIN, P., BOUTIGNY, S., RIOUX, J. B., SALVI, D., SEIGNEURIN-BERNY, D., RICHAUD, P., JOYARD, J., PIGNOL, D., SABATY, M., DESNOS, T., PEBAY-PEYROULA, E., DARROUZET, E., VERNET, T. & ROLLAND, N. 2011. Heterologous Expression of Membrane Proteins: Choosing the Appropriate Host. *Plos One,* 6.

BESSIRE, M., BOREL, S., FABRE, G., CARRACA, L., EFREMOVA, N., YEPHREMOV, A., CAO, Y., JETTER, R., JACQUAT, A. C., METRAUX, J. P. & NAWRATH, C. 2011. A member of the PLEIOTROPIC DRUG RESISTANCE family of ATP binding cassette transporters is required for the formation of a functional cuticle in Arabidopsis. *Plant Cell,* 23**,** 1958-70.

BIALA, W., BANASIAK, J., JARZYNIAK, K., PAWELA, A. & JASINSKI, M. 2017. Medicago truncatula ABCG10 is a transporter of 4-coumarate and liquiritigenin in the medicarpin biosynthetic pathway. *Journal of Experimental Botany,* 68**,** 3231-3241.

BIEMANS-OLDEHINKEL, E., DOEVEN, M. K. & POOLMAN, B. 2006. ABC transporter architecture and regulatory roles of accessory domains. *Febs Letters,* 580**,** 1023-1035.

BIENERT, M. D., SIEGMUND, S. E. G., DROZAK, A., TROMBIK, T., BULTREYS, A., BALDWIN, I. T. & BOUTRY, M. 2012. A pleiotropic drug resistance transporter in Nicotiana tabacum is involved in defense against the herbivore Manduca sexta. *Plant Journal,* 72**,** 745-757.

BLAKESLEE, J. J., PEER, W. A. & MURPHY, A. S. 2005. Auxin transport. *Current Opinion in Plant Biology,* 8**,** 494-500.

BOGDANOV, M. & DOWHAN, W. 1998. Phospholipid-assisted protein folding: phosphatidylethanolamine is required at a late step of the conformational maturation of the polytopic membrane protein lactose permease. *Embo Journal,* 17**,** 5255-5264.

BOGDANOV, M., HEACOCK, P. N. & DOWHAN, W. 2002. A polytopic membrane protein displays a reversible topology dependent on membrane lipid composition. *Embo Journal,* 21**,** 2107-2116.

BULTREYS, A., TROMBIK, T., DROZAK, A. & BOUTRY, M. 2009. Nicotiana plumbaginifolia plants silenced for the ATP-binding cassette transporter gene NpPDR1 show increased susceptibility to a group of fungal and oomycete pathogens. *Molecular Plant Pathology,* 10**,** 651-663.

BUSSO, D., KIM, R. & KIM, S. H. 2003. Expression of soluble recombinant proteins in a cell-free system using a 96-well format. *Journal of Biochemical and Biophysical Methods,* 55**,** 233-240.

BYRNE, J. A., STRAUTNIEKS, S. S., IHRKE, G., PAGANI, F., KINSELY, A. S., LINTON, K. J., MIELI-VERGANI, G. & THOMPSON, R. J. 2009. Missense Mutations and Single Nucleotide Polymorphisms in ABCB11 Impair Bile Salt Export Pump Processing and Function or Disrupt Pre-Messenger RNA Splicing. *Hepatology,* 49**,** 553-567.

BYRNE, J. A., STRAUTNIEKS, S. S., MIELI-VERGANI, G., HIGGINS, C. F., LINTON, K. J. & THOMPSON, R. J. 2002. The human bile salt export pump: Characterization of substrate specificity and identification of inhibitors. *Gastroenterology,* 123**,** 1649-1658.

CAMPBELL, E. J., SCHENK, P. M., KAZAN, K., PENNINCKX, I. A. M. A., ANDERSON, J. P., MACLEAN, D. J., CAMMUE, B. P. A., EBERT, P. R. & MANNERS, J. M. 2003. Pathogen-responsive expression of a putative ATP-binding cassette transporter gene conferring resistance to the diterpenoid sclareol is regulated by multiple defense signaling pathways in Arabidopsis. *Plant Physiology,* 133**,** 1272-1284.

CAMPE, R., LANGENBACH, C., LEISSING, F., POPESCU, G. V., POPESCU, S. C., GOELLNER, K., BECKERS, G. J. M. & CONRATH, U. 2016. ABC transporter PEN3/PDR8/ABCG36 interacts with calmodulin that, like PEN3, is required for Arabidopsis nonhost resistance. *New Phytologist,* 209**,** 294-306.

CEREGHINO, J. L. & CREGG, J. M. 2000. Heterologous protein expression in the methylotrophic yeast Pichia pastoris. *Fems Microbiology Reviews,* 24**,** 45-66.

CHAE, P. S., RASMUSSEN, S. G., RANA, R. R., GOTFRYD, K., CHANDRA, R., GOREN, M. A., KRUSE, A. C., NURVA, S., LOLAND, C. J., PIERRE, Y., DREW, D., POPOT, J. L., PICOT, D., FOX, B. G., GUAN, L., GETHER, U., BYRNE, B., KOBILKA, B. & GELLMAN, S. H. 2010. Maltose-neopentyl glycol (MNG) amphiphiles for solubilization, stabilization and crystallization of membrane proteins. *Nat Methods,* 7**,** 1003-8.

CHAKRABURTTY, K. 2001. Translational regulation by ABC systems. *Research in Microbiology,* 152**,** 391-399.

CHEN, C. C. & WILSON, T. H. 1984. The Phospholipid Requirement for Activity of the Lactose Carrier of Escherichia-Coli. *Journal of Biological Chemistry,* 259**,** 150-158.

CHEN, G. F. T. & INOUYE, M. 1990. Suppression of the Negative Effect of Minor Arginine Codons on Gene-Expression - Preferential Usage of Minor Codons within the 1st 25 Codons of the Escherichia-Coli Genes. *Nucleic Acids Research,* 18**,** 1465-1473.

CHEN, G. X., KOMATSUDA, T., MA, J. F., NAWRATH, C., POURKHEIRANDISH, M., TAGIRI, A., HU, Y. G., SAMERI, M., LI, X. R., ZHAO, X., LIU, Y. B., LI, C., MA, X. Y., WANG, A. D., NAIR, S., WANG, N., MIYAO, A., SAKUMA, S., YAMAJI, N., ZHENG, X. T. & NEVO, E. 2011. An ATP-binding cassette subfamily G full transporter is essential for the retention of leaf water in both wild barley and rice. *Proceedings of the National Academy of Sciences of the United States of America,* 108**,** 12354-12359.

CHEN, J. 2013. Molecular mechanism of the Escherichia coli maltose transporter. *Current Opinion in Structural Biology,* 23**,** 492-498.

CHEN, J., LU, G., LIN, J., DAVIDSON, A. L. & QUIOCHO, F. A. 2003. A tweezers-like motion of the ATP-binding cassette dimer in an ABC transport cycle. *Molecular Cell,* 12**,** 651-661.

CHEN, Y. L., FELDER, L., JIANG, X. Y. & NAIDONG, W. 2002. Determination of ketoconazole in human plasma by high-performance liquid chromatography - tandem

mass spectrometry. *Journal of Chromatography B-Analytical Technologies in the Biomedical and Life Sciences,* 774**,** 67-78.

CHERRY, J. M., HONG, E. L., AMUNDSEN, C., BALAKRISHNAN, R., BINKLEY, G., CHAN, E. T., CHRISTIE, K. R., COSTANZO, M. C., DWIGHT, S. S., ENGEL, S. R., FISK, D. G., HIRSCHMAN, J. E., HITZ, B. C., KARRA, K., KRIEGER, C. J., MIYASATO, S. R., NASH, R. S., PARK, J., SKRZYPEK, M. S., SIMISON, M., WENG, S. & WONG, E. D. 2012. Saccharomyces Genome Database: the genomics resource of budding yeast. *Nucleic Acids Research,* 40**,** D700-D705.

CHINCHILLA, D., BAUER, Z., REGENASS, M., BOLLER, T. & FELIX, G. 2006. The Arabidopsis receptor kinase FLS2 binds flg22 and determines the specificity of flagellin perception. *Plant Cell,* 18**,** 465-76.

CHINCHILLA, D., ZIPFEL, C., ROBATZEK, S., KEMMERLING, B., NURNBERGER, T., JONES, J. D., FELIX, G. & BOLLER, T. 2007. A flagellin-induced complex of the receptor FLS2 and BAK1 initiates plant defence. *Nature,* 448**,** 497-500.

CHLOUPKOVA, M., PICKERT, A., LEE, J. Y., SOUZA, S., TRINH, Y. T., CONNELLY, S. M., DUMONT, M. E., DEAN, M. & URBATSCH, I. L. 2007. Expression of 25 human ABC transporters in the yeast Pichia pastoris and characterization of the purified ABCC3 ATPase activity. *Biochemistry,* 46**,** 7992-8003.

CHOI, H., OHYAMA, K., KIM, Y. Y., JIN, J. Y., LEE, S. B., YAMAOKA, Y., MURANAKA, T., SUH, M. C., FUJIOKA, S. & LEE, Y. 2014. The role of Arabidopsis ABCG9 and ABCG31 ATP binding cassette transporters in pollen fitness and the deposition of steryl glycosides on the pollen coat. *Plant Cell,* 26**,** 310-24.

COCK, J. M., STERCK, L., ROUZE, P., SCORNET, D., ALLEN, A. E., AMOUTZIAS, G., ANTHOUARD, V., ARTIGUENAVE, F., AURY, J. M., BADGER, J. H., BESZTERI, B., BILLIAU, K., BONNET, E., BOTHWELL, J. H., BOWLER, C., BOYEN, C., BROWNLEE, C., CARRANO, C. J., CHARRIER, B., CHO, G. Y., COELHO, S. M., COLLEN, J., CORRE, E., DA SILVA, C., DELAGE, L., DELAROQUE, N., DITTAMI, S. M., DOULBEAU, S., ELIAS, M., FARNHAM, G., GACHON, C. M. M., GSCHLOESSL, B., HEESCH, S., JABBARI, K., JUBIN, C., KAWAI, H., KIMURA, K., KLOAREG, B., KUPPER, F. C., LANG, D., LE BAIL, A., LEBLANC, C., LEROUGE, P., LOHR, M., LOPEZ, P. J., MARTENS, C., MAUMUS, F., MICHEL, G., MIRANDA-SAAVEDRA, D., MORALES, J., MOREAU, H., MOTOMURA, T., NAGASATO, C., NAPOLI, C. A., NELSON, D. R., NYVALL-COLLEN, P., PETERS, A. F., POMMIER, C., POTIN, P., POULAIN, J., QUESNEVILLE, H., READ, B., RENSING, S. A., RITTER, A., ROUSVOAL, S., SAMANTA, M., SAMSON, G., SCHROEDER, D. C., SEGURENS, B., STRITTMATTER, M., TONON, T., TREGEAR, J. W., VALENTIN, K., VON DASSOW, P., YAMAGISHI, T., VAN DE PEER, Y. & WINCKER, P. 2010. The Ectocarpus genome and the independent evolution of multicellularity in brown algae. *Nature,* 465**,** 617-621.

COLEMAN, J., INOUYE, M. & NAKAMURA, K. 1985. Mutations Upstream of the Ribosome-Binding Site Affect Translational Efficiency. *Journal of Molecular Biology,* 181**,** 139-143.

COLEMAN, J. O. D., BLAKEKALFF, M. M. A. & DAVIES, T. G. E. 1997. Detoxification of xenobiotics by plants: Chemical modification and vacuolar compartmentation. *Trends in Plant Science,* 2**,** 144-151.

COVIC, L. & LEW, R. R. 1996. Arabidopsis thaliana cDNA isolated by functional complementation shows homology to serine threonine protein kinases. *Biochimica Et Biophysica Acta-Gene Structure and Expression,* 1305**,** 125-129.

CREGG, J. M., CEREGHINO, J. L., SHI, J. Y. & HIGGINS, D. R. 2000. Recombinant protein expression in Pichia pastoris. *Molecular Biotechnology,* 16**,** 23-52.

CROUZET, J., ROLAND, J., PEETERS, E., TROMBIK, T., DUCOS, E., NADER, J. & BOUTRY, M. 2013. NtPDR1, a plasma membrane ABC transporter from Nicotiana tabacum, is involved in diterpene transport. *Plant Mol Biol,* 82**,** 181-92.

CROUZET, J., TROMBIK, T., FRAYSSE, A. S. & BOUTRY, M. 2006. Organization and function of the plant pleiotropic drug resistance ABC transporter family. *FEBS Lett,* 580**,** 1123-30.

CURRAN, A., CHANG, I. F., CHANG, C. L., GARG, S., MIGUEL, R. M., BARRON, Y. D., LI, Y., ROMANOWSKY, S., CUSHMAN, J. C., GRIBSKOV, M., HARMON, A. C. & HARPER, J. F. 2011. Calcium-dependent protein kinases from Arabidopsis show substrate specificity differences in an analysis of 103 substrates. *Frontiers in Plant Science,* 2.

DAWSON, R. J. P. & LOCHER, K. P. 2006. Structure of a bacterial multidrug ABC transporter. *Nature,* 443**,** 180-185.

DEBIEVRE, P. & TAYLOR, P. D. P. 1993. Table of the Isotopic Compositions of the Elements. *International Journal of Mass Spectrometry and Ion Processes,* 123**,** 149-166.

DEMESSIE, Z., WOOLFSON, K. N., YU, F., QU, Y. & DE LUCA, V. 2017. The ATP binding cassette transporter, VmTPT2/VmABCG1, is involved in export of the monoterpenoid indole alkaloid, vincamine in Vinca minor leaves. *Phytochemistry,* 140**,** 118-124.

DICKE, M. & HILKER, M. 2003. Induced plant defences: from molecular biology to evolutionary ecology. *Basic and Applied Ecology,* 4**,** 3-14.

DICKE, M., VAN POECKE, R. M. P. & DE BOER, J. G. 2003. Inducible indirect defence of plants: from mechanisms to ecological functions. *Basic and Applied Ecology,* 4**,** 27-42.

DRULEY, T. E., STEIN, W. D. & RONINSON, I. B. 2001. Analysis of MDR1 P-glycoprotein conformational changes in permeabilized cells using differential immunoreactivity. *Biochemistry,* 40**,** 4312-4322.

DUCOS, E., FRAYSSE, S. & BOUTRY, M. 2005. NtPDR3, an iron-deficiency inducible ABC transporter in Nicotiana tabacum. *FEBS Lett,* 579**,** 6791-5.

EGNER, R., MAHE, Y., PANDJAITAN, R. & KUCHLER, K. 1995. Endocytosis and Vacuolar Degradation of the Plasma Membrane-Localized Pdr5 Atp-Binding Cassette Multidrug Transporter in Saccharomyces-Cerevisiae. *Molecular and Cellular Biology,* 15**,** 5879-5887.

EGUSA, M., MIWA, T., KAMINAKA, H., TAKANO, Y. & KODAMA, M. 2013. Nonhost Resistance of Arabidopsis thaliana Against Alternaria alternata Involves both Pre- and Postinvasive Defenses but Is Collapsed by AAL-Toxin in the Absence of LOH2. *Phytopathology,* 103**,** 733-740.

ELLINGER, P., KLUTH, M., STINDT, J., SMITS, S. H. & SCHMITT, L. 2013. Detergent screening and purification of the human liver ABC transporters BSEP (ABCB11) and MDR3 (ABCB4) expressed in the yeast Pichia pastoris. *PLoS One,* 8**,** e60620.

ERNST, R., KLEMM, R., SCHMITT, L. & KUCHLER, K. 2005. Yeast ATP-binding cassette transporters: cellular cleaning pumps. *Methods Enzymol,* 400**,** 460-84.

ERNST, R., KOCH, J., HORN, C., TAMPE, R. & SCHMITT, L. 2006. Engineering ATPase activity in the isolated ABC cassette of human TAP1. *Journal of Biological Chemistry,* 281**,** 27471-27480.

ERNST, R., KUEPPERS, P., KLEIN, C. M., SCHWARZMUELLER, T., KUCHLER, K. & SCHMITT, L. 2008. A mutation of the H-loop selectively affects rhodamine transport by the yeast multidrug ABC transporter Pdr5. *Proceedings of the National Academy of Sciences of the United States of America,* 105**,** 5069-5074.

FAN, J. L., ZHAI, Z. Y., YAN, C. S. & XU, C. C. 2015. Arabidopsis TRIGALACTOSYLDIACYLGLYCEROL5 Interacts with TGD1, TGD2, and TGD4 to Facilitate Lipid Transfer from the Endoplasmic Reticulum to Plastids. *Plant Cell,* 27**,** 2941-2955.

FOURCROY, P., SISO-TERRAZA, P., SUDRE, D., SAVIRON, M., REYT, G., GAYMARD, F., ABADIA, A., ABADIA, J., ALVAREZ-FERNANDEZ, A. & BRIAT, J. F. 2014. Involvement of the ABCG37 transporter in secretion of scopoletin and derivatives by Arabidopsis roots in response to iron deficiency. *New Phytol,* 201**,** 155-67.

FUHRMANN, M., HAUSHERR, A., FERBITZ, L., SCHODL, T., HEITZER, M. & HEGEMANN, P. 2004. Monitoring dynamic expression of nuclear genes in Chlamydomonas reinhardtii by using a synthetic luciferase reporter gene. *Plant Molecular Biology,* 55**,** 869-881.

GAUDET, R. & WILEY, D. C. 2001. Structure of the ABC ATPase domain of human TAP1, the transporter associated with antigen processing. *Embo Journal,* 20**,** 4964-4972.

GECHEV, T. S. & HILLE, J. 2012. Molecular basis of plant stress. *Cellular and Molecular Life Sciences,* 69**,** 3161-3163.

GEERTSMA, E. R., MAHMOOD, N. A. B. N., SCHUURMAN-WOLTERS, G. K. & POOLMAN, B. 2008. Membrane reconstitution of ABC transporters and assays of translocator function. *Nature Protocols,* 3**,** 256-266.

GEISLER, M., BLAKESLEE, J. J., BOUCHARD, R., LEE, O. R., VINCENZETTI, V., BANDYOPADHYAY, A., TITAPIWATANAKUN, B., PEER, W. A., BAILLY, A., RICHARDS, E. L., EJENDA, K. F. K., SMITH, A. P., BAROUX, C., GROSSNIKLAUS, U., MULLER, A., HRYCYNA, C. A., DUDLER, R., MURPHY, A. S. & MARTINOIA, E. 2005. Cellular efflux of auxin catalyzed by the Arabidopsis MDR/PGP transporter AtPGP1. *Plant Journal,* 44**,** 179-194.

GLAVINAS, H., MEHN, D., JANI, M., OOSTERHUIS, B., HEREDI-SZABO, K. & KRAJCSI, P. 2008. Utilization of membrane vesicle preparations to study drug-ABC transporter interactions. *Expert Opinion on Drug Metabolism & Toxicology,* 4**,** 721-732.

GOOSEN, N. & MOOLENAAR, G. F. 2001. Role of ATP hydrolysis by UvrA and UvrB during nucleotide excision repair. *Research in Microbiology,* 152**,** 401-409.

GRÄFE, K., SHANMUGARAJAH, K., ZOBEL, T., WEIDTKAMP-PETERS, S., KLEINSCHRODT, D., SMITS, S. H. J. & SCHMITT, L. in preparation. Cloning and expression of selected ABC transporters from the *Arabidopsis thaliana* ABCG family in *Pichia pastoris*.

GREC, S., VANHAM, D., DE RIBAUCOURT, J. C., PURNELLE, B. & BOUTRY, M. 2003. Identification of regulatory sequence elements within the transcription promoter region of NpABC1, a gene encoding a plant ABC transporter induced by diterpenes. *Plant Journal,* 35**,** 237-250.

GRILLITSCH, K., TARAZONA, P., KLUG, L., WRIESSNEGGER, T., ZELLNIG, G., LEITNER, E., FEUSSNER, I. & DAUM, G. 2014. Isolation and characterization of the plasma membrane from the yeast Pichia pastoris. *Biochimica Et Biophysica Acta-Biomembranes,* 1838**,** 1889-1897.

GRISSHAMMER, R. 2006. Understanding recombinant expression of membrane proteins. *Current Opinion in Biotechnology,* 17**,** 337-340.

GRISWOLD, K. E., MAHMOOD, N. A., IVERSON, B. L. & GEORGIOU, G. 2003. Effects of codon usage versus putative 5 '-mRNA structure on the expression of Fusarium solani cutinase in the Escherichia coli cytoplasm. *Protein Expression and Purification,* 27**,** 134-142.

GUL, N., LINARES, D. M., HO, F. Y. & POOLMAN, B. 2014. Evolved Escherichia coli Strains for Amplified, Functional Expression of Membrane Proteins. *Journal of Molecular Biology,* 426**,** 136-149.

GUO, H. W. & ECKER, J. R. 2004. The ethylene signaling pathway: new insights. *Current Opinion in Plant Biology,* 7**,** 40-49.

GUPTA, R. P., KUEPPERS, P., HANEKOP, N. & SCHMITT, L. 2014. Generating Symmetry in the Asymmetric ATP-binding Cassette (ABC) Transporter Pdr5 from Saccharomyces cerevisiae. *Journal of Biological Chemistry,* 289**,** 15272-15279.

HAYASHI, M., YAGI, M., KAMADA, T., NITO, K. & NISHIMURA, M. 2004. Ped3p is a novel type of peroxisomal ATP-binding cassette transporter involved in peroxisomal fatty acid beta-oxidation. *Plant and Cell Physiology,* 45**,** S1-S1.

HENRIKSEN, U., GETHER, U. & LITMAN, T. 2005. Effect of Walker A mutation (K86M) on oligomerization and surface targeting of the multidrug resistance transporter ABCG2. *Journal of Cell Science,* 118**,** 1417-1426.

HILL, T. L. & MORALES, M. F. 1951. On High Energy Phosphate Bonds of Biochemical Interest. *Journal of the American Chemical Society,* 73**,** 1656-1660.

HOLLENSTEIN, K., DAWSON, R. J. P. & LOCHER, K. P. 2007. Structure and mechanism of ABC transporter proteins. *Current Opinion in Structural Biology,* 17**,** 412-418.

HOPFNER, K. P., KARCHER, A., SHIN, D. S., CRAIG, L., ARTHUR, L. M., CARNEY, J. P. & TAINER, J. A. 2000. Structural biology of Rad50 ATPase: ATP-driven conformational control in DNA double-strand break repair and the ABC-ATPase superfamily. *Cell,* 101**,** 789-800.

HORN, C., BREMER, E. & SCHMITT, L. 2003. Nucleotide dependent monomer/dimer equilibrium of OpuAA, the nucleotide-binding protein of the osmotically regulated ABC transporter OpuA from Bacillus subtilis. *Journal of Molecular Biology,* 334**,** 403-419.

HOSEINI, S. S. & SAUER, M. G. 2015. Molecular cloning using polymerase chain reaction, an educational guide for cellular engineering. *Journal of Biological Engineering,* 9.

HOVERS, J., POTSCHIES, M., POLIDORI, A., PUCCI, B., RAYNAL, S., BONNETE, F., SERRANO-VEGA, M. J., TATE, C. G., PICOT, D., PIERRE, Y., POPOT, J. L., NEHME, R., BIDET, M., MUS-VETEAU, I., BUSSKAMP, H., JUNG, K. H., MARX, A., TIMMINS, P. A. & WELTE, W. 2011a. A class of mild surfactants that keep integral membrane proteins water-soluble for functional studies and crystallization. *Molecular Membrane Biology,* 28**,** 170-180.

HOVERS, J., POTSCHIES, M., POLIDORI, A., PUCCI, B., RAYNAL, S., BONNETE, F., SERRANO-VEGA, M. J., TATE, C. G., PICOT, D., PIERRE, Y., POPOT, J. L., NEHME, R., BIDET, M., MUS-VETEAU, I., BUSSKAMP, H., JUNG, K. H., MARX, A., TIMMINS, P. A. & WELTE, W. 2011b. A class of mild surfactants that keep integral membrane proteins water-soluble for functional studies and crystallization. *Mol Membr Biol,* 28**,** 171-81.

HUALA, E., DICKERMAN, A. W., GARCIA-HERNANDEZ, M., WEEMS, D., REISER, L., LAFOND, F., HANLEY, D., KIPHART, D., ZHUANG, M., HUANG, W., MUELLER, L. A., BHATTACHARYYA, D., BHAYA, D., SOBRAL, B. W., BEAVIS, W., MEINKE, D. W., TOWN, C. D., SOMERVILLE, C. & RHEE, S. Y. 2001. The Arabidopsis Information Resource (TAIR): a comprehensive database and web-based information retrieval, analysis, and visualization system for a model plant. *Nucleic Acids Res,* 29**,** 102-5.

HUANG, C. F., YAMAJI, N. & MA, J. F. 2010. Knockout of a Bacterial-Type ATP-Binding Cassette Transporter Gene, AtSTAR1, Results in Increased Aluminum Sensitivity in Arabidopsis. *Plant Physiology,* 153**,** 1669-1677.

HUANG, C. F., YAMAJI, N., MITANI, N., YANO, M., NAGAMURA, Y. & MA, J. F. 2009. A bacterial-type ABC transporter is involved in aluminum tolerance in rice. *Plant Cell,* 21**,** 655-67.

HUANG, Q., WANG, G. J., SUN, J. G., HU, X. L., LU, Y. H. & ZHANG, Q. 2007. Simultaneous determination of docetaxel and ketoconazole in rat plasma by liquid chromatography/electrospray ionization tandem mass spectrometry. *Rapid Communications in Mass Spectrometry,* 21**,** 1009-1018.

HUSSAIN, M. M., TRANUMJENSEN, J., NOREN, O., SJOSTROM, H. & CHRISTIANSEN, K. 1981. Reconstitution of Purified Amphiphilic Pig Intestinal Microvillus Aminopeptidase - Mode of Membrane Insertion and Morphology. *Biochemical Journal,* 199**,** 179-&.

HWANG, J. U., SONG, W. Y., HONG, D., KO, D., YAMAOKA, Y., JANG, S., YIM, S., LEE, E., KHARE, D., KIM, K., PALMGREN, M., YOON, H. S., MARTINOIA, E. & LEE, Y. 2016. Plant ABC Transporters Enable Many Unique Aspects of a Terrestrial Plant's Lifestyle. *Molecular Plant,* 9**,** 338-355.

ITO, H. & GRAY, W. M. 2006. A gain-of-function mutation in the Arabidopsis pleiotropic drug resistance transporter PDR9 confers resistance to auxinic herbicides. *Plant Physiology,* 142**,** 63-74.

JANAS, E., HOFACKER, M., CHEN, M., GOMPF, S., VAN DER DOES, C. & TAMPE, R. 2003. The ATP hydrolysis cycle of the nucleotide-binding domain of the mitochondrial ATP-binding cassette transporter Mdl1p. *Journal of Biological Chemistry,* 278**,** 26862-26869.

JAQUINOD, M., VILLIERS, F., KIEFFER-JAQUINOD, S., HUGOUVIEU, V., BRULEY, C., GARIN, J. & BOURGUIGNON, J. 2007. A proteomics dissection of Arabidopsis thaliana vacuoles isolated from cell culture. *Molecular & Cellular Proteomics,* 6**,** 394-412.

JASINSKI, M., STUKKENS, Y., DEGAND, H., PURNELLE, B., MARCHAND-BRYNAERT, J. & BOUTRY, M. 2001. A plant plasma membrane ATP binding cassette-type transporter is involved in antifungal terpenoid secretion. *Plant Cell,* 13**,** 1095-1107.

JOHANSSON, O. N., FANTOZZI, E., FAHLBERG, P., NILSSON, A. K., BUHOT, N., TOR, M. & ANDERSSON, M. X. 2014. Role of the penetration-resistance genes PEN1, PEN2 and PEN3 in the hypersensitive response and race-specific resistance in Arabidopsis thaliana. *Plant Journal,* 79**,** 466-476.

JONES, P. M. & GEORGE, A. M. 2004. The ABC transporter structure and mechanism: perspectives on recent research. *Cellular and Molecular Life Sciences,* 61**,** 682-699.

KADABA, N. S., KAISER, J. T., JOHNSON, E., LEE, A. & REES, D. C. 2008. The high-affinity E-coli methionine ABC transporter: Structure and allosteric regulation. *Science,* 321**,** 250-253.

KANG, J., HWANG, J. U., LEE, M., KIM, Y. Y., ASSMANN, S. M., MARTINOIA, E. & LEE, Y. 2010. PDR-type ABC transporter mediates cellular uptake of the phytohormone abscisic acid. *Proc Natl Acad Sci U S A,* 107**,** 2355-60.

KANG, J., PARK, J., CHOI, H., BURLA, B., KRETZSCHMAR, T., LEE, Y. & MARTINOIA, E. 2011. Plant ABC Transporters. *Arabidopsis Book,* 9**,** e0153.

KANG, J., YIM, S., CHOI, H., KIM, A., LEE, K. P., LOPEZ-MOLINA, L., MARTINOIA, E. & LEE, Y. 2015. Abscisic acid transporters cooperate to control seed germination. *Nature Communications,* 6.

KHARE, D., CHOI, H., HUH, S. U., BASSIN, B., KIM, J., MARTINOIA, E., SOHN, K. H., PAEK, K. H. & LEE, Y. 2017. Arabidopsis ABCG34 contributes to defense against necrotrophic pathogens by mediating the secretion of camalexin. *Proceedings of the National Academy of Sciences of the United States of America,* 114**,** E5712-E5720.

KIM, D. Y., BOVET, L., KUSHNIR, S., NOH, E. W., MARTINOIA, E. & LEE, Y. 2006. AtATM3 is involved in heavy metal resistance in Arabidopsis. *Plant Physiology,* 140**,** 922-932.

KIM, D. Y., BOVET, L., MAESHIMA, M., MARTINOIA, E. & LEE, Y. 2007. The ABC transporter AtPDR8 is a cadmium extrusion pump conferring heavy metal resistance. *Plant Journal,* 50**,** 207-218.

KIM, D. Y., JIN, J. Y., ALEJANDRO, S., MARTINOIA, E. & LEE, Y. 2010. Overexpression of AtABCG36 improves drought and salt stress resistance in Arabidopsis. *Physiologia Plantarum,* 139**,** 170-180.

KOBAE, Y., SEKINO, T., YOSHIOKA, H., NAKAGAWA, T., MARTINOIA, E. & MAESHIMA, M. 2006. Loss of AtPDR8, a plasma membrane ABC transporter of Arabidopsis thaliana, causes hypersensitive cell death upon pathogen infection. *Plant Cell Physiol,* 47**,** 309-18.

KOBAYASHI, T., NAKAYAMA, Y., ITAI, R. N., NAKANISHI, H., YOSHIHARA, T., MORI, S. & NISHIZAWA, N. K. 2003. Identification of novel cis-acting elements, IDE1 and IDE2, of the barley IDS2 gene promoter conferring iron-deficiency-inducible, root-specific expression in heterogeneous tobacco plants. *Plant Journal,* 36**,** 780-793.

KOLACZKOWSKI, M., VAN DER REST, M., CYBULARZ-KOLACZKOWSKA, A., SOUMILLION, J. P., KONINGS, W. N. & GOFFEAU, A. 1996a. Anticancer drugs, ionophoric peptides, and steroids as substrates of the yeast multidrug transporter Pdr5p. *J Biol Chem,* 271**,** 31543-8.

KOLACZKOWSKI, M., VANDERREST, M., CYBULARZKOLACZKOWSKA, A., SOUMILLION, J. P., KONINGS, W. N. & GOFFEAU, A. 1996b. Drugs, ionophoric peptides, and steroids as substrates of the yeast multidrug transporter Pdr5p. *Journal of Biological Chemistry,* 271**,** 31543-31548.

KORKHOV, V. M., MIREKU, S. A., VEPRINTSEV, D. B. & LOCHER, K. P. 2014. Structure of AMP-PNP-bound BtuCD and mechanism of ATP-powered vitamin B12 transport by BtuCD-F. *Nature Structural & Molecular Biology,* 21**,** 1097-1099.

KORONAKIS, E., HUGHES, C., MILISAV, I. & KORONAKIS, V. 1995. Protein Exporter Function and in-Vitro Atpase Activity Are Correlated in Abc-Domain Mutants of Hlyb. *Molecular Microbiology,* 16**,** 87-96.

KOZAK, L., GOPAL, G., YOON, J. H., SAUNA, Z. E., AMBUDKAR, S. V., THAKURTA, A. G. & DHAR, R. 2002. Elf1p, a member of the ABC class of ATPases, functions as a mRNA export factor in Schizosacchromyces pombe. *Journal of Biological Chemistry,* 277**,** 33580-33589.

KRATTINGER, S. G., LAGUDAH, E. S., SPIELMEYER, W., SINGH, R. P., HUERTA-ESPINO, J., MCFADDEN, H., BOSSOLINI, E., SELTER, L. L. & KELLER, B. 2009. A Putative ABC Transporter Confers Durable Resistance to Multiple Fungal Pathogens in Wheat. *Science,* 323**,** 1360-1363.

KRATTINGER, S. G., LAGUDAH, E. S., WICKER, T., RISK, J. M., ASHTON, A. R., SELTER, L. L., MATSUMOTO, T. & KELLER, B. 2011. Lr34 multi-pathogen resistance ABC transporter: molecular analysis of homoeologous and orthologous genes in hexaploid wheat and other grass species. *Plant Journal,* 65**,** 392-403.

KRETZSCHMAR, T., BURLA, B., LEE, Y., MARTINOIA, E. & NAGY, R. 2011. Functions of ABC transporters in plants. *Essays Biochem,* 50**,** 145-60.

KRETZSCHMAR, T., KOHLEN, W., SASSE, J., BORGHI, L., SCHLEGEL, M., BACHELIER, J. B., REINHARDT, D., BOURS, R., BOUWMEESTER, H. J. & MARTINOIA, E. 2012. A petunia ABC protein controls strigolactone-dependent symbiotic signalling and branching. *Nature,* 483**,** 341-U135.

KRUMPOCHOVA, P., SAPTHU, S., BROUWERS, J. F., DE HAAS, M., DE VOS, R., BORST, P. & VAN DE WETERING, K. 2012. Transportomics: screening for substrates of ABC transporters in body fluids using vesicular transport assays. *Faseb Journal,* 26**,** 738-747.

KUROMORI, T., MIYAJI, T., YABUUCHI, H., SHIMIZU, H., SUGIMOTO, E., KAMIYA, A., MORIYAMA, Y. & SHINOZAKI, K. 2010. ABC transporter AtABCG25 is involved in abscisic acid transport and responses. *Proceedings of the National Academy of Sciences of the United States of America,* 107**,** 2361-2366.

KUSHNIR, S., BABIYCHUK, E., STOROZHENKO, S., DAVEY, M. W., PAPENBROCK, J., DE RYCKE, R., ENGLER, G., STEPHAN, U. W., LANGE, H., KISPAL, G., LILL, R. & VAN MONTAGU, M. 2001. A mutation of the mitochondrial ABC transporter Sta1 leads to dwarfism and chlorosis in the Arabidopsis mutant starik. *Plant Cell,* 13**,** 89-100.

LANFERMEIJER, F. C., VENEMA, K. & PALMGREN, M. G. 1998. Purification of a histidine-tagged plant plasma membrane H+-ATPase expressed in yeast. *Protein Expression and Purification,* 12**,** 29-37.

LANGE, C., NETT, J. H., TRUMPOWER, B. L. & HUNTE, C. 2001. Specific roles of protein-phospholipid interactions in the yeast cytochrome bc(1) complex structure. *Embo Journal,* 20**,** 6591-6600.

LARSEN, P. B., GEISLER, M. J. B., JONES, C. A., WILLIAMS, K. M. & CANCEL, J. D. 2005. ALS3 encodes a phloem-localized ABC transporter-like protein that is required for aluminum tolerance in Arabidopsis. *Plant Journal,* 41**,** 353-363.

LE MAIRE, M., CHAMPEIL, P. & MOLLER, J. V. 2000. Interaction of membrane proteins and lipids with solubilizing detergents. *Biochimica Et Biophysica Acta-Biomembranes,* 1508**,** 86-111.

LEBA, L. J., CHEVAL, C., ORTIZ-MARTIN, I., RANTY, B., BEUZON, C. R., GALAUD, J. P. & ALDON, D. 2012. CML9, an Arabidopsis calmodulin-like protein, contributes to plant innate immunity through a flagellin-dependent signalling pathway. *Plant Journal,* 71**,** 976-989.

LEE, M., CHOI, Y., BURLA, B., KIM, Y. Y., JEON, B., MAESHIMA, M., YOO, J. Y., MARTINOIA, E. & LEE, Y. 2008. The ABC transporter AtABCB14 is a malate importer and modulates stomatal response to CO2. *Nature Cell Biology,* 10**,** 1217-1223.

LEE, M., LEE, K., LEE, J., NOH, E. W. & LEE, Y. 2005. AtPDR12 contributes to lead resistance in arabidopsis. *Plant Physiology,* 138**,** 827-836.

LEE, S. H. S., D. M. 2009. Cloning and maintenance of the housefly sodium channel gene using low copy number vector and two sequential host strains. *Journal of Asia-Pacific Entomology,* 12**,** 51-53.

LEFEVRE, F., BAIJOT, A. & BOUTRY, M. 2015. Plant ABC transporters: time for biochemistry? *Biochemical Society Transactions,* 43**,** 931-936.

LENOBLE, M. E., SPOLLEN, W. G. & SHARP, R. E. 2004. Maintenance of shoot growth by endogenous ABA: genetic assessment of the involvement of ethylene suppression. *Journal of Experimental Botany,* 55**,** 237-245.

LICHTENBERG, D., AHYAYAUCH, H., ALONSO, A. & GONI, F. M. 2013. Detergent solubilization of lipid bilayers: a balance of driving forces. *Trends in Biochemical Sciences,* 38**,** 85-93.

LIPKA, V., DITTGEN, J., BEDNAREK, P., BHAT, R., WIERMER, M., STEIN, M., LANDTAG, J., BRANDT, W., ROSAHL, S., SCHEEL, D., LLORENTE, F., MOLINA, A., PARKER, J., SOMERVILLE, S. & SCHULZE-LEFERT, P. 2005. Pre- and postinvasion defenses both contribute to nonhost resistance in Arabidopsis. *Science,* 310**,** 1180-1183.

LOCHER, K. P. 2016. Mechanistic diversity in ATP-binding cassette (ABC) transporters. *Nature Structural & Molecular Biology,* 23**,** 487-493.

LOCHER, K. P., LEE, A. T. & REES, D. C. 2002. The E-coli BtuCD structure: A framework for ABC transporter architecture and mechanism. *Science,* 296**,** 1091-1098.

LOO, T. W. & CLARKE, D. M. 1995. Rapid Purification of Human P-Glycoprotein Mutants Expressed Transiently in Hek-293 Cells by Nickel-Chelate Chromatography and Characterization of Their Drug-Stimulated Atpase Activities. *Journal of Biological Chemistry,* 270**,** 21449-21452.

LU, B. B., XU, C. C., AWAI, K., JONES, A. D. & BENNING, C. 2007. A small ATPase protein of Arabidopsis, TGD3, involved in chloroplast lipid import. *Journal of Biological Chemistry,* 282**,** 35945-35953.

LU, X. L., DITTGEN, J., PISLEWSKA-BEDNAREK, M., MOLINA, A., SCHNEIDER, B., SVATOS, A., DOUBSKY, J., SCHNEEBERGER, K., WEIGEL, D., BEDNAREK, P. & SCHULZE-LEFERT, P. 2015. Mutant Allele-Specific Uncoupling of PENETRATION3 Functions Reveals Engagement of the ATP-Binding Cassette Transporter in Distinct Tryptophan Metabolic Pathways. *Plant Physiology,* 168**,** 814-+.

MACAULEY-PATRICK, S., FAZENDA, M. L., MCNEIL, B. & HARVEY, L. M. 2005. Heterologous protein production using the Pichia pastoris expression system. *Yeast,* 22**,** 249-270.

MALINVERNI, J. C. & SILHAVY, T. J. 2009. An ABC transport system that maintains lipid asymmetry in the Gram-negative outer membrane. *Proceedings of the National Academy of Sciences of the United States of America,* 106**,** 8009-8014.

MARTINOIA, E., KLEIN, M., GEISLER, M., BOVET, L., FORESTIER, C., KOLUKISAOGLU, U., MULLER-ROBER, B. & SCHULZ, B. 2002. Multifunctionality of plant ABC transporters--more than just detoxifiers. *Planta,* 214**,** 345-55.

MARTON, M. J., DEALDANA, C. R. V., QIU, H. F., CHAKRABURTTY, K. & HINNEBUSCH, A. G. 1997. Evidence that GCN1 and GCN20, translational regulators of GCN4, function on elongating ribosomes in activation of eIF2 alpha kinase GCN2. *Molecular and Cellular Biology,* 17**,** 4474-4489.

MASON, D. L. & MICHAELIS, S. 2002. Requirement of the N-terminal extension for vacuolar trafficking and transport activity of yeast Ycf1p, an ATP-binding cassette transporter. *Molecular Biology of the Cell,* 13**,** 4443-4455.

MCFARLANE, H. E., SHIN, J. J. H., BIRD, D. A. & SAMUELS, A. L. 2010. Arabidopsis ABCG Transporters, Which Are Required for Export of Diverse Cuticular Lipids, Dimerize in Different Combinations. *Plant Cell,* 22**,** 3066-3075.

MILDVAN, A. S. 1979. The role of metals in enzyme-catalyzed substitutions at each of the phosphorus atoms of ATP. *Adv Enzymol Relat Areas Mol Biol,* 49**,** 103-26.

MOHR, P. G. & CAHILL, D. M. 2003. Abscisic acid influences the susceptibility of Arabidopsis thaliana to Pseudomonas syringae pv. tomato and Peronospora parasitica. *Functional Plant Biology,* 30**,** 461-469.

MOODY, J. E., MILLEN, L., BINNS, D., HUNT, J. F. & THOMAS, P. J. 2002. Cooperative, ATP-dependent association of the nucleotide binding cassettes during the catalytic cycle of ATP-binding cassette transporters. *Journal of Biological Chemistry,* 277**,** 21111-21114.

MUMBERG, D., MULLER, R. & FUNK, M. 1995. Yeast Vectors for the Controlled Expression of Heterologous Proteins in Different Genetic Backgrounds. *Gene,* 156**,** 119-122.

MUSIELAK, T. J., SCHENKEL, L., KOLB, M., HENSCHEN, A. & BAYER, M. 2015. A simple and versatile cell wall staining protocol to study plant reproduction. *Plant Reproduction,* 28**,** 161-169.

MYSORE, K. S. & RYU, C. M. 2004. Nonhost resistance: how much do we know? *Trends in Plant Science,* 9**,** 97-104.

NIELSEN, M. E. & THORDAL-CHRISTENSEN, H. 2013. Transcytosis shuts the door for an unwanted guest. *Trends in Plant Science,* 18**,** 611-616.

NIKS, R. E. & MARCEL, T. C. 2009. Nonhost and basal resistance: how to explain specificity? *New Phytologist,* 182**,** 817-828.

NOE, J., STIEGER, B. & MEIER, P. J. 2002. Functional expression of the canalicular bile salt export pump of human liver. *Gastroenterology,* 123**,** 1659-1666.

NUHSE, T. S., BOTTRILL, A. R., JONES, A. M. E. & PECK, S. C. 2007. Quantitative phosphoproteomic analysis of plasma membrane proteins reveals regulatory mechanisms of plant innate immune responses. *Plant Journal,* 51**,** 931-940.

NURUZZAMAN, M., ZHANG, R., CAO, H. Z. & LUO, Z. Y. 2014. Plant pleiotropic drug resistance transporters: transport mechanism, gene expression, and function. *J Integr Plant Biol,* 56**,** 729-40.

OLDHAM, M. L. & CHEN, J. 2011. Snapshots of the maltose transporter during ATP hydrolysis. *Proceedings of the National Academy of Sciences of the United States of America,* 108**,** 15152-15156.

OLDHAM, M. L., DAVIDSON, A. L. & CHEN, J. 2008. Structural insights into ABC transporter mechanism. *Current Opinion in Structural Biology,* 18**,** 726-733.

OPEKAROVA, M. & TANNER, W. 2003. Specific lipid requirements of membrane proteins - a putative bottleneck in heterologous expression. *Biochimica Et Biophysica Acta-Biomembranes,* 1610**,** 11-22.

ORELLE, C., DALMAS, O., GROS, P., DI PIETRO, A. & JAULT, J. M. 2003. The conserved glutamate residue adjacent to the Walker-B motif is the catalytic base for ATP hydrolysis in the ATP-binding cassette transporter BmrA. *Journal of Biological Chemistry,* 278**,** 47002-47008.

PANAGIOTIDIS, C. H., REYES, M., SIEVERTSEN, A., BOOS, W. & SHUMAN, H. A. 1993. Characterization of the Structural Requirements for Assembly and Nucleotide-Binding of an Atp-Binding Cassette Transporter - the Maltose Transport-System of Escherichia-Coli. *Journal of Biological Chemistry,* 268**,** 23685-23696.

PANDEY, P., IRULAPPAN, V., BAGAVATHIANNAN, M. V. & SENTHIL-KUMAR, M. 2017. Impact of Combined Abiotic and Biotic Stresses on Plant Growth and Avenues for Crop Improvement by Exploiting Physio-morphological Traits. *Frontiers in Plant Science,* 8.

PEREZ, C., GERBER, S., BOILEVIN, J., BUCHER, M., DARBRE, T., AEBI, M., REYMOND, J. L. & LOCHER, K. P. 2015. Structure and mechanism of an active lipid-linked oligosaccharide flippase. *Nature,* 524**,** 433-+.

PIERMAN, B., TOUSSAINT, F., BERTIN, A., LEVY, D., SMARGIASSO, N., DE PAUW, E. & BOUTRY, M. 2017. Activity of the purified plant ABC transporter NtPDR1 is stimulated by diterpenes and sesquiterpenes involved in constitutive and induced defenses. *Journal of Biological Chemistry,* 292**,** 19491-19502.

PROCKO, E., RAGHURAMAN, G., WILEY, D. C., RAGHAVAN, M. & GAUDET, R. 2005. Identification of domain boundaries within the N-termini of TAP1 and TAP2 and their importance in tapasin binding and tapasin-mediated increase in peptide loading of MHC class I. *Immunology and Cell Biology,* 83**,** 475-482.

QU, Q., CHU, J. W. K. & SHAROM, F. J. 2003. Transition state P-glycoprotein binds drugs and modulators with unchanged affinity, suggesting a concerted transport mechanism. *Biochemistry,* 42**,** 1345-1353.

RAMESH, V., DE, A. & NAGARAJA, V. 1994. Engineering Hyperexpression of Bacteriophage-Mu C-Protein by Removal of Secondary Structure at the Translation Initiation Region. *Protein Engineering,* 7**,** 1053-1057.

REA, P. A. 2007. Plant ATP-binding cassette transporters. *Annu Rev Plant Biol,* 58**,** 347-75.

REES, D. C., JOHNSON, E. & LEWINSON, O. 2009. ABC transporters: the power to change. *Nature Reviews Molecular Cell Biology,* 10**,** 218-227.

REISER, L., BERARDINI, T. Z., LI, D., MULLER, R., STRAIT, E. M., LI, Q., MEZHERITSKY, Y., VETUSHKO, A. & HUALA, E. 2016. Sustainable funding for biocuration: The Arabidopsis Information Resource (TAIR) as a case study of a subscription-based funding model. *Database (Oxford),* 2016.

RIGAUD, J. L., PITARD, B. & LEVY, D. 1995. Reconstitution of Membrane-Proteins into Liposomes - Application to Energy-Transducing Membrane-Proteins. *Biochimica Et Biophysica Acta-Bioenergetics,* 1231**,** 223-246.

ROSTON, R. L., GAO, J. P., MURCHA, M. W., WHELAN, J. & BENNING, C. 2012. TGD1,-2, and-3 Proteins Involved in Lipid Trafficking Form ATP-binding Cassette (ABC) Transporter with Multiple Substrate-binding Proteins. *Journal of Biological Chemistry,* 287**,** 21406-21415.

RUSHTON, P. J., SOMSSICH, I. E., RINGLER, P. & SHEN, Q. X. J. 2010. WRKY transcription factors. *Trends in Plant Science,* 15**,** 247-258.

RUZICKA, K., STRADER, L. C., BAILLY, A., YANG, H., BLAKESLEE, J., LANGOWSKI, L., NEJEDLA, E., FUJITA, H., ITOH, H., SYONO, K., HEJATKO, J., GRAY, W. M., MARTINOIA, E., GEISLER, M., BARTEL, B., MURPHY, A. S. & FRIML, J. 2010. Arabidopsis PIS1 encodes the ABCG37 transporter of auxinic compounds including the auxin precursor indole-3-butyric acid. *Proc Natl Acad Sci U S A,* 107**,** 10749-53.

SACHDEV, D. & CHIRGWIN, J. M. 1998. Order of fusions between bacterial and mammalian proteins can determine solubility in Escherichia coli. *Biochemical and Biophysical Research Communications,* 244**,** 933-937.

SAEKI, T., SHIMABUKU, A. M., AZUMA, Y., SHIBANO, Y., KOMANO, T. & UEDA, K. 1991. Expression of Human P-Glycoprotein in Yeast-Cells - Effects of Membrane Component Sterols on the Activity of P-Glycoprotein. *Agricultural and Biological Chemistry,* 55**,** 1859-1865.

SAKAMOTO, K., MARGOLLES, A., VAN VEEN, H. W. & KONINGS, W. N. 2001. Hop resistance in the beer spoilage bacterium Lactobacillus brevis is mediated by the ATP-binding cassette multidrug transporter HorA. *Journal of Bacteriology,* 183**,** 5371-5375.

SAMI, M., YAMASHITA, H., HIRONO, T., KADOKURA, H., KITAMOTO, K., YODA, K. & YAMASAKI, M. 1997. Hop-resistant Lactobacillus brevis contains a novel plasmid harboring a multidrug resistance-like gene. *Journal of Fermentation and Bioengineering,* 84**,** 1-6.

SANCHEZ-FERNANDEZ, R., DAVIES, T. G., COLEMAN, J. O. & REA, P. A. 2001a. The Arabidopsis thaliana ABC protein superfamily, a complete inventory. *J Biol Chem,* 276**,** 30231-44.

SANCHEZ-FERNANDEZ, R., REA, P. A., DAVIES, T. G. & COLEMAN, J. O. 2001b. Do plants have more genes than humans? Yes, when it comes to ABC proteins. *Trends Plant Sci,* 6**,** 347-8.

SANCHEZ-VALLET, A., RAMOS, B., BEDNAREK, P., LOPEZ, G., PISLEWSKA-BEDNAREK, M., SCHULZE-LEFERT, P. & MOLINA, A. 2010. Tryptophan-derived secondary metabolites in Arabidopsis thaliana confer non-host resistance to necrotrophic Plectosphaerella cucumerina fungi. *Plant Journal,* 63**,** 115-127.

SASABE, M., TOYODA, K., SHIRAISHI, T., INAGAKI, Y. & ICHINOSE, Y. 2002. cDNA cloning and characterization of tobacco ABC transporter: NtPDR1 is a novel elicitor-responsive gene. *Febs Letters,* 518**,** 164-168.

SASSE, J., SCHLEGEL, M., BORGHI, L., ULLRICH, F., LEE, M., LIU, G. W., GINER, J. L., KAYSER, O., BIGLER, L., MARTINOIA, E. & KRETZSCHMAR, T. 2016. Petunia hybrida PDR2 is involved in herbivore defense by controlling steroidal contents in trichomes. *Plant Cell and Environment,* 39**,** 2725-2739.

SAUER, N., CASPARI, T., KLEBL, F. & TANNER, W. 1990. Functional Expression of the Chlorella Hexose Transporter in Schizosaccharomyces-Pombe. *Proceedings of the National Academy of Sciences of the United States of America,* 87**,** 7949-7952.

SAZUKA, T., KETA, S., SHIRATAKE, K., YAMAKI, S. & SHIBATA, D. 2004. A proteomic approach to identification of transmembrane proteins and membrane-anchored proteins of Arabidopsis thaliana by peptide Sequencing. *DNA Research,* 11**,** 101-113.

SCHIESTL, R. H. & GIETZ, R. D. 1989. High-Efficiency Transformation of Intact Yeast-Cells Using Single Stranded Nucleic-Acids as a Carrier. *Current Genetics,* 16**,** 339-346.

SCHMITT, L., BENABDELHAK, H., BLIGHT, M. A., HOLLAND, B. I. & STUBBS, M. T. 2003. Crystal structure of the nucleotide-binding domain of the ABC-transporter haemolysin B: Identification of a variable region within ABC helical domains. *Journal of Molecular Biology,* 330**,** 333-342.

SCHMITT, L. & TAMPE, R. 2000. Affinity, specificity, diversity: a challenge for the ABC transporter TAP in cellular immunity. *Chembiochem,* 1**,** 16-35.

SCHNEIDER, E. & HUNKE, S. 1998. ATP-binding-cassette (ABC) transport systems: Functional and structural aspects of the ATP-hydrolyzing subunits/domains. *Fems Microbiology Reviews,* 22**,** 1-20.

SCHNEIDER, E., WILKEN, S. & SCHMID, R. 1994. Nucleotide-Induced Conformational-Changes of Malk, a Bacterial Atp Binding Cassette Transporter Protein. *Journal of Biological Chemistry,* 269**,** 20456-20461.

SENIOR, A. E., ALSHAWI, M. K. & URBATSCH, I. L. 1995. The catalytic cycle of P-glycoprotein. *Febs Letters,* 377**,** 285-289.

SHANG, Y., XIAO, J., MA, L. L., WANG, H. Y., QI, Z. J., CHEN, P. D., LIU, D. J. & WANG, X. E. 2009. Characterization of a PDR type ABC transporter gene from wheat (Triticum aestivum L.). *Chinese Science Bulletin,* 54**,** 3249-3257.

SHAROM, F. J. 1997. The P-glycoprotein multidrug transporter: interactions with membrane lipids, and their modulation of activity. *Biochemical Society Transactions,* 25**,** 1088-1096.

SHAROM, F. J., YU, X. H., LU, P. H., LIU, R. H., CHU, J. W. K., SZABO, K., MULLER, M., HOSE, C. D., MONKS, A., VARADI, A., SEPRODI, J. & SARKADI, B. 1999. Interaction of the P-glycoprotein multidrug transporter (MDR1) with high affinity peptide chemosensitizers in isolated membranes, reconstituted systems, and intact cells. *Biochemical Pharmacology,* 58**,** 571-586.

SIKORSKI, R. S. & HIETER, P. 1989. A System of Shuttle Vectors and Yeast Host Strains Designed for Efficient Manipulation of DNA in Saccharomyces-Cerevisiae. *Genetics,* 122**,** 19-27.

SMART, C. C. & FLEMING, A. J. 1996. Hormonal and environmental regulation of a plant PDR5-like ABC transporter. *Journal of Biological Chemistry,* 271**,** 19351-19357.

SMITH, P. C., KARPOWICH, N., MILLEN, L., MOODY, J. E., ROSEN, J., THOMAS, P. J. & HUNT, J. F. 2002. ATP binding to the motor domain from an ABC transporter drives formation of a nucleotide sandwich dimer. *Molecular Cell,* 10**,** 139-149.

SREEKRISHNA, K., BRANKAMP, R. G., KROPP, K. E., BLANKENSHIP, D. T., TSAY, J. T., SMITH, P. L., WIERSCHKE, J. D., SUBRAMANIAM, A. & BIRKENBERGER, L. A. 1997. Strategies for optimal synthesis and secretion of heterologous proteins in the methylotrophic yeast Pichia pastoris. *Gene,* 190**,** 55-62.

STEIN, M., DITTGEN, J., SANCHEZ-RODRIGUEZ, C., HOU, B. H., MOLINA, A., SCHULZE-LEFERT, P., LIPKA, V. & SOMERVILLE, S. 2006. Arabidopsis PEN3/PDR8, an ATP binding cassette transporter, contributes to nonhost resistance to inappropriate pathogens that enter by direct penetration. *Plant Cell,* 18**,** 731-46.

STINDT, J., ELLINGER, P., STROSS, C., KEITEL, V., HAUSSINGER, D., SMITS, S. H. J., KUBITZ, R. & SCHMITT, L. 2011. Heterologous Overexpression and Mutagenesis of the Human Bile Salt Export Pump (ABCB11) Using DREAM (Directed REcombination-Assisted Mutagenesis). *Plos One,* 6.

STRADER, L. C. & BARTEL, B. 2009. The Arabidopsis PLEIOTROPIC DRUG RESISTANCE8/ABCG36 ATP binding cassette transporter modulates sensitivity to the auxin precursor indole-3-butyric acid. *Plant Cell,* 21**,** 1992-2007.

STUKKENS, Y., BULTREYS, A., GREC, S., TROMBIK, T., VANHAM, D. & BOUTRY, M. 2005. NpPDR1, a pleiotropic drug resistance-type ATP-binding cassette transporter from Nicotiana plumbaginifolia, plays a major role in plant pathogen defense. *Plant Physiology,* 139**,** 341-352.

SUN, Y., LI, L., MACHO, A. P., HAN, Z., HU, Z., ZIPFEL, C., ZHOU, J. M. & CHAI, J. 2013. Structural basis for flg22-induced activation of the Arabidopsis FLS2-BAK1 immune complex. *Science,* 342**,** 624-8.

SVENSSON, J., ANDERSSON, C., RESELAND, J. E., LYNGSTADAAS, P. & BULOW, L. 2006. Histidine tag fusion increases expression levels of active recombinant amelogenin in Escherichia coli. *Protein Expression and Purification,* 48**,** 134-141.

SYMMONS, M. F., BOKMA, E., KORONAKIS, E., HUGHES, C. & KORONAKIS, V. 2009. The assembled structure of a complete tripartite bacterial multidrug efflux pump. *Proceedings of the National Academy of Sciences of the United States of America,* 106**,** 7173-7178.

TAKEUCHI, M., KEGASA, T., WATANABE, A., TAMURA, M. & TSUTSUMI, Y. 2018. Expression analysis of transporter genes for screening candidate monolignol transporters using Arabidopsis thaliana cell suspensions during tracheary element differentiation. *Journal of Plant Research,* 131**,** 297-305.

TATE, C. G., WHITELEY, E. & BETENBAUGH, M. J. 1999. Molecular chaperones stimulate the functional expression of the cocaine-sensitive serotonin transporter. *Journal of Biological Chemistry,* 274**,** 17551-17558.

TERASAKA, K., BLAKESLEE, J. J., TITAPIWATANAKUN, B., PEER, W. A., BANDYOPADHYAY, A., MAKAM, S. N., LEE, O. R., RICHARDS, E. L., MURPHY, A. S., SATO, F. & YAZAKI, K. 2005. PGP4, an ATP binding cassette P-glycoprotein, catalyzes auxin transport in Arabidopsis thaliana roots. *Plant Cell,* 17**,** 2922-2939.

THEODOULOU, F. L. 2000. Plant ABC transporters. *Biochim Biophys Acta,* 1465**,** 79-103.

THEODOULOU, F. L., HOLDSWORTH, M. & BAKER, A. 2006. Peroxisomal ABC transporters. *FEBS Lett,* 580**,** 1139-55.

TILLER, G. E., MUELLER, T. J., DOCKTER, M. E. & STRUVE, W. G. 1984. Hydrogenation of triton X-100 eliminates its fluorescence and ultraviolet light absorption while preserving its detergent properties. *Anal Biochem,* 141**,** 262-6.

TOUSSAINT, F., PIERMAN, B., BERTIN, A., LEVY, D. & BOUTRY, M. 2017. Purification and biochemical characterization of NpABCG5/NpPDR5, a plant pleiotropic drug resistance transporter expressed in Nicotiana tabacum BY-2 suspension cells. *Biochemical Journal,* 474**,** 1689-1703.

TROMBIK, T., JASINSKI, M., CROUZET, J. & BOUTRY, M. 2008. Identification of a cluster IV pleiotropic drug resistance transporter gene expressed in the style of Nicotiana plumbaginifolia. *Plant Mol Biol,* 66**,** 165-75.

TSIRIGOS, K. D., PETERS, C., SHU, N., KALL, L. & ELOFSSON, A. 2015. The TOPCONS web server for consensus prediction of membrane protein topology and signal peptides. *Nucleic Acids Res,* 43**,** W401-7.

TYLER, B. M., TRIPATHY, S., ZHANG, X. M., DEHAL, P., JIANG, R. H. Y., AERTS, A., ARREDONDO, F. D., BAXTER, L., BENSASSON, D., BEYNON, J. L., CHAPMAN, J., DAMASCENO, C. M. B., DORRANCE, A. E., DOU, D. L., DICKERMAN, A. W., DUBCHAK, I. L., GARBELOTTO, M., GIJZEN, M., GORDON, S. G., GOVERS, F., GRUNWALD, N. J., HUANG, W., IVORS, K. L., JONES, R. W., KAMOUN, S., KRAMPIS, K., LAMOUR, K. H., LEE, M. K., MCDONALD, W. H., MEDINA, M., MEIJER, H. J. G., NORDBERG, E. K., MACLEAN, D. J., OSPINA-GIRALDO, M. D., MORRIS, P. F., PHUNTUMART, V., PUTNAM, N. H., RASH, S., ROSE, J. K. C., SAKIHAMA, Y., SALAMOV, A. A., SAVIDOR, A., SCHEURING, C. F., SMITH, B. M., SOBRAL, B. W. S., TERRY, A., TORTO-ALALIBO, T. A., WIN, J., XU, Z. Y., ZHANG, H. B., GRIGORIEV, I. V., ROKHSAR, D. S. & BOORE, J. L. 2006. Phytophthora genome sequences uncover evolutionary origins and mechanisms of pathogenesis. *Science,* 313**,** 1261-1266.

UNDERWOOD, W. & SOMERVILLE, S. C. 2013. Perception of conserved pathogen elicitors at the plasma membrane leads to relocalization of the Arabidopsis PEN3 transporter. *Proc Natl Acad Sci U S A,* 110**,** 12492-7.

VAN DEN BRULE, S., MULLER, A., FLEMING, A. J. & SMART, C. C. 2002. The ABC transporter SpTUR2 confers resistance to the antifungal diterpene sclareol. *Plant Journal,* 30**,** 649-662.

VAN DEN BRULE, S. & SMART, C. C. 2002. The plant PDR family of ABC transporters. *Planta,* 216**,** 95-106.

VERDON, G., ALBERS, S. V., VAN OOSTERWIJK, N., DIJKSTRA, B. W., DRIESSEN, A. J. M. & THUNNISSEN, A. M. W. H. 2003. Formation of the productive ATP-Mg2+-bound dimer of GlcV, an ABC-ATPase from Sulfolobus solfataricus. *Journal of Molecular Biology,* 334**,** 255-267.

VERRIER, P. J., BIRD, D., BURLA, B., DASSA, E., FORESTIER, C., GEISLER, M., KLEIN, M., KOLUKISAOGLU, U., LEE, Y., MARTINOIA, E., MURPHY, A., REA, P. A., SAMUELS, L., SCHULZ, B., SPALDING, E. J., YAZAKI, K. & THEODOULOU, F. L. 2008. Plant ABC proteins--a unified nomenclature and updated inventory. *Trends Plant Sci,* 13**,** 151-9.

VETTER, I. R. & WITTINGHOFER, A. 1999. Nucleoside triphosphate-binding proteins: different scaffolds to achieve phosphoryl transfer. *Q Rev Biophys,* 32**,** 1-56.

VOGL, T., THALLINGER, G. G., ZELLNIG, G., DREW, D., CREGG, J. M., GLIEDER, A. & FREIGASSNER, M. 2014. Towards improved membrane protein production in Pichia pastoris: General and specific transcriptional response to membrane protein overexpression. *New Biotechnology,* 31**,** 538-552.

VU, K., BAUTOS, J., HONG, M. P. & GELLI, A. 2009. The functional expression of toxic genes: Lessons learned from molecular cloning of CCH1, a high-affinity Ca2+ channel. *Analytical Biochemistry,* 393**,** 234-241.

WAGNER, S., BADER, M. L., DREW, D. & DE GIER, J. W. 2006. Rationalizing membrane protein overexpression. *Trends in Biotechnology,* 24**,** 364-371.

WALLIN, E. & VON HEIJNE, G. 1998. Genome-wide analysis of integral membrane proteins from eubacterial, archaean, and eukaryotic organisms. *Protein Science,* 7**,** 1029-1038.

WANG, Z. L., STALCUP, L. D., HARVEY, B. J., WEBER, J., CHLOUPKOVA, M., DUMONT, M. E., DEAN, M. & URBATSCH, I. L. 2006. Purification and ATP hydrolysis of the putative cholesterol transporters ABCG5 and ABCG8. *Biochemistry,* 45**,** 9929-9939.

WARD, A., REYES, C. L., YU, J., ROTH, C. B. & CHANG, G. 2007. Flexibility in the ABC transporter MsbA: Alternating access with a twist. *Proceedings of the National Academy of Sciences of the United States of America,* 104**,** 19005-19010.

WARNE, T., SERRANO-VEGA, M. J., BAKER, J. G., MOUKHAMETZIANOV, R., EDWARDS, P. C., HENDERSON, R., LESLIE, A. G. W., TATE, C. G. & SCHERTLER, G. F. X. 2008. Structure of a beta(1)-adrenergic G-protein-coupled receptor. *Nature,* 454**,** 486-491.

WESTLAKE, C. J., COLE, S. P. C. & DEELEY, R. G. 2005. Role of the NH2-terminal membrane spanning domain of multidrug resistance protein 1/ABCC1 in protein processing and trafficking. *Molecular Biology of the Cell,* 16**,** 2483-2492.

WOODWARD, A. W. & BARTEL, B. 2005. Auxin: Regulation, action, and interaction. *Annals of Botany,* 95**,** 707-735.

XIN, X. F., NOMURA, K., UNDERWOOD, W. & HE, S. Y. 2013. Induction and suppression of PEN3 focal accumulation during Pseudomonas syringae pv. tomato DC3000 infection of Arabidopsis. *Mol Plant Microbe Interact,* 26**,** 861-7.

XU, C. C., FAN, J. L., RIEKHOF, W., FROEHLICH, J. E. & BENNING, C. 2003. A permease-like protein involved in ER to thylakoid lipid transfer in Arabidopsis. *Embo Journal,* 22**,** 2370-2379.

YADAV, V., MOLINA, I., RANATHUNGE, K., CASTILLO, I. Q., ROTHSTEIN, S. J. & REED, J. W. 2014. ABCG Transporters Are Required for Suberin and Pollen Wall Extracellular Barriers in Arabidopsis. *Plant Cell,* 26**,** 3569-3588.

YANG, Z. R., HILDEBRANDT, E., JIANG, F., ALEKSANDROV, A. A., KHAZANOV, N., ZHOU, Q. X., AN, J. L., MEZZELL, A. T., XAVIER, B. M., DING, H., RIORDAN, J. R., SENDEROWITZ, H., KAPPES, J. C., BROUILLETTE, C. G. & URBATSCH, I. L. 2018. Structural stability of purified human CFTR is systematically improved by mutations in nucleotide binding domain 1. *Biochimica Et Biophysica Acta-Biomembranes,* 1860**,** 1193-1204.

YAZAKI, K. 2006. ABC transporters involved in the transport of plant secondary metabolites. *FEBS Lett,* 580**,** 1183-91.

YIM, S., KHARE, D., KANG, J., HWANG, J. U., LIANG, W. Q., MARTINOIA, E., ZHANG, D. B., KANG, B. H. & LEE, Y. 2016. Postmeiotic development of pollen surface layers requires two Arabidopsis ABCG-type transporters. *Plant Cell Reports,* 35**,** 1863-1873.

YU, F. & DE LUCA, V. 2013. ATP-binding cassette transporter controls leaf surface secretion of anticancer drug components in Catharanthus roseus. *Proceedings of the National Academy of Sciences of the United States of America,* 110**,** 15830-15835.

YUAN, Y. R., BLECKER, S., MARTSINKEVICH, O., MILLEN, L., THOMAS, P. J. & HUNT, J. F. 2001. The crystal structure of the MJ0796 ATP-binding cassette - Implications for the structural consequences of ATP hydrolysis in the active site of an ABC transporter. *Journal of Biological Chemistry,* 276**,** 32313-32321.

ZAITSEVA, J., JENEWEIN, S., JUMPERTZ, T., HOLLAND, I. B. & SCHMITT, L. 2005. H662 is the linchpin of ATP hydrolysis in the nucleotide-binding domain of the ABC transporter HlyB. *Embo Journal,* 24**,** 1901-1910.

ZENG, H., LIU, G. S., REA, P. A. & KRUH, G. D. 2000. Transport of amphipathic anions by human multidrug resistance protein 3. *Cancer Research,* 60**,** 4779-4784.

ZHAO, J., DAVIS, L. C. & VERPOORTE, R. 2005. Elicitor signal transduction leading to production of plant secondary metabolites. *Biotechnology Advances,* 23**,** 283-333.

ZIEGLER, J., SCHMIDT, S., STREHMEL, N., SCHEEL, D. & ABEL, S. 2017. Arabidopsis Transporter ABCG37/PDR9 contributes primarily highly oxygenated Coumarins to Root Exudation. *Scientific Reports,* 7.

Acknowledgements

An dieser Stelle möchte ich allen danken, die mich während meiner Promotionszeit unterstützt haben.

Mein besonderer Dank gilt Prof. Dr. Lutz Schmitt. Danke für die Möglichkeit zu promovieren, für die permanente Unterstützung in allen beruflichen Lebenslagen, für fachliche Diskussionen, für die Möglichkeit, Ideen einzubringen und die Schaffung eines Umfeldes in dem ich mich weiterentwickeln konnte.

Bei Prof. Dr. Karl-Erich Jaeger bedanke ich mich für die Übernahme des Korreferats und für das wissenschaftliche Interesse an meiner Arbeit. Vielen Dank für das Engagement durch welches meine Promotion voran getrieben werden konnte.

Dr. Sander Smits möchte ich für viele anregende Diskussionen danken, für einen anderen Blickwinkel auf Ergebnisse und Fragestellungen und für die Unterstützung und Rückendeckung in vielen Situationen.

Dr. Diana Kleinschrodt danke ich für die Unterstützung zu Begin meiner Arbeit. Vielen Dank für die Zuversicht wenn es bei der Klonierung und Expression nicht weitergehen wollte, für wertvolle Ratschläge und Ideen und dafür, dass Du immer ein Ansprechpartner in schwierigen Situationen warst.

Liebe Kalpana, Dir möchte ich ganz besonders dafür danken, dass Du mich in all der Zeit begleitet hast, dass Du meine Projektpartnerin warst, Ansprechpartnerin und Freundin. Wir haben in der Zeit Vieles geteilt, Erfahrungen gesammelt und uns gegenseitig unterstützt. Danke dafür.

Rebecca und Sakshi, Euch vielen Dank für die unendliche Unterstützung während unserer Zeit in der Arbeitsgruppe und darüber hinaus. Ihr habt mir in so vielen Situationen geholfen und mich unterstützt. Und wenn ich mal eine Auszeit brauchte wart ihr auch immer da.

Ich danke Jens und Martina für die gute Atmosphäre bei uns im Labor und dafür, dass ich so sein konnte, wie ich bin.

Den “Mädels” Katja, Julia, Sandra, Olivia und Isabelle danke ich für eine tolle gemeinsame Zeit mit Kaffeepausen, Disneyabenden und kulinarischen Ausflügen. Es wird kein Morgen geben.

Ich danke den Mitgliedern der MDR-Gruppe Manuel, Tim und Martin für konstruktive Meetings, Diskussionen und Ratschläge.

Ich bedanke mich bei PD Dr. Ulrich Schulte für die Möglichkeit, Studenten bei ihren Abschlussarbeiten und im Praktikum zu betreuen, wobei ich sehr viel gelernt habe und auch gewachsen bin.

Bei Frau Blum bedanke ich mich für die organisatorische Unterstützung während meiner Promotion.

Allen derzeitigen und ehemaligen Mitarbeitern des Instituts für Biochemie danke ich für die gute Atmosphäre und die schöne Zeit bei der Arbeit, aber auch bei Betriebsausflügen, Grillabenden und bei Kaffee und Kuchen.

Ich danke dem Cluster of Excellence on Plant Sciences (CEPLAS) für die Förderung meines Projektes und die Möglichkeit, mich im Rahmen der CEPLAS Graduate School weiterzubilden. Den Mitarbeitern des CEPLAS Office möchte ich für die Unterstützung und Betreuung während meiner Promotionszeit danken. Bei den Mitgliedern von CEPLAS bedanke ich mich für viele interessante wissenschaftliche Diskussionen und Anregungen während diverser CEPLAS-Veranstaltungen.

Dr. Sabine Metzger von der CEPLAS Plant Metabolism and Metabolomics Facility danke ich für die fachliche Kompetenz in der Massenspektrometrie.

Dr. Thomas Zobel und Dr. Stefanie Weidtkamp-Peters vom Center for Advanced Imaging der Heinrich-Heine-Universität Düsseldorf danke ich für die Unterstützung bei den Fluoreszenzmessungen.

Meinen Freunden danke ich für die Anteilnahme, das Verständnis und die Ablenkung während dieser stressige Zeit.

Liebe Esther und liebe Meike, ich kann kaum sagen wie wichtig ihr mir in den letzten Jahren geworden seid. Vielen Dank für die fachlichen Diskussionen, die Schreibgruppe mit viel konstruktiv deutscher (aka in your face) Kritik und darüber hinaus für unzählige Mädelsabende, Wasted Wednesdays, und Kaffeeeinladungen. Ihr versteht mich.

Ein weiterer besonderer Dank gilt meiner Familie, die mich auf so vielfältige Weise während meiner Ausbildung unterstützt hat, mich ermutigt hat und Verständnis gezeigt hat. Ich danke vor allem meinen Eltern, meinen Großeltern und meinem Patenonkel.

Patrick, Du bist der wichtigste Mensch in meinem Leben. Danke, dass Du immer da bist. Du bist mein Rückhalt, mein Rückzugsort und gibst mir Kraft. Mit Dir bin ich zuversichtlich.

Eidestattliche Versicherung

Ich versichere an Eides Statt, dass die Dissertation von mir selbständig und ohne unzulässige fremde Hilfe unter Beachtung der „Grundsätze zur Sicherung guter wissenschaftlicher Praxis an der Heinrich-Heine-Universität Düsseldorf“ erstellt worden ist. Die Dissertation wurde in der vorgelegten oder in ähnlicher Form noch bei keiner anderen Institution eingereicht. Ich habe bisher keine erfolglosen Promotionsversuche unternommen.

Düsseldorf, den

_____

Katharina Gräfe

Curriculum vitae

Personal Details

Name: Katharina Gräfe
Date of birth: November 17th 1986
Place of birth: Krefeld, Germany

Education

- 2013 – present Heinrich Heine University Düsseldorf, Germany
  PhD Thesis in Biochemistry at the Institute for Biochemistry
  Member of the Cluster of Excellence on Plant Sciences Graduate School
  Title of Thesis: "Establishing an *in vitro* system for the ABC transporter Pleiotropic Drug Resistance 8 from *A. thaliana*"

- 2011 – 2013 Bremerhaven University of Applied Sciences, Germany
  Master of Science in Biotechnology, ECTS grade A
  Master Thesis (in English) in the Plant Adaptive Genomics and Genetics Group at the Max Planck Institute for Plant Breeding Research, Cologne, Germany
  Title of Thesis: "Functional Characterization of *EARLY FLOWERING3* Homologs from different Tomato Species"

- 2007 – 2010: Bremerhaven University of Applied Sciences, Germany
  Bachelor of Science in Maritime Technologies, specialization in Biotechnology
  Bachelor Thesis (in German) in the Biogeochemistry Group at the Max Planck Institute for Marine Microbiology in Bremen, Germany
  Title of Thesis: "Extraction of dissolved gases of marine sediment porewaters for concentration and isotope analysis by mass spectrometry"

- 2006 – 2007 Berufskolleg Glockenspitz, Krefeld
  Trained as a state-certified chemical-technical assistant

- 1997 – 2006 Gymnasium am Stadtpark, Krefeld
  "Allgemeine Hochschulreife", university entrance qualification

Appendix

A1. List of detergents used in the detergent screening for the solubilization of *At*PDR8 out of the *P. pastoris* membrane. The cmc of the respective detergents, the used concentration, the position on the DotBlot membrane as well as the nature of the detergents are listed. N, neutral; A, anionic; Z, zwitterionic

Position	Detergent	cmc	% used	Nature
A1	Anameg®-7	0.65	1	N
A2	Anapoe®-20	0.0072	1	N
A3	Anapoe®-35	0.001	1	N
A4	Anapoe®-58	0.00045	1	N
A5	Anapoe®-80	0.0016	1	N
A6	Anapoe®-C10E6	0.025	1	N
A7	Anapoe®-C10E9	0.053	1	N
A8	Anapoe®-C12E8	0.0048	1	N
A9	Anapoe®-C12E9	0.003	1	N
A10	Anapoe®-C12E10	0.2	1	N
A11	Anapoe®-C13E8	0.0055	1	N
A12	Anapoe®-X-100	0.015	1	N
B1	Anapoe®-X-114	0.011	1	N
B2	Anapoe®-X-305	0.09919	1	N
B3	Anapoe®-X-405	0.16	1	N
B4	Big CHAP	0.25	1	N
B5	Big CHAP deoxy	0.12	1	N
B6	CYGLU®-3	0.86	2	N
B7	CYMAL®-1	15	2	N
B8	CYMAL®-2	5.4	2	N
B9	CYMAL®-3	0.37	1	N
B10	2,6-Dimethyl-4-heptyl-β-D-maltopyranoside	1.2	2	N
B11	n-Decyl-α-D-maltopyranoside		2	N
B12	n-Decyl-ß-D-maltopyranoside	0.087	2	N
C1	n-Decyl-ß-D-Thiomaltopyranosid	0.045	2	N
C2	n-Decyl-N,N-Dimethylglycin	0.046	2	Z
C3	n-Dodecyl-α-D-maltopyranoside	0.0076	1	N
C4	n-Dodecyl-β-D-maltopyranoside	0.0087	1	N
C5	n-Heptyl-β-D-thioglucopyranoside	0.85	2	N
C6	n-Heptyl-ß-D-Glucopyranoside	1.9	2	N
C7	n-Nonyl-β-D-thiomaltopyranoside	0.15	1	N
C8	n-Dodecyl-β-D-thiomaltopyranoside	0.0026	1	N
C9	CYMAL 4	0.12	2	N
C10	CYMAL®-5	0.12	2	N
C11	CYMAL 6	0.028	1	N
C12	CYMAL 7	0.0099	1	N

D1	Anzergent 3-8	10.9	2	Z
D2	Anzergent® 3-10	1.2	2	Z
D3	Anzergent®3-12	0.094	1	Z
D4	Anzergent® 3-14	0.007	1	Z
D5	CHAPS	0.49	2	Z
D6	CHAPSO	0.5	2	Z
D7	Cyclofos™-4	0.45	2	Z
D8	Cyclofos™-5	0.15	1	Z
D9	Cyclofos™-6	0.094	1	Z
D10	Cyclofos™-7	0.022	1	Z
D11	Fos-Choline®-9	1.2	2	Z
D12	Fos-Choline-10	0.35	1	Z
E1	Cyclofos™-3	1.3	2	Z
E2	Fos-Choline®-11	0.062	1	Z
E3	Fos-Choline®-12	0.047	1	Z
E4	Fos-Choline®-13	0.027	1	Z
E5	Fos-Choline®-14	0.0046	1	Z
E6	Fos-Choline®-15	0.0027	1	Z
E7	Fos-Choline®-16	0.00053	1	Z
E8	Fos-Choline®-Iso-9	0.99	2	Z
E9	Fos-Choline®-Iso-11	0.9	2	Z
E10	Fos-Choline®-Unisat-11-10	0.21	1	Z
E11	Fos-Choline®-8	3.4	2	Z
E12	n-Dodecyl-N,N-dimethylglycine	0.041	1	Z
F1	n-Dodecyl-N,N-dimethylamine-N-oxide (DDAO)	0.023	1	Z
F2	Cholic acid, sodium salt	0.60 (pH 7)	1	A
F3	Deoxycholic acid, sodium salt	0.24	1	A
F4	Fosmea - 8	0.59	1	A
F5	Fosmea®-10	0.15	1	A
F6	Hexaethylene Glycol Monooctyl Ether (C8E6)	0.39	1	N
F7	n-Hexyl-ß-D-Glucopyranoside	6.6	2	N
F8	n-Hexyl-ß-D-Maltopyranoside	8.9	2	N
F9	n-Nonyl-ß-D- Glucopyranoside	0.2	1	N
F10	n-Nonyl-ß-D-Maltopyranoside	0.28	1	N
F11	MEGA-8	2.5	2	N
F12	Octaethylene Glycol Monodecyl Ether (C12E8)	0.0048	1	N
G1	n-Octyl-ß-D-Glucopyranoside	0.53	1	N
G2	n-Octyl-ß-D-Thiomaltopyranoside	0.4	1	N
G3	n-Octyl−β−D-Maltopyranoside	0.89	2	N
G4	Cyclofos™-2	7.5	1	Z
G5	Pentaethylene Glycol Monodecyl Ether (C10E5)	0.031	1	N
G6	PMAL-C8		1	Z
G7	2-Propyl-1-Pentyl Maltopyranoside	1.9	2	N
G8	Sodium Dodecanoyl Sarcosine	0.42	1	A
G9	Sucrose Monododecanoate	0.016	1	N
G10	n-Tetradecyl−β−D-Maltopyranoside	0.00054	1	N
G11	n-Tetradecyl-N,N-Dimethylamine-N-Oxide (TDAO)	0.0075	1	Z

G12	Tetraethylene Glycol Monooctyl Ether (C8E4)	0.25	1	N
H1	n-Tridecyl−β−D-Maltopyranoside	0.0017	1	N
H2	n-Undecyl−α−D-Maltopyranoside	0.029	1	N
H3	n-Undecyl−β−D-Maltopyranoside	0.029	1	N
H4	n-Undecyl−β−D-Thiomaltopyranoside	0.011	1	N
H5	SDS			A
H6	Buffer			

A2. Blotting membranes of the linear sucrose gradient. Sucrose concentration increases with increasing fraction numbers (top of each membrane). The detected proteins of each row are listed on the very left side.

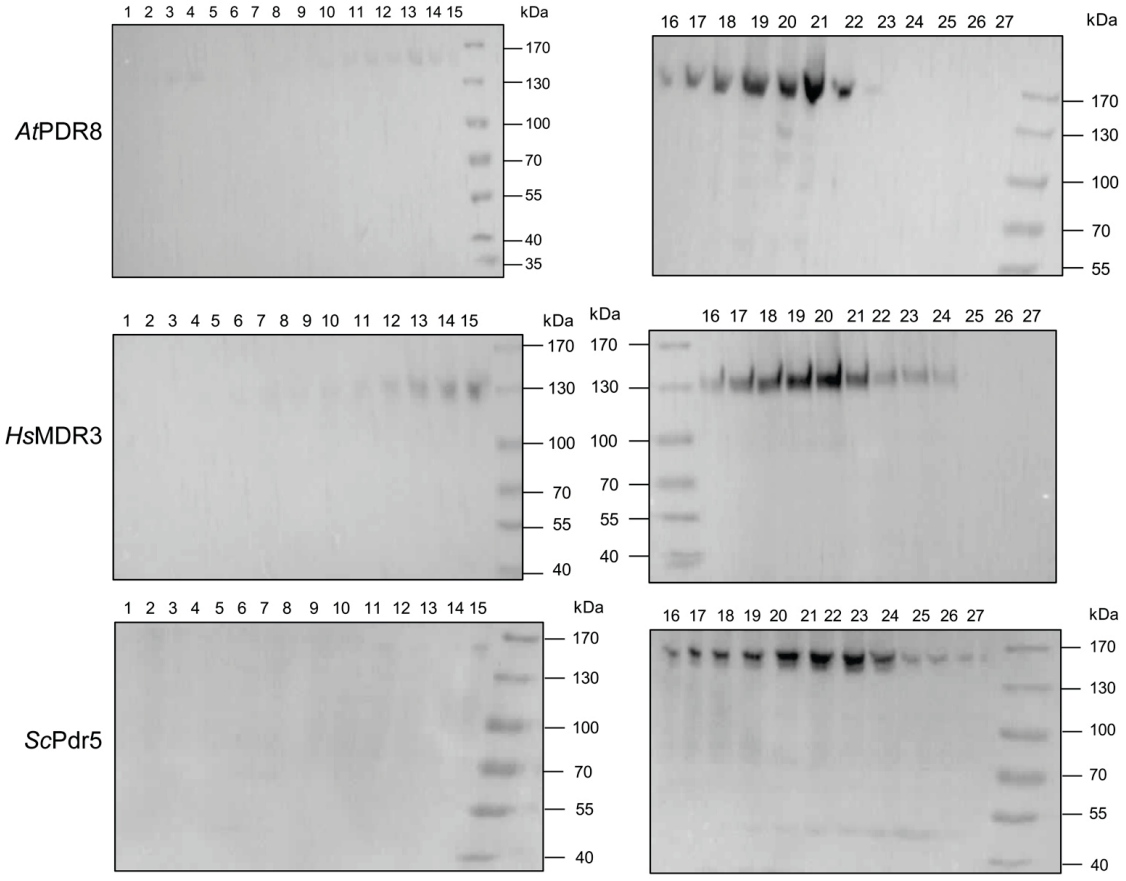

A3. Mass spectrometry results of the complete elution fraction after *At*PDR8 CBP-AC. The table lists the accession numbers of the detected proteins, the number of the identified peptides and the coverage. Furthermore the molecular weight of the detected proteins is listed as well as the number of amino acids.

Accession	Description	Coverage	# Unique Peptides	# AAs	MW [kDa]
AtPDR8	AtPDR8_HIS PE=1 SV=1 - [AtPDR8_HIS]	51.78	120	1518	170.7
C4R3X8	ATPase involved in protein folding and the response to stress OS=Komagataella pastoris (strain GS115 / ATCC 20864) GN=PAS_chr3_0230 PE=3 SV=1 - [C4R3X8_PICPG]	57.84	24	657	70.7
C4R5D4	Fusion protein that is cleaved to yield a ribosomal protein of the small (40S) subunit and ubiquitin OS=Komagataella pastoris (strain GS115 / ATCC 20864) GN=PAS_chr3_0722 PE=4 SV=1 - [C4R5D4_PICPG]	53.33	13	150	17.2
C4R887	ATPase involved in protein folding and nuclear localization signal (NLS)-directed nuclear transport OS=Komagataella pastoris (strain GS115 / ATCC 20864) GN=PAS_chr4_0552 PE=3 SV=1 - [C4R887_PICPG]	47.60	17	645	69.6
C4R1Z2	Mitochondrial porin (Voltage-dependent anion channel), outer membrane protein OS=Komagataella pastoris (strain GS115 / ATCC 20864) GN=PAS_chr2-2_0392 PE=4 SV=1 - [C4R1Z2_PICPG]	78.80	22	283	29.6
C4QVS9	Plasma membrane H+-ATPase, pumps protons out of the cell OS=Komagataella pastoris (strain GS115 / ATCC 20864) GN=PAS_chr1-1_0002 PE=3 SV=1 - [C4QVS9_PICPG]	25.78	20	896	97.8
C4R5Q0	Transketolase, similar to Tkl2p OS=Komagataella pastoris (strain GS115 / ATCC 20864) GN=PAS_chr3_0834 PE=4 SV=1 - [C4R5Q0_PICPG]	24.89	9	707	78.5
C4R4Y8	ATP synthase subunit alpha OS=Komagataella pastoris (strain GS115 / ATCC 20864) GN=PAS_chr3_0576 PE=3 SV=1 - [C4R4Y8_PICPG]	34.25	20	546	58.7
C4R6R6	Protein involved in synthesis of the thiamine hydroxymethylpyrimidine (HMP) OS=Komagataella pastoris (strain GS115 / ATCC 20864) GN=PAS_chr4_0065 PE=4 SV=1 - [C4R6R6_PICPG]	47.35	14	340	38.2
C4R5P8	Transketolase, similar to Tkl2p OS=Komagataella pastoris (strain GS115 / ATCC 20864) GN=PAS_chr3_0832 PE=4 SV=1 - [C4R5P8_PICPG]	23.76	7	707	78.8
C4R5N2	Uncharacterized protein OS=Komagataella pastoris (strain GS115 / ATCC 20864) GN=PAS_chr3_0815 PE=4 SV=1 - [C4R5N2_PICPG]	18.02	16	838	94.6
C4QXI5	Heat shock protein Hsp90 OS=Komagataella pastoris (strain GS115 / ATCC 20864) GN=PAS_chr1-4_0130 PE=3 SV=1 - [C4QXI5_PICPG]	26.77	17	706	80.9
C4QVY8	Translation initiation factor eIF4G, subunit of the mRNA cap-binding protein complex (EIF4F) OS=Komagataella pastoris (strain GS115 / ATCC 20864) GN=PAS_chr1-1_0053 PE=4 SV=1 - [C4QVY8_PICPG]	17.30	15	1098	121.4
C4R4H7	Serine/threonine-protein phosphatase OS=Komagataella pastoris (strain GS115 / ATCC 20864) GN=PAS_chr3_0414 PE=3 SV=1 - [C4R4H7_PICPG]	25.22	15	579	66.3
C4R606	NAD(+)-dependent formate dehydrogenase, may protect cells from exogenous formate OS=Komagataella pastoris (strain GS115 / ATCC 20864) GN=PAS_chr3_0932 PE=3 SV=1 - [C4R606_PICPG]	24.11	8	365	40.3
C4R2N5	ATP synthase subunit beta OS=Komagataella pastoris (strain GS115 / ATCC 20864) GN=PAS_chr2-2_0165 PE=3 SV=1 - [C4R2N5_PICPG]	28.03	11	503	54.0
C4QZL3	Ribosomal protein L30 of the large (60S) ribosomal subunit, nearly identical to Rpl24Ap and has simi OS=Komagataella pastoris (strain GS115 / ATCC 20864) GN=PAS_chr2-1_0086 PE=4 SV=1 - [C4QZL3_PICPG]	35.44	10	158	17.9
C4R4C3	Mitochondrial matrix ATPase OS=Komagataella pastoris (strain GS115 / ATCC 20864) GN=PAS_chr3_0365 PE=3 SV=1 - [C4R4C3_PICPG]	24.42	12	647	69.7
C4R4D1	Uncharacterized protein OS=Komagataella pastoris (strain GS115 / ATCC 20864) GN=PAS_chr3_0374 PE=4 SV=1 - [C4R4D1_PICPG]	26.55	13	629	71.8
C4R1H5	Uncharacterized protein OS=Komagataella pastoris (strain GS115 / ATCC 20864) GN=PAS_chr2-1_0701 PE=4 SV=1 - [C4R1H5_PICPG]	33.92	14	513	57.7
C4R2Z2	Protein chaperone involved in regulation of the HSP90 and HSP70 functions OS=Komagataella pastoris (strain GS115 / ATCC 20864) GN=PAS_chr2-2_0066 PE=3 SV=1 - [C4R2Z2_PICPG]	35.07	11	402	43.4
P04842	Alcohol oxidase 1 OS=Komagataella pastoris (strain GS115 / ATCC 20864) GN=AOX1 PE=1 SV=2 - [ALOX1_PICPG]	20.66	11	663	73.9
C4QZS3	ATPase involved in protein import into the ER, also acts as a chaperone to mediate protein folding i OS=Komagataella pastoris (strain GS115 / ATCC 20864) GN=PAS_chr2-1_0140 PE=3 SV=1 - [C4QZS3_PICPG]	17.99	13	678	74.2
C4QWG3	Ribosomal protein L4 of the large (60S) ribosomal subunit, nearly identical to Rpl8Ap OS=Komagataella pastoris (strain GS115 / ATCC 20864) GN=PAS_chr1-1_0216 PE=4 SV=1 - [C4QWG3_PICPG]	30.45	9	243	26.8

C4R416	Ferrochelatase OS=Komagataella pastoris (strain GS115 / ATCC 20864) GN=PAS_chr3_0264 PE=3 SV=1 - [C4R416_PICPG]	30.21	11	374	42.0
C4QY19	Calmodulin-dependent protein kinase OS=Komagataella pastoris (strain GS115 / ATCC 20864) GN=PAS_chr1-4_0302 PE=4 SV=1 - [C4QY19_PICPG]	29.04	10	396	45.0
C4R6Z0	Protein component of the large (60S) ribosomal subunit OS=Komagataella pastoris (strain GS115 / ATCC 20864) GN=PAS_chr4_0139 PE=3 SV=1 - [C4R6Z0_PICPG]	30.15	11	388	43.6
C4R560	Thiazole synthase, catalyzes formation of the thiazole moiety of thiamin pyrophosphate OS=Komagataella pastoris (strain GS115 / ATCC 20864) GN=PAS_chr3_0648 PE=3 SV=1 - [C4R560_PICPG]	36.23	8	345	37.0
C4QWH2	Vacuolar proteinase B (YscB), a serine protease of the subtilisin family OS=Komagataella pastoris (strain GS115 / ATCC 20864) GN=PAS_chr1-1_0226 PE=3 SV=1 - [C4QWH2_PICPG]	14.31	8	559	59.1
C4R1R9	Long chain fatty acyl-CoA synthetase with a preference for C12:0-C16:0 fatty acids OS=Komagataella pastoris (strain GS115 / ATCC 20864) GN=PAS_chr2-1_0785 PE=4 SV=1 - [C4R1R9_PICPG]	13.69	9	701	78.3
C4QZB0	Elongation factor 1-alpha OS=Komagataella pastoris (strain GS115 / ATCC 20864) GN=PAS_FragB_0052 PE=3 SV=1 - [C4QZB0_PICPG]	20.92	11	459	50.1
C4R0Q9	Uncharacterized protein OS=Komagataella pastoris (strain GS115 / ATCC 20864) GN=PAS_chr2-1_0456 PE=3 SV=1 - [C4R0Q9_PICPG]	18.73	9	726	79.5
C4R2D0	Putative magnesium transporter OS=Komagataella pastoris (strain GS115 / ATCC 20864) GN=PAS_chr2-2_0260 PE=4 SV=1 - [C4R2D0_PICPG]	12.39	7	815	91.8
C4R2Q1	Type II HSP40 co-chaperone that interacts with the HSP70 protein Ssa1p OS=Komagataella pastoris (strain GS115 / ATCC 20864) GN=PAS_chr2-2_0151 PE=4 SV=1 - [C4R2Q1_PICPG]	32.37	8	346	37.0
C4R6J2	Succinate dehydrogenase [ubiquinone] iron-sulfur subunit, mitochondrial OS=Komagataella pastoris (strain GS115 / ATCC 20864) GN=PAS_chr3_1111 PE=3 SV=1 - [C4R6J2_PICPG]	27.72	7	267	30.5
C4QV89	Heat shock protein that cooperates with Ydj1p (Hsp40) and Ssa1p (Hsp70) OS=Komagataella pastoris (strain GS115 / ATCC 20864) GN=PAS_chr1-3_0102 PE=3 SV=1 - [C4QV89_PICPG]	10.41	9	903	100.2
C4R6T1	Uncharacterized protein OS=Komagataella pastoris (strain GS115 / ATCC 20864) GN=PAS_chr4_0080 PE=4 SV=1 - [C4R6T1_PICPG]	22.70	7	392	45.2
C4R6U6	40S ribosomal protein S6 OS=Komagataella pastoris (strain GS115 / ATCC 20864) GN=PAS_chr4_0094 PE=3 SV=1 - [C4R6U6_PICPG]	32.20	7	236	27.0
C4R0W4	Uncharacterized protein OS=Komagataella pastoris (strain GS115 / ATCC 20864) GN=PAS_chr2-1_0853 PE=3 SV=1 - [C4R0W4_PICPG]	17.14	7	525	56.8
C4R6A5	S-(hydroxymethyl)glutathione dehydrogenase OS=Komagataella pastoris (strain GS115 / ATCC 20864) GN=PAS_chr3_1028 PE=3 SV=1 - [C4R6A5_PICPG]	18.21	7	379	40.5
C4R6R5	Uncharacterized protein OS=Komagataella pastoris (strain GS115 / ATCC 20864) GN=PAS_chr4_0064 PE=4 SV=1 - [C4R6R5_PICPG]	19.77	5	258	29.2
C4R5L9	Uncharacterized protein OS=Komagataella pastoris (strain GS115 / ATCC 20864) GN=PAS_chr3_0802 PE=4 SV=1 - [C4R5L9_PICPG]	10.32	6	785	86.9
C4QZM5	Polyadenylate-binding protein OS=Komagataella pastoris (strain GS115 / ATCC 20864) GN=PAS_chr2-1_0097 PE=3 SV=1 - [C4QZM5_PICPG]	10.06	6	626	70.0
C4QVW4	Cytoplasmic pre-60S factor OS=Komagataella pastoris (strain GS115 / ATCC 20864) GN=PAS_chr1-1_0031 PE=4 SV=1 - [C4QVW4_PICPG]	15.48	5	407	47.0
C4R8S1	Succinate dehydrogenase [ubiquinone] flavoprotein subunit, mitochondrial OS=Komagataella pastoris (strain GS115 / ATCC 20864) GN=PAS_chr4_0733 PE=3 SV=1 - [C4R8S1_PICPG]	13.03	7	637	70.2
C4R5A5	Uncharacterized protein OS=Komagataella pastoris (strain GS115 / ATCC 20864) GN=PAS_chr3_0692 PE=4 SV=1 - [C4R5A5_PICPG]	18.21	7	313	35.8
C4R2U4	Protein component of the large (60S) ribosomal subunit OS=Komagataella pastoris (strain GS115 / ATCC 20864) GN=PAS_chr2-2_0109 PE=3 SV=1 - [C4R2U4_PICPG]	32.35	5	170	19.1
C4QY16	Mitochondrial external NADH dehydrogenase, a type II NAD(P)H:quinone oxidoreductase OS=Komagataella pastoris (strain GS115 / ATCC 20864) GN=PAS_chr1-4_0299 PE=4 SV=1 - [C4QY16_PICPG]	17.05	7	569	62.7
C4R4M3	Subunit b of the stator stalk of mitochondrial F1F0 ATP synthase OS=Komagataella pastoris (strain GS115 / ATCC 20864) GN=PAS_chr3_0460 PE=4 SV=1 - [C4R4M3_PICPG]	39.66	8	232	25.3
C4R6Y9	Small subunit of carbamoyl phosphate synthetase OS=Komagataella pastoris (strain GS115 / ATCC 20864) GN=PAS_chr4_0138 PE=3 SV=1 - [C4R6Y9_PICPG]	17.14	6	420	46.4
C4R6G5	Sulfite reductase beta subunit, involved in amino acid biosynthesis, transcription repressed by meth OS=Komagataella pastoris (strain GS115 / ATCC 20864) GN=PAS_chr3_1084 PE=4 SV=1 - [C4R6G5_PICPG]	4.67	7	1414	157.2
C4R4Q2	High affinity sulfate permease OS=Komagataella pastoris (strain GS115 / ATCC 20864) GN=PAS_chr3_0489 PE=3 SV=1 - [C4R4Q2_PICPG]	8.21	5	853	95.5
C4R7Z3	Uncharacterized protein OS=Komagataella pastoris (strain GS115 / ATCC 20864) GN=PAS_chr4_0465 PE=4 SV=1 - [C4R7Z3_PICPG]	11.25	5	489	56.2

C4R9G1	Peptidyl-prolyl isomerase OS=Komagataella pastoris (strain GS115 / ATCC 20864) GN=PAS_c034_0039 PE=3 SV=1 - [C4R9G1_PICPG]	10.19	6	756	85.5
C4R3D4	Peroxisomal integral membrane protein OS=Komagataella pastoris (strain GS115 / ATCC 20864) GN=PAS_chr3_0043 PE=4 SV=1 - [C4R3D4_PICPG]	12.15	6	461	52.2
C4R6G8	Vacuolar aspartyl protease (Proteinase A) OS=Komagataella pastoris (strain GS115 / ATCC 20864) GN=PAS_chr3_1087 PE=3 SV=1 - [C4R6G8_PICPG]	23.41	5	410	44.3
C4QWD5	Mitochondrial ribosomal protein of the large subunit, has similarity to E. coli L2 ribosomal protein OS=Komagataella pastoris (strain GS115 / ATCC 20864) GN=PAS_chr1-1_0192 PE=4 SV=1 - [C4QWD5_PICPG]	12.73	6	377	42.1
C4QWE4	Aspartate aminotransferase OS=Komagataella pastoris (strain GS115 / ATCC 20864) GN=PAS_chr1-1_0200 PE=3 SV=1 - [C4QWE4_PICPG]	13.38	5	426	47.8
C4R6P6	Mitochondrial aldehyde dehydrogenase OS=Komagataella pastoris (strain GS115 / ATCC 20864) GN=PAS_chr4_0043 PE=3 SV=1 - [C4R6P6_PICPG]	16.77	5	501	54.3
C4R7C6	Protein component of the large (60S) ribosomal subunit OS=Komagataella pastoris (strain GS115 / ATCC 20864) GN=PAS_chr4_0267 PE=3 SV=1 - [C4R7C6_PICPG]	44.09	6	127	14.3
C4R146	Protein component of the small (40S) ribosomal subunit OS=Komagataella pastoris (strain GS115 / ATCC 20864) GN=PAS_chr2-1_0584 PE=3 SV=1 - [C4R146_PICPG]	30.97	5	155	17.6
C4QW56	Uncharacterized protein OS=Komagataella pastoris (strain GS115 / ATCC 20864) GN=PAS_chr1-1_0118 PE=4 SV=1 - [C4QW56_PICPG]	14.95	5	408	46.3
C4QWD4	Subunit 5 of the stator stalk of mitochondrial F1F0 ATP synthase OS=Komagataella pastoris (strain GS115 / ATCC 20864) GN=PAS_chr1-1_0191 PE=3 SV=1 - [C4QWD4_PICPG]	26.34	4	205	21.7
Q9P4D1	Actin OS=Komagataella pastoris (strain GS115 / ATCC 20864) GN=ACT1 PE=1 SV=1 - [ACT_PICPG]	14.36	5	376	41.7
C4R5L3	Protein involved in the organization of the actin cytoskeleton OS=Komagataella pastoris (strain GS115 / ATCC 20864) GN=PAS_chr3_0795 PE=4 SV=1 - [C4R5L3_PICPG]	12.17	5	411	44.4
C4QWG6	Protein component of the large (60S) ribosomal subunit OS=Komagataella pastoris (strain GS115 / ATCC 20864) GN=PAS_chr1-1_0219 PE=4 SV=1 - [C4QWG6_PICPG]	17.32	4	254	27.2
C4QV16	Protein component of the large (60S) ribosomal subunit, nearly identical to Rpl4Ap OS=Komagataella pastoris (strain GS115 / ATCC 20864) GN=PAS_chr1-3_0034 PE=4 SV=1 - [C4QV16_PICPG]	15.93	5	339	36.9
C4QZ87	Uncharacterized protein OS=Komagataella pastoris (strain GS115 / ATCC 20864) GN=PAS_FragB_0031 PE=4 SV=1 - [C4QZ87_PICPG]	9.55	3	398	44.6
C4QXA0	Glucose-6-phosphate 1-epimerase (Hexose-6-phosphate mutarotase) OS=Komagataella pastoris (strain GS115 / ATCC 20864) GN=PAS_chr1-4_0042 PE=4 SV=1 - [C4QXA0_PICPG]	18.79	4	298	33.9
C4R370	Protein that forms a complex with Spt4p OS=Komagataella pastoris (strain GS115 / ATCC 20864) GN=PAS_chr3_1136 PE=4 SV=1 - [C4R370_PICPG]	4.30	5	908	101.0
C4R8L5	GTP-binding protein OS=Komagataella pastoris (strain GS115 / ATCC 20864) GN=PAS_chr4_0680 PE=4 SV=1 - [C4R8L5_PICPG]	17.21	4	215	23.7
C4R9A6	ATPase in ER, nuclear membrane and cytosol with homology to mammalian p97 OS=Komagataella pastoris (strain GS115 / ATCC 20864) GN=PAS_FragD_0026 PE=3 SV=1 - [C4R9A6_PICPG]	9.28	6	830	91.1
C4R760	Major ADP/ATP carrier of the mitochondrial inner membrane OS=Komagataella pastoris (strain GS115 / ATCC 20864) GN=PAS_chr4_0210 PE=3 SV=1 - [C4R760_PICPG]	17.43	5	304	33.2
C4R1C0	Uncharacterized protein OS=Komagataella pastoris (strain GS115 / ATCC 20864) GN=PAS_chr2-1_0874 PE=4 SV=1 - [C4R1C0_PICPG]	10.07	2	268	29.0
C4QY33	Member of silencing information regulator 2 (Sir2) family of NAD(+)-dependent protein deacetylases OS=Komagataella pastoris (strain GS115 / ATCC 20864) GN=PAS_chr1-4_0315 PE=4 SV=1 - [C4QY33_PICPG]	19.89	5	352	40.1
C4QWU1	Ribosomal protein L37 OS=Komagataella pastoris (strain GS115 / ATCC 20864) GN=PAS_chr1-1_0337 PE=3 SV=1 - [C4QWU1_PICPG]	29.76	4	84	9.7
C4R1T0	Uncharacterized protein OS=Komagataella pastoris (strain GS115 / ATCC 20864) GN=PAS_chr2-1_0891 PE=4 SV=1 - [C4R1T0_PICPG]	10.78	3	269	31.2
C4R1C9	Ribosomal protein L15 OS=Komagataella pastoris (strain GS115 / ATCC 20864) GN=PAS_chr2-1_0658 PE=3 SV=1 - [C4R1C9_PICPG]	21.08	4	204	24.2
C4R5M5	Uncharacterized protein OS=Komagataella pastoris (strain GS115 / ATCC 20864) GN=PAS_chr3_0808 PE=3 SV=1 - [C4R5M5_PICPG]	10.17	4	482	54.8
C4R836	Subunit of the prohibitin complex (Phb1p-Phb2p) OS=Komagataella pastoris (strain GS115 / ATCC 20864) GN=PAS_chr4_0505 PE=4 SV=1 - [C4R836_PICPG]	21.35	5	267	29.2
C4QYJ4	ATP synthase subunit gamma OS=Komagataella pastoris (strain GS115 / ATCC 20864) GN=PAS_chr1-4_0465 PE=3 SV=1 - [C4QYJ4_PICPG]	16.26	4	289	31.6
C4QWU8	Protein component of the large (60S) ribosomal subunit OS=Komagataella pastoris (strain GS115 / ATCC 20864) GN=PAS_chr1-1_0345 PE=3 SV=1 - [C4QWU8_PICPG]	14.14	4	297	34.1

C4R9F6	Putative uncharacterized protein OS=Komagataella pastoris (strain GS115 / ATCC 20864) GN=PAS_c034_0034 PE=4 SV=1 - [C4R9F6_PICPG]	7.16	2	433	45.2
C4R853	40S ribosomal protein S1 OS=Komagataella pastoris (strain GS115 / ATCC 20864) GN=RPS1 PE=3 SV=1 - [RS3A_PICPG]	19.53	5	256	28.9
C4QVA2	Protein component of the small (40S) ribosomal subunit OS=Komagataella pastoris (strain GS115 / ATCC 20864) GN=PAS_chr1-3_0115 PE=3 SV=1 - [C4QVA2_PICPG]	13.99	3	243	26.9
C4QX22	Putative transmembrane protein involved in export of ammonia OS=Komagataella pastoris (strain GS115 / ATCC 20864) GN=PAS_chr1-1_0417 PE=4 SV=1 - [C4QX22_PICPG]	20.50	3	278	30.1
C4R2P4	Uncharacterized protein OS=Komagataella pastoris (strain GS115 / ATCC 20864) GN=PAS_chr2-2_0463 PE=4 SV=1 - [C4R2P4_PICPG]	28.97	4	214	23.6
C4R7R5	Component of the TOM (Translocase of outer membrane) complex OS=Komagataella pastoris (strain GS115 / ATCC 20864) GN=PAS_chr4_0391 PE=4 SV=1 - [C4R7R5_PICPG]	16.20	4	389	42.7
C4R2S1	Catalase OS=Komagataella pastoris (strain GS115 / ATCC 20864) GN=PAS_chr2-2_0131 PE=3 SV=1 - [C4R2S1_PICPG]	9.22	4	510	57.8
C4R339	Pyruvate carboxylase OS=Komagataella pastoris (strain GS115 / ATCC 20864) GN=PAS_chr2-2_0024 PE=4 SV=1 - [C4R339_PICPG]	3.24	5	1174	129.2
C4R8Z3	Mitochondrial ribosomal protein of the large subunit OS=Komagataella pastoris (strain GS115 / ATCC 20864) GN=PAS_chr4_0799 PE=4 SV=1 - [C4R8Z3_PICPG]	15.10	4	298	33.9
C4R7T7	Protein component of the large (60S) ribosomal subunit, nearly identical to Rpl13Bp OS=Komagataella pastoris (strain GS115 / ATCC 20864) GN=PAS_chr4_0413 PE=4 SV=1 - [C4R7T7_PICPG]	22.34	4	197	22.2
C4R926	Plasma membrane ATP-binding cassette (ABC) transporter OS=Komagataella pastoris (strain GS115 / ATCC 20864) GN=PAS_chr4_0832 PE=3 SV=1 - [C4R926_PICPG]	2.46	3	1503	170.5
C4R4G2	Uncharacterized protein OS=Komagataella pastoris (strain GS115 / ATCC 20864) GN=PAS_chr3_1188 PE=4 SV=1 - [C4R4G2_PICPG]	14.84	4	384	43.3
C4R6X2	Uncharacterized protein OS=Komagataella pastoris (strain GS115 / ATCC 20864) GN=PAS_chr4_0120 PE=3 SV=1 - [C4R6X2_PICPG]	17.99	4	289	33.1
C4QXC0	G-protein beta subunit and guanine nucleotide dissociation inhibitor for Gpa2p OS=Komagataella pastoris (strain GS115 / ATCC 20864) GN=PAS_chr1-4_0063 PE=4 SV=1 - [C4QXC0_PICPG]	17.41	4	316	34.7
C4QWF3	Uncharacterized protein OS=Komagataella pastoris (strain GS115 / ATCC 20864) GN=PAS_chr1-1_0484 PE=4 SV=1 - [C4QWF3_PICPG]	33.14	4	175	19.7
C4R5C0	Uncharacterized protein OS=Komagataella pastoris (strain GS115 / ATCC 20864) GN=PAS_chr3_0705 PE=4 SV=1 - [C4R5C0_PICPG]	3.96	3	858	94.9
C4R6Y3	Protein component of the large (60S) ribosomal subunit OS=Komagataella pastoris (strain GS115 / ATCC 20864) GN=PAS_chr4_0131 PE=4 SV=1 - [C4R6Y3_PICPG]	26.95	4	167	18.6
C4R650	Cytoplasmic mRNA cap binding protein OS=Komagataella pastoris (strain GS115 / ATCC 20864) GN=PAS_chr3_0972 PE=3 SV=1 - [C4R650_PICPG]	17.82	4	202	23.1
C4R1Z0	Uncharacterized protein OS=Komagataella pastoris (strain GS115 / ATCC 20864) GN=PAS_chr2-2_0394 PE=4 SV=1 - [C4R1Z0_PICPG]	8.84	3	328	35.9
C4R0S8	Mitochondrial alcohol dehydrogenase isozyme III OS=Komagataella pastoris (strain GS115 / ATCC 20864) GN=PAS_chr2-1_0472 PE=3 SV=1 - [C4R0S8_PICPG]	15.43	3	350	37.0
C4R5E4	Cytoplasmic ATPase that is a ribosome-associated molecular chaperone OS=Komagataella pastoris (strain GS115 / ATCC 20864) GN=PAS_chr3_0731 PE=3 SV=1 - [C4R5E4_PICPG]	5.71	3	613	66.5
C4R5U7	S-adenosylmethionine synthase OS=Komagataella pastoris (strain GS115 / ATCC 20864) GN=PAS_chr3_0876 PE=3 SV=1 - [C4R5U7_PICPG]	9.90	4	384	42.3
C4QZ00	Mitochondrial phosphate carrier protein OS=Komagataella pastoris (strain GS115 / ATCC 20864) GN=PAS_chr1-4_0615 PE=3 SV=1 - [C4QZ00_PICPG]	14.56	3	316	32.9
C4QX36	Acetohydroxyacid reductoisomerase OS=Komagataella pastoris (strain GS115 / ATCC 20864) GN=PAS_chr1-1_0432 PE=4 SV=1 - [C4QX36_PICPG]	11.31	3	398	44.3
C4R2S0	Uncharacterized protein OS=Komagataella pastoris (strain GS115 / ATCC 20864) GN=PAS_chr2-2_0462 PE=4 SV=1 - [C4R2S0_PICPG]	5.29	3	473	52.1
C4R1H6	Protein that recognizes and binds damaged DNA during nucleotide excision repair OS=Komagataella pastoris (strain GS115 / ATCC 20864) GN=PAS_chr2-1_0702 PE=4 SV=1 - [C4R1H6_PICPG]	13.49	4	341	40.1
C4R7T5	Uncharacterized protein OS=Komagataella pastoris (strain GS115 / ATCC 20864) GN=PAS_chr4_0411 PE=4 SV=1 - [C4R7T5_PICPG]	6.24	2	481	54.8
C4R3E7	60S ribosomal protein L20 OS=Komagataella pastoris (strain GS115 / ATCC 20864) GN=PAS_chr3_0054 PE=3 SV=1 - [C4R3E7_PICPG]	16.57	3	181	21.5
C4QXY5	Uncharacterized protein OS=Komagataella pastoris (strain GS115 / ATCC 20864) GN=PAS_chr1-4_0274 PE=4 SV=1 - [C4QXY5_PICPG]	16.00	2	150	17.4
C4QVA0	Small rho-like GTPase, essential for establishment and maintenance of cell polarity OS=Komagataella pastoris (strain GS115 / ATCC 20864) GN=PAS_chr1-	20.16	3	253	27.9

	3_0113 PE=3 SV=1 - [C4QVA0_PICPG]				
C4QZ92	60S ribosomal protein L36 OS=Komagataella pastoris (strain GS115 / ATCC 20864) GN=PAS_FragB_0036 PE=3 SV=1 - [C4QZ92_PICPG]	16.83	2	101	11.5
C4R697	D-lactate dehydrogenase, oxidizes D-lactate to pyruvate, transcription is heme-dependent OS=Komagataella pastoris (strain GS115 / ATCC 20864) GN=PAS_chr3_1021 PE=4 SV=1 - [C4R697_PICPG]	3.05	3	590	64.4
C4QVE0	Plasma membrane pyridoxine (Vitamin B6) transporter OS=Komagataella pastoris (strain GS115 / ATCC 20864) GN=PAS_chr1-3_0153 PE=3 SV=1 - [C4QVE0_PICPG]	7.68	3	508	56.4
C4R8S3	One of six ATPases of the 19S regulatory particle of the 26S proteasome OS=Komagataella pastoris (strain GS115 / ATCC 20864) GN=PAS_chr4_0736 PE=3 SV=1 - [C4R8S3_PICPG]	7.26	3	441	49.4
C4QZZ6	Protein O-mannosyltransferase, transfers mannose residues from dolichyl phosphate-D-mannose to prote OS=Komagataella pastoris (strain GS115 / ATCC 20864) GN=PAS_chr2-1_0212 PE=4 SV=1 - [C4QZZ6_PICPG]	4.94	3	789	89.5
C4QYS9	Peroxiredoxin OS=Komagataella pastoris (strain GS115 / ATCC 20864) GN=PAS_chr1-4_0547 PE=4 SV=1 - [C4QYS9_PICPG]	19.41	3	170	18.4
C4QWP7	Coatomer subunit alpha OS=Komagataella pastoris (strain GS115 / ATCC 20864) GN=PAS_chr1-1_0294 PE=4 SV=1 - [C4QWP7_PICPG]	2.82	3	1206	136.7
C4R7S1	Heme-binding protein involved in regulation of cytochrome P450 protein Erg11p OS=Komagataella pastoris (strain GS115 / ATCC 20864) GN=PAS_chr4_0396 PE=4 SV=1 - [C4R7S1_PICPG]	23.72	3	156	17.4
C4R0F7	Subunit IV of cytochrome c oxidase OS=Komagataella pastoris (strain GS115 / ATCC 20864) GN=PAS_chr2-1_0361 PE=4 SV=1 - [C4R0F7_PICPG]	26.09	3	161	18.1
C4R487	Protein component of the large (60S) ribosomal subunit, identical to Rpl43Ap OS=Komagataella pastoris (strain GS115 / ATCC 20864) GN=PAS_chr3_0335 PE=3 SV=1 - [C4R487_PICPG]	27.17	2	92	10.1
C4R9C8	ER membrane protein involved in regulation of OLE1 transcription, acts with homolog Spt23p OS=Komagataella pastoris (strain GS115 / ATCC 20864) GN=PAS_FragD_0002 PE=4 SV=1 - [C4R9C8_PICPG]	2.65	3	1095	121.4
C4R5Q6	Dihydroxyacetone kinase, required for detoxification of dihydroxyacetone (DHA) OS=Komagataella pastoris (strain GS115 / ATCC 20864) GN=PAS_chr3_0841 PE=4 SV=1 - [C4R5Q6_PICPG]	7.89	3	608	65.3
C4R362	Alpha 5 subunit of the 20S proteasome involved in ubiquitin-dependent catabolism OS=Komagataella pastoris (strain GS115 / ATCC 20864) GN=PAS_chr3_1129 PE=4 SV=1 - [C4R362_PICPG]	10.59	3	255	28.0
C4R290	Pyruvate dehydrogenase E1 component subunit alpha OS=Komagataella pastoris (strain GS115 / ATCC 20864) GN=PAS_chr2-2_0294 PE=4 SV=1 - [C4R290_PICPG]	7.32	3	396	44.0
C4R673	Cytochrome c1, component of the mitochondrial respiratory chain OS=Komagataella pastoris (strain GS115 / ATCC 20864) GN=PAS_chr3_0997 PE=4 SV=1 - [C4R673_PICPG]	13.54	3	288	31.9
C4R4J8	Mitochondrial amino acid transporter OS=Komagataella pastoris (strain GS115 / ATCC 20864) GN=PAS_chr3_0434 PE=3 SV=1 - [C4R4J8_PICPG]	4.43	3	700	77.9
C4R5Q7	Multifunctional protein with both hydroxymethylpyrimidine kinase and thiaminase activities OS=Komagataella pastoris (strain GS115 / ATCC 20864) GN=PAS_chr3_0842 PE=4 SV=1 - [C4R5Q7_PICPG]	3.62	2	553	61.5
C4R1D2	Catalytic subunit of 1,3-beta-D-glucan synthase OS=Komagataella pastoris (strain GS115 / ATCC 20864) GN=PAS_chr2-1_0661 PE=4 SV=1 - [C4R1D2_PICPG]	1.54	3	1878	215.1
C4R8U8	C3HC4-type RING-finger peroxisomal membrane peroxin OS=Komagataella pastoris (strain GS115 / ATCC 20864) GN=PAS_chr4_0759 PE=4 SV=1 - [C4R8U8_PICPG]	6.36	2	409	47.5
C4R235	GTP-binding protein of the ras superfamily required for bud site selection OS=Komagataella pastoris (strain GS115 / ATCC 20864) GN=PAS_chr2-2_0347 PE=4 SV=1 - [C4R235_PICPG]	8.70	2	230	25.7
C4QZ39	Subunit of SAGA histone acetyltransferase complex OS=Komagataella pastoris (strain GS115 / ATCC 20864) GN=PAS_chr1-4_0651 PE=4 SV=1 - [C4QZ39_PICPG]	5.43	2	644	74.0
C4QZJ9	Delta(9) fatty acid desaturase OS=Komagataella pastoris (strain GS115 / ATCC 20864) GN=PAS_chr2-1_0072 PE=3 SV=1 - [C4QZJ9_PICPG]	6.46	3	495	55.9
C4QX33	P-type ATPase sodium pump, involved in Na+ and Li+ efflux to allow salt tolerance OS=Komagataella pastoris (strain GS115 / ATCC 20864) GN=PAS_chr1-1_0428 PE=3 SV=1 - [C4QX33_PICPG]	3.76	3	1089	120.4
C4QXC1	Aldehyde dehydrogenase OS=Komagataella pastoris (strain GS115 / ATCC 20864) GN=PAS_chr1-4_0064 PE=3 SV=1 - [C4QXC1_PICPG]	6.05	3	512	57.6
C4R6A0	NAD(+)-dependent glutamate synthase (GOGAT) OS=Komagataella pastoris (strain GS115 / ATCC 20864) GN=PAS_chr3_1024 PE=4 SV=1 - [C4R6A0_PICPG]	1.64	3	2138	236.7
C4R612	3-hydroxyisobutyryl-CoA hydrolase, member of a family of enoyl-CoA hydratase/isomerases OS=Komagataella pastoris (strain GS115 / ATCC 20864)	3.57	2	504	56.4

	GN=PAS_chr3_0937 PE=4 SV=1 - [C4R612_PICPG]				
C4R259	Co-chaperone that stimulates the ATPase activity of the HSP70 protein Ssc1p OS=Komagataella pastoris (strain GS115 / ATCC 20864) GN=PAS_chr2-2_0323 PE=3 SV=1 - [C4R259_PICPG]	7.72	2	492	53.1
C4R789	Glutamine-dependent NAD(+) synthetase OS=Komagataella pastoris (strain GS115 / ATCC 20864) GN=PAS_chr4_0233 PE=4 SV=1 - [C4R789_PICPG]	3.93	3	712	80.4
C4QW05	Plasma membrane protein involved in remodeling GPI anchors OS=Komagataella pastoris (strain GS115 / ATCC 20864) GN=PAS_chr1-1_0069 PE=4 SV=1 - [C4QW05_PICPG]	4.04	2	569	66.8
C4QYS8	Clathrin heavy chain OS=Komagataella pastoris (strain GS115 / ATCC 20864) GN=PAS_chr1-4_0546 PE=3 SV=1 - [C4QYS8_PICPG]	1.21	2	1656	187.1
C4R5U9	Uncharacterized protein OS=Komagataella pastoris (strain GS115 / ATCC 20864) GN=PAS_chr3_1234 PE=4 SV=1 - [C4R5U9_PICPG]	9.49	3	390	44.0
C4R5T5	Non-essential intracellular esterase that can function as an S-formylglutathione hydrolase OS=Komagataella pastoris (strain GS115 / ATCC 20864) GN=PAS_chr3_0867 PE=4 SV=1 - [C4R5T5_PICPG]	9.36	2	299	33.3
C4R4C6	P-type ATPase, ion transporter of the ER membrane involved in ER function and Ca2+ homeostasis OS=Komagataella pastoris (strain GS115 / ATCC 20864) GN=PAS_chr3_0368 PE=3 SV=1 - [C4R4C6_PICPG]	2.96	3	1217	136.0
C4R2M0	Uncharacterized protein OS=Komagataella pastoris (strain GS115 / ATCC 20864) GN=PAS_chr2-2_0177 PE=4 SV=1 - [C4R2M0_PICPG]	10.74	2	242	27.2
C4R1L1	Uncharacterized protein OS=Komagataella pastoris (strain GS115 / ATCC 20864) GN=PAS_chr2-1_0735 PE=4 SV=1 - [C4R1L1_PICPG]	10.17	2	177	20.0
C4R6Q0	Peripheral membrane protein located at Vid (Vacuole import and degradation) vesicles OS=Komagataella pastoris (strain GS115 / ATCC 20864) GN=PAS_chr4_0047 PE=4 SV=1 - [C4R6Q0_PICPG]	15.31	2	294	33.2
C4R1W6	Uncharacterized protein OS=Komagataella pastoris (strain GS115 / ATCC 20864) GN=PAS_chr2-2_0419 PE=4 SV=1 - [C4R1W6_PICPG]	3.80	2	526	58.3
C4QX63	Mevalonate pyrophosphate decarboxylase OS=Komagataella pastoris (strain GS115 / ATCC 20864) GN=PAS_chr1-4_0003 PE=4 SV=1 - [C4QX63_PICPG]	6.28	2	382	41.9
C4R883	Component of the septin ring of the mother-bud neck that is required for cytokinesis OS=Komagataella pastoris (strain GS115 / ATCC 20864) GN=PAS_chr4_0548 PE=3 SV=1 - [C4R883_PICPG]	3.80	2	474	54.5
C4QXV1	Protein component of the large (60S) ribosomal subunit, nearly identical to Rpl34Bp OS=Komagataella pastoris (strain GS115 / ATCC 20864) GN=PAS_chr1-4_0239 PE=4 SV=1 - [C4QXV1_PICPG]	12.10	2	124	14.0
C4R6D4	Putative integral membrane protein OS=Komagataella pastoris (strain GS115 / ATCC 20864) GN=PAS_chr3_1058 PE=4 SV=1 - [C4R6D4_PICPG]	6.92	2	289	31.7
C4R5P1	Subunit VI of cytochrome c oxidase OS=Komagataella pastoris (strain GS115 / ATCC 20864) GN=PAS_chr3_0824 PE=4 SV=1 - [C4R5P1_PICPG]	15.97	2	144	16.7
C4R0B4	Calnexin OS=Komagataella pastoris (strain GS115 / ATCC 20864) GN=PAS_chr2-1_0322 PE=3 SV=1 - [C4R0B4_PICPG]	4.96	2	565	63.0
C4R4R9	C-22 sterol desaturase OS=Komagataella pastoris (strain GS115 / ATCC 20864) GN=PAS_chr3_0507 PE=3 SV=1 - [C4R4R9_PICPG]	3.60	2	528	60.1
C4R389	Uncharacterized protein OS=Komagataella pastoris (strain GS115 / ATCC 20864) GN=PAS_c131_0011 PE=4 SV=1 - [C4R389_PICPG]	15.04	2	133	14.9
C4R4X4	Elongation factor Tu OS=Komagataella pastoris (strain GS115 / ATCC 20864) GN=PAS_chr3_0562 PE=3 SV=1 - [C4R4X4_PICPG]	7.53	2	425	46.8
C4R8J5	Phospholipid-transporting ATPase OS=Komagataella pastoris (strain GS115 / ATCC 20864) GN=PAS_chr4_0662 PE=3 SV=1 - [C4R8J5_PICPG]	1.50	2	1265	143.2
C4R526	Subunit Va of cytochrome c oxidase OS=Komagataella pastoris (strain GS115 / ATCC 20864) GN=PAS_chr3_0615 PE=4 SV=1 - [C4R526_PICPG]	15.13	2	152	17.6
Q9P4C8	Small COPII coat GTPase SAR1 OS=Komagataella pastoris (strain GS115 / ATCC 20864) GN=SAR1 PE=3 SV=1 - [SAR1_PICPG]	12.11	2	190	21.7
C4QYX3	Protein component of the small (40S) subunit, essential for control of translational accuracy OS=Komagataella pastoris (strain GS115 / ATCC 20864) GN=PAS_chr1-4_0589 PE=3 SV=1 - [C4QYX3_PICPG]	5.32	2	263	28.2
C4R696	Uncharacterized protein OS=Komagataella pastoris (strain GS115 / ATCC 20864) GN=PAS_chr3_1020 PE=4 SV=1 - [C4R696_PICPG]	8.71	2	333	37.9
C4R0L2	Alpha-isopropylmalate synthase (2-isopropylmalate synthase) OS=Komagataella pastoris (strain GS115 / ATCC 20864) GN=PAS_chr2-1_0415 PE=3 SV=1 - [C4R0L2_PICPG]	2.45	2	571	63.6
C4QXI8	AAA-peroxin that heterodimerizes with AAA-peroxin Pex1p OS=Komagataella pastoris (strain GS115 / ATCC 20864) GN=PAS_chr1-4_0133 PE=3 SV=1 - [C4QXI8_PICPG]	1.46	2	1166	129.1
C4R2L7	Cytoplasmic serine/threonine protein kinase OS=Komagataella pastoris (strain GS115 / ATCC 20864) GN=PAS_chr2-2_0179 PE=3 SV=1 - [C4R2L7_PICPG]	5.23	2	421	48.0
C4QWJ9	Uncharacterized protein OS=Komagataella pastoris (strain GS115 / ATCC 20864) GN=PAS_chr1-1_0252 PE=4 SV=1 - [C4QWJ9_PICPG]	10.11	2	178	19.3
C4QWZ8	Uncharacterized protein OS=Komagataella pastoris (strain GS115 / ATCC 20864) GN=PAS_chr1-1_0394 PE=3 SV=1 - [C4QWZ8_PICPG]	3.36	2	536	60.1

C4R3J8	Uncharacterized protein OS=Komagataella pastoris (strain GS115 / ATCC 20864) GN=PAS_chr3_0104 PE=4 SV=1 - [C4R3J8_PICPG]	9.89	2	182	21.2
C4R0T7	Ribosomal protein 59 of small subunit, required for ribosome assembly and 20S pre-rRNA processing OS=Komagataella pastoris (strain GS115 / ATCC 20864) GN=PAS_chr2-1_0481 PE=3 SV=1 - [C4R0T7_PICPG]	16.67	2	144	15.2
C4R0Q2	GTP binding protein (Mammalian Ranp homolog) OS=Komagataella pastoris (strain GS115 / ATCC 20864) GN=PAS_chr2-1_0449 PE=4 SV=1 - [C4R0Q2_PICPG]	8.45	2	213	24.1
C4R0I2	Mitochondrial ribosomal protein of the small subunit OS=Komagataella pastoris (strain GS115 / ATCC 20864) GN=PAS_chr2-1_0384 PE=3 SV=1 - [C4R0I2_PICPG]	7.38	2	298	35.0
C4R4F4	Transcription factor OS=Komagataella pastoris (strain GS115 / ATCC 20864) GN=PAS_chr3_0393 PE=4 SV=1 - [C4R4F4_PICPG]	4.15	2	603	67.9
C4QXC8	Co-chaperone that binds to Hsp82p and activates its ATPase activity OS=Komagataella pastoris (strain GS115 / ATCC 20864) GN=PAS_chr1-4_0072 PE=4 SV=1 - [C4QXC8_PICPG]	8.38	2	334	37.5
C4R0T8	Protein component of the small (40S) ribosomal subunit OS=Komagataella pastoris (strain GS115 / ATCC 20864) GN=PAS_chr2-1_0482 PE=3 SV=1 - [C4R0T8_PICPG]	13.08	2	130	14.6
C4R3X9	Uncharacterized protein OS=Komagataella pastoris (strain GS115 / ATCC 20864) GN=PAS_chr3_1167 PE=3 SV=1 - [C4R3X9_PICPG]	7.88	2	203	22.6
C4R4B9	Uncharacterized protein OS=Komagataella pastoris (strain GS115 / ATCC 20864) GN=PAS_chr3_0362 PE=4 SV=1 - [C4R4B9_PICPG]	8.42	2	285	32.6
C4R8X8	Uncharacterized protein OS=Komagataella pastoris (strain GS115 / ATCC 20864) GN=PAS_chr4_0787 PE=4 SV=1 - [C4R8X8_PICPG]	7.42	2	310	35.6
C4R7R1	Uncharacterized protein OS=Komagataella pastoris (strain GS115 / ATCC 20864) GN=PAS_chr4_0956 PE=4 SV=1 - [C4R7R1_PICPG]	7.74	2	310	36.3
C4QX37	Mitochondrial peroxiredoxin (1-Cys Prx) with thioredoxin peroxidase activity OS=Komagataella pastoris (strain GS115 / ATCC 20864) GN=PAS_chr1-1_0433 PE=4 SV=1 - [C4QX37_PICPG]	8.41	2	226	25.1
C4R7A1	40S ribosomal protein S4 OS=Komagataella pastoris (strain GS115 / ATCC 20864) GN=PAS_chr4_0246 PE=3 SV=1 - [C4R7A1_PICPG]	6.03	2	282	31.7
C4R8K2	Beta 5 subunit of the 20S proteasome, responsible for the chymotryptic activity of the proteasome OS=Komagataella pastoris (strain GS115 / ATCC 20864) GN=PAS_chr4_0668 PE=3 SV=1 - [C4R8K2_PICPG]	9.96	2	281	31.1
C4QZ54	Uncharacterized protein OS=Komagataella pastoris (strain GS115 / ATCC 20864) GN=PAS_c121_0014 PE=4 SV=1 - [C4QZ54_PICPG]	13.66	2	161	18.6
C4R7L7	Ribosomal protein 28 (Rp28) of the small (40S) ribosomal subunit OS=Komagataella pastoris (strain GS115 / ATCC 20864) GN=PAS_chr4_0348 PE=3 SV=1 - [C4R7L7_PICPG]	11.03	2	145	15.9
C4R3K4	Nucleolar protein involved in pre-rRNA processing OS=Komagataella pastoris (strain GS115 / ATCC 20864) GN=PAS_chr3_0110 PE=4 SV=1 - [C4R3K4_PICPG]	3.67	2	654	75.9
C4R347	Histone deacetylase OS=Komagataella pastoris (strain GS115 / ATCC 20864) GN=PAS_chr2-2_0016 PE=3 SV=1 - [C4R347_PICPG]	5.41	2	462	52.8
C4QW50	Protein involved in negative regulation of transcription of iron regulon OS=Komagataella pastoris (strain GS115 / ATCC 20864) GN=PAS_chr1-1_0111 PE=3 SV=1 - [C4QW50_PICPG]	2.81	2	711	79.2
C4QWS2	Fructose 1,6-bisphosphate aldolase, required for glycolysis and gluconeogenesis OS=Komagataella pastoris (strain GS115 / ATCC 20864) GN=PAS_chr1-1_0319 PE=4 SV=1 - [C4QWS2_PICPG]	4.82	2	353	38.9
C4R5Z1	ATPase of the ATP-binding cassette (ABC) family involved in 40S and 60S ribosome biogenesis OS=Komagataella pastoris (strain GS115 / ATCC 20864) GN=PAS_chr3_0918 PE=3 SV=1 - [C4R5Z1_PICPG]	3.16	2	601	67.3
C4QYX8	E1 beta subunit of the pyruvate dehydrogenase (PDH) complex OS=Komagataella pastoris (strain GS115 / ATCC 20864) GN=PAS_chr1-4_0593 PE=4 SV=1 - [C4QYX8_PICPG]	7.12	2	365	39.6
C4R986	DNA helicase OS=Komagataella pastoris (strain GS115 / ATCC 20864) GN=PAS_chr4_0891 PE=3 SV=1 - [C4R986_PICPG]	3.15	2	794	89.5
C4R1P7	Acetyl-coenzyme A synthetase OS=Komagataella pastoris (strain GS115 / ATCC 20864) GN=PAS_chr2-1_0767 PE=3 SV=1 - [C4R1P7_PICPG]	3.14	2	668	73.9
C4QVJ9	Mitochondrial peripheral inner membrane protein OS=Komagataella pastoris (strain GS115 / ATCC 20864) GN=PAS_chr1-3_0208 PE=4 SV=1 - [C4QVJ9_PICPG]	2.63	2	494	56.8
C4R7T8	Protein component of the small (40S) ribosomal subunit OS=Komagataella pastoris (strain GS115 / ATCC 20864) GN=PAS_chr4_0414 PE=3 SV=1 - [C4R7T8_PICPG]	14.29	2	147	16.4
C4R8K0	Nucleolar protein, component of the small subunit (SSU) processome containing the U3 snoRNA OS=Komagataella pastoris (strain GS115 / ATCC 20864) GN=PAS_chr4_0667 PE=4 SV=1 - [C4R8K0_PICPG]	2.08	2	864	98.9
C4QZY3	NADH-cytochrome b5 reductase OS=Komagataella pastoris (strain GS115 / ATCC	6.23	2	305	34.6

	20864) GN=PAS_chr2-1_0199 PE=3 SV=1 - [C4QZY3_PICPG]				
C4QZL4	Protein component of the large (60S) ribosomal subunit, has similarity to rat L30 ribosomal protein OS=Komagataella pastoris (strain GS115 / ATCC 20864) GN=PAS_chr2-1_0087 PE=3 SV=1 - [C4QZL4_PICPG]	16.82	2	107	11.6
C4QZE7	Protein component of the large (60S) ribosomal subunit, nearly identical to Rpl7Ap and has similarit OS=Komagataella pastoris (strain GS115 / ATCC 20864) GN=PAS_chr2-1_0022 PE=4 SV=1 - [C4QZE7_PICPG]	9.84	2	244	27.9
C4R4Z1	Glycerol-3-phosphate dehydrogenase OS=Komagataella pastoris (strain GS115 / ATCC 20864) GN=PAS_chr3_0579 PE=3 SV=1 - [C4R4Z1_PICPG]	1.95	2	667	74.2
C4R3C3	Uncharacterized protein OS=Komagataella pastoris (strain GS115 / ATCC 20864) GN=PAS_chr3_0029 PE=4 SV=1 - [C4R3C3_PICPG]	3.34	2	539	60.6
C4R3E4	Subunit of the SAGA and SAGA-like transcriptional regulatory complexes, interacts with Spt15p to act OS=Komagataella pastoris (strain GS115 / ATCC 20864) GN=PAS_chr3_0051 PE=4 SV=1 - [C4R3E4_PICPG]	5.57	2	341	38.9

A4. Mass spectrometry results of the 70 kDa band of the *At*PDR8 CBP-AC elution fraction. The table lists the accession numbers of the detected proteins, the number of the identified peptides and the coverage. Furthermore the molecular weight of the detected proteins is listed as well as the number of amino acids.

Accession	Description	Coverage	# Unique Peptides	MW [kDa]
AtPDR8	AtPDR8_HIS GN=AtPDR8_HIS PE=1 SV=1 - [AtPDR8_HIS]	40.97	103	170.7
C4R8V1	Ubiquitin OS=Komagataella pastoris (strain GS115 / ATCC 20864) GN=PAS_chr4_0762 PE=4 SV=1 - [C4R8V1_PICPG]	72.26	10	34.8
C4R3X8	ATPase involved in protein folding and the response to stress OS=Komagataella pastoris (strain GS115 / ATCC 20864) GN=PAS_chr3_0230 PE=3 SV=1 - [C4R3X8_PICPG]	37.29	22	70.7
C4R5Q0	Transketolase, similar to Tkl2p OS=Komagataella pastoris (strain GS115 / ATCC 20864) GN=PAS_chr3_0834 PE=4 SV=1 - [C4R5Q0_PICPG]	20.79	12	78.5
C4R4H7	Serine/threonine-protein phosphatase OS=Komagataella pastoris (strain GS115 / ATCC 20864) GN=PAS_chr3_0414 PE=3 SV=1 - [C4R4H7_PICPG]	23.83	18	66.3
C4R4J8	Mitochondrial amino acid transporter OS=Komagataella pastoris (strain GS115 / ATCC 20864) GN=PAS_chr3_0434 PE=3 SV=1 - [C4R4J8_PICPG]	18.57	12	77.9
C4R697	D-lactate dehydrogenase, oxidizes D-lactate to pyruvate, transcription is heme-dependent OS=Komagataella pastoris (strain GS115 / ATCC 20864) GN=PAS_chr3_1021 PE=4 SV=1 - [C4R697_PICPG]	18.31	11	64.4
C4R708	Tetradecameric mitochondrial chaperonin OS=Komagataella pastoris (strain GS115 / ATCC 20864) GN=PAS_chr4_0158 PE=3 SV=1 - [C4R708_PICPG]	22.07	12	60.2
C4R4D1	Uncharacterized protein OS=Komagataella pastoris (strain GS115 / ATCC 20864) GN=PAS_chr3_0374 PE=4 SV=1 - [C4R4D1_PICPG]	13.51	10	71.8
C4R0W4	Uncharacterized protein OS=Komagataella pastoris (strain GS115 / ATCC 20864) GN=PAS_chr2-1_0853 PE=3 SV=1 - [C4R0W4_PICPG]	21.33	9	56.8
C4QXI5	Heat shock protein Hsp90 OS=Komagataella pastoris (strain GS115 / ATCC 20864) GN=PAS_chr1-4_0130 PE=3 SV=1 - [C4QXI5_PICPG]	11.61	8	80.9
C4R7I1	Uncharacterized protein OS=Komagataella pastoris (strain GS115 / ATCC 20864) GN=PAS_chr4_0945 PE=4 SV=1 - [C4R7I1_PICPG]	15.67	6	52.7
P04842	Alcohol oxidase 1 OS=Komagataella pastoris (strain GS115 / ATCC 20864) GN=AOX1 PE=1 SV=2 - [ALOX1_PICPG]	11.01	8	73.9
C4R8M0	Vacuolar carboxypeptidase yscS OS=Komagataella pastoris (strain GS115 / ATCC 20864) GN=PAS_chr4_0686 PE=4 SV=1 - [C4R8M0_PICPG]	13.71	7	65.8
C4R1R9	Long chain fatty acyl-CoA synthetase with a preference for C12:0-C16:0 fatty acids OS=Komagataella pastoris (strain GS115 / ATCC 20864) GN=PAS_chr2-1_0785 PE=4 SV=1 - [C4R1R9_PICPG]	12.84	8	78.3
C4R5P8	Transketolase, similar to Tkl2p OS=Komagataella pastoris (strain GS115 / ATCC 20864) GN=PAS_chr3_0832 PE=4 SV=1 - [C4R5P8_PICPG]	9.19	2	78.8
C4R938	Protein disulfide isomerase, multifunctional protein resident in the endoplasmic reticulum lumen OS=Komagataella pastoris (strain GS115 / ATCC 20864) GN=PAS_chr4_0844 PE=3 SV=1 - [C4R938_PICPG]	12.74	5	52.6
C4R8S1	Succinate dehydrogenase [ubiquinone] flavoprotein subunit, mitochondrial OS=Komagataella pastoris (strain GS115 / ATCC 20864) GN=PAS_chr4_0733 PE=3 SV=1 - [C4R8S1_PICPG]	8.16	5	70.2
C4R773	Vacuolar cation channel OS=Komagataella pastoris (strain GS115 / ATCC 20864) GN=PAS_chr4_0220 PE=4 SV=1 - [C4R773_PICPG]	8.07	6	73.8

C4R5E4	Cytoplasmic ATPase that is a ribosome-associated molecular chaperone OS=Komagataella pastoris (strain GS115 / ATCC 20864) GN=PAS_chr3_0731 PE=3 SV=1 - [C4R5E4_PICPG]	7.67	4	66.5
C4R1Q2	Phosphoglucomutase, catalyzes interconversion of glucose-1-phosphate and glucose-6-phospate OS=Komagataella pastoris (strain GS115 / ATCC 20864) GN=PAS_chr2-1_0771 PE=3 SV=1 - [C4R1Q2_PICPG]	8.71	6	67.1
C4R9F2	Nuclear protein localization protein OS=Komagataella pastoris (strain GS115 / ATCC 20864) GN=PAS_c034_0030 PE=4 SV=1 - [C4R9F2_PICPG]	7.37	5	63.8
C4QXF2	Cytoplasmic aspartyl-tRNA synthetase, homodimeric enzyme OS=Komagataella pastoris (strain GS115 / ATCC 20864) GN=PAS_chr1-4_0095 PE=3 SV=1 - [C4QXF2_PICPG]	9.19	5	63.0
C4R404	Acetyl-coA hydrolase OS=Komagataella pastoris (strain GS115 / ATCC 20864) GN=PAS_chr3_0253 PE=4 SV=1 - [C4R404_PICPG]	3.82	4	58.2
C4R6R6	Protein involved in synthesis of the thiamine hydroxymethylpyrimidine (HMP) OS=Komagataella pastoris (strain GS115 / ATCC 20864) GN=PAS_chr4_0065 PE=4 SV=1 - [C4R6R6_PICPG]	10.88	4	38.2
C4R090	Protein involved in proteasome-dependent catabolite degradation of fructose-1,6-bisphosphatase OS=Komagataella pastoris (strain GS115 / ATCC 20864) GN=PAS_chr2-1_0299 PE=4 SV=1 - [C4R090_PICPG]	6.68	4	64.0
C4R4Y8	ATP synthase subunit alpha OS=Komagataella pastoris (strain GS115 / ATCC 20864) GN=PAS_chr3_0576 PE=3 SV=1 - [C4R4Y8_PICPG]	6.23	3	58.7
C4R3K5	Restriction of telomere capping protein 5 OS=Komagataella pastoris (strain GS115 / ATCC 20864) GN=RTC5 PE=3 SV=1 - [RTC5_PICPG]	5.72	3	65.2
C4R0H8	Protein involved in nuclear export of the large ribosomal subunit OS=Komagataella pastoris (strain GS115 / ATCC 20864) GN=PAS_chr2-1_0380 PE=4 SV=1 - [C4R0H8_PICPG]	5.14	2	57.4
C4QWZ4	Cytosolic asparaginyl-tRNA synthetase, required for protein synthesis OS=Komagataella pastoris (strain GS115 / ATCC 20864) GN=PAS_chr1-1_0390 PE=3 SV=1 - [C4QWZ4_PICPG]	5.99	3	61.4
C4R1J1	5-aminolevulinate synthase OS=Komagataella pastoris (strain GS115 / ATCC 20864) GN=PAS_chr2-1_0716 PE=3 SV=1 - [C4R1J1_PICPG]	7.14	3	61.5
C4R1Z2	Mitochondrial porin (Voltage-dependent anion channel), outer membrane protein OS=Komagataella pastoris (strain GS115 / ATCC 20864) GN=PAS_chr2-2_0392 PE=4 SV=1 - [C4R1Z2_PICPG]	16.25	4	29.6
C4R1X5	Uncharacterized protein OS=Komagataella pastoris (strain GS115 / ATCC 20864) GN=PAS_chr2-2_0496 PE=3 SV=1 - [C4R1X5_PICPG]	6.83	3	64.8
C4R560	Thiazole synthase, catalyzes formation of the thiazole moiety of thiamin pyrophosphate OS=Komagataella pastoris (strain GS115 / ATCC 20864) GN=PAS_chr3_0648 PE=3 SV=1 - [C4R560_PICPG]	4.93	3	37.0
C4R605	Phosphoinositide binding protein required for vesicle formation in autophagy OS=Komagataella pastoris (strain GS115 / ATCC 20864) GN=PAS_chr3_0931 PE=4 SV=1 - [C4R605_PICPG]	4.24	3	59.9
C4R0L2	Alpha-isopropylmalate synthase (2-isopropylmalate synthase) OS=Komagataella pastoris (strain GS115 / ATCC 20864) GN=PAS_chr2-1_0415 PE=3 SV=1 - [C4R0L2_PICPG]	4.55	3	63.6
C4R6H6	Phosphoesterase involved in downregulation of the unfolded protein response OS=Komagataella pastoris (strain GS115 / ATCC 20864) GN=PAS_chr3_1097 PE=4 SV=1 - [C4R6H6_PICPG]	4.66	3	66.1
C4QVE8	Uncharacterized protein OS=Komagataella pastoris (strain GS115 / ATCC 20864) GN=PAS_chr1-3_0160 PE=4 SV=1 - [C4QVE8_PICPG]	2.56	2	71.9
C4R3C3	Uncharacterized protein OS=Komagataella pastoris (strain GS115 / ATCC 20864) GN=PAS_chr3_0029 PE=4 SV=1 - [C4R3C3_PICPG]	3.34	2	60.6
C4QZN4	Shuttling pre-60S factor OS=Komagataella pastoris (strain GS115 / ATCC 20864) GN=PAS_chr2-1_0105 PE=4 SV=1 - [C4QZN4_PICPG]	3.67	3	59.3
C4R1W6	Uncharacterized protein OS=Komagataella pastoris (strain GS115 / ATCC 20864) GN=PAS_chr2-2_0419 PE=4 SV=1 - [C4R1W6_PICPG]	3.42	2	58.3
C4R6Z1	ATP-dependent DEAD (Asp-Glu-Ala-Asp)-box RNA helicase OS=Komagataella pastoris (strain GS115 / ATCC 20864) GN=PAS_chr4_0140 PE=3 SV=1 - [C4R6Z1_PICPG]	4.29	2	66.4
C4R9A4	Subunit of the NuA3 histone acetyltransferase complex that acetylates histone H3 OS=Komagataella pastoris (strain GS115 / ATCC 20864) GN=PAS_FragD_0029 PE=4 SV=1 - [C4R9A4_PICPG]	3.86	2	71.9
C4R153	Uncharacterized protein OS=Komagataella pastoris (strain GS115 / ATCC 20864) GN=PAS_chr2-1_0590 PE=4 SV=1 - [C4R153_PICPG]	4.07	2	68.8
C4R2S1	Catalase OS=Komagataella pastoris (strain GS115 / ATCC 20864) GN=PAS_chr2-2_0131 PE=3 SV=1 - [C4R2S1_PICPG]	4.71	2	57.8
C4QXD6	Fatty acid transporter and very long-chain fatty acyl-CoA synthetase OS=Komagataella pastoris (strain GS115 / ATCC 20864) GN=PAS_chr1-4_0080 PE=4 SV=1 - [C4QXD6_PICPG]	2.39	2	72.2
C4R606	NAD(+)-dependent formate dehydrogenase, may protect cells from exogenous formate OS=Komagataella pastoris (strain GS115 / ATCC 20864)	5.21	2	40.3

	GN=PAS_chr3_0932 PE=3 SV=1 - [C4R606_PICPG]			
C4R0Q9	Uncharacterized protein OS=Komagataella pastoris (strain GS115 / ATCC 20864) GN=PAS_chr2-1_0456 PE=3 SV=1 - [C4R0Q9_PICPG]	3.44	2	79.5
C4R3N8	Beta subunit of cytoplasmic phenylalanyl-tRNA synthetase, forms a tetramer with Frs2p to generate ac OS=Komagataella pastoris (strain GS115 / ATCC 20864) GN=PAS_chr3_0144 PE=4 SV=1 - [C4R3N8_PICPG]	4.24	2	66.1
C4R1M9	Cystathionine gamma-synthase, converts cysteine into cystathionine OS=Komagataella pastoris (strain GS115 / ATCC 20864) GN=PAS_chr2-1_0752 PE=3 SV=1 - [C4R1M9_PICPG]	4.07	2	66.5
C4QZ28	Actin-interacting protein OS=Komagataella pastoris (strain GS115 / ATCC 20864) GN=PAS_chr1-4_0641 PE=4 SV=1 - [C4QZ28_PICPG]	3.85	2	62.3
C4R6T1	Uncharacterized protein OS=Komagataella pastoris (strain GS115 / ATCC 20864) GN=PAS_chr4_0080 PE=4 SV=1 - [C4R6T1_PICPG]	5.10	2	45.2